The Anatomy of the Ancestral Iceland Plume: a chemical and isotopic Study of the Tertiary Basalts and Picrites from Baffin Island

Solveigh Laß-Evans

Thesis submitted as partial fulfilment of the requirements for the degree of Doctor of Philosophy (Ph. D) in Geology

University of Edinburgh

2004

To my son Aneirin

and

in memory of my grandparents

Anne and Hanfried Laß

Abstract

Around 62 Ma, large outpourings of basalt occurred in the North Atlantic region, from Baffin Island in the north-west, to the British Isles in the south-east, nearly simultaneously, over a lateral distance of 2000 km. This event may be best explained by the arrival of the ancestral Iceland plume beneath Greenland at this time. This research comprises a detailed chemical and isotopic study of picritic and basaltic lava flows and dykes from Baffin Island, the most westerly and least studied part of the North Atlantic Igneous Province (NAIP).

Most of the Baffin Island olivine phenocrysts are not in equilibrium with their host rock composition (MgO = 8-28 wt. %) and lavas with >14 wt. % MgO contain accumulated olivines. The wide range of calculated liquid compositions (9-20 wt. % MgO) indicates a complex magmatic system, in which several batches of magmas have been mixed and of which only a small proportion has reached the surface. The Baffin Island rocks were generated over a wide range of depths with estimated parental liquidus temperatures of 1211-1430° C and segregation pressures of 1.7-3.1 GPa.

Trace element and isotope ratios show that two distinct mantle sources were available: (1) a relatively depleted source with $(La/Sm)_n$ <1, negative ΔNb, $^{87}Sr/^{86}Sr$: 0.7030-0.7034 and $^{143}Nd/^{144}Nd$: 0.5130 and (2) a relatively enriched source with $(La/Sm)_n$ <1, positive ΔNb, $^{87}Sr/^{86}Sr$: 0.7039-0.7042 and $^{143}Nd/^{144}Nd$: 0.51280-0.51284. With the exception of Pb-isotope ratios, which show interaction with Precambrian basement rocks, isotope and trace element ratios are not significantly affected by crustal material. Therefore, the high-$^{87}Sr/^{86}Sr$, low-$^{143}Nd/^{144}Nd$ samples represent the most enriched endmember of the ancestral Iceland plume, which was present 62 Ma, but of which the geochemical signatures are not evident today.

The highest $^{3}He/^{4}He$ isotope ratios (up to 50 R_a) yet recorded from any terrestrial rocks are found in the low-$^{87}Sr/^{86}Sr$, high-$^{143}Nd/^{144}Nd$ rocks, probably generated by mixing at the 670-km thermal boundary of depleted mantle material with primordial helium from the lower mantle. An origin of the Baffin Island lava flows at such a reservoir could explain the high $^{176}Hf/^{177}Hf$ relative to $^{143}Nd/^{144}Nd$ ratios. Therefore, the depleted rocks are not derived from a N-MORB source, but may instead represent a plume 'sheath' with a long history of trace element depletion and isolation from the convecting upper mantle.

Acknowledgements

I am extremely grateful to my supervisor, Godfrey Fitton, for trusting me with the Baffin Island samples and for his help and support during the project. I would also like to express my gratitude to my other supervisor Rob Ellam, for his help and encouragement throughout the project and for his constant reminders to keep an open mind.

My third supervisor, Brian Upton, lent me his diary and pictures from his trip to Baffin Island in 1969. I am very grateful for this information as well as his moral support and his constant supply of chocolate and cakes to keep me going. Thanks also to Fin Stuart, my fourth supervisor, for help and advice with the helium isotope analyses.

This project would not have been possible without the efforts of Ian Snape, Coleen Cole and Sally Brown, who collected the rocks during a 1996 Edinburgh University expedition to Baffin Island, partly funded by the Sheila Hall Trust.

This work was supported by a NERC scholarship (GT04/99/ES/79).

I would like to thank Dodie James for her help with the XRF analyses and for her wise words. Peter Hill and Paula McDade provided invaluable help with the electron probe. For their expert and professional help at SUERC, I thank Valerie Olive for supervising my work with the ICP-MS and Anne Kelly and Vinny Gallagher for their help with the isotope analyses; I would also like to thank them for their friendship and generosity.

I gratefully acknowledge the expertise of Pamela Kempton for her comprehensive instruction in hafnium isotope analyses and for her help and supervision in carrying these out at NIGL.

Colin Devey, my diploma supervisor in Kiel, encouraged and supported me in my early contacts with Scotland - I am most grateful to him.

In Edinburgh and East Kilbride, I thank Alice Williams, Estelle Mortimer, Fiona Fordyce, Johannes Barth, Katalin Juhasz-Bodnar, Lynne Chambers, Martin Howard, Mat Hardenberg and Salima Baraka-Lokmane for their good company and friendship shared over food and coffee. I am grateful to my flatmate Kathryn Hardacre for her friendship and advice during my first year in Edinburgh. Above all, I would like to thank Friðbjørg Biskopstø for her constant companionship and support as a fellow foreign student, flatmate and particularly as a good dear friend.

I would like to thank my family for believing in me and for their support and encouragement throughout my time at University. Finally, I would not have been able to finish this project without the love and patience of my husband, Richard. I am deeply grateful for his support at home, for proof-reading and for encouraging me to keep going.

Contents

Figures

Tables

I Rationale

1 Introduction

1.1 Models for LIPs origin

Large igneous provinces (LIPs) represent major global magmatic events, and their emplacement could have influenced the environment on a regional or even global scale, with implications for climate change and mass extinctions (e.g. Coffin & Eldholm, 1993). The voluminous magma production of LIPs, including continental flood basalts and associated intrusive rocks, oceanic plateaus, submarine ridges, ocean basin flood basalts, seamount groups and the large volumes of magma emplaced along passive volcanic margins, clearly record major thermal perturbations in the mantle (e.g. Coffin & Eldholm, 1992, 1993). It has become popular to attribute this extensive magmatism to mantle plumes originating from a thermal boundary layer deep within the mantle (e.g. Morgan, 1971; White & McKenzie, 1989; Campbell & Griffiths, 1990). The acceptance of mantle plumes, however, has not been universal and suggestions for other forms of mantle convection model remain (e.g. Mutter et al., 1988; Anderson et al., 1992; Anderson, 1998). One model for such a non-plume origin of LIPs suggests that regions of warmer-than-ambient mantle ("hotcells", Anderson et al., 1992) are caused partly by a long-term continental insulation and partly by the cooling effect of distant subduction zones (Anderson et a., 1992; Anderson, 1998). Another non-plume model (Fig. 1.1) relies on the sharp thermal contrast between the normal-temperature asthenosphere and the cooler, steep rift-flanks of the continental lithosphere inducing local convection cells beneath the developing rift zone (Mutter et al., 1988).

Alternatively, the necessary thermal energy for the voluminous magma production of LIPs is supplied from an external source, for example from a mantle plume. This model, in various forms, is widely supported and represents so far the most plausible explanation for the origin of LIPs (e.g. H.C.Larsen et al., 1994). Mantle plumes are

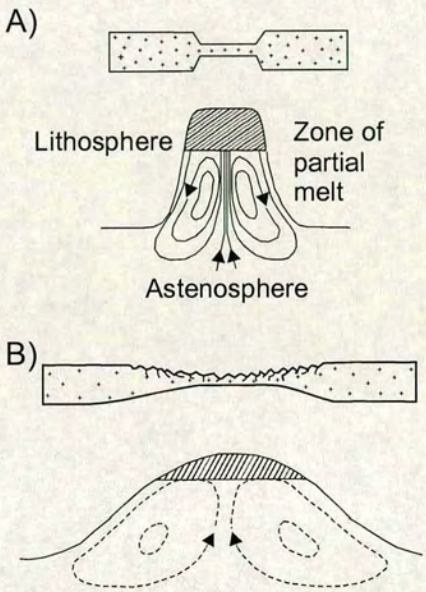

Fig. 1.1. Convective partial melting (Mutter et al., 1988) showing a schematic cross section of the lithosphere and astenosphere after rifting for a narrow and a wide rifting zone. The rate of induced mantle flow is greater for a narrow margin, leading to enhanced partial melting (for further explanation, see text). In this model, no external source of heat, such as a plume, is required.

thought to be solid, narrow upwelling convection currents in the mantle. Because they entrain large amounts of mantle material on the way from their origin to the surface they represent significant carriers of heat and material within the Earth's interior (Morgan, 1971; Davies, 1988; Sleep, 1990). They are believed to be up to 200° C hotter than the surrounding mantle through which they penetrate and rise. The classical thesis predicts that they originate from a hot low-density layer within the mantle. This source is located either above the seismic discontinuity at a depth of 670 km between upper and lower mantle (White & McKenzie, 1989) or at the D"-layer at the core-mantle boundary (CMB) at a depth of 2,900 km (Richards et al., 1989; Griffiths & Campbell, 1990). It is difficult to image narrow conduits of rapidly rising mantle plumes by seismic tomographic methods (Nataf, 1993) and therefore, it has not yet been possible to date to determine definitively by this method whether plumes rise from the 670 km discontinuity, from the CMB, or even from both (Cserepes & Yuen, 2000).

Two fundamentally different classes of plume model have been developed. The model of Courtney & White (1988), further developed by White & McKenzie (1989) (the "incubating plume" hypothesis; Fig. 1.2), is based on observations of crustal structures along volcanic margins and on petrologic modelling (Coffin & Eldholm, 1992). In this model a mantle plume originates either from the 670 km discontinuity or from the lower mantle. It accumulates gradually and incubates slowly beneath the overlying lithosphere. The plume behaves passively and extensive melting occurs by decompression only, when the plume head is crossed by pre-existing 'thinspots' (Thompson & Gibson, 1991), for example young ocean basins, or when the lithosphere is pulled apart as a result of plate divergence (McKenzie & Bickle, 1988; White & McKenzie, 1989; Kent et al., 1992). In the second class of model, the plume plays a more active role. In this model (the "starting plume" hypothesis; Fig. 1.2), based primarily on the results of laboratory experiments, a large start-up plume originates at the CMB (Richards et al., 1989; Campbell & Griffiths, 1990; Griffiths & Campbell, 1990). When the plume head impacts at the base of the lithosphere, the continent ruptures and vulcanism occurs. If

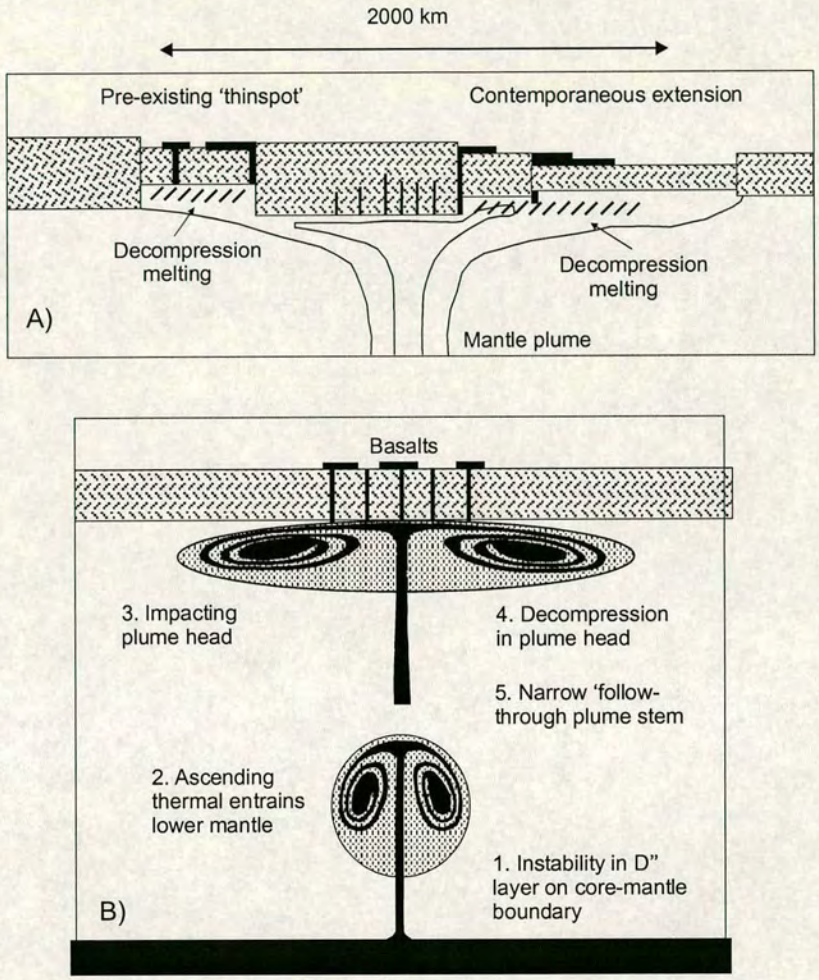

Fig. 1.2. Schematic diagrams of plume-lithosphere interactions from H.C.Larsen et al. (1994). (A) The incubating plume model of White & McKenzie (1989). (B) The impacting plume model of Richards et al. (1989) and Campbell & Griffiths (1990) and Griffiths & Campbell (1990). For explanation see text.

there is a continuous supply of hot material from the source region, the starting plume consists of a large mushroom-shaped head and a relatively narrow feeder conduit or tail.

Alternatively, a short-lived plume originates at the CMB, rises to the 670 km discontinuity, injects hot material in the upper mantle (Tackley et al., 1993) and eventually triggers convective instability in this thermal boundary, which could produce one or more secondary plumes (Fitton et al., 1997). Recently, a further kind of plume has been proposed, originating neither from the CMB, nor the 670 km discontinuity, but from below the 670 km boundary (mid-mantle plume, Cserepes & Yuen, 2000). This plume does not, in contrast to the classical plume models, develop from a thermal boundary within the mantle. Instead, it is fed by lower-mantle material immediately below the 670 km discontinuity with no deep source rising in the upper mantle in a form of a narrow, cylindrical plume (Cserepes & Yuen, 2000).

1.2 The North Atlantic Igneous Province (NAIP)

The North Atlantic Igneous Province (NAIP) is perhaps the best place in which to study the structure, origin and composition of a mantle plume and its evolution through time. Around 61 Ma, continental magmatism occurred nearly simultaneously in Baffin Island (Clarke & Upton, 1971), West Greenland (Storey et al., 1998), SE Greenland (Sinton & Duncan, 1998), central E Greenland (Sinton & Duncan, 1998; Storey et al., 1998), the Faeroe Islands (L.M.Larsen et al., 1999) and in the British Isles (Pearson et al., 1996; Chambers & Pringle, 2001) over a lateral distance of 2000 km (Fig. 1.3 and 1.4). This early (pre-break-up) phase ended around 58 Ma. The later (break-up) phase along the North Atlantic rift zone was accompanied both by the formation of thick, seaward-dipping reflector sequences (SDRS) along the E Greenland and NW European margins and by voluminous on-shore magmatism in E Greenland (e.g. Saunders et al., 1997; H.C.Larsen & Saunders, 1998). This phase of igneous activity started around 56 Ma and

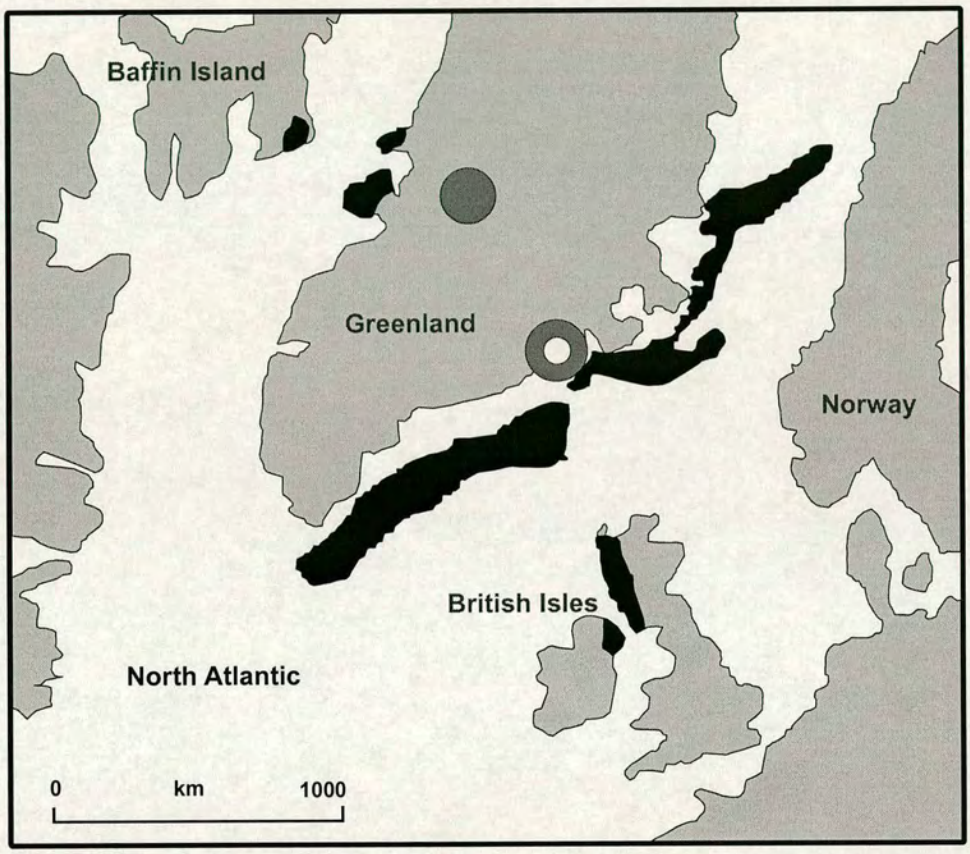

Fig. 1.3. Reconstruction of the North Atlantic region at 55 Ma (adapted from Nadin et al., 1995) showing the distribution of the Tertiary volcanic activity and the estimated locations of the ancestral Iceland plume (non-filled circle: White & McKenzie, 1989; filled-circle: Lawver & Müller, 1994).

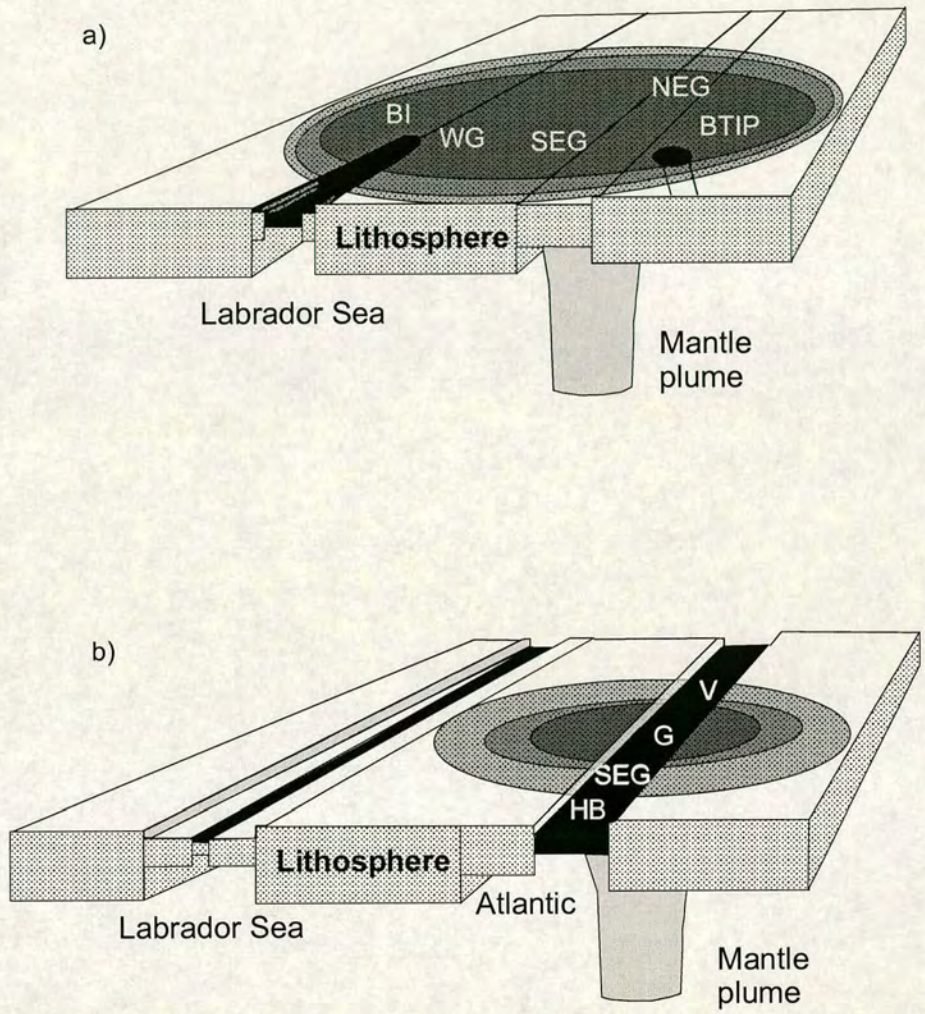

Fig. 1.4. Schematic diagrams of the development of the Iceland plume during (a) Palaeocene and (b) Eocene times (from Saunders et al., 1997). Abbreviations: NEG- Northeast Greenland; BTIP- British Tertiary Igneous Province; SEG- Southeast Greenland; WG- West Greenland; B- Baffin Island; V- Voring Plateau; G- central East Greenland; HB- Hatton Bank margin.

is still active along the North Atlantic rift system today (e.g. Saunders et al., 1998).

The widespread volcanic event required a broad thermal anomaly (White et al., 1987; White, 1988) and can be explained by the arrival of the ancestral Iceland plume beneath Greenland at 61 Ma (Chalmers et al., 1995b). The precise location of the ancestral Iceland plume in the North Atlantic region, however, is open to some doubt. Some authors propose that the axis of the ancestral Iceland plume was centred beneath eastern Greenland at 61 Ma (Brooks, 1973; White & McKenzie, 1989), whereas others (Lawver & Müller, 1994) suggest that its location was beneath West Greenland at this time. Not only the location of the ancestral Iceland plume, but also the widespread occurrence of high-temperature magmas in the North Atlantic Igneous Province remain unresolved problems. The classical plume models (the starting plume model and the incubating plume model, see above) make fairly specific predictions in respect to the temperature distribution within the plume head. They predict that high- temperature magmas (such as picrites) should be restricted to above the central plume stem (e.g. Campbell & Griffiths, 1990), or at most to a few hundred kilometres around it (e.g. White & McKenzie, 1989). This seems to be in conflict with the actual distribution of picrites in the NAIP. These high-temperature, magnesian magmas occur in Baffin Island (e.g. Clarke & Upton, 1971; Francis, 1985), West Greenland (Clarke & Pedersen, 1976; Pedersen, 1985b; Gill et al., 1992), central East Greenland (Nielsen et al., 1981; Gill et al., 1988; Fram & Lesher, 1997), SE Greenland (H.C.Larsen et al., 1994; Fram et al., 1998; L.M.Larsen et al., 1998; Thy et al., 1998; Fitton et al., 2000) and in the British Tertiary Igneous Province (e.g. Kent, 1995). The outstanding question in the NAIP is, therefore, how the extremely high-temperature melts from a single plume could erupt in such volumes over a distance of 2000 km, and the lack of a satisfactory answer to this question has led to the development of additional plume models. Earlier work includes suggestions that either (1) the Kangerlussuaq-Iceland plume is responsible for the magmatism in NW Europe, but that a second plume accounts for the volcanism in West Greenland (Gill et al., 1992), or (2) the rising plume may have been split at depth by the underside

topography of the Greenland craton leading to the production of hot, picritic magmas at significant distances away from the plume axis (Hill, 1991; L.M.Larsen et al., 1992; Holm et al., 1993) or (3) that picrites erupt not only close to the plume axis but also over its margin (Chalmers et al., 1995b).

In recent studies various workers (e.g. Graham et al., 1998; Storey et al., 1998; H.C.Larsen & Saunders, 1998; Saunders et al., 1998; T.B.Larsen et al., 1999) have suggested that rapid lateral channelling of hot mantle plume material in the shallow mantle ("surging plume model", H.C.Larsen & Saunders, 1998) could have caused the wide geographical spread of volcanism in the North Atlantic region. Numerical models demonstrated that hot plume head material could ascend at ultra-fast rates (1-10 m/yr) and spread out horizontally (~0.5 m/yr) as a thin layer beneath the lithosphere (assuming a non-Newtonian [i.e. non-linear] temperature- and depth-dependent upper mantle rheology operating at an effective Rayleigh number of $\sim 10^6$) (T.B.Larsen & Yuen, 1997; T.B.Larsen et al., 1999). In applying a more realistic non-Newtonian rheology, plumes can rise more quickly through the mantle, causing higher temperatures in the plume head and thus will be more effective in producing flood basalt volcanism than will the Newtonian rheology (Van Keken, 1997). Sedimentary (Dam et al., 1998), geochemical (Graham et al., 1998; H.C.Larsen & Saunders, 1998; Saunders et al., 1998; Tegner et al., 1998) and geochronological (Storey et al., 1998) data support the hypothesis that the contemporaneous emplacement of hot mantle material throughout the North Atlantic region could have been caused by such anomalous high mantle flux rates. In this case, melt generation within the plume head took place nearly simultaneously through lithosphere thinspots in widely separated locations (H.C.Larsen & Saunders, 1998). The emplacement of hot Iceland mantle material in separate locations could have occurred in episodic or pulsing events (e.g. Saunders et al., 1997; White & Lovell, 1997; O'Connor et al., 2000; Johnston & Thorkelson, 2000). On the basis of $^{40}Ar/^{39}Ar$ data from dredged samples from three Rockall seamounts, O'Connor et al. (2000) pointed out that volcanic activity took place in pulses on timescales of 5-10 Myr dating backwards into the late

Cretaceous. According to O'Connor et al. (2000), this model is compatible with models of ultrafast mantle plumes (e.g. T.B.Larsen & Yuen, 1997; T.B.Larsen et al., 1999), which show evidence of very focused activities with calm periods, pulses ranging from a few Myr (T.B.Larsen et al., 1999) to about 10 Myr (T.B.Larsen & Yuen, 1997).

1.3 The Iceland mantle plume

1.3.1 Geophysical signatures

Various interpretations of seismic data are seemingly in disagreement as to whether Iceland is underlain by a mantle plume originating from the CMB (e.g. Shen et al., 1998; Helmberger et al., 1998; Bijwaard & Spakman, 1999), or if buoyant upwelling is restricted to the upper mantle beneath Iceland (e.g. Ritsema et al., 1999; Megnin & Romanowisz, 2000; Foulger et al., 2000; Foulger & Pearson, 2001).

Several recent seismic whole-mantle tomography experiments support the hypothesis that the North Atlantic at the latitude of Iceland is underlain by a low seismic velocity anomaly in the upper mantle (Bijwaard & Spakman, 1999; Ritsema et al., 1999; Megnin & Romanowisz, 2000). As summarised by Foulger and Pearson (2001), Ritsema et al. (1999), for example, determined an s-wave-velocity model. They found that the resolution of the structure beneath the North Atlantic is ~1000 km laterally and ~150 km vertically in the transition zone, similar to the ~900 km horizontal and ~100 km vertical resolution modelled by Megnin & Romanowisz (2000). Local seismic experiments detected a relatively narrow, approximately vertical, low seismic velocity anomaly beneath Iceland (e.g. Allen et al., 1999), of which the structure could be resolved down to 400 km, but not deeper (Wolfe et al., 1997). A more recent teleseismic tomographic experiment (Foulger et al., 2000) suggested that the low-wave-speed anomaly beneath Iceland is confined to the upper mantle.

In search of evidence for a mantle plume originating in the lower mantle, Bijwaard & Spakman (1999) found a continuous, weak low seismic velocity body in the lower mantle. According to them, the anomaly lies beneath Iceland in the upper mantle, shifts towards the Faeroe Isles at 1000 km depth, returns to southern Iceland at 1900 km depth, broadens and extends westwards with depth and underlies Greenland in the depth range of 2000-2500 km. However, Foulger & Pearson (2001) pointed out that Bijwaard & Spakman (1999) had to saturate the colour scale they used at <10 % of the maximum anomaly in order to illustrate an apparently continuous low seismic velocity structure extending throughout the mantle. In comparison to other recent whole-mantle tomographic experiments (e.g. Ritsema et al., 1999; Megnin & Romanowisz, 2000), which imply an upper mantle origin for the Iceland plume, the inconsistency with Bijwaard & Spakman (1999) model could rely only on the colour scale used and, therefore, to the first-order, the three models are in agreement (Foulger & Pearson, 2001). Other seismic evidence for a deeper structure beneath Iceland is presented by Shen et al. (1998), who used receiver functions to study the two seismic discontinuities marking the top (at 400 km) and bottom (at 650 km) of the mantle transition zone beneath Iceland. They found that the transition zone is 20 km thinner compared to the average Earth (Kennet & Engdahl, 1991). They interpreted this observation as a result of a hot and narrow plume originating from the lower mantle and convecting through both discontinuities. In supporting a deeper structure beneath the Iceland region, Helmberger et al. (1998) modelled the interference of shear waves through, and refracted at, the CMB beneath Iceland. They found the presence of a localised patch of material with ultra-low seismic wave speed at the CMB and suggested that this zone represents the hot, partially molten source region of the Iceland mantle plume.

1.3.2 Geochemical signatures

Geochemical data (trace element and isotopic) offer a powerful opportunity to study several facts of LIP development, including the interactions between a mantle plume and the lithosphere, relative contributions of the crust, and the role of mantle plumes in LIP formation. Fitton et al. (1997) summarised the compositional and thermal structures of different plume types (Fig. 1.5). A plume, whose source lies in the thermal boundary layer at the 670 km discontinuity (Model 1), is likely to be composed of an outer layer of hot upper mantle, which is similar in composition to the depleted mantle source of mid-ocean ridge basalts (MORB). Its axial zone would consist of lower mantle material, which is less depleted in incompatible elements and therefore would show different chemical and isotopic signatures compared with MORB-source mantle. If a plume has its source at the core-mantle boundary (Model 2), it will be mainly composed of hot material from the D"-layer, with a thin outer shell of heated upper mantle material. A slowly incubating plume (Model 1) would heat the adjacent asthenosphere and thus, the compositional and thermal components of this plume would be decoupled. In contrast, an impacting plume (Model 2) would have had far less time to transfer energy to the adjacent mantle, and therefore the chemical and thermal effects would be coincident (H.C.Larsen et al., 1994). A plume originating at the D"-layer might stall at the 670 km discontinuity (Model 3), heat the upper mantle and create one or more secondary plumes. These could be similar in composition to Model 1, but with a central part composed of material from the core-mantle boundary (Fitton et al., 1997) or they might consist only of upper mantle material.

The NAIP offers a unique opportunity to study the compositional structure of a large mantle plume. While most plumes remain trapped beneath a lithospheric cap, the juxtaposition of the Iceland plume and the North Atlantic ridge allows the plume to decompress and melt at shallow levels. Not only does this provide material from the entire width of the plume head, but also from the Palaeogene to the present day.

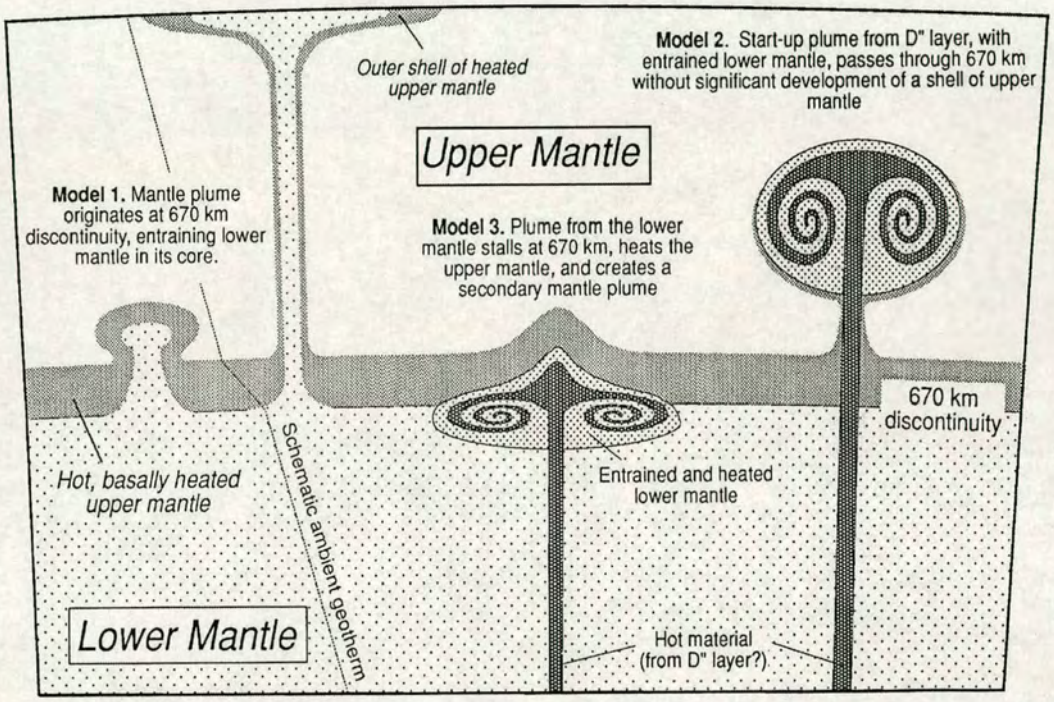

Fig. 1.5. Schematic representation of different mantle plumes (from Fitton et al., 1997) For explanation see text.

Numerous studies have shown that Icelandic volcanic rocks can be distinguished in their geochemical and isotopic characteristics with respect to North Atlantic mid-ocean ridge basalts (MORB), by having higher abundances of incompatible trace elements, high $^{87}Sr/^{86}Sr$, low $^{143}Nd/^{144}Nd$ and radiogenic Pb (e.g. O'Nions & Pankhurst, 1973; Sun & Jahn, 1975; Zindler et al., 1979). In order to generate the observed range of isotopic ratios, the mantle beneath Iceland must be heterogeneous and requires contributions from isotopically distinct sources (e.g. Zindler et al., 1979; Elliot et al., 1991; Hémond et al., 1993). In general, the range of lava compositions on Iceland require interaction between a relatively high-$^{87}Sr/^{86}Sr$, low-$^{143}Nd/^{144}Nd$ and incompatible-rich end-member and a relatively low-$^{87}Sr/^{86}Sr$, high-$^{143}Nd/^{144}Nd$ and incompatible-element-poor end-member (e.g. Hanan et al., 2000; Hanan & Schilling, 1997; Fitton et al., 2003). The depleted component has been interpreted as either MORB-source mantle (Schilling, 1973; Hart et al., 1973; Sun & Jahn, 1975; Schilling et al., 1983; Hanan & Schilling, 1997; Hanan et al., 2000) or as an intrinsic component of the plume itself (Hards et al., 1995; Kerr, 1995; Kerr et al., 1995; Thirlwall, 1995; Fitton et al., 1997, 2003; Nowell et al., 1998; Kempton et al., 1998, 2000; Chauvel & Hémond, 1999). However, the enriched signatures of the plume do not fit a simple two-component model either (Prestvik et al., 2001). It has been suggested that the plume may contain more than one enriched component (Hanan & Schilling, 1997; Hanan et al., 2000) and is perhaps heterogeneous only on a relatively small scale (Furman et al., 1995).

1.4 Aims of this thesis

Although the NAIP is one of the best-studied LIPs with a large amount of geochemical data from Iceland itself and other parts of the NAIP, there are still several gaps in our knowledge and further work is necessary in order to improve understanding of plume dynamics. In particular, data from the periphery of the NAIP is required to allow a more direct comparison between Iceland and the 61 Ma plume axis. Baffin Island lies at the

most extreme western margin of the NAIP and has been little studied. Existing publications are based on a relatively small and old collection, and analyses have not included the latest geochemical techniques. This thesis comprises a detailed chemical and isotopic study of a suite of new samples of Baffin Island.

The broad aim was to constrain better the evolution of the Iceland mantle plume and the thesis focused on four main areas:

1. The magnesian rocks of West Greenland/Baffin Island have been a focal point of controversy concerning the MgO contents of primary magmas in general. In order to establish the nature of the Baffin Island picrites and to help resolve, if the high MgO values either (1) represent primary liquids rising from the mantle, or (2) reflect the mechanical accumulation of olivine phenocrysts, a detailed analysis of olivine compositions from Durban Island has been carried out. These analyses also help to estimate the liquidus temperature.

2. Magmas passing through continental crust may modify their composition by assimilation of crustal material. Because the Baffin Island magmas erupted through Archaean and Proterozoic crust, as well as Tertiary sedimentary sequences, it is necessary to consider whether or not the lavas interacted with their basement rocks before the mantle source characteristics or the melting regime of the Tertiary rocks on Baffin Island can be investigated.

3. Fundamental questions in Earth science concern the mineralogy of the basalt source region and the temperatures and depths at which basalts form. In order to examine the geochemical variations due to partial melting processes, major and trace element mantle source models help to evaluate the melting processes responsible for the generation of the Baffin Island lavas.

4. Investigation of the nature of the Baffin Island mantle source and to establish (1) whether the geochemical signature of the Iceland plume was present in the outer edge of the NAIP; and (2) if so whether its compositional signature was the same at the time of break-up; or instead (3) if the Baffin Island Tertiary lavas were only the result of a local volcanic eruption event, unrelated to the NAIP.

2 Geological history

2.1 Tectonic development

The tectonic history of the Labrador Sea, Davis Strait and Baffin Bay (Fig. 2.1) has been a source of much controversy, and the interpretation of the available data in this area has led to different reconstructions of the plate tectonic movements.

Lithospheric stretching between the North American and Greenland plates started ~130 Ma (Balkwill, 1987). During this stretching, complex graben systems developed from the present day Labrador Sea to the northern end of Baffin Bay (Ziegler, 1988; Whittaker, 1997). These basins subsided and were filled with sediments during the Cretaceous (e.g. Henderson et al., 1976; Balkwill, 1987).

2.1.1 Labrador Sea

Marine magnetic, gravity and seismic data all indicate that sea-floor spreading took place in the Labrador Sea, but the timing of the onset of spreading and the distribution of continental and oceanic crust in the Labrador Sea has been a matter of debate for many years. Essentially, the subject of the debate has been the transition zone between 59° N and 62° N in the Labrador Sea, where small-amplitude and variable-shape anomalies occur. These less clearly defined, low-amplitude anomalies have been interpreted as: (1) sea-floor spreading anomalies (Srivastava, 1978; Roest & Srivastava, 1989; Srivastava & Roest, 1999); (2) dyke injections through foundered and stretched continental crust (Chalmers, 1991; Chalmers & Laursen, 1995); (3) foundered continental crust underlain by partly serpentinized mantle (Chian & Louden, 1994; Chian et al., 1995); or (4) serpentinized peridotites through which dykes may have been injected (Geoffrey

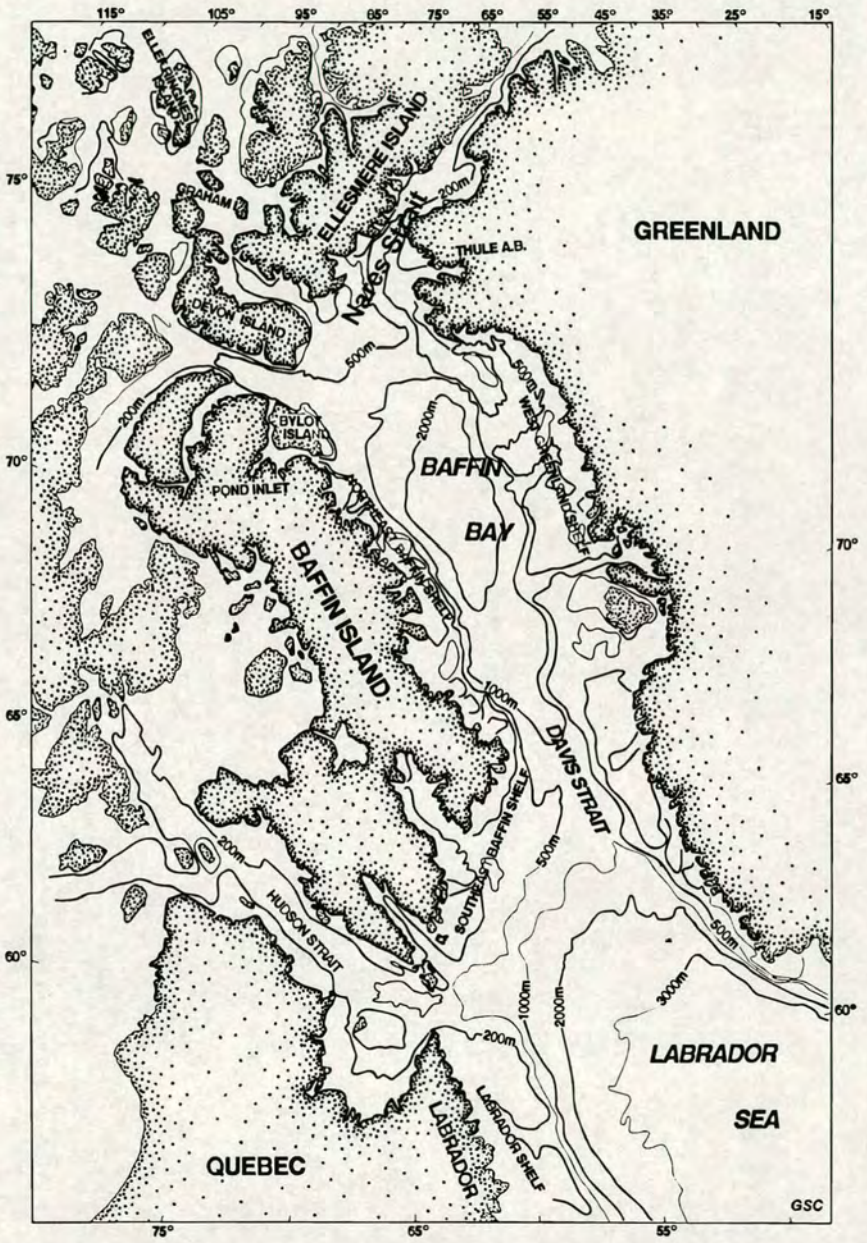

Fig. 2.1. General map of Labrador Sea, Davis Strait and Baffin Bay showing the bathymetry in meters below sea level (after Balkwill et al., 1990).

et al., 2001). Continental plate break-up and reorganisation propagated from south to north in the Labrador Sea. Roest & Srivastava (1989) and Srivastava & Roest (1999) argued that sea-floor spreading began in the Late Cretaceous (Fig. 2.2) and they interpreted the low-amplitude magnetic anomalies as sea-floor spreading anomalies Chron 33-27 (78-62 Ma, Fig. 2.3). In contrast, others (Chalmers, 1991; Chalmers & Laursen, 1995; Chian & Louden, 1994; Chian et al., 1995) favoured an Early Tertiary age (Chron 27n) for the onset of sea-floor spreading (Fig. 2.4). In this model, the continent-ocean-boundary (COB) is placed ~120 km farther seaward than the previously suggested position (Chalmers, 1991).

Apart from disagreement over the interpretation of the transitional zone, it seems to be generally accepted that sea-floor spreading took place between Chrons 27 and 21 (62-48 Ma respectively, according to the time scale of Kent & Gradstein, 1986). Transform-like faults in the southern Labrador Sea are characterised by two trends, N60°-70° E and N20°-30° E (Kristoffersen & Talwani, 1977; Roest & Srivastava, 1989; Chalmers & Laursen, 1995; Whittaker et al., 1997). According to Roest & Srivastava (1989) the former trend indicates the ENE direction of the Greenland plate relative to the North American plate until Chron 25 (59 Ma), while the latter trend indicates a major change of the spreading direction to NNE between Chrons 25 and 24. This change was caused by the development of a triple junction as Greenland separated from both North America and Europe (e.g. Roest & Srivastava, 1989). The first phase of spreading, ending at Chron 24r, took place along a NNW axis, while the second phase of spreading (Chrons 24-13) took place along a NW-trending axis (Whittaker et al., 1997). The direction of the northern part of the extinct Labrador Sea rift is distinguishable, trending approximately N125° E (Geoffrey et al., 2001). As a result of this shift, the spreading in the Labrador Sea became oblique and stopped after Chron 20 (45 Ma) but prior to Chron 13 (36 Ma) (e.g. Roest & Srivastava, 1989). Figure 2.5 demonstrates the evolution of the Labrador Sea after Roest & Srivastava (1989).

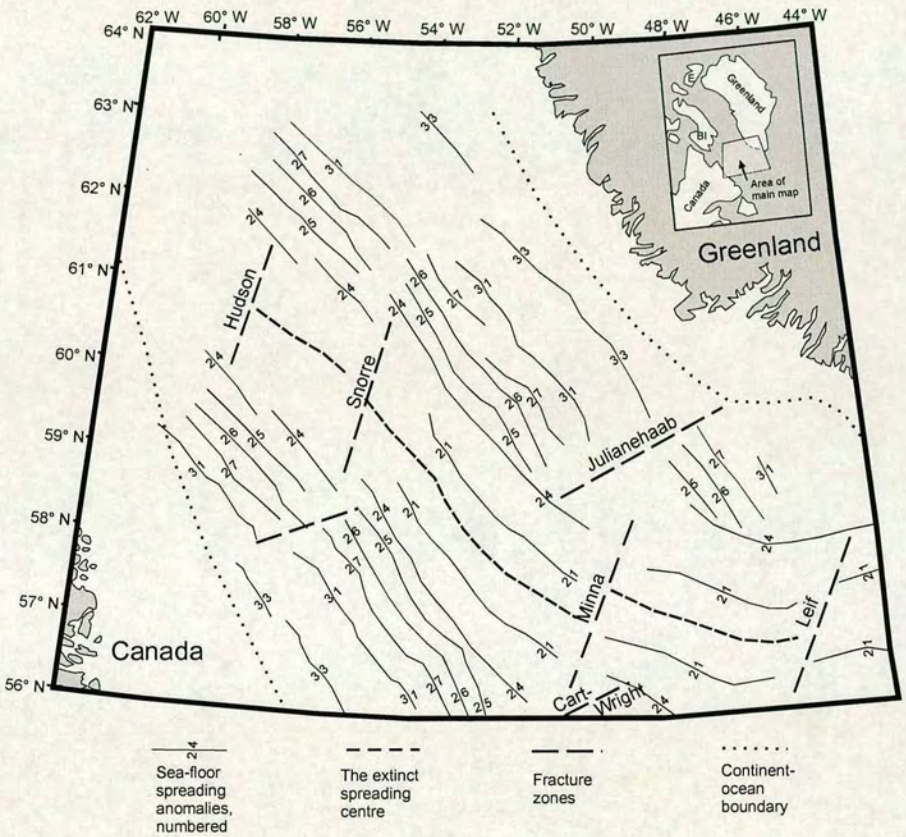

Fig. 2.2. Map of the Labrador Sea (taken from Chalmers, 1991). Sea-floor spreading anomalies and the boundary between continental and oceanic crust are from Roest & Srivastava (1989). Note that the extent of the oceanic crust is a debatable issue: for a different interpretation see Fig. 2.4.

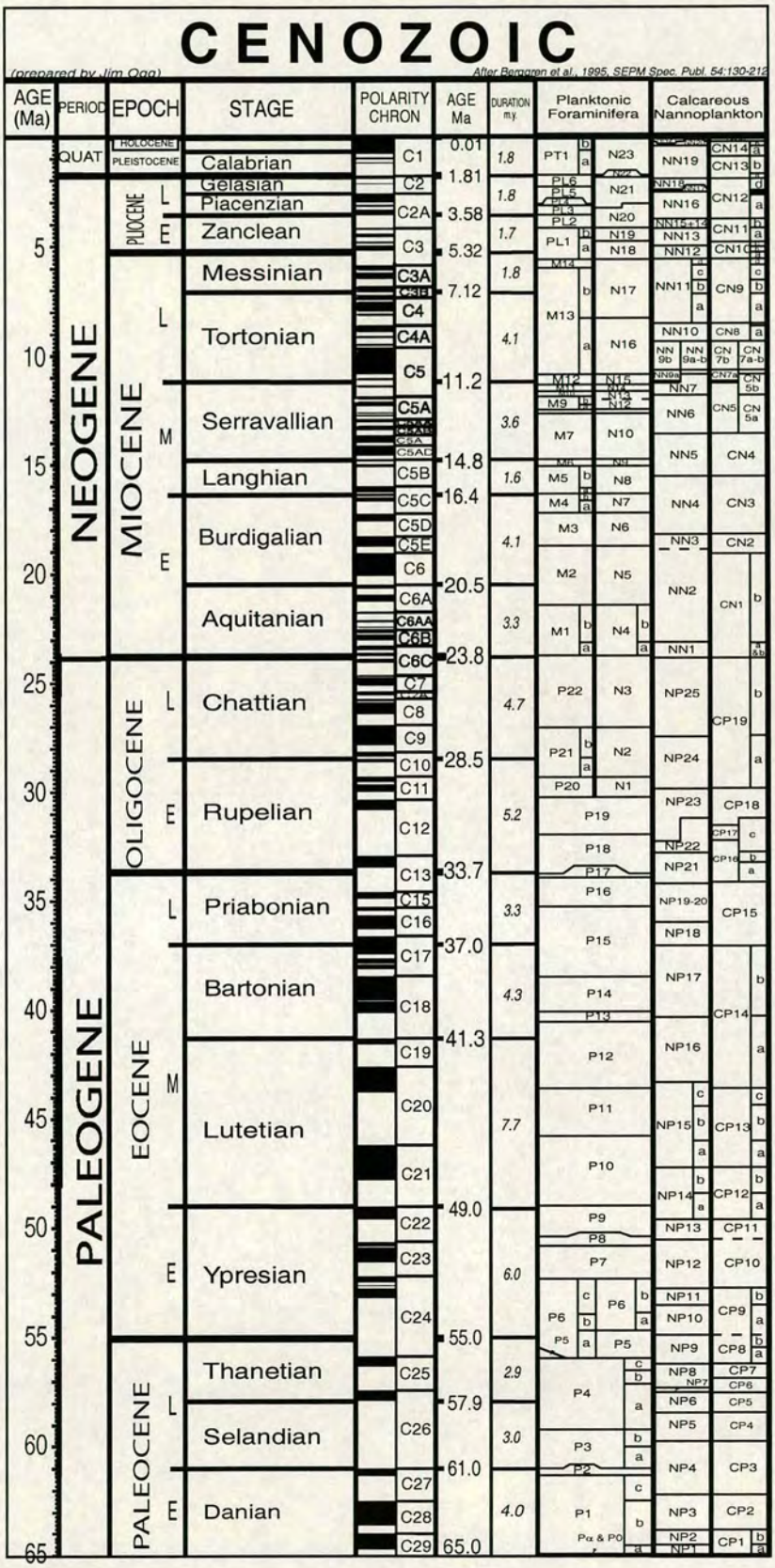

Fig. 2.3. Geomagnetic time scale after Berggren et al. (1995).

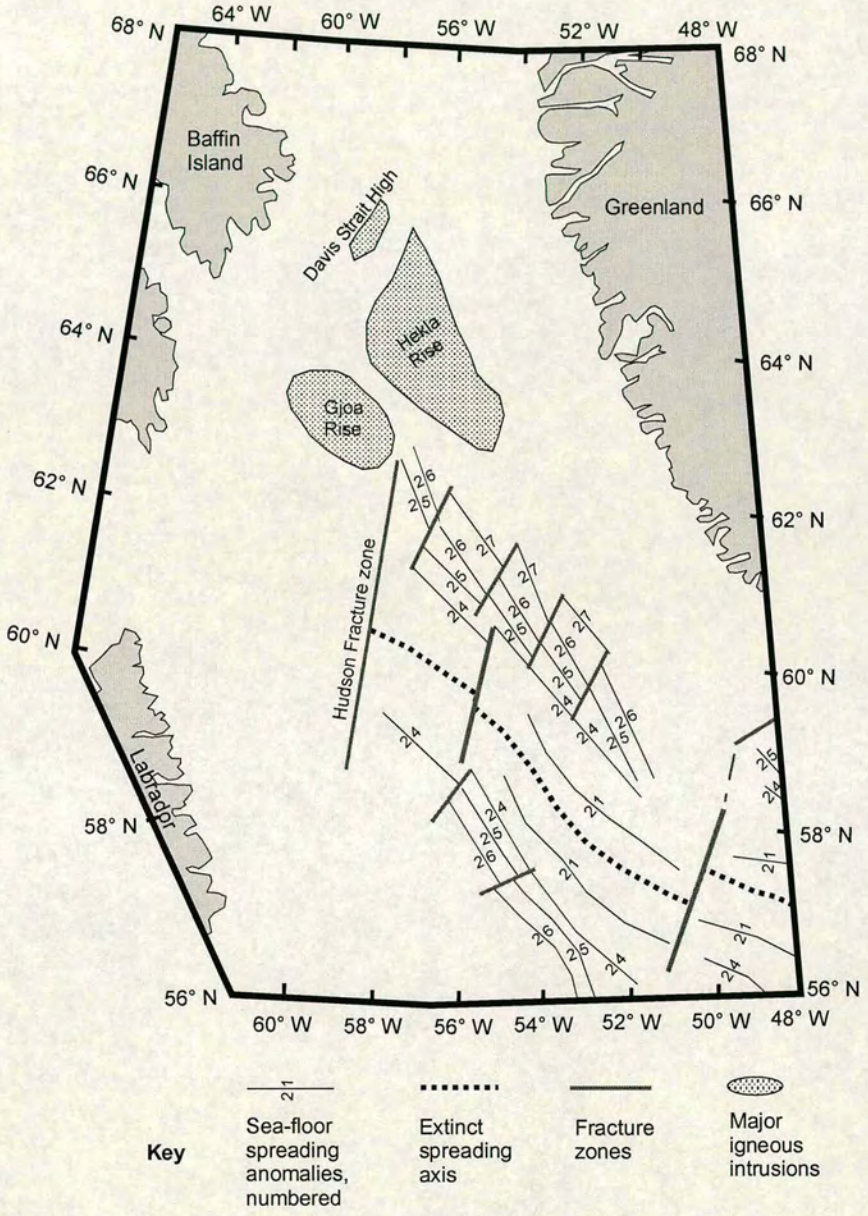

Fig. 2.4. Tectonic map of the northern Labrador Sea after the interpretation of Chalmers and co-workers (e.g. Chalmers et al., 1993; Chalmers & Laursen, 1995)

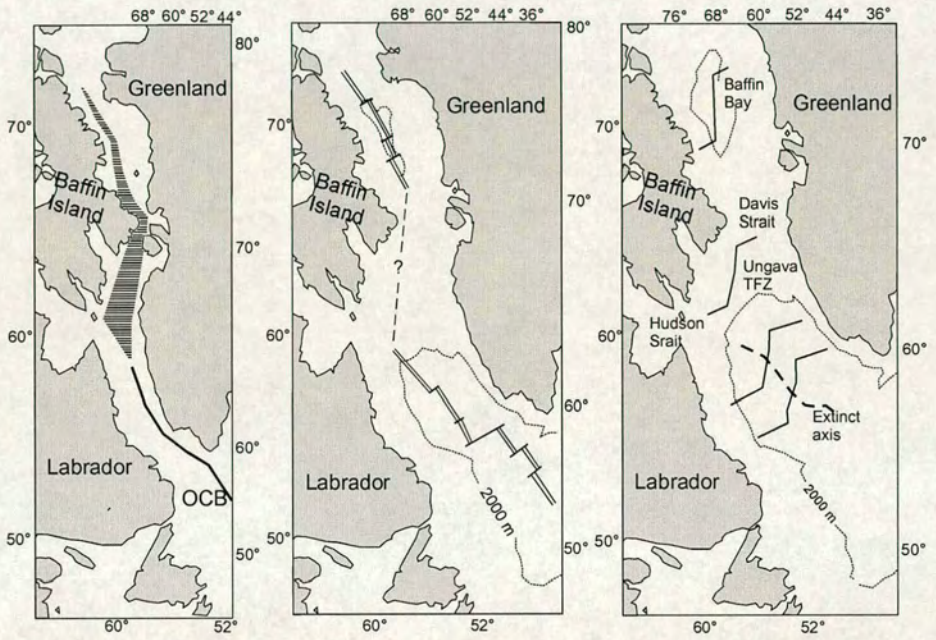

a) Closure Labrador Sea (92 Ma)

b) Chron 25 (59 Ma)

c) Present

Fig. 2.5. Evolution of the Labrador Sea according to Roest & Srivastava (1989). Three stages are shown: (a) initial opening 92 Ma; (b) Chron 25 and (c) present. The North American plate is fixed in these reconstructions.

More recently, Roest & Srivastava (1999) reviewed earlier models and provided a re-evaluation of the plate tectonics of the Labrador Sea. They came to the conclusion that faulted and thinned oceanic crust exists across the northern margins of the Labrador Sea and that very slow sea-floor spreading took place prior to Chron 31. From their interpretation of gravity, magnetic and seismic data, the width of the crust seems to be much greater on the Greenland side than on the Labrador side and they suggested that this is because a ridge had initially been present closer to Greenland. This ridge intersected with the Labrador margin and had to propagate gradually to the NW until it could spread evenly between the Greenland and Labrador plates. Roest & Srivastava (1999) also noted that the mean rate of spreading changed from 5.8 to 12 mm/year soon after Chron 30 and suggested this might have been the result of initiation of a mantle plume west of Greenland (see chapter 1).

2.1.2 Davis Strait

The Labrador Sea and Baffin Bay are separated by the Davis Strait, whose present crustal composition and complex structure are poorly understood. Chalmers (1993) and Chalmers et al. (1995a), assuming that oceanic crust developed in Baffin Bay (section 2.1.3), proposed that the areas of sea-floor spreading in Labrador Sea and Baffin Bay were connected through continental crust in the Davis Strait area. A bathymetric ridge, the Ungava transform zone (e.g. Kerr, 1967; Srivastava, 1978; Srivastava et al., 1981; Klose et al., 1982), appears to be an intra-continental complex system of strike-slip faults, on to which the relative motion of Greenland and Canada in the Labrador Sea to Baffin Bay were transferred (Chalmers, 1993; Chalmers et al., 1995a). In contrast, Roest & Srivastava (1989) thought that an oceanic ridge axis existed in the Davis Strait, even if it is difficult to reconstruct its geometry (Fig. 2.5). According to them, the complex structure of the Ungava fault system in Davis Strait was caused both by the change of the spreading direction from E-NE to N-NW after Chron 25 and through compression,

which existed in Davis Strait and Baffin Bay during the last stages of spreading. More recently, Geoffrey et al. (2001) suggested that Davis Strait was never a large transform fault as suggested by Srivastava et al. (1982), but rather a simple N10°- trending bend of the Labrador Sea- Baffin Bay opening axis, which could have been accommodated by several small transform faults.

Other important features (see Fig. 2.4 for location) in Davis Strait are the Gjoa Rise (Tucholke & Frey, 1985), the Hecla Rise (Tucholke & Frey, 1985) and the Davis Strait High (Srivastava et al., 1982), all of which were also the subject of controversy. The Gjoa Rise was interpreted by Tucholke & Frey (1985) as the result of off-axis volcanism, while Chalmers et al. (1995a) and Chalmers & Laursen (1995) thought it was a volcanic continental margin. The Hecla Rise was initially thought to be an oceanic rise (Tucholke & Frey, 1985), but was more recently interpreted as an area of shallow continental basement (Chalmers et al., 1993; Chalmers & Laursen, 1995). The Davis Strait High (Srivastava et al., 1982) either contains both oceanic and continental crust (e.g. Srivastava et al., 1982) or is composed of continental crust with volcanism occurring in an entirely intra-cratonic setting (Chalmers & Laursen, 1995). The Davis Strait High may have formed a land bridge between the Labrador Sea and Baffin Bay during the Tertiary, and therefore may have played a major role in determining the pattern of oceanic circulation at that time (Rolle, 1985).

A major aspect of the geology of the Davis Strait is the voluminous basaltic lavas that occur onshore north of Cape Dyer on the eastern coast of Baffin Island (Clarke & Upton, 1971) and in the Disko-Svartenhuk area of West Greenland (Clarke & Pedersen, 1976) (see also section 2.2). The volcanism took place mainly in the early Tertiary. The basalts that outcrop northward of Cape Dyer on Baffin Island have a potassium-argon age of 58 ±2 Ma (Clarke & Upton, 1971) and are normally magnetized (Deutsch et al., 1971). According to Pedersen et al. (2002), they are most likely time-equivalent to the Anaanaa Member of the Vaigat Formation in West Greenland (section 2.2.1 and Fig. 2.3) and

erupted during Chron 27n (61.3 - 60.9 Ma, J.Riisager et al., 1999). At the same time as the volcanism in West Greenland, a range of marine, limnic and fluviatile clastic sediments were deposited. Biostratigraphic dinoflagellate dating of these sediments suggested that eruption of the onshore West Greenland volcanics took place between Chrons 27r and 25n (Piasecki et al., 1992). $^{40}Ar/^{39}Ar$ dating by Storey et al. (1998) of the Vaigat and Maligât Formations of the Greenland volcanic province (section 2.2) has shown that the main volcanism lasted around 1 million years (60.4 ±0.5 to 59.4 ±0.5). As already suggested by Srivastava (1978), these volcanic rocks are thought to have formed contemporaneously with the early stages of sea-floor spreading in Baffin Bay. According to P.Riisager & Abrahamsen (1999) and J. Riisager et al. (1999), the lowermost lavas of the Vaigat Formation are normally magnetized and erupted during Chron 27n (60.9-61.3 Ma; Cande & Kent, 1995) a duration of less than 0.35 M.y., while the upper part of the Vaigat Formation and all of the Maligât Formation lavas belong to the long reversely magnetized interval of Chron 26r (57.0-60.9 Ma; Cande & Kent, 1995). Pedersen et al. (2002) estimated, for the volcanism within the Nuussuaq Basin during the C27n-C26r transition, that the magma production rate was a minimum of ~0.042 $km^3\ a^{-1}$. They concluded that the Vaigat Formation volcanism occurred during periods of high eruption rates over short periods, separated by low activity periods or even inactivity, over a combined time span in excess of 70 ka.

2.1.3 Baffin Bay

While it seems to be generally accepted that oceanic crust with magnetic stripes and transform faults does exist in the Labrador Sea, definitive evidence for the presence of oceanic crust in Baffin Bay is lacking. The aeromagnetic anomalies in the deeper basins of Baffin Bay are weak and to date neither linear sea-floor spreading anomalies in the basins nor the location of the extinct spreading ridge have been clearly identified, although their presence is extremely likely (e.g. Geoffrey et al., 1998). An

approximately north-south feature that extends from 71° N, 64° W to 73° N, 65° W (Rice & Shade, 1982) coincides with a relative negative gravity anomaly (Jackson et al., 1979). McWhae (1981) and Rice & Shade (1982) suggested that this feature represents an extinct spreading centre. However, because this feature runs roughly parallel to the Hudson transform fracture zone and other transform faults in the Labrador Sea in the south, more recent publications (Whittaker et al., 1997; Geoffrey et al., 2001) interpreted this feature as a transform fault, as earlier proposed by Jackson et al. (1979) and favoured by Roest & Srivastava (1989). A relative negative gravity anomaly trending WNW from 73° N, 66° W to 74° N, 75° W, the direction of which is roughly parallel to the extinct northern Labrador Sea, may mark the position of an extinct spreading centre in Baffin Bay (Whittaker et al., 1997). This axis seems to join N-S trending Baffin Bay transform faults in the north and south (Geoffrey et al., 2001). The similarity between the magnetic anomalies in Baffin Bay and central Labrador Sea, the identical approximately N-S trending transform faults in Baffin Bay and the northern Labrador Sea, and the identification of an extinct rift axis immediately north of Davis Strait in Baffin Bay led Geoffrey et al. (2001) to suggest that Baffin Bay acted as the northern termination of the northward-propagating Labrador Sea oceanic rift system.

If the above interpretations are correct, then sea-floor spreading was oblique (Srivastava et al., 1987) and this could explain the lack of distinct sea-floor spreading magnetic anomalies (Roots & Srivastava, 1989) in Baffin Bay. If spreading took place in Baffin Bay, it started either during Chron 31 (Roest & Srivastava, 1989; Jackson et al., 1992), or later, during the second phase (Chron 24) of spreading in the Labrador Sea (McWhae, 1981; Whittaker et al., 1997).

The area in northern Baffin Bay (Fig. 2.1) between the Canadian Arctic Islands and northern Greenland has also been subject of considerable controvery and the arguments centre on whether or not movements took place between Ellesmere Island and northern Greenland in Nares Strait (e.g. Dawes & Kerr, 1982; Frisch & Dawes, 1994; Jackson et

al., 1992; Jackson & Marillier, 1994). Reid & Jackson (1997) developed a plate tectonic model for Baffin Bay, based on the Roest & Srivastava (1989) model and observations of Jackson et al. (1992). According to this model, from anomaly 31 to 25 (65 to 57 Ma, using the time scale of Harland et al., 1990) the North American plate moved apart in northern Baffin Bay. From anomaly 25 to anomaly 24 (57-54 Ma) strike-slip was the dominant motion followed by compressional phases between anomalies 24 and 13 (54-24 Ma). The result of this work and associated studies showed that north of 76° N, the crust is continental but thins markedly in the central part between Devon and Ellesmere Islands and Greenland. Reid & Jackson (1997) concluded that rifting took place in the northern Baffin Bay, at least initially, with little or no melt production. The plate reconstruction model of Roest & Srivastava (1989) demands large-scale strike-slip displacement between Canada and Greenland along Nares Strait. However, if the movements between Greenland and North America did not start in the late Cretaceous (Chron 33) but during the Tertiary (Chron 27) (for discussion on this issue see section 2.1.1), the need for large strike-slip movements along Nares Strait would be reduced (Chalmers, 1991; Frisch & Dawes, 1994). Jackson & Marillier (1994) asked in a discussion paper how to resolve the 'Nares Strait problem'. Geophysical data from the seas surrounding Greenland and geological data from Baffin Island, West to South Greenland and Labrador imply movement along Nares Strait, whereas geological information from Ellesmere Island, Northwest Greenland and the western part of North Greenland do not indicate motion.

The interpretations above all imply an oceanic origin for Baffin Bay, while in contrast, Kerr (1967) and Grant (1975, 1980, 1982) favour the interpretation that Baffin Bay is underlain by foundered or attenuated continental crust in which Tertiary basaltic rocks intruded. According to this hypothesis, Baffin Bay is not oceanic in origin, but rather resulted from vertical movements.

2.2 Previous work

2.2.1 West Greenland

The Tertiary volcanic province of West Greenland covers an area of at least 55,000 km^2 on land and the adjoining continental shelf, and it is geographically divisible into four main areas, namely Svartenhuk Halvø, Ubekendt Ejland, Nûgssuaq, and Disko (Clarke & Pedersen, 1976) (Fig. 2.6). The volcanic stratigraphy of West Greenland (Fig. 2.7) has been classified mainly using lithostratigraphic rather than geochemical criteria. Three lithostratigraphic units are defined, from oldest to youngest, Vaigat, Maligât and Hareøen Formations (Hald & Pedersen, 1975). The volcanism of the Vaigat Formation occurred in three main episodes which, from lowest to highest, are the Anaanaa, Naujánguit and Ordlingassoq Members. Each episode started with olivine-rich magmas and ended with more evolved, often contaminated magmas (e.g. L.M.Larsen & Pedersen, 2000). The Anaanaa Member consists of the oldest known Tertiary volcanic rocks in West Greenland (picrites, olivine-rich basalts, feldspar-phyric basalts and siliceous contaminated basalts) and is known only from a limited area in western Nuussuaq (Pedersen et al., 1996). The Naujánguit Member (Pedersen, 1985a) consists predominantly of picritic lavas and hyaloclastites with horizons of contaminated basalts (Asûk Member and Kûgánguaq Member). Uppermost part of the Naujánguit Member represents the eruption of olivine-poor tholeiitic basalts of the Qordlortorssuaq Member in a waning stage of volcanic activity (Pedersen, 1985b). The youngest, Ordlingassoq Member of the Vaigat Formation consists of picrites with three horizons of contaminated lavas, including the alkaline rocks of the Manîtdlat Member (Pedersen, 1985b). While in the Vaigat Formation picritic lavas, hyaloclastites and a small number of basalt horizons are present, the overlying Maligât Formation consists of feldspar-phyric tholeiitic basalts (Hald & Pedersen, 1975). The youngest, Hareøen Formation, is separated from the Maligât Formation by shales and coal seams and is mainly dominated by transitional olivine-phyric basalts (Hald & Pedersen, 1975).

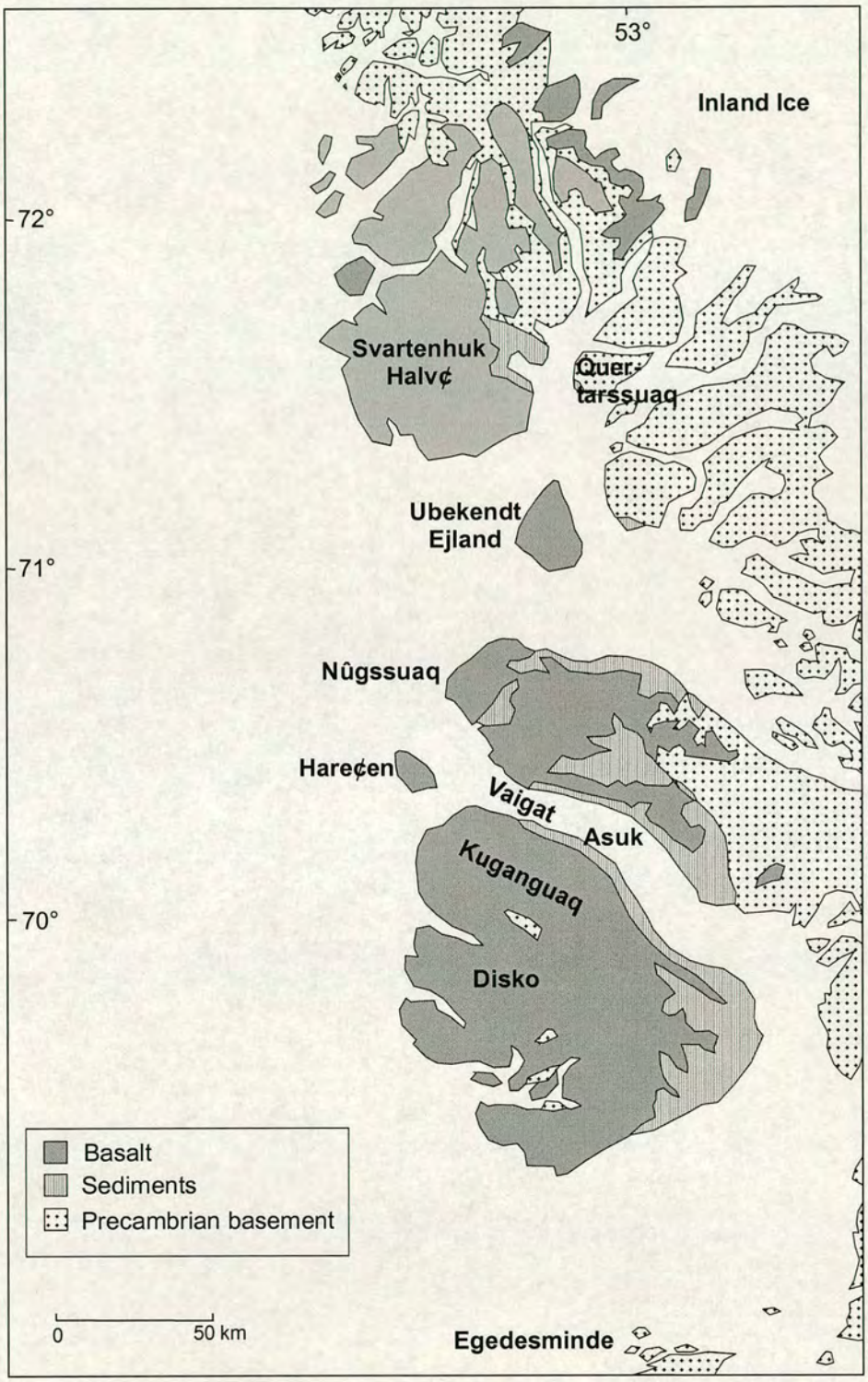

Fig. 2.6. Simplified geological map of the West Greenland Igneous Province (after Clarke & Pedersen, 1976).

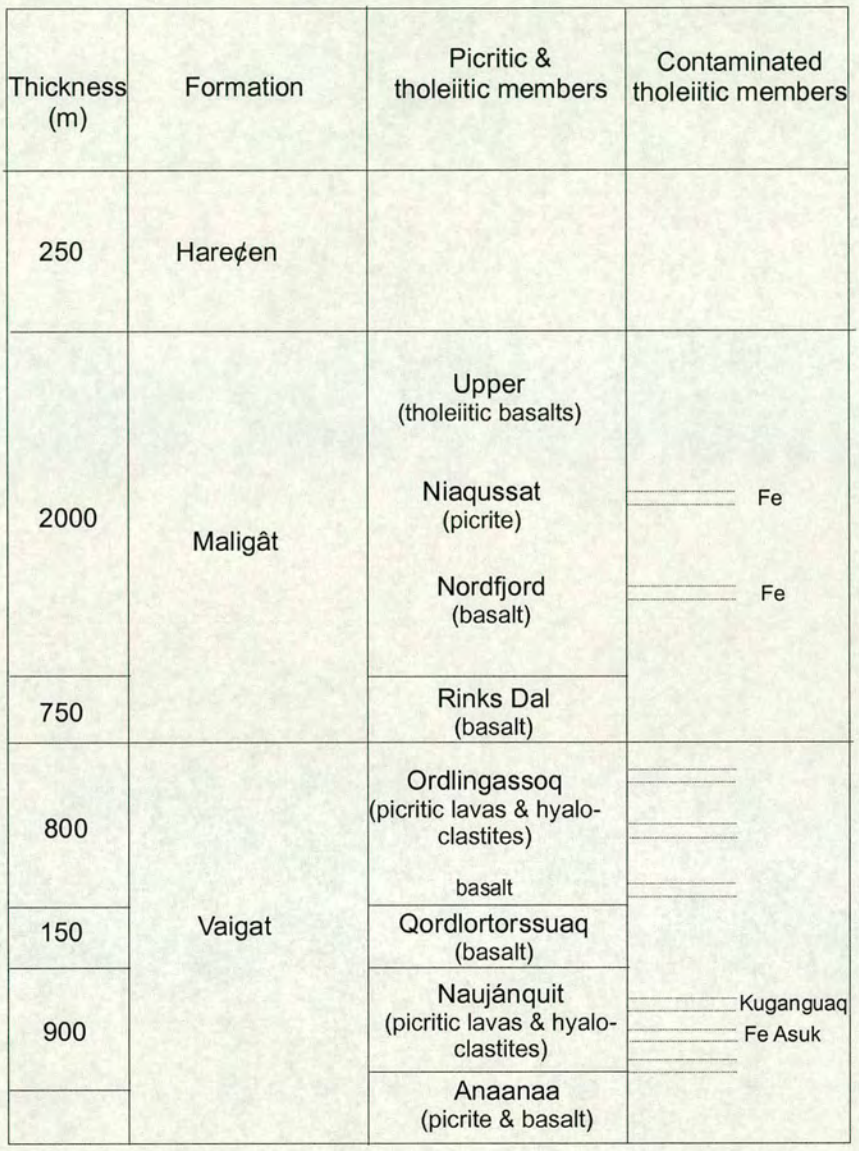

Fig. 2.7. Simplified volcanic stratigraphy of the West Greenland Tertiary Volcanic Province (based on Pedersen (1985a,b) and Lightfoot et al. (1997).

The West Greenland flood basalts show a wide range of trace element ratios and isotopic compositions (e.g. Pedersen & Pedersen, 1987; Goodrich & Patchett, 1991; Holm et al., 1993; Lightfoot et al., 1997; Lightfoot & Hawkesworth, 1997; Graham et al., 1998; Schäfer et al., 2000; L.M. Larsen et al., 2003). Detailed chemical information on the earliest Tertiary rocks on Nussuaq (Anaanaa Member) are not yet available (Graham et al., 1998), but picrites from the lowest member of the Vaigat Formation on Disko have the most depleted compositions (εNd: +8 to +10; εSr: -22 to –15) of the entire volcanic province and overlap with present-day North Atlantic MORB (e.g. Holm et al., 1993). Most other picrites from Ubekendt Ejland and Svartenhuk Halvø are more enriched (εNd > 6; εSr < -10) and overlap both with MORB and with Icelandic basalts (e.g. Holm et al., 1993). Graham et al. (1998) found $^{3}He/^{4}He$ ratios up to $31R_a$ (where R_a is the atmospheric ratio of 1.39×10^{-6}) in picrites from the Vaigat Formation on Nussuaq. They interpreted the isotope variations of He, Pb, Nd and Sr as a result of the interaction between the early Iceland mantle plume and the upper mantle during ascent and dispersion beneath the continental lithosphere. Calculations following McKenzie & Bickle (1988) point to high degrees of melting (24-30 %) for the West Greenland lavas at depths of 60-90 km in the underlying mantle, requiring potential temperatures of 1540-1600°C (Gill et al., 1992). For primary magmas from West Greenland and Baffin Island, Herzberg & O'Hara (1998, 2002) calculated eruption temperatures of 1400-1440°C and pressures of initial melting on the anhydrous solidus of 3.8-4.7 GPa.

The effects of crustal contamination on the tholeiitic rocks on Disko and Nussuaq are well described (Pedersen, 1985b; Pedersen & Pedersen, 1987; Goodrich & Patchett, 1991; Pedersen et al., 1996; Lightfoot et al., 1997). Contamination of picritic and basaltic magma could have occurred by (1) assimilation-fractionational-crystallisation (AFC)-processes involving shale and sandstone (Pedersen & Pedersen, 1997) or (2) by simply mixing with Cretaceous to early Tertiary sediments (Goodrich & Patchett, 1991). Lightfoot et al. (1997) identified contamination of the Vaigat Formation with material

from two distinct crustal sources (sediment and a granodioritic end-member). Their sample collection was further analysed by Schäfer et al. (2000) for osmium isotope ratios and the results are consistent with the conclusions of Lightfoot et al. (1997). The picrites show little evidence for crustal contamination and their compositional variation might reflect source heterogeneity of the mantle plume. By contrast, the basalts of the Vaigat Formation do indicate evidence for crustal contamination processes (Lightfoot et al., 1997; Schäfer et al., 2000). The Os-isotope analyses of Schäfer et al. (2000) agree with the work of Lightfoot et al. (1997), suggesting that both sedimentary and felsic continental crust components produced the observed isotopic ratios. Schäfer et al. (2000) postulated that portions of the West Greenland continental flood basalt province might represent the first direct sampling of unmodified plume head material derived either from the lower mantle or from lower portions of the upper mantle. Recently, L.M. Larsen et al. (2003) studied alkaline rocks of the Manîtdlat Member of the Vaigat Formation, which show very unusual geochemical signatures (enriched in incompatible elements, negative εNd and mostly negative εSr). They suggested that the alkaline magmas erupted within a regional zone of eruption centres that mainly produced tholeiitic magmas, and that mixing between alkaline and tholeiitic magmas and their phenocrysts took place in the conduit system. In order to produce the various magma types of the Manîtdlat Member, a number of enriched source areas with different mineralogies may have been present in the lithospheric mantle (L.M. Larsen et al., 2003).

2.2.2 Study area

The first geological publications on Baffin Island were mainly restricted to descriptions of the coastal rocks (Sutherland, 1853; McMillan, 1910). In 1964, detailed mapping and sampling of the Baffin Bay Igneous Province began, in order to examine possible

correlations between the igneous rocks of Baffin Island (Wilson & Clarke, 1965; Clarke, 1967) and West Greenland (Pulvertaft & Clarke, 1966; Clarke, 1968b). Clarke and co-workers published the first geochemical results on lava flows from Baffin Island (Clarke, 1968a, 1970, 1975; Clarke & Upton, 1971; O'Nions & Clarke, 1972; Keen & Clarke, 1974; Clarke & O'Hara, 1979; Clarke et al., 1988). The Baffin Island lavas are olivine-rich, with MgO contents >8 wt. %, and show the following phase assemblages: (1) olivine and glass, (2) olivine, plagioclase and glass and (3) olivine, plagioclase, microlites (cpx?) and glass (Clarke, 1970). Chrome spinel is always present as an early phenocryst in all phase assemblages. Clarke (1970) divided the lava flows of West Greenland and Baffin Island into three groups: (1) olivine-enriched bases of thick flows (mainly on Baffin Island) or cumulitic flows (mainly on West Greenland), characterised by large olivine phenocrysts, (2) flows with olivine-microphenocrysts (or skeletal olivine) at the base of the volcanic pile (first eruptions) and (3) leucocratic segration veins in thick flows (mainly on Baffin Island), olivine-poor basalts in both locations and feldspar-phyric basalts (in West Greenland only). By comparing the bulk-chemical compositions of the basalts with phase relations, Clarke (1970) suggested that, at a pressure of 30 kbar, the second group was parental and possibly primary with 19-20 wt. % MgO. The first group is of accumulative origin with MgO >21 wt. %, while the third group has undergone fractional crystallisation (MgO <16 wt. %). The lava flows have low concentrations of incompatible elements and an average $^{87}Sr/^{86}Sr$ ratio of 0.7030 (Clarke, 1968a, 1970; O'Nions & Clarke, 1972). Stratigraphic and chemical relations between the Baffin Island and West Greenland suites showed that they belonged to the same era of volcanic activity, related to the continental break-up of the Labrador Sea - Baffin Bay area (Clarke 1970; Clarke & Upton, 1971). The Baffin Island basalts are generally more depleted in light rare earth elements (LREE) and incompatible trace elements than are the lavas of West Greenland (O'Nions & Clarke, 1972). The first eruptions on Baffin Island were generated from a depleted mantle source, while the later lavas from Baffin Island and all lavas from West Greenland were derived from relatively more enriched mantle (Clarke et al., 1989). While Clarke (1970), Clarke & O'Hara

(1979) and Elthon & Ridley (1979) all argued for the existence of liquids with 19-20 wt. % MgO on Baffin Island, Hart & Davies (1978, 1979) claimed, on the basis of Ni-partitioning between olivine and liquid, that rocks with more than 11-13 wt. % MgO contain accumulated olivine (see chapter 4). Francis (1985, 1986) analysed lavas from Padloping Island and demonstrated that, although the chilled margins of picritic lavas are crystal-liquid mixtures, their composition can be used to provide analogues of primary liquids. He concluded that the olivine phenocryst compositions (Fo_{86-89}) require liquids with 10-13.5 wt. % MgO, but the olivine xenocrysts (up to Fo_{93}) suggest that primary liquids for the Padloping Island magmas contained at least 18 wt. % MgO. The same suite on Padloping Island was analysed by Robillard et al. (1992), who identified two compositional types: (1) a light-REE depleted suite (N-MORB), with $(La/Sm)_n \sim$ 0.6-0.7 and $^{87}Sr/^{86}Sr_{\text{present day (pd) (unleached)}} = 0.7031$- 0.7032 and (2) a suite (E-MORB) that shows slight REE enrichment $(La/Sm)_n \sim$ 1-1.2 and $^{87}Sr/^{86}Sr_{(pd)}$ (0.7032-0.7039). Because the N- and E-type samples are intermixed throughout the volcanic succession, Robillard et al. (1992) suggested that both types of magma erupted contemporaneously, originating from two distinct mantle sources on the periphery of the ancestral Iceland plume. More recently, Kent et al. (1998) studied glass inclusions from the same samples reported by Robillard et al. (1992). With their new isotope data for the depleted ($^{143}Nd/^{144}Nd >0.51300$) and enriched ($^{143}Nd/^{144}Nd <0.51300$) lava flows, their results are consistent with the suggestions of Robillard et al. (1992). The depleted samples are similar to other depleted North Atlantic MORB, while the enriched samples are more extreme than plume-related samples from the North Atlantic (Kent et al., 1998). Because the glass inclusions of the E-MORB-like samples are more varied in their degree of incompatible enrichment, Kent et al. (1998) suggested that they represent mixtures of melts from both depleted and enriched sources.

2.3 Geology of the Study Area

The eastern coast of Baffin Island consists of Precambrian basement, early Tertiary continental sediments and Tertiary volcanic breccias and basaltic lava flows (e.g. Clarke & Upton, 1971).

2.3.1 Precambrian basement

The Precambrian basement (Fig. 2.8) of the study area belongs to the Churchill Structural Province (Taylor, 1971). In more detail, the Precambrian rocks of the study area are part of the Hoare Bay Group (Jackson et al., 1990) and are equivalent to the Proterozoic Nagssugtoquidian mobile belt in West Greenland (Jackson et al., 1990; Peterson et al., 2002). The alignment of the Precambrian Provinces on both sides of Baffin Bay supports the theory of sea-floor spreading processes in this area (Jackson et al., 1992).

The Hoare Bay Group in general consists of mica-hornblende-feldspar-quartz-gneiss and schist, amphibolite and biotite-hornblende- gneiss and schist, and minor ultrabasic rocks (Taylor, 1981), while the the Precambrian rocks of the study area consist of gneisses and migmatites, with a common mineral assemblage of quartz, two feldspars, biotite, often garnet and/or muscovite and accessories, including apatite, zircon and magnetite (Clarke & Upton, 1971). The metamorphic grade is generally amphibolite facies but locally reaches granulite facies (Clarke & Upton, 1971). On Durban Island a non-foliated muscovite-tourmaline granite occurs, which might have been the source of the pre-volcanic, tourmaline-bearing sediments on that island (Clarke, 1968a; Clarke & Upton, 1971). North and northwest of the sample locations, a major fault separates the Nagssugtoqidian mobile belt from the Cumberland Batholith, at ~66° N 60° W (Fig. 2.8).

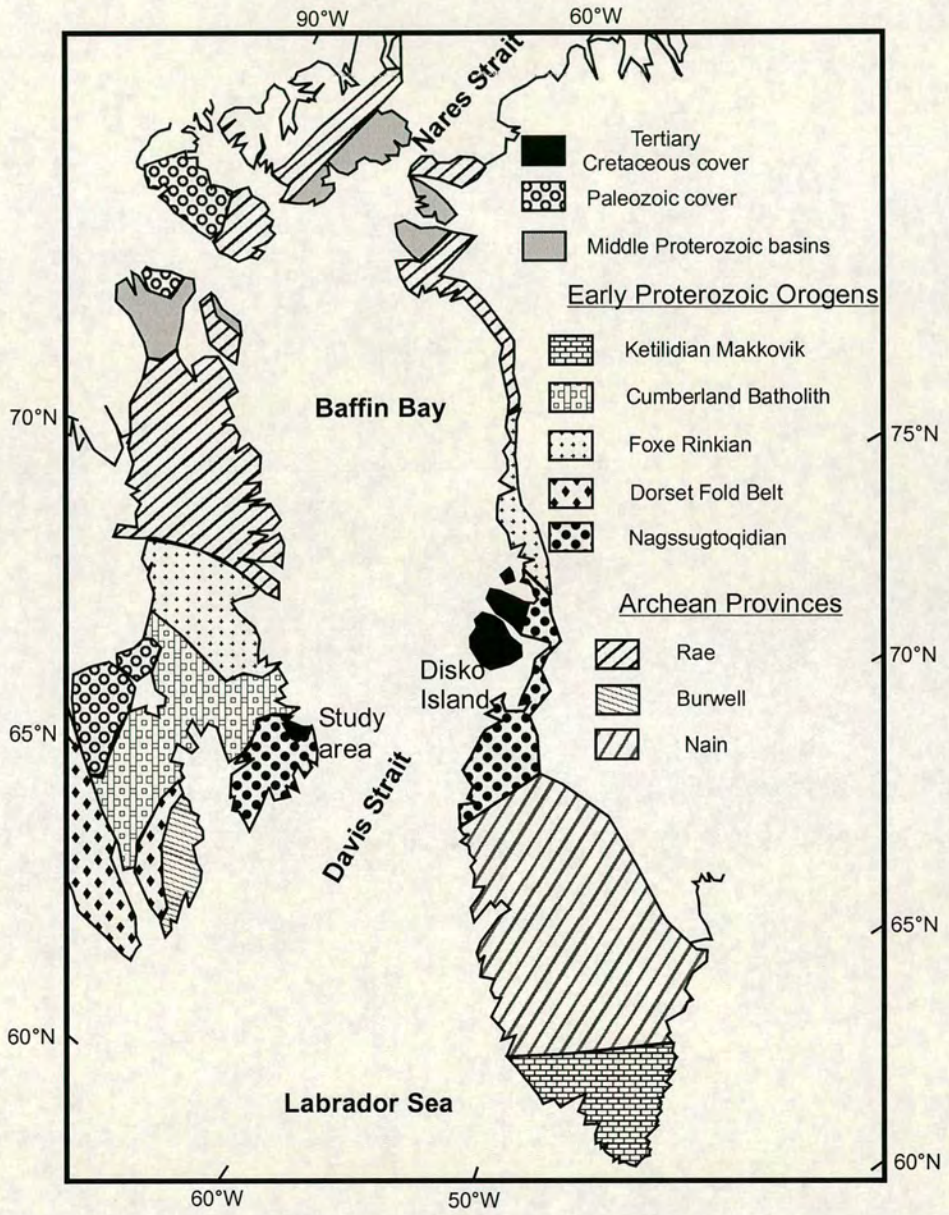

Fig. 2.8. Geological map of Baffin Island and the West Greenland coast (after Jackson et al., 1992).

2.3.2 Cretaceous and Tertiary sediments

Cretaceous and Tertiary sediments overlie the Precambrian rocks in many locations, and their thickness and frequency increases from Cape Dyer northwestward to Cape Searle (Carke, 1968a; Clarke & Upton, 1971). They were briefly described by Clarke & Upton (1971) as having a continental origin, containing unconsolidated white quartz sands, impure sandstones, shales, minor coal and conglomerate layers. At Cape Searle, sands show cross-bedding, pointing generally to a southwesterly source area for this formation. The sediments at Cape Searle and elsewhere form shallow basins and were probably faulted at an unknown time (Clarke & Upton, 1971). Burden & Langille (1990) described the stratigraphy in more detail as well as the sedimentology of Cretaceous and Tertiary outliers, which occur in half-grabens along the coast of Baffin Island (Fig. 2.9). They also related their observations to the tectonic history of this area. These sediments and the location of the half-grabens are of particular interest, because they occur directly next to and beneath the studied volcanic rocks on Padloping Island and Durban Island and therefore give more information about the tectonic history of this area. Because the first sedimentary strata were deposited on deeply weathered Precambrian basement in the lower Cretaceous, Burden & Langille (1990) support the hypothesis of Pierce (1982) for even earlier rifting (middle Cretaceous) than proposed by e.g. Srivastava & Roest (1989) (see section 2.1.1). The non-marine sediments show a long history of rifting, starting with locally derived sheet deposits (lower Quqaluit Fm) of northward extending, high energy, meandering rivers partly controlled by episodes of subsidence. They were followed by vertical, narrower meander belts (Upper Quqaluit Fm). In the Tertiary, extensional tectonism and crustal subsidence is characterised by rapid aggradation of gravel-bedload stream deposits and volcanic ash layers (Cape Searle Fm), followed immediately by large outpourings of basalt breccia and lava into the rapidly subsiding half-grabens (Burden & Langille, 1990).

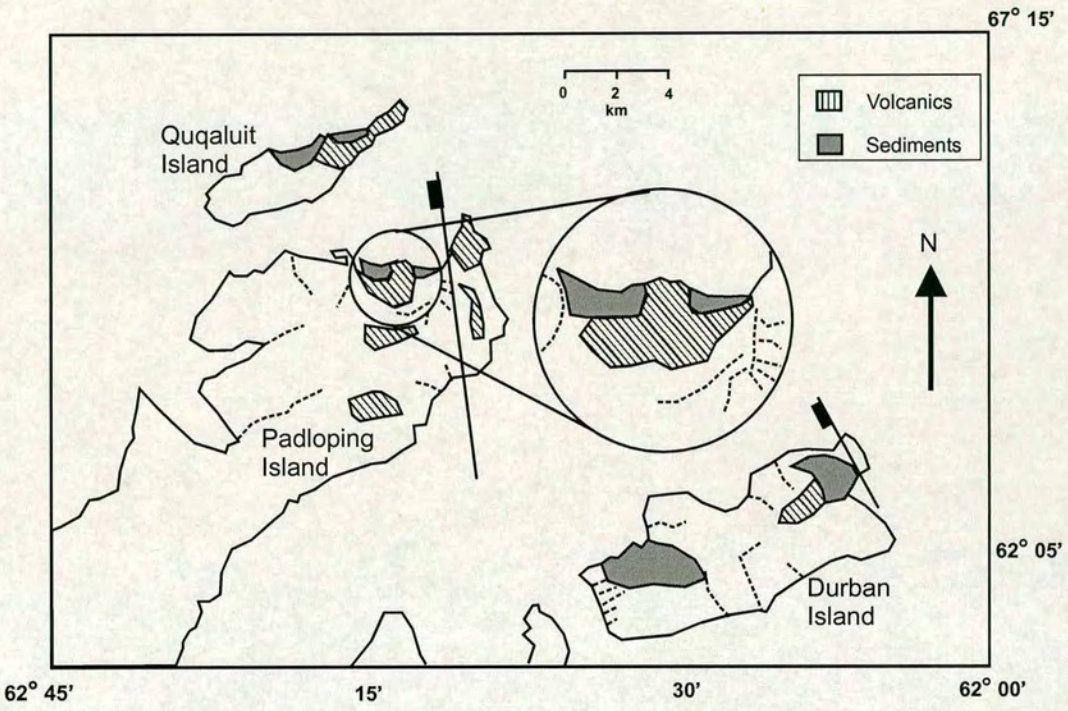

Fig. 2.9. Generalised geology of half-grabens (hatchure on down-thrown block) on Padloping Island and Durban Island (after Burden & Langille, 1990).

2.3.3 Tertiary volcanic rocks

Small patches of Tertiary volcanic rocks occur along the Baffin Island coast 90 km northwest of Cape Dyer (Fig. 2.10). In 1996, an Edinburgh University expedition to Baffin Island collected 75 samples at three sites along this coast. The collection consists of picritic and basaltic lava flows and dykes. Stratigraphic profiles of the three sample locations (Cape Searle, Padloping Island and Durban Island) are shown in Fig. 2.11.

The lavas overlie the Precambrian basement either directly or, at some locations, with a thin sequence of continental sediments intervening between the basement and the volcanic rocks (Clarke & Upton, 1971). Where sediments occur, the overlying volcanic rocks tend to be divisible into a lower subaqueous volcanic breccia and an upper sequence of subaerial flows (Clarke & Upton, 1971).

Two types of different coloured (orange and black), but mineralogically identical, breccias have been identified: their difference in colour is explicable by greater hydration of the glass (palagonitization) and oxidation of the iron in the orange material (Clarke & Upton, 1971). Both breccias contain hyaloclastite, basaltic fragments and massive basaltic blocks. Giant cross-bedding is present and its attitude in both breccias indicates a northeastward source area of the volcanics (Clarke & Upton, 1971). Clarke (1968a) and Clarke & Upton (1971) noted that, if the tops of the breccia units erupted contemporaneously and close to the Tertiary sea-level, a slight differential movement of the main outcrops during a post-volcanic uplift must have taken place. The extent of uplift was up to 400-500 m, except on Cape Searle, where the top of the breccia is only about 150 m above sea-level.

Following the field descriptions of Clarke (1968a) and Clarke & Upton (1971), the picritic and olivine-rich lava flows occupy depressions in the Precambrian basement. They are generally horizontal, but sometimes tilted as a result of slumping caused by

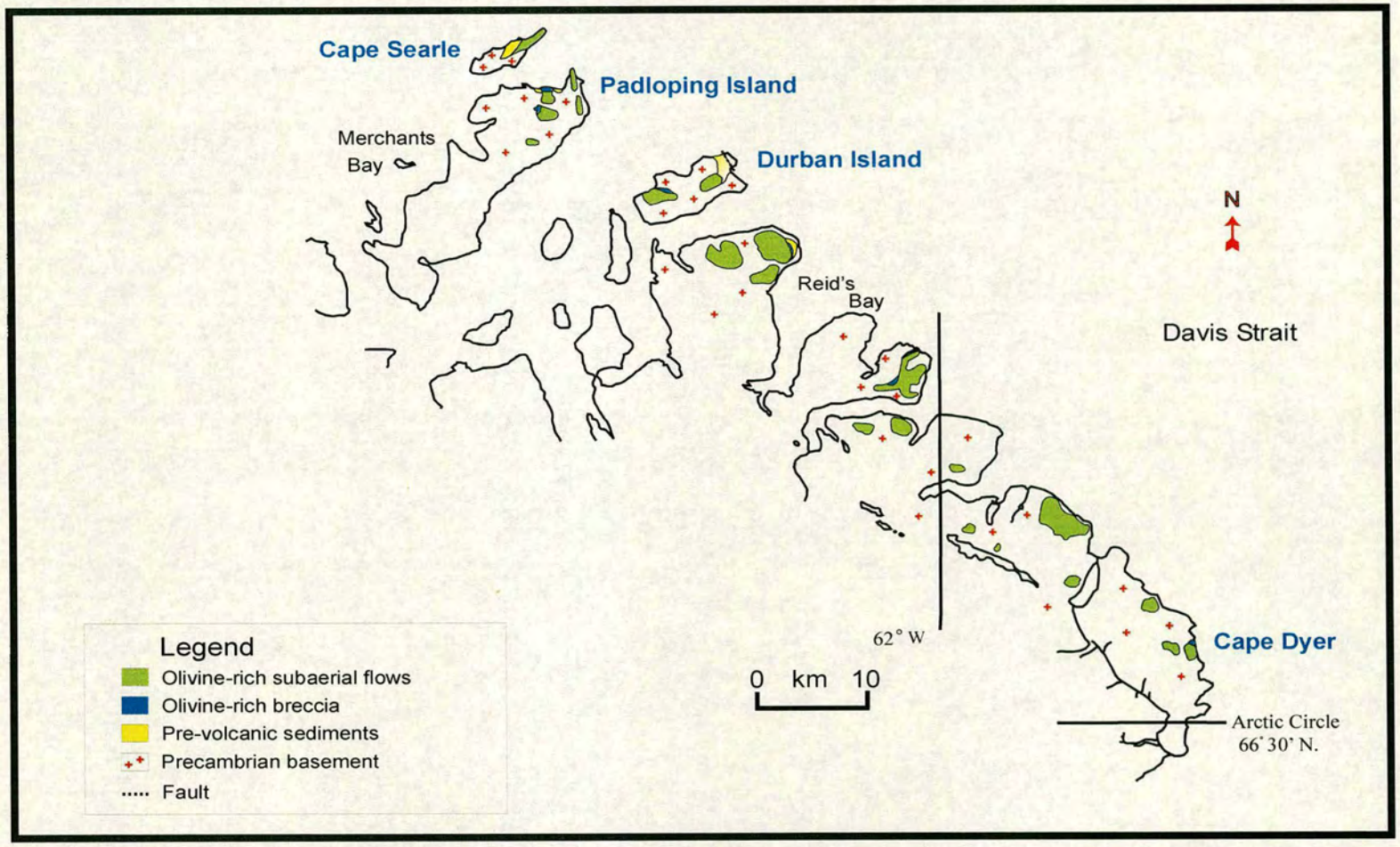

Fig. 2.10. Geological map of the eastern coast of Baffin Island (after Clarke & Upton, 1971)

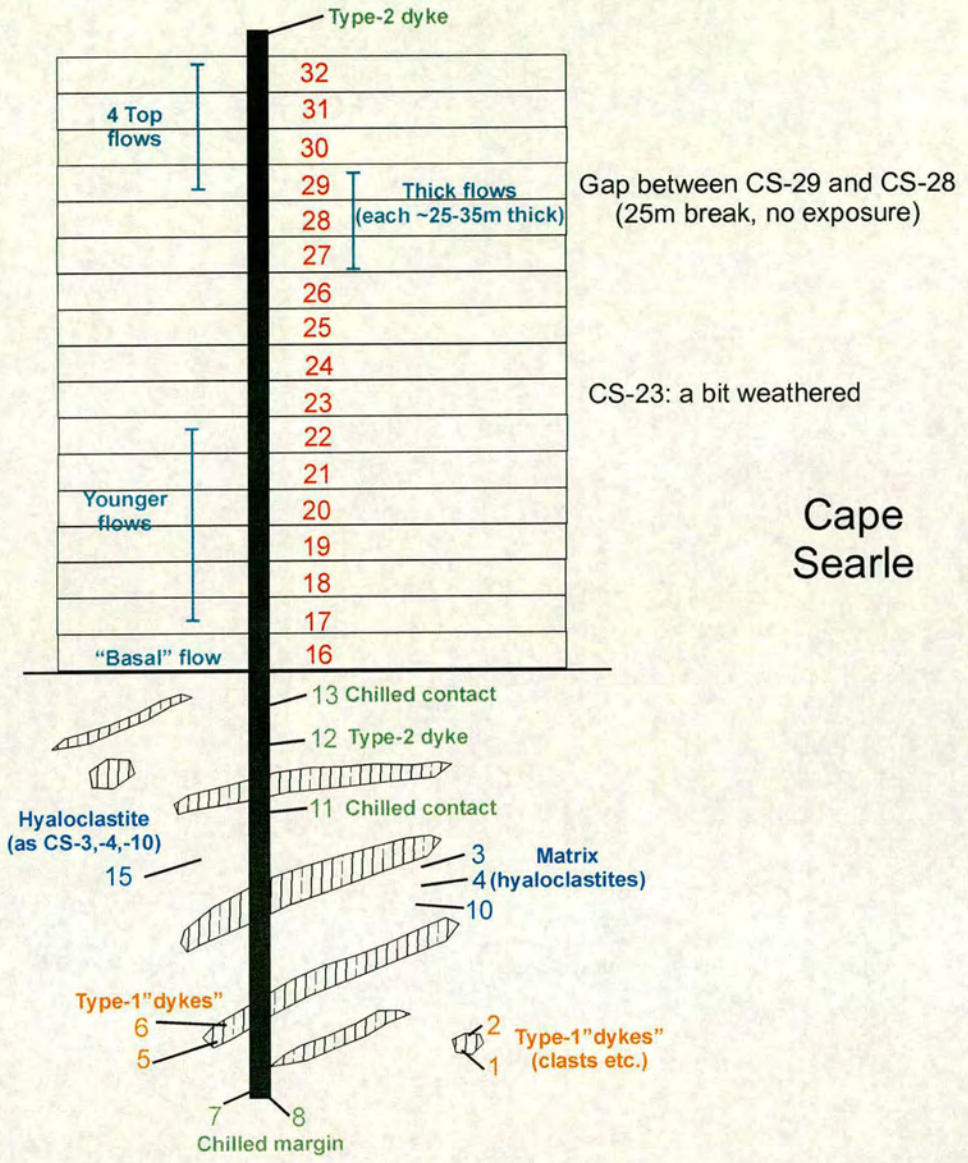

Fig. 2.11a. Stratigraphic lava sequence of the Cape Searle samples.

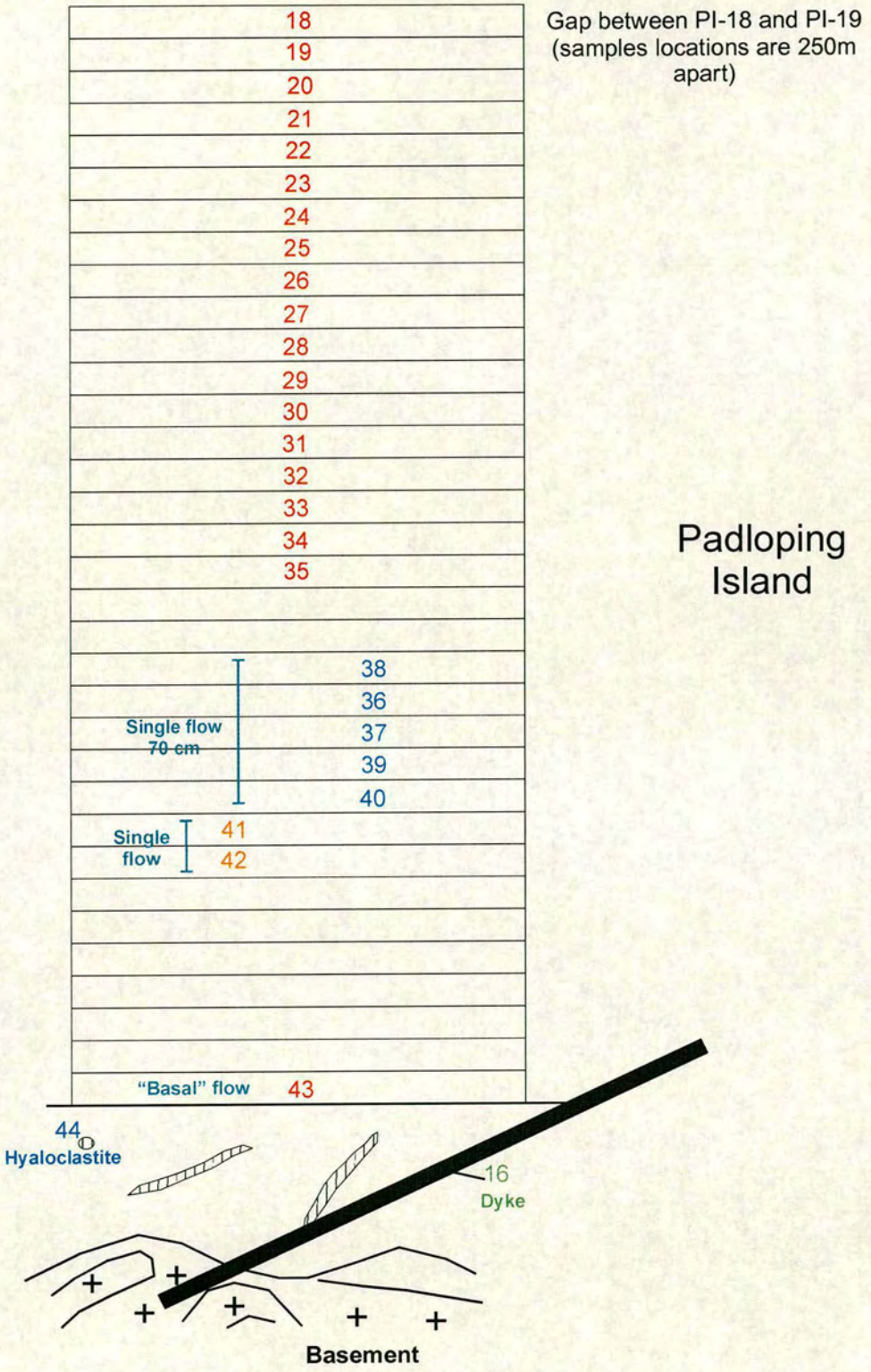

Fig. 2.11b. Stratigraphic lava sequence of the Padloping Island samples.

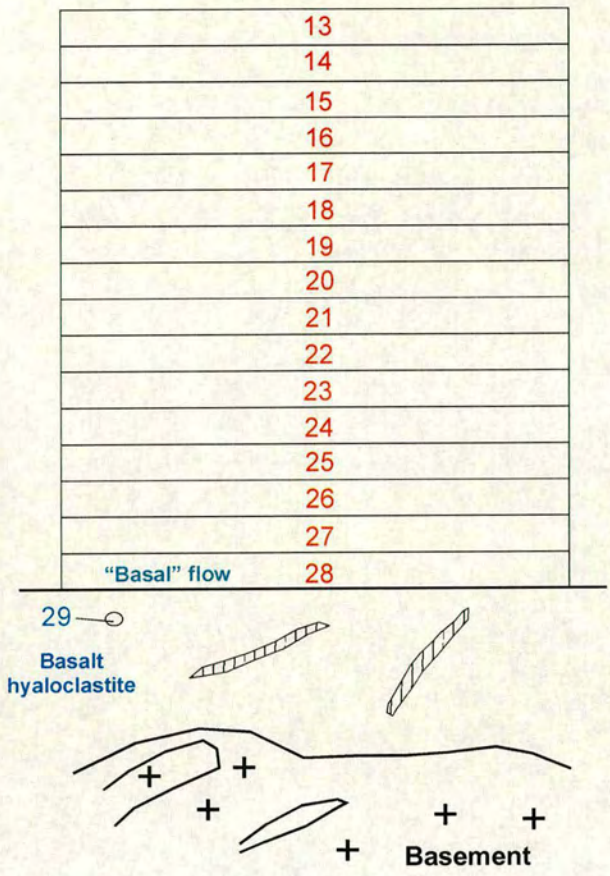

Fig. 2.11c. Stratigraphic lava sequence of the Durban Island samples.

undermining of the sediments beneath. The tops of the outcrops show no evidence of erosion during Pleistocene glaciation, suggesting that they are virtually complete. According to Clarke & Upton (1971) the most complete succession of the volcanic rocks is exposed on the cliffs of Cape Searle, with at least 150 m of breccias (their base is below sea-level) overlain by approximately 300 m of subaerial lava flows.
The lava flows thin rapidly inland from a prominent seaward-facing cliff and pinch out 10 km inland from the coastline. Although the thickness of individual flows varies between 1 and 35 m, flows thicker than 10 m are rare and the average is less than 5 m. The horizontal flows become increasingly thin and reddened toward the top of each section.

It seems to be impossible to correlate the flows from one location to another and most of the eruptions, particularly the later ones, were local phenomena (Clarke, 1968a; Clarke & Upton, 1971). The only correlatable stratigraphic feature between the outcrops is the general progression from subaqueous breccias, through thick subaerial flows, to thin flows with oxidised tops. This progression and the wedge-shaped cross-sections of the outcrops (if original features) show evidence for waning volcanism and therefore the later flows are smaller in volume and extent (Clarke & Upton, 1971).

In the north, at Padloping Island and Cape Searle, vertical basaltic dykes cut both the Tertiary volcanics and underlying sediments, but not the Precambrian rocks inland from the coastal outcrops. These dykes, roughly 20 in number, average 2 m wide (none thicker than 7 m) and strike approximately parallel to the coastline (Clarke, 1968a; Clarke & Upton, 1971).

Compared to the West Greenland volcanic province and also to the other igneous provinces in the North Atlantic, the Baffin Island sequences are relatively thin (Fig. 2.12). The feldspar-phyric basalts, which erupted in the later stage of the volcanic activity on West Greenland are absent in Baffin Island. Therefore, Clarke (1968a) and

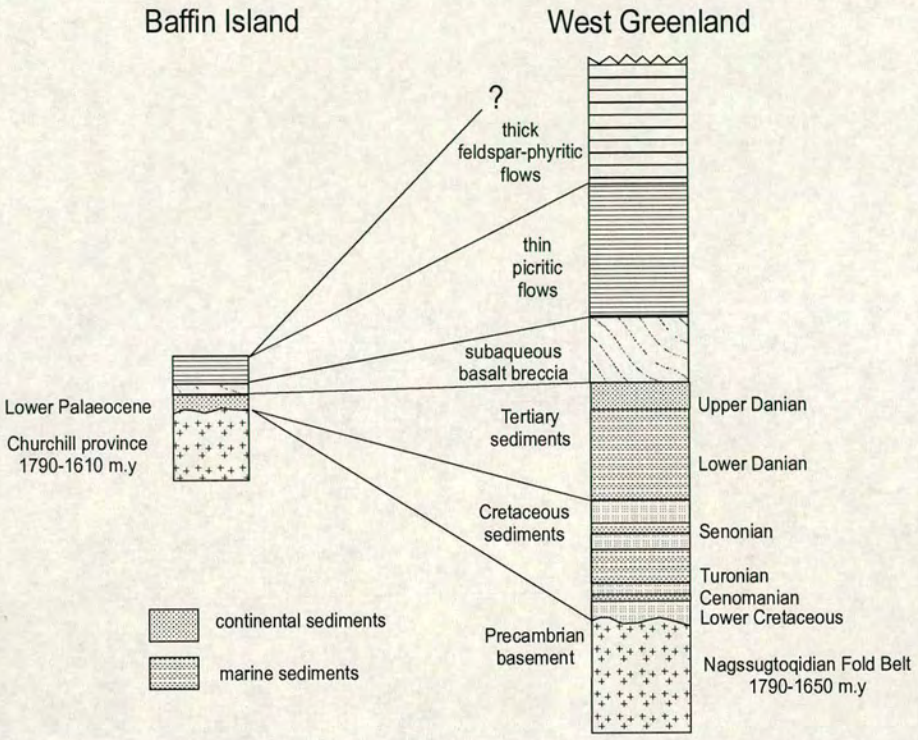

Fig. 2.12. A comparison of the stratigraphic columns in Baffin Island and West Greenland (after Clarke, 1975).

Clarke & Upton (1971) came to the conclusion in their plate tectonic model for the Labrador Sea- Baffin Bay area that, during sea-floor spreading processes, the source of the volcanics on Baffin Island was carried away on the Greenland plate. While the volcanic activity ended in Baffin Island, volcanism continued with the eruption of further picrites, basalts, and feldspar-phyric basalts in West Greenland.

II Results

3 Results

3.1 Petrography

The majority of the investigated rocks from Baffin Island contain olivine phenocrysts, ranging in abundance from 5 to 50 modal % (estimated from thin sections). The olivines show complex textures (polyhedral, skeletal and sometimes parallel-growth) and several morphology types occur within one sample. Spinifex textures have not been observed. The crystal size is generally 1-1.5 mm, but some olivines up to 3.5 mm in size are also present in the magnesian rocks. In rocks with MgO contents <15 wt. % the crystal-sizes become smaller with decreasing MgO, but rocks with MgO contents >15 wt. % show a large variety of phenocryst sizes (1-3.5 mm) (Fig. 3.1). All crystal types may contain spinel and glass-inclusions. Olivine crystals with strained kink bands occur occasionally. The olivine phenocrysts are often accompanied by an opaque phenocryst phase (chromite) up to 0.1 mm in size. Rocks with plagioclase phenocrysts are present, but rare, and no rocks with clinopyroxene phenocrysts have been found in either this or previous studies on Baffin Island (e.g. Clarke & Upton, 1971; Francis, 1985). The rocks are either porphyritic with mainly olivine phenocrysts (±chromite, ±plagioclase phenocrysts), or non-porphyritic. Most of the lavas are holocrystalline or hypocrystalline, apart from the hyaloclastites, which are holohyaline. Groundmass minerals are olivine, chromian spinel, plagioclase and clinopyroxene. The rocks often have a glomeroporphyritic texture with clusters of olivine or olivine and plagioclase crystals. Clinopyroxene (augite) appears, generally in the groundmass with a subophitic texture wholly or partly enclosing plagioclase laths, or occasionally with an ophimottled texture.

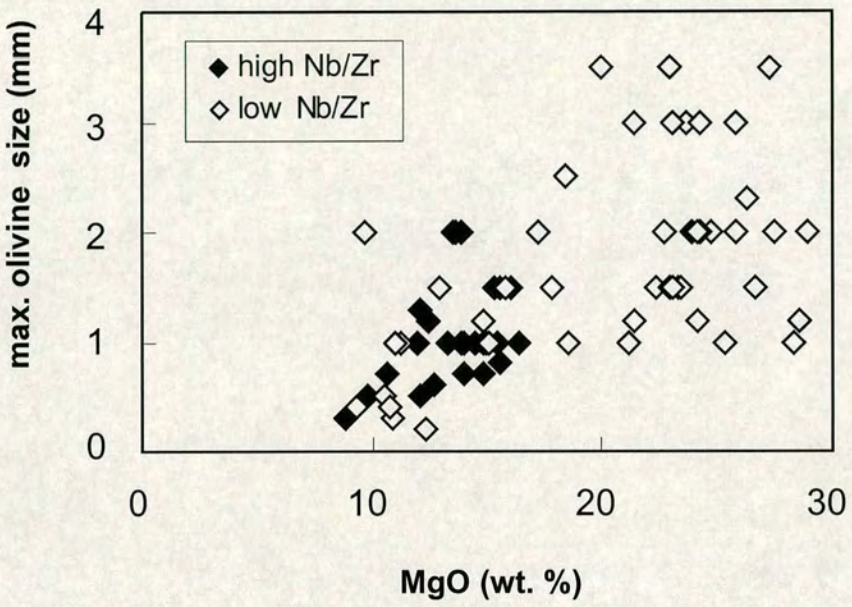

Fig. 3.1. The maximum size of olivine crystals determined (by thin section examination) in the rock versus the MgO content (calculated on a volatile-free basis) of the rock.

Two geochemical groups (see chapter 3.4) on Baffin Island may be also distinguished by their petrography (Fig. 3.2). Low-Nb/Zr lavas on both Padloping Island (lower series) and Durban Island (lower and upper series) are in general more magnesium-rich and contain large olivine crystals with several shapes (polyhedral, skeletal- and parallel-growth). On the other hand, high-Nb/Zr lava flows on Padloping Island (upper series) and on Durban Island (middle series) show lower magnesium contents (except DI-23) and less frequent occurrence of large olivine crystals, whose shapes are restricted to euhedral and subhedral forms. Cape Searle, however, shows a reverse picture. The upper lavas (low Nb/Zr), which are magnesium-rich, contain only olivines with euhedral/subhedral shapes, while the olivines of the stratigraphically lower (high Nb/Zr) are texturally complex. Moreover, a sort of rhythm is recognisable rising up the stratigraphic sequence, showing two cycles of olivines with euhedral/subhedral and euhedral/ subhedral/ anhedral/ skeletal-growth shapes (Fig. 3.2). At all three locations, low-magnesium lavas show skeletal shapes in the high- but not in the low-Nb/Zr lava flows.

A more detailed petrographic description of each Baffin Island sample is given in the Appendix.

3.2 Olivine chemistry/composition

The olivine compositions of Baffin Island were determined to investigate whether the lava flows and dykes represent liquids or were formed by olivine accumulation. As Padloping Island lavas had already been analysed by Francis (1985, 1986), olivines from Durban Island were analysed in detail in this study. For Padloping Island and Cape Searle, only the dykes and some representative olivine compositions of the different lava

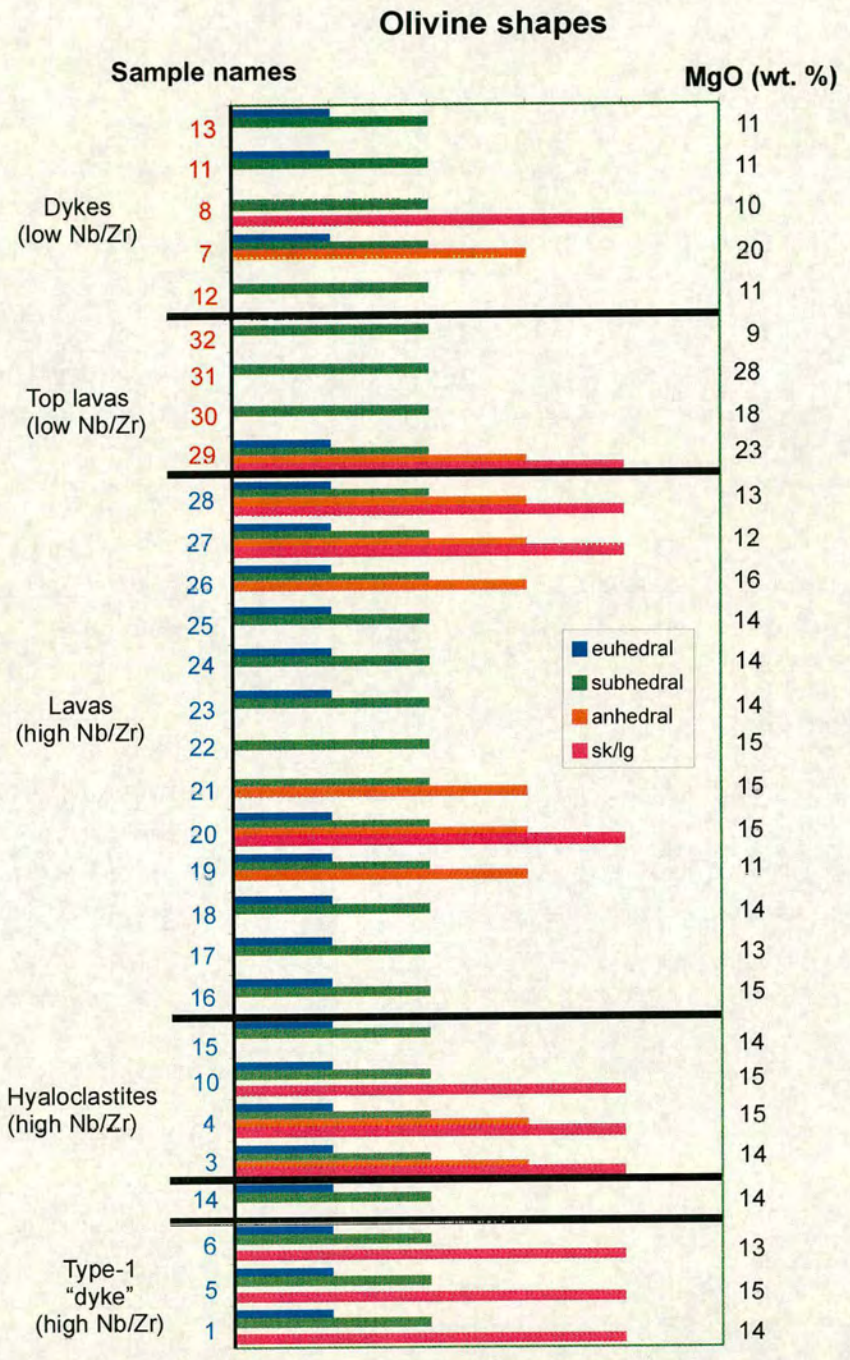

Fig. 3.2a. Simplified diagram showing the petrography of the stratigraphic sequence of Cape Searle (sk: skeletal olivine; lg: long-growth olivine)

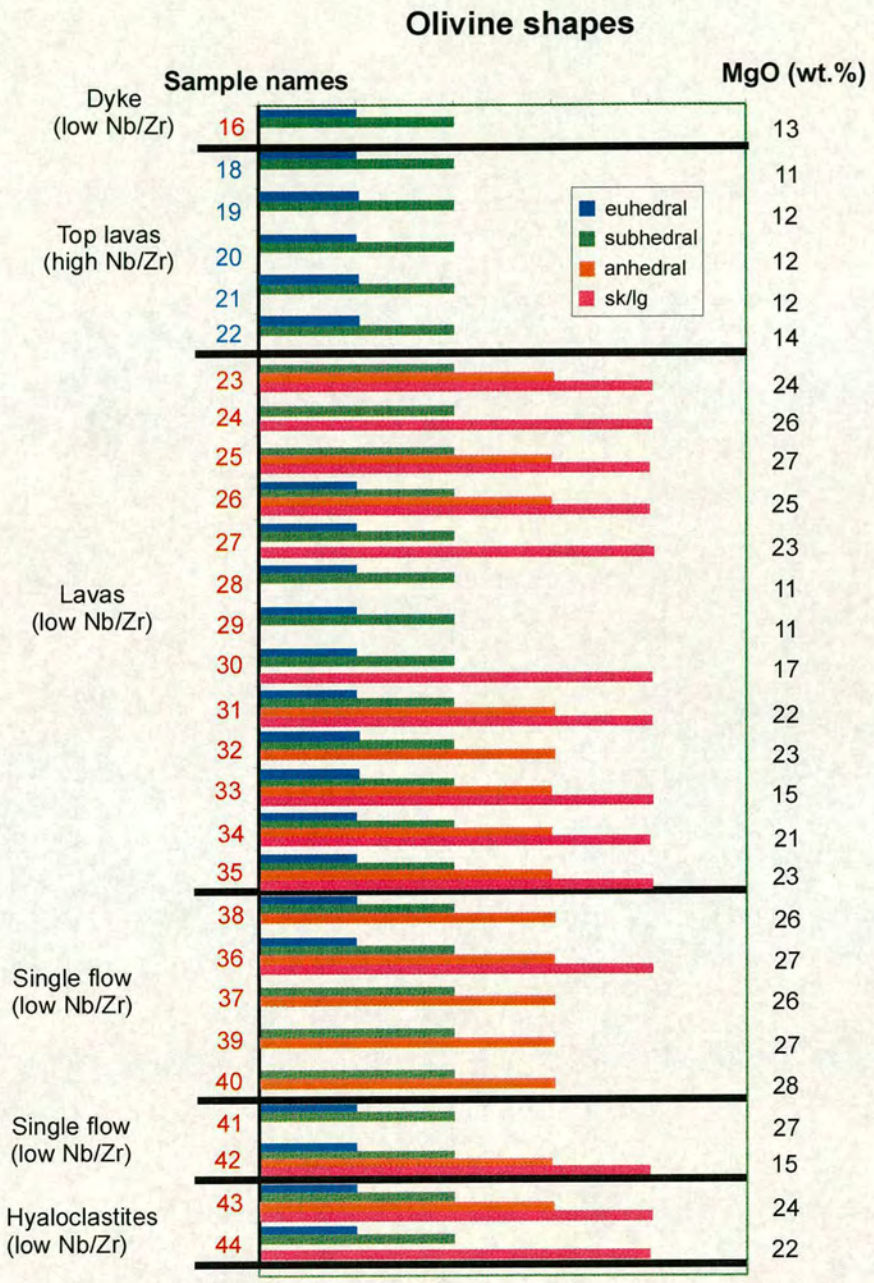

Fig. 3.2b. Simplified diagram showing the petrography of the stratigraphic sequence of Padloping Island (sk: skeletal olivine; lg: long-growth olivine).

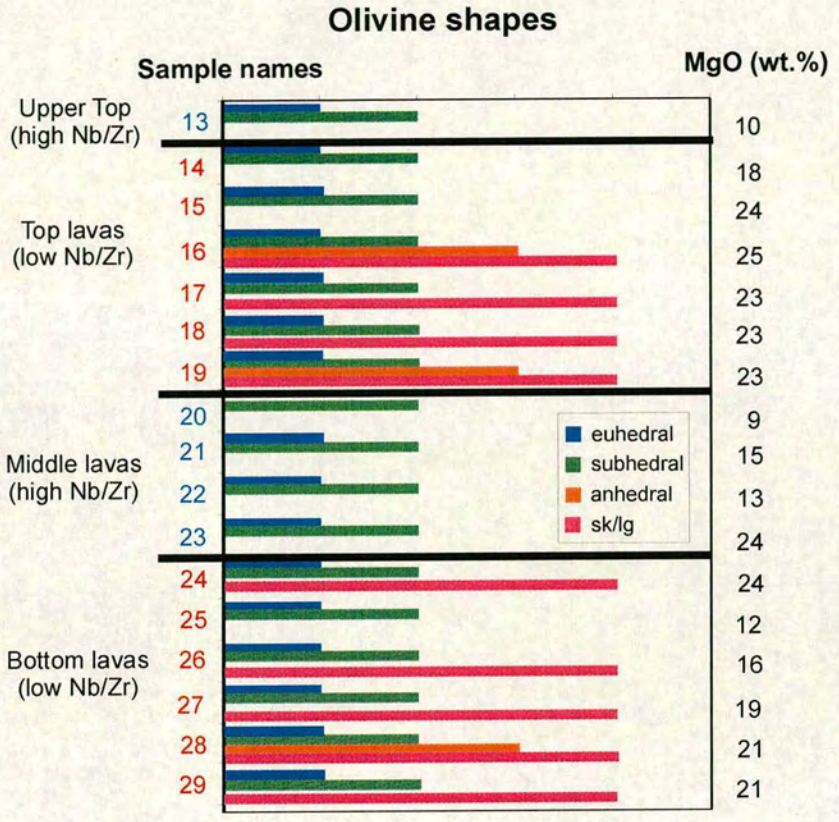

Fig. 3.2c. Simplified diagram showing the petrography of the stratigraphic sequence of Durban Island (sk: skeletal olivine; lg: long-growth olivine).

groups (see chapter 3.4 and 3.5) were analysed. Phenocryst core and rim compositions are summarised in Fig. 3.3 and all olivine analyses are given in the Appendix.

Most of the olivine phenocrysts are normally zoned with margins enriched in Fe. However, some olivines were measured which are nearly unzoned, or even show reverse zoning (for example CS-18 and PI-16). Olivine core composition for the lava flows range from Fo_{81} to Fo_{92}, except for the stratigraphically highest and more evolved lava flow (DI-13) which only contains olivine microphenocrysts with forsterite contents of 64-72 mol. %. The core compositions of the dykes are more magnesian with forsterite contents between 89 and 93 mol. %. The rims of the olivine phenocrysts range in composition from Fo_{78} to Fo_{88} (Fo_{63-72} for DI-13) for the lava flows and from Fo_{82} to Fo_{93} for the dykes. As shown in Fig. 3.4, some lava flows have a restricted range of olivine core compositions (Fo_{max}-Fo_{min}= 0.2 mol. %), while most of the lavas show a wide range of core compositions (Fo_{max}-Fo_{min} = up to 4.2 mol. %).

The two different geochemical groups are distinguishable not only by their olivine sizes and morphologies (see above section 3.1), but also by their olivine composition. The magnesium-rich (low Nb/Zr) lavas contain more-forsteritic olivines than the less-magnesian (high Nb/Zr) lavas. While these forsteritic olivines are generally larger in size, no systematic compositional difference between euhedral and skeletal olivine crystals was found (Fig. 3.4).

The olivines of Baffin Island contain a significant amount of CaO (0.23-0.38 wt. %), NiO (0.04-0.5 wt. %) and Cr_2O_3 (0.02-0.2 wt. %) (Fig. 3.5). The core compositions show a positive correlation between the forsterite content and both NiO and Cr_2O_3, but a negative correlation with CaO (Fig. 3.5). Note that the most evolved lava sample (DI-13) and some core measurements of DI-25 do not show such clear correlation in the latter diagram. The olivines in lava flows and dykes of Baffin Island show much higher

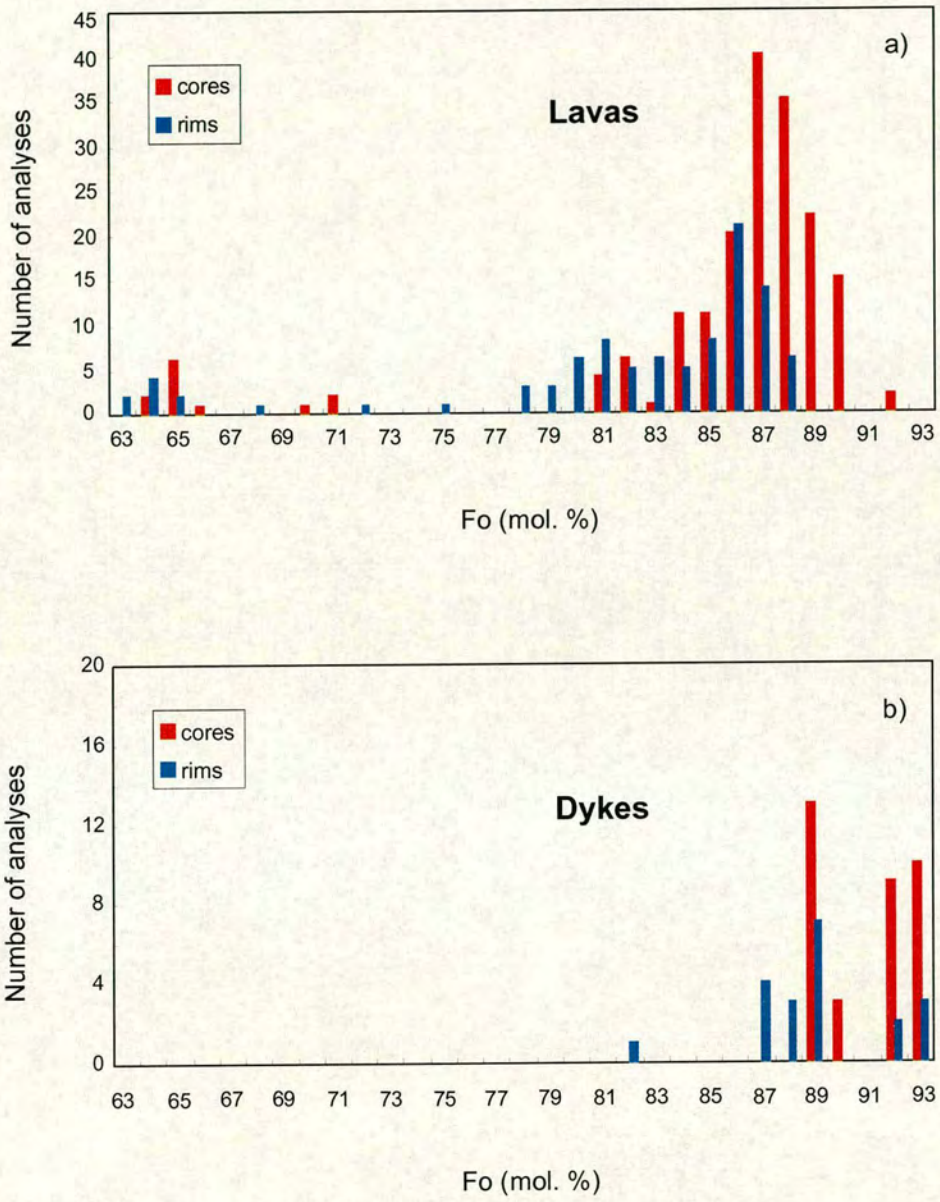

Fig. 3.3. Histogram of forsterite content (mol. %) of the olivines in the (a) lava flows (cores [n=179] and rims [n=96]) and (b) dykes (cores [n=35] and rims [n=20]).

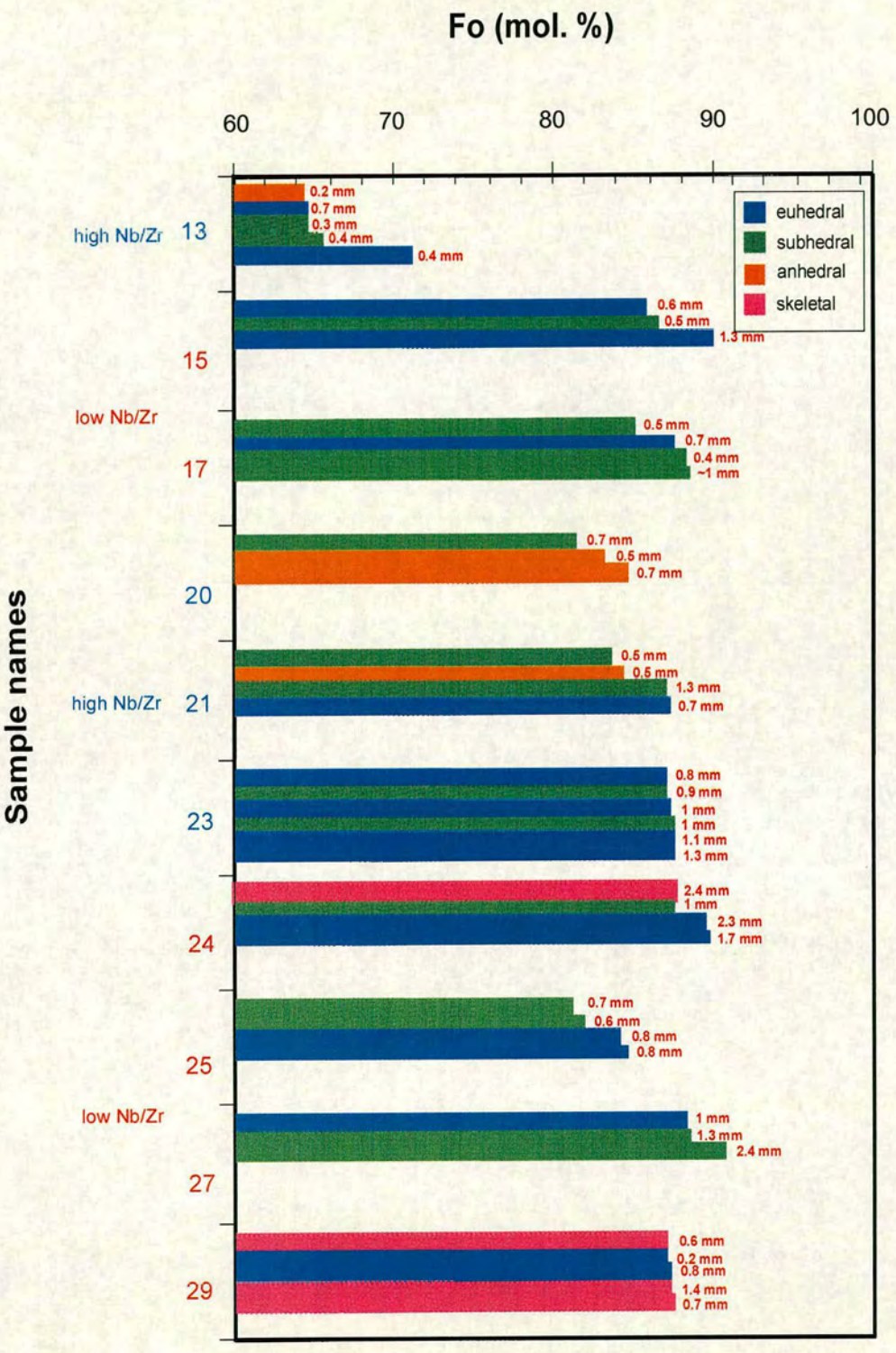

Fig. 3.4a. Forsterite content of olivines from the lava flows arranged in stratigraphic order on Durban Island. For each crystal, around three core measurements have been carried out and the mean forsterite composition is presented here.

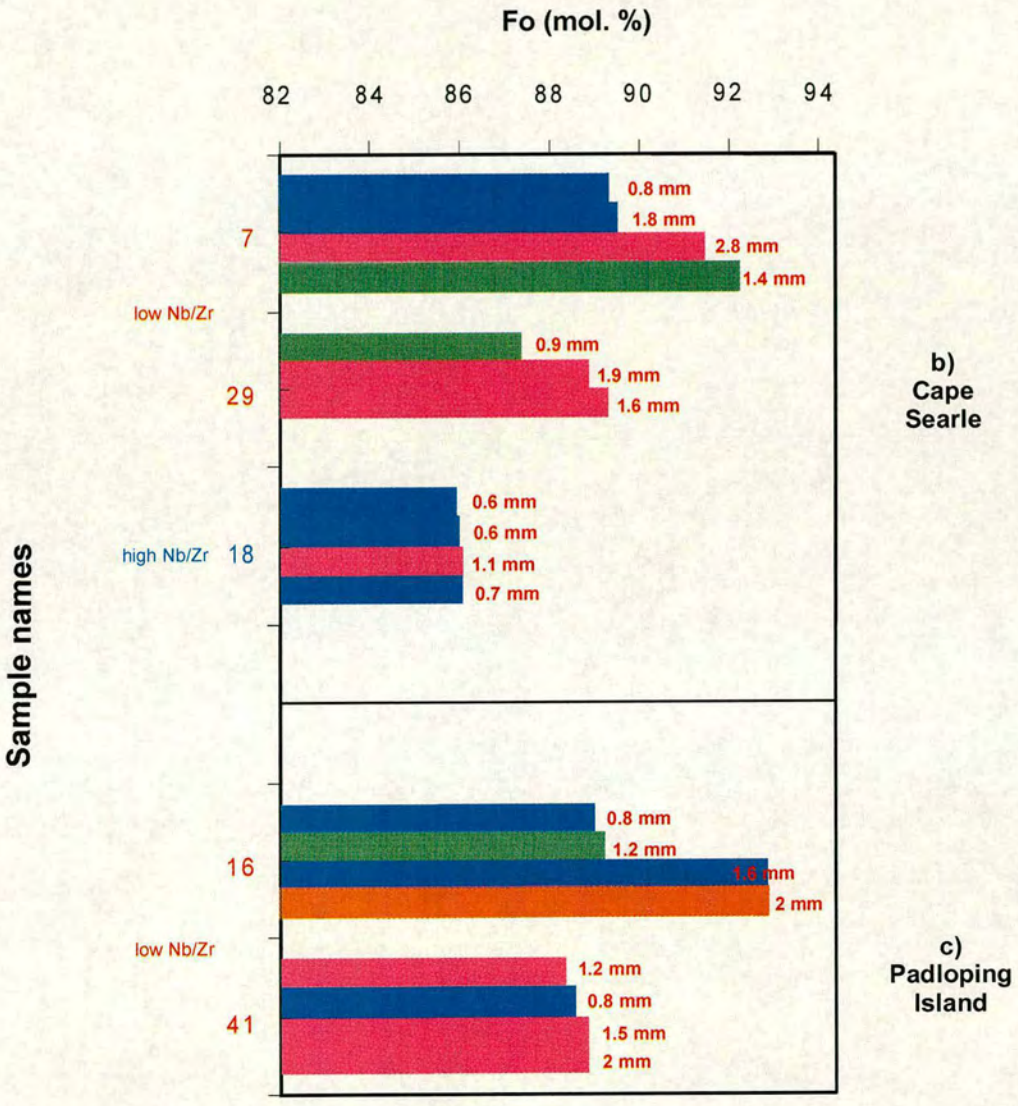

Fig. 3.4. Forsterite content of olivines from the lava flows arranged in stratigraphic order on (b) Cape Searle and (c) Padloping Island. For each crystal, around three core measurements have been carried out and the mean forsterite composition is presented here.

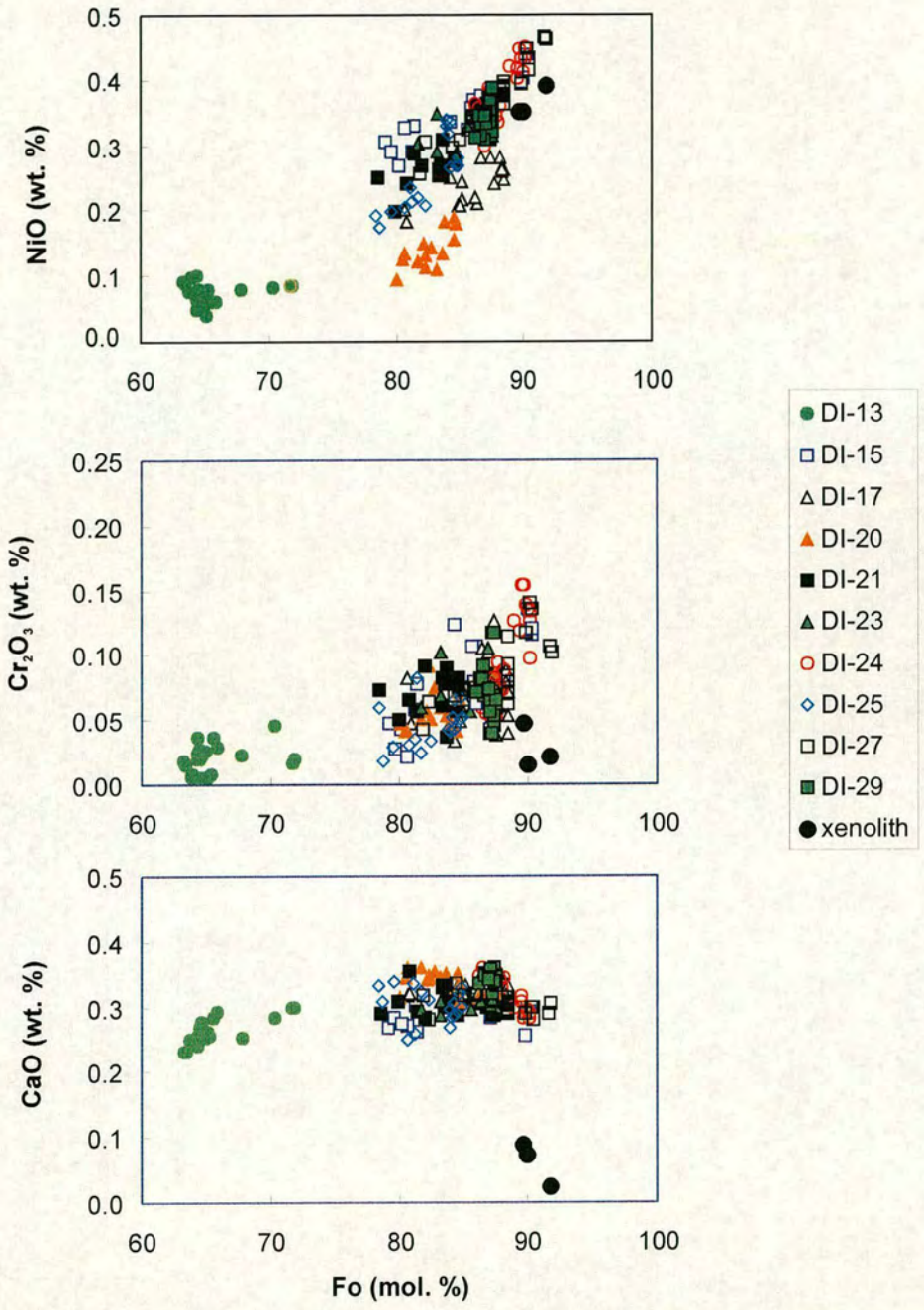

Fig. 3.5a. Minor elements (NiO, Cr_2O_3, CaO wt. %) versus forsterite contents of olivine cores from Durban Island. Some mantle olivine analyses [xenolith] (Hervik et al., 1986) are included for comparison.

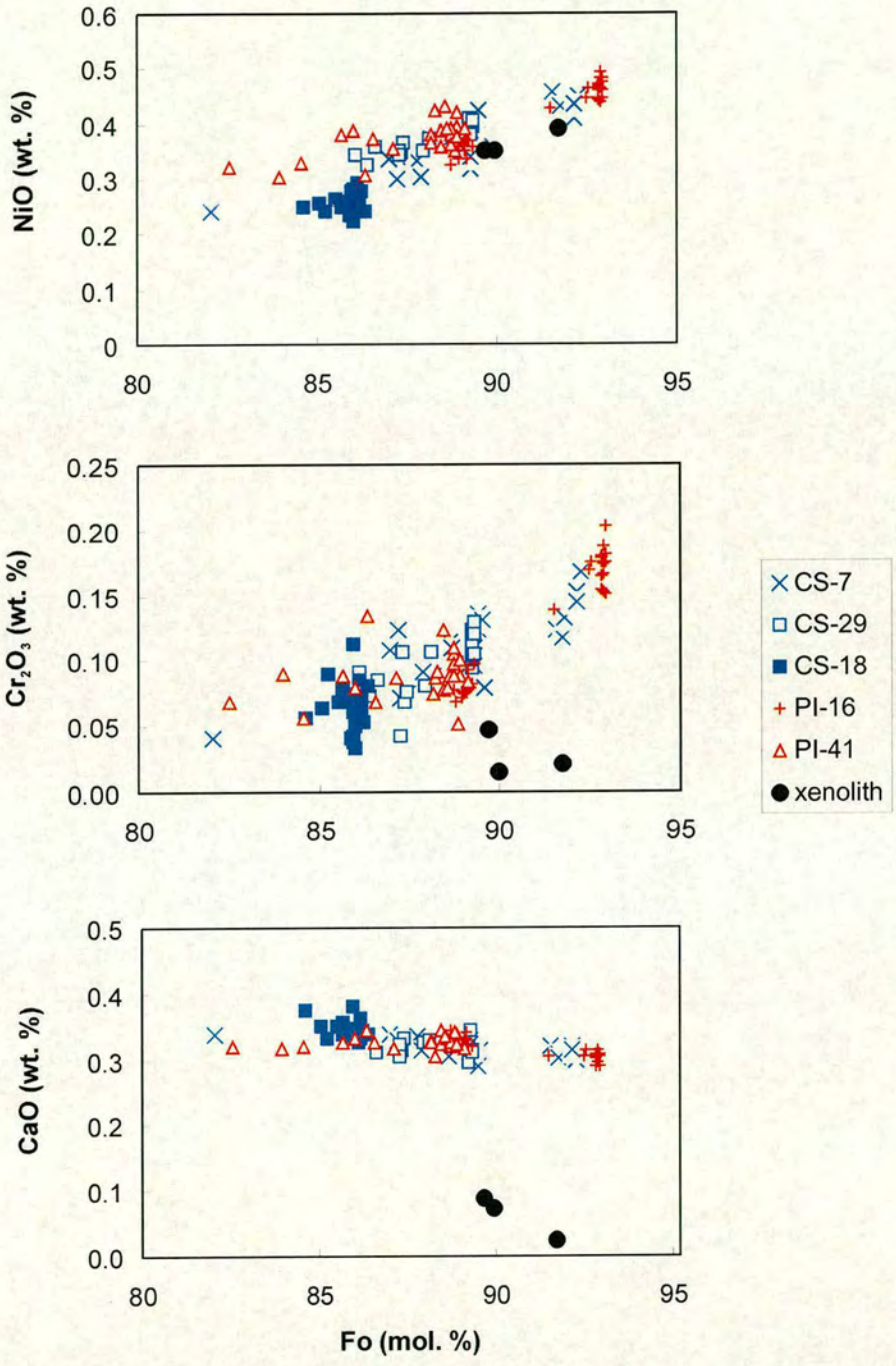

Fig. 3.5b. Minor elements (NiO, Cr_2O_3, CaO wt. %) versus forsterite contents of olivine cores from Cape Searle and Padloping Island. Some mantle olivine analyses [xenolith] (Hervig et al., 1986) are included for comparison.

values of CaO and Cr_2O_3 than mantle olivines (Hervig et al., 1986), which are also presented in Fig. 3.5 for comparison (for discussion see section 4.2.2).

3.3 Major elements

3.3.1 Classification

The Baffin Island lava flows and dykes can be classified in a total alkalis-silica (TAS) diagram (Le Maitre, 1989). According to this, the rocks are divided into ultrabasic and basic rocks; the majority of the rocks are basalts with the exception of the stratigraphically lower lava flows on Padloping Island which are picrobasalts (Fig. 3.6). However, while the TAS system works well with common rocks, it is inadequate for many low-silica rocks, and high-Mg volcanic rocks have to be further separated by their MgO and TiO_2 contents (Le Bas & Streckeisen, 1991). In Fig. 3.7, the International Union of Geological Sciences (IUGS) reclassification for high-Mg and picritic volcanic rocks is used (Le Bas, 2000). Using this chemical classification, all of the Baffin Island samples are either basalts, picrites or komatiites. However, if the rocks contain accumulated olivines, the classification has to be used with caution (e.g. Le Maitre, 1989; Le Bas, 2001). Further discussion of this issue, as well as classification of the Baffin Island rocks used for this study, is given in section 4.1 and 4.2.1.

3.3.2 Variation diagrams

The major element data have been recalculated to 100% on a volatile-free basis and all iron is reported as Fe_2O_3. In oxide variation diagrams, most elements define linear trends (Fig. 3.8). For the lava flows, as MgO decreases (28.3 to 8.8 wt. %), there is a general

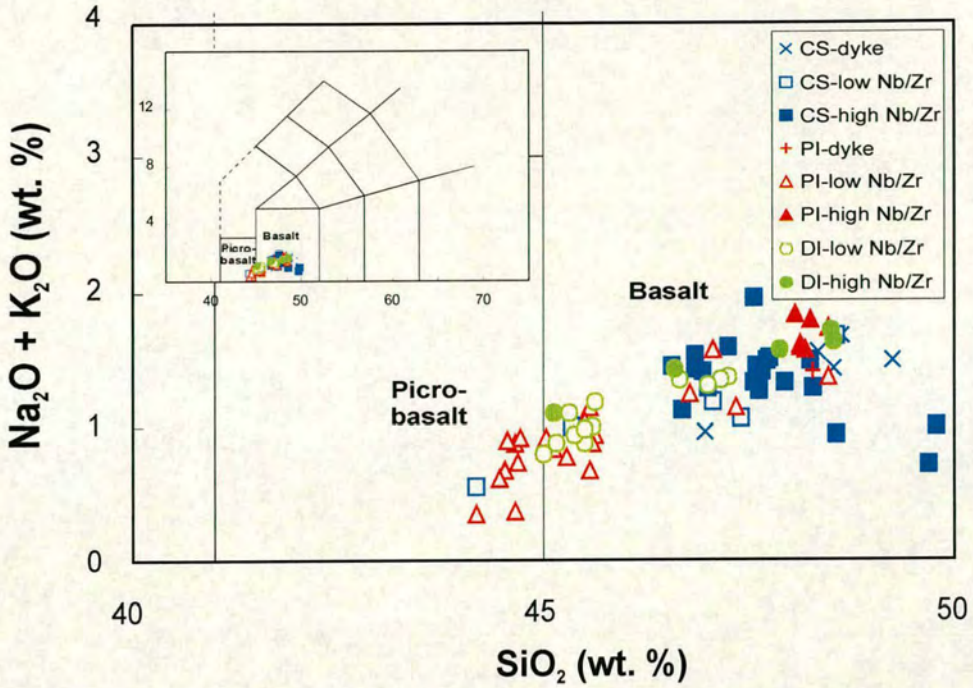

Fig. 3.6. The total alkalis versus silica diagram (TAS) after Le Maitre et al. (1989). The analyses have been recalculated to 100% on a volatile-free basis.

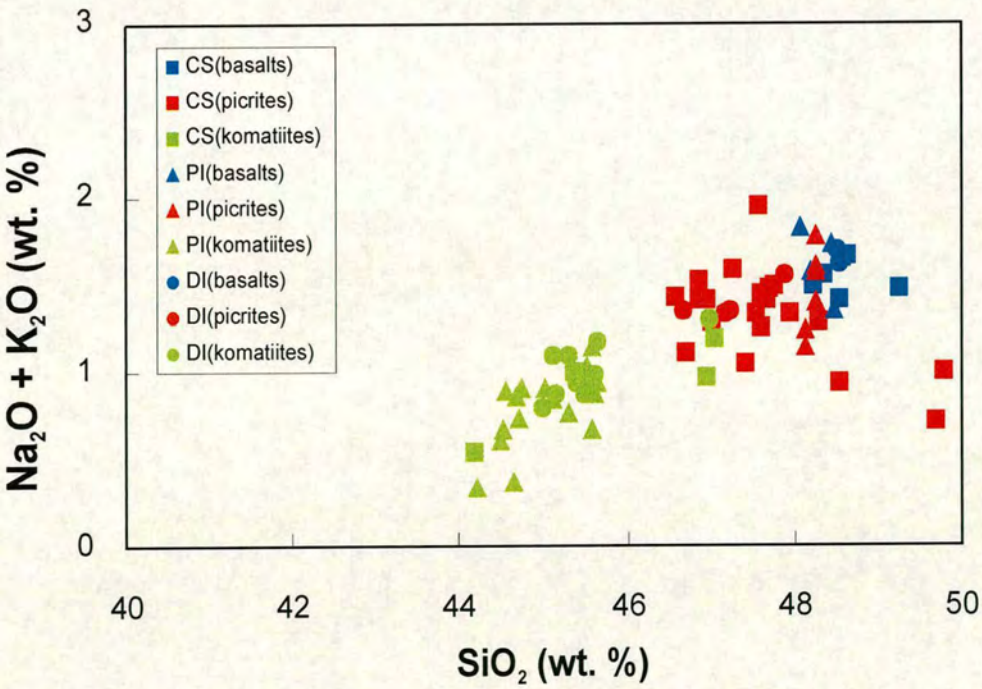

Fig. 3.7. The total alkalis versus silica diagram (TAS) after Le Maitre et al. (1989) with IUGS reclassification for high-Mg and picritic volcanic rocks (Le Bas, 2000). The Baffin Island rocks can be classified as basalts (MgO <12 wt. %; SiO_2 >45 wt. %), picrites (MgO >12 wt. %; SiO_2 between 30 and 52 wt. %) and komatiites (MgO >18 wt. %; SiO_2 between 30 and 52 wt. %; ($Na_2O + K_2O$) <2 wt. %; TiO_2 <1 wt. %). The analyses have been recalculated to 100% on a volatile-free basis.

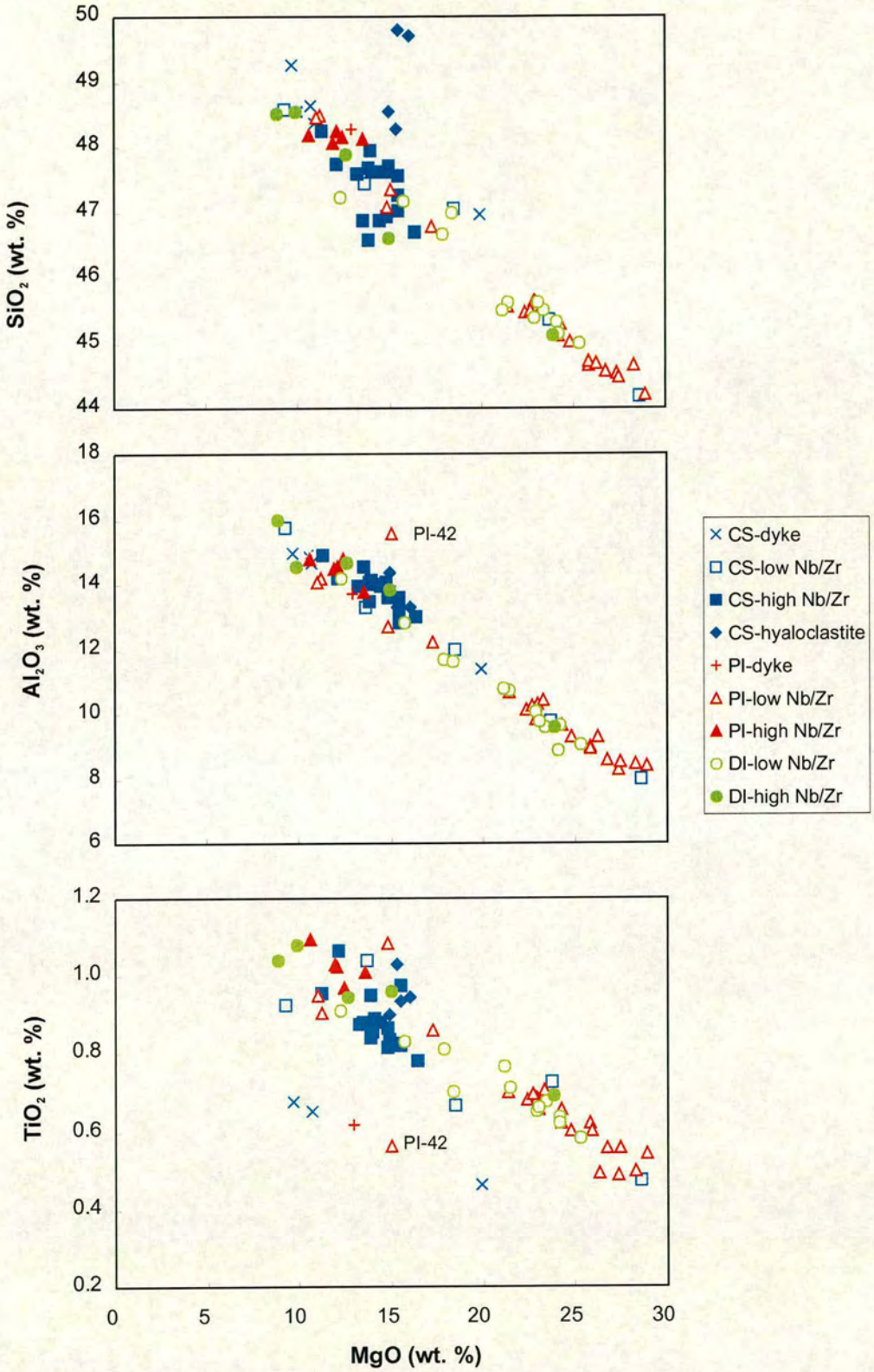

Fig. 3.8. Oxide variations (wt. %) diagrams showing SiO_2, Al_2O_3, TiO_2, Fe_2O_3, CaO, Na_2O, K_2O, MnO and P_2O_5 versus MgO.The analyses have been recalculated to 100% on a volatile-free basis.

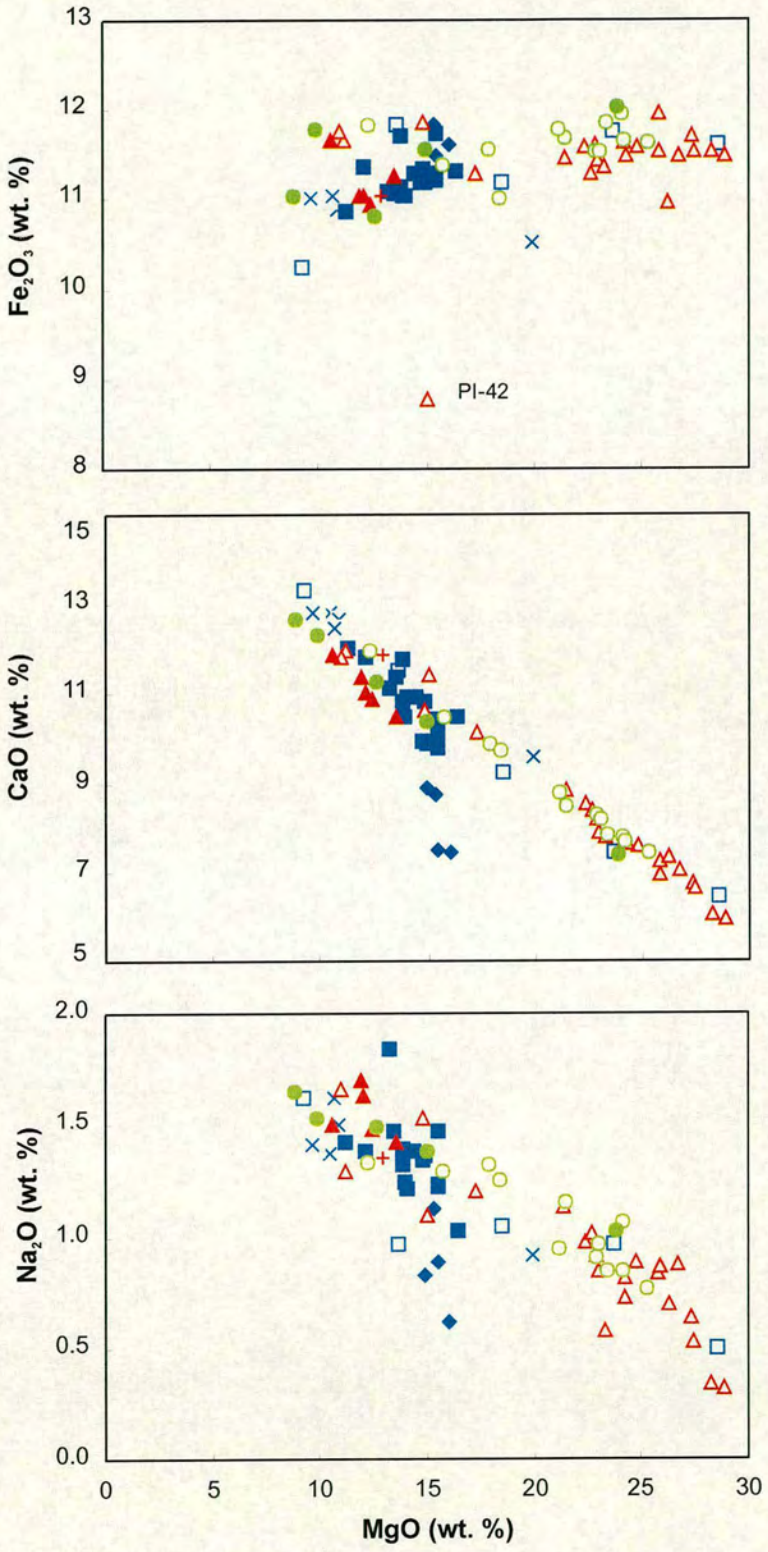

Fig. 3.8. (continued)

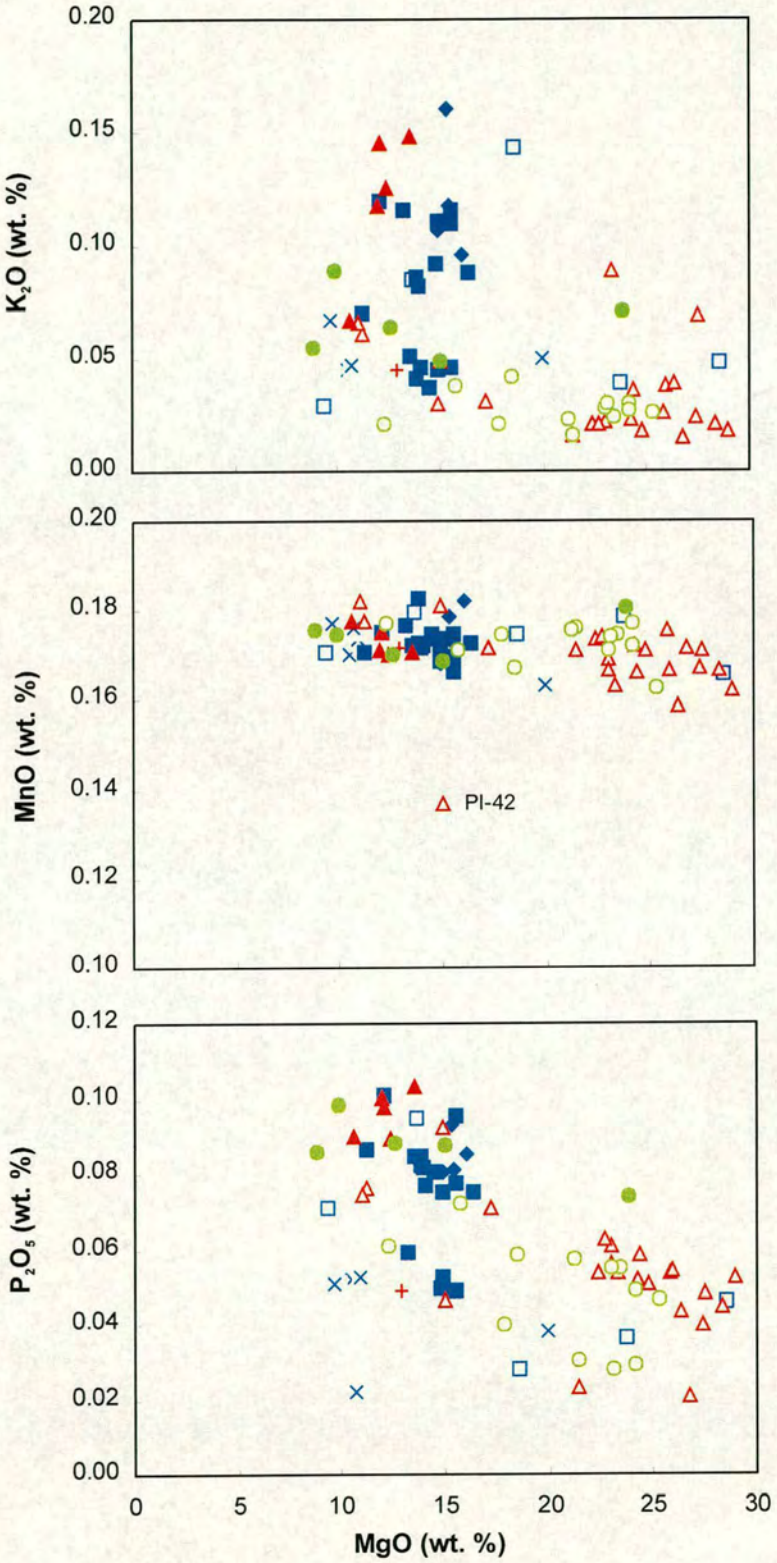

Fig. 3.8. (continued)

increase in SiO_2 (42.2 to 49.7 wt. %), Al_2O_3 (8.3 to 15.9 wt. %), CaO (5.9 to 13.3 wt. %), TiO_2 (0.5 to 1.1 wt. %) and Na_2O (0.3 to 1.8 wt. %). For Fe_2O_3 (10.3 to 12.0 wt. %) the data are scattered, but stay largely constant with declining MgO. K_2O (0.02 to 0.16 wt. %), MnO (0.16 to 0.18 wt. %) and P_2O_5 (0.02 to 0.10 wt. %) display a scatter of values, but MnO and P_2O_5 increase slightly with decreasing MgO. The dyke samples of Padloping Island and Cape Searle generally lie within the trend defined by the lava flows, except for TiO_2 versus MgO, where the samples define a parallel trend to the lava flows with lower TiO_2 values (0.5 to 0.7 wt. %). Note that in most variation diagrams PI-42 does not follow the general trend; depending on the element in question, it shows either higher or lower values than the other samples. The hyaloclastites (CS-15, -10, -4, -3) are more altered (volatile contents between 5.29 and 7.55) and display higher SiO_2 and lower CaO and Na_2O values compared to the remaining lava flows.

3.4 Trace elements

3.4.1 Variation diagrams

In variation diagrams of MgO versus trace elements (Fig. 3.9), most elements define linear trends. For Zr (23 to 66 ppm), Y (9 to 24 ppm), Sr (38 to 257 ppm), Rb (0.1 to 2.5 ppm), Sc (24 to 53 ppm) and Cu (65 to 152 ppm), the values of the lava flows increase slightly with decreasing MgO contents (28.1 to 8.9 wt%). The dykes, however, have lower values of Zr (23 to 43 ppm) and Sr (37 to 52 ppm), covering a narrow range with decreasing MgO (20 to 10 wt. %). No correlation with MgO is apparent for Zn (58 to 85 ppm), while Ni (152 to 1373 ppm) and Cr (462 to 2353 ppm) correlate positively with MgO for both lava flows and dykes on Baffin Island. With decreasing MgO, Nb stays nearly constant at low values (~1 ppm) until it reaches 16 wt. % MgO, then it scatters (0.5-6.7 ppm) at lower MgO.

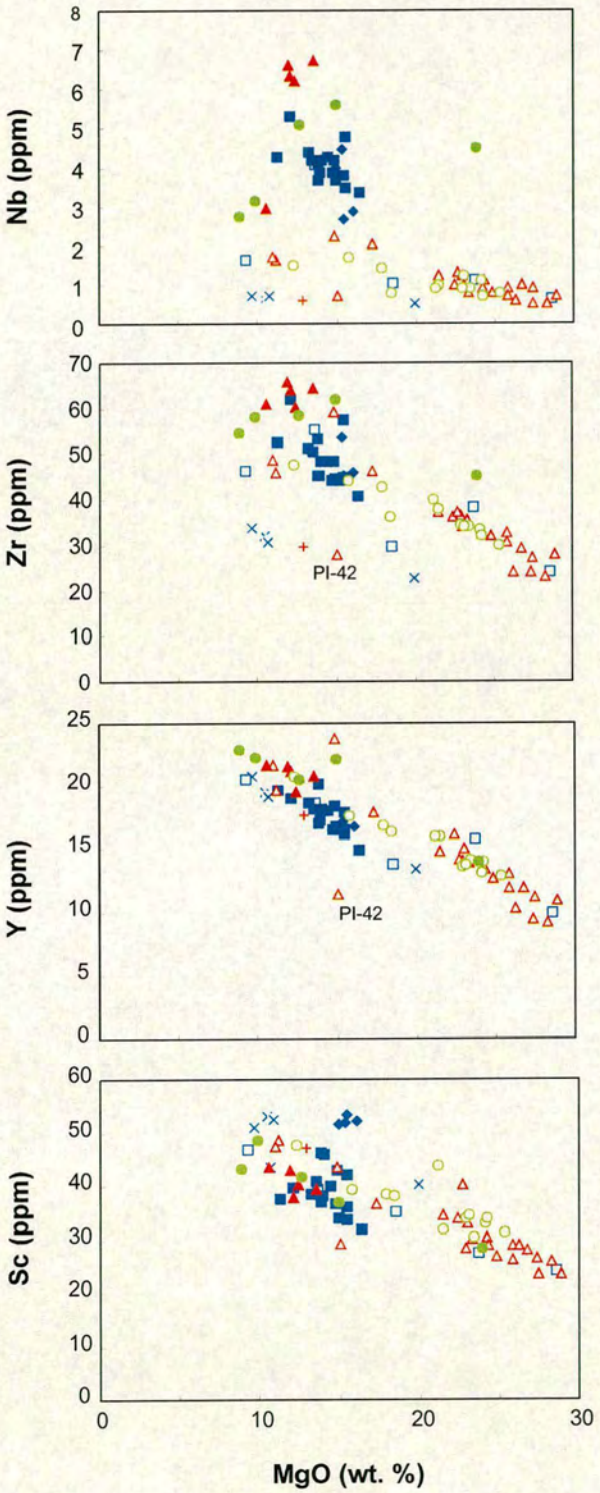

Fig. 3.9. Trace elements in ppm (Nb, Zr, Y, Sc, Sr, Rb, Zn, Cu, Ni, Cr, V) versus MgO (wt. %). MgO contents are recalculated on a volatile-free basis. Symbols as in Fig. 3.8.

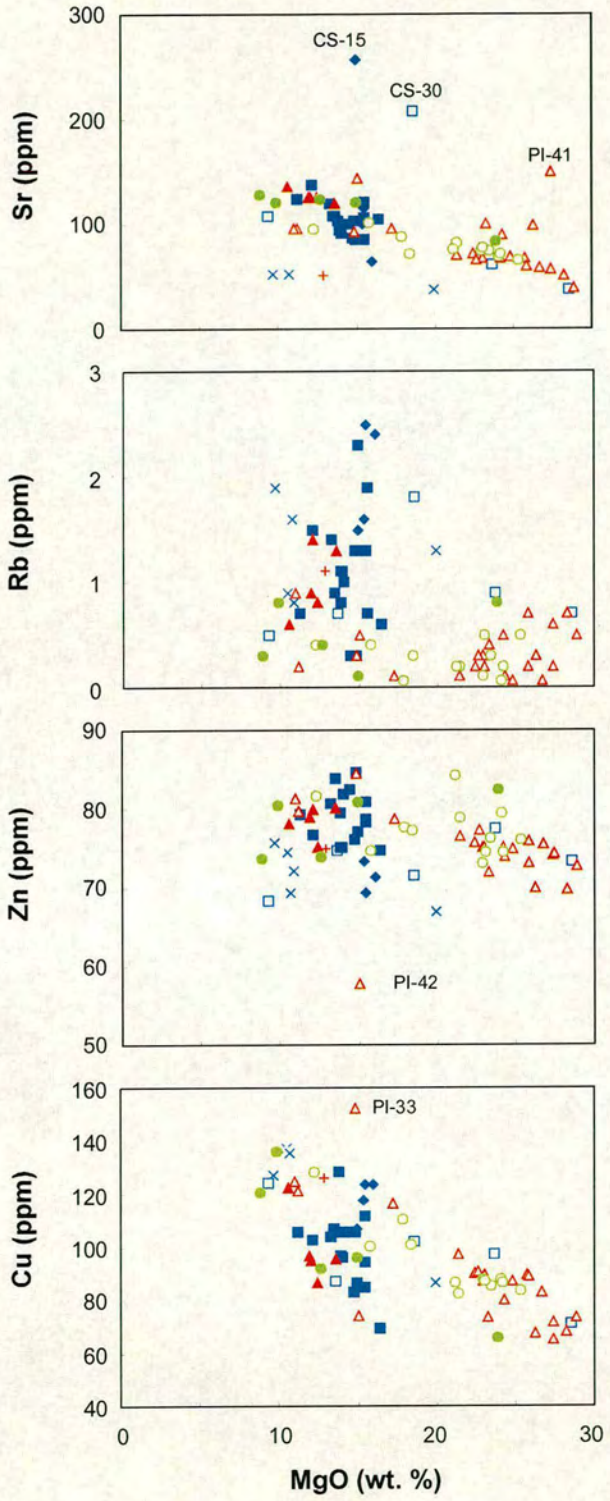

Fig. 3.9. (continued)

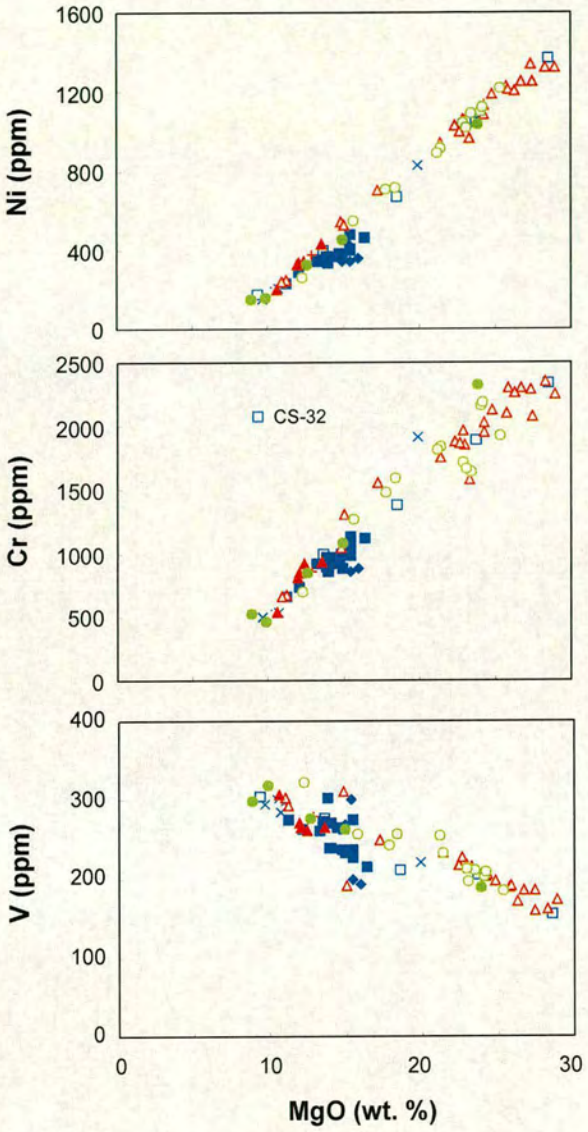

Fig. 3.9. (continued)

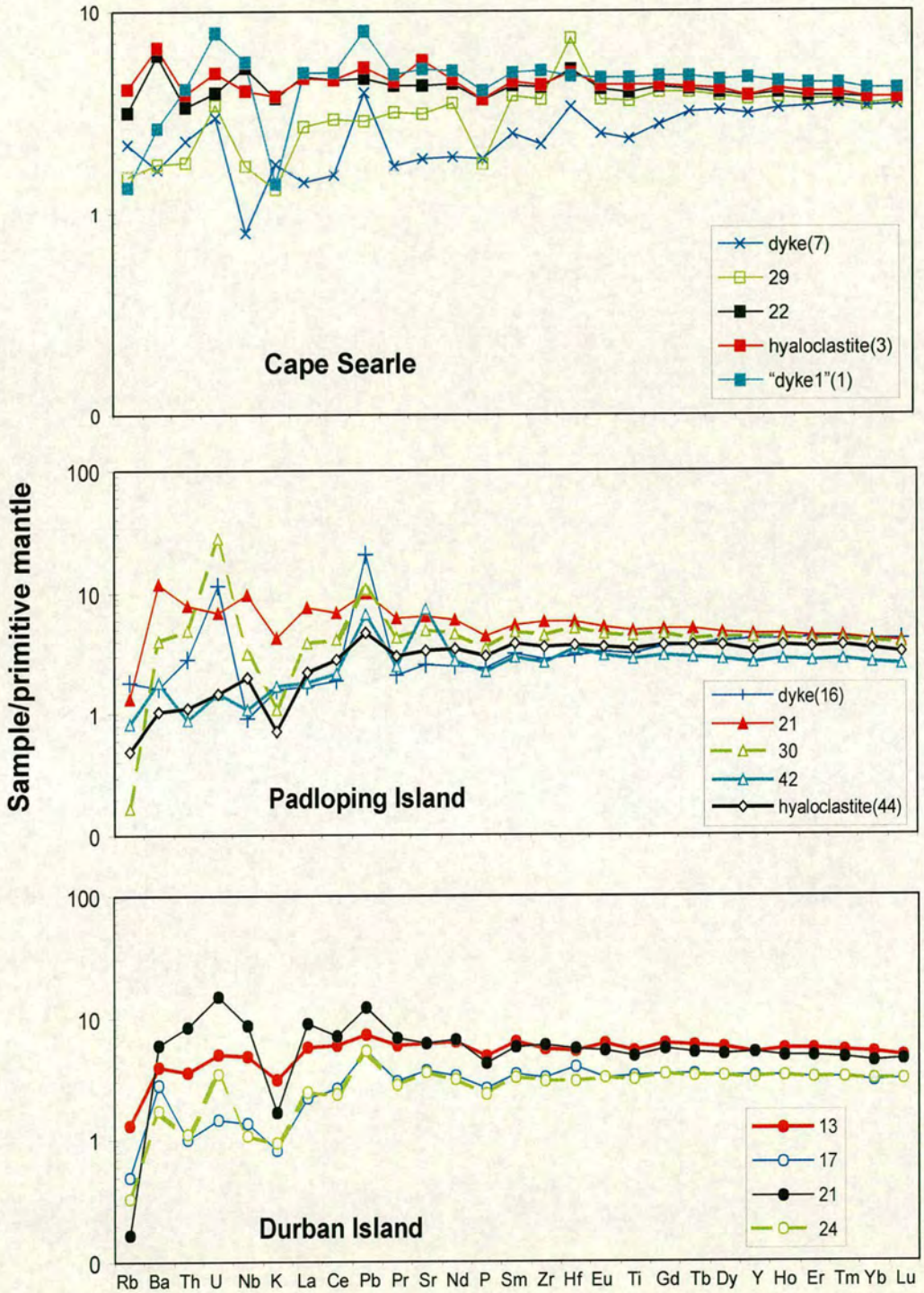

Fig. 3.10. Primitive-mantle-normalised trace element patterns of selected samples (low Nb/Zr: open symbols; high Nb/Zr: closed symbols) from Cape Searle, Padloping Island and Durban Island. Primitive mantle values are from McDonough & Sun (1995).

3.4.2 Incompatible element plots

The Baffin Island lava flows and dykes show a wide range of geochemical signatures (Fig. 3.10). The samples can be broadly divided into two groups, which are represented throughout the stratigraphic sequences in each of the three locations. The dykes and upper lava flows on Cape Searle, the dyke and the lower lava flows on Padloping Island and the upper and lower lava flows on Durban Island have Nb/Zr <0.05 and $(La/Sm)_n$ <1, while the lower lava flows on Cape Searle, the upper lava flows on Padloping Island and the middle lava flows on Durban Island have Nb/Zr >0.07 and $(La/Sm)_n$ >1 (Fig. 3.11 and 3.12). The Hf results of twelve samples (CS-31,-29,-28,-25,-23,-21 and PI-31,-32,-34,-36,-38,-39,-40) are too high. It was not possible to identify the cause of these errors and the results have been excluded. The Pb result (100 ppm) of PI-25 is also too high and has been excluded. Some lavas, in particular the dykes, show an enrichment in Pb, often coupled with a depletion in Nb, which is generally the signature of continental crust. Whether the volcanic rocks on Baffin Island are contaminated with continental crust, will be discussed in detail in chapter 5.

3.5 Isotopes

3.5.1 Strontium and Neodymium

The lava flows and dykes on Baffin Island define a negative correlation on a plot of $^{87}Sr/^{86}Sr$ versus $^{143}Nd/^{144}Nd$ (Fig. 3.13). The low-Nb/Zr lavas of Durban Island and Padloping Island have high $^{143}Nd/^{144}Nd$ (0.51304-0.51313) and low $^{87}Sr/^{86}Sr$ (0.7030-0.7034). The high-Nb/Zr lava flows of Cape Searle have $^{143}Nd/^{144}Nd$ between 0.51298 and 0.51300 and $^{87}Sr/^{86}Sr$ between 0.7034 and 0.7035, while the hyaloclastites scatter at even lower $^{143}Nd/^{144}Nd$ (0.51293-0.51304) and higher $^{87}Sr/^{86}Sr$ (0.7038-0.7040). The

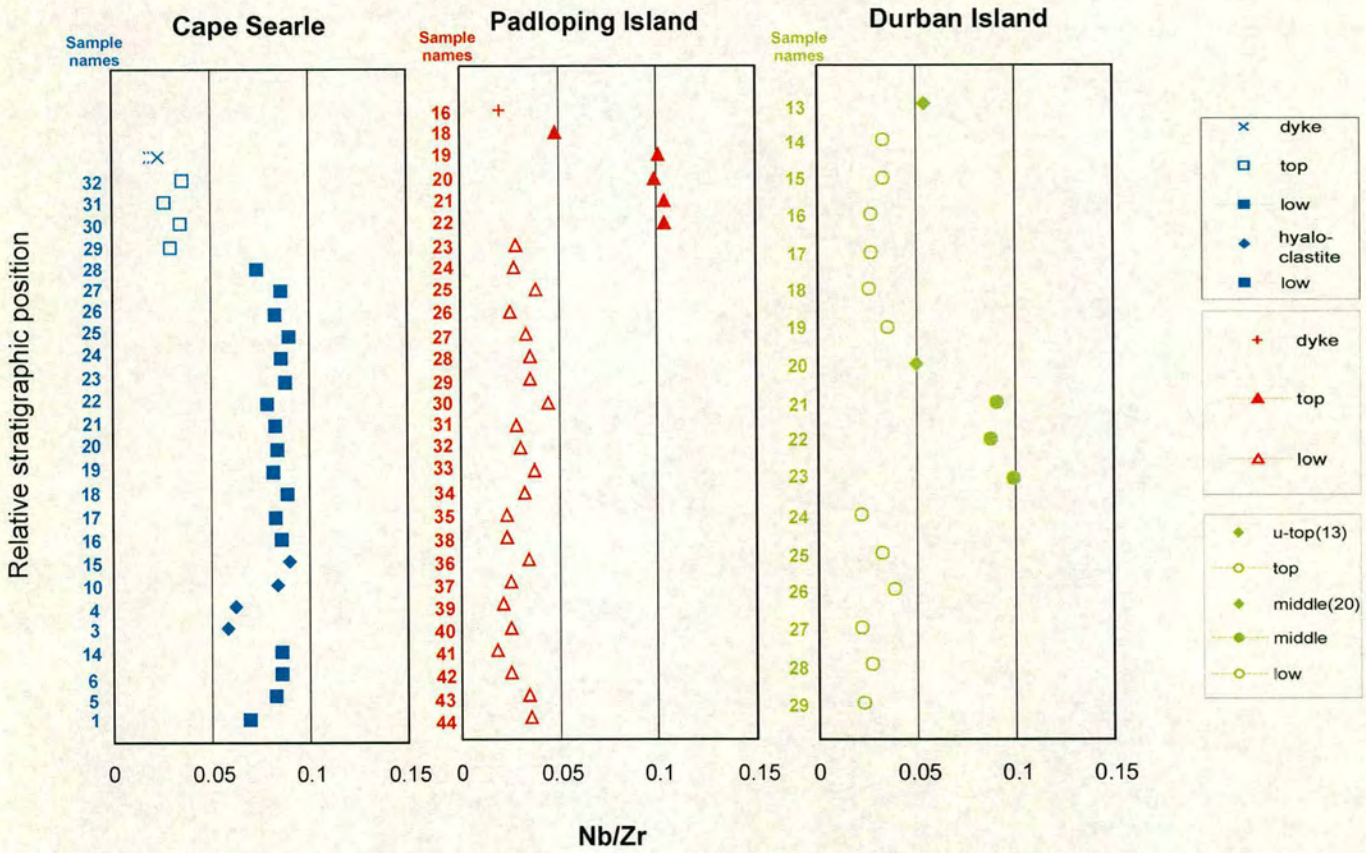

Fig. 3.11. Stratigraphic variation of Nb/Zr in lavas from Cape Searle, Padloping Island and Durban Island.

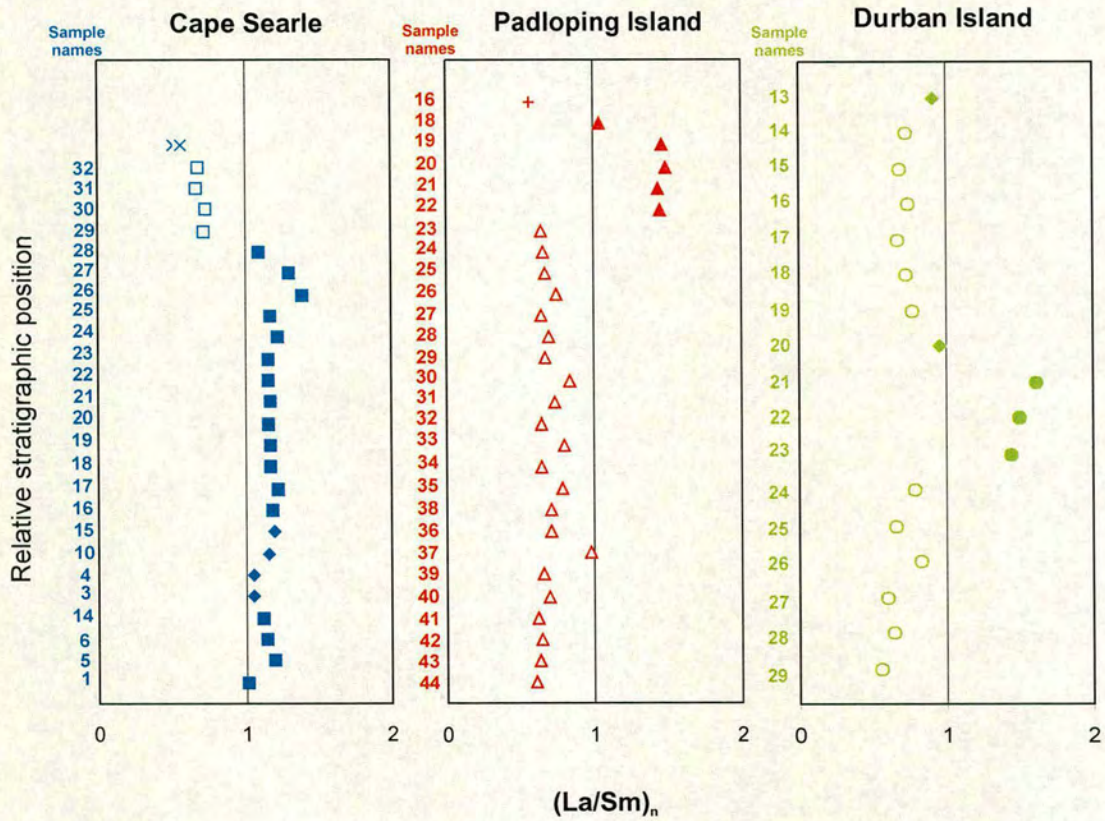

Fig. 3.12. Stratigraphic variation of $(La/Sm)_n$ in lavas from Cape Searle, Padloping Island and Durban Island. Symbols as in Fig. 3.11.

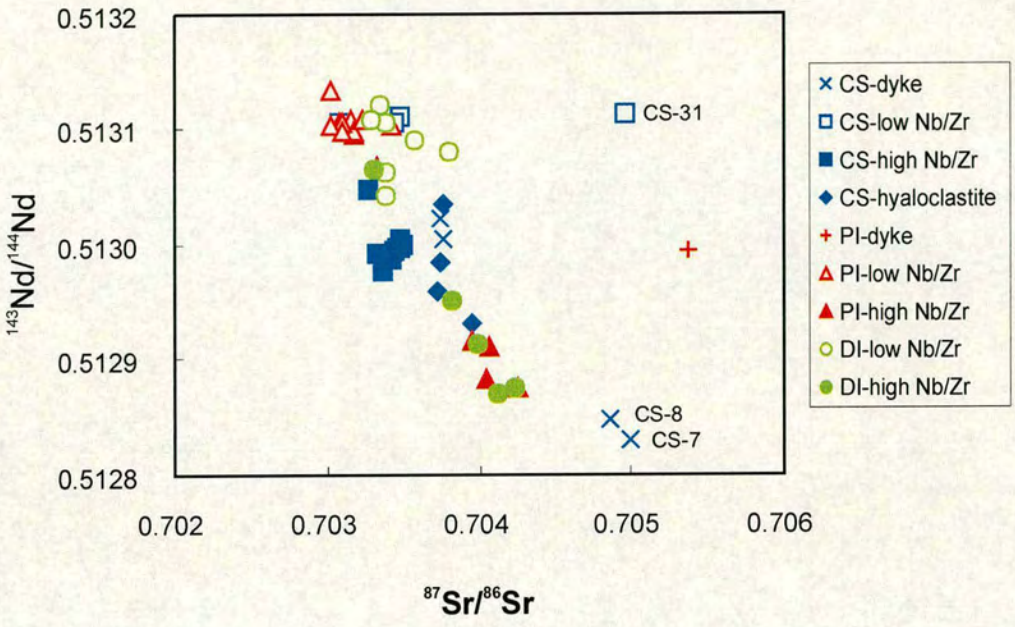

Fig. 3.13. Measured values of $^{143}Nd/^{144}Nd$ versus $^{87}Sr/^{86}Sr$ of the Baffin Island samples.

high-Nb/Zr lavas of Padloping Island and Durban Island have low $^{143}Nd/^{144}Nd$ (0.51288-0.51292) and high $^{87}Sr/^{86}Sr$ (0.7040-0.7042). The chilled margins of the dyke on Cape Searle (CS-7, CS-8) have the lowest $^{143}Nd/^{144}Nd$ (0.51283-0.51285) and highest $^{87}Sr/^{86}Sr$ (0.7049-0.7050) of any of the analysed samples on Baffin Island. The Padloping dyke (PI-16) lies off the trend defined by the remaining samples and instead shows very different $^{143}Nd/^{144}Nd$ (0.51300) and $^{87}Sr/^{86}Sr$ (0.7054) ratios. CS-31 has high $^{143}Nd/^{144}Nd$ (0.513110), but also high $^{87}Sr/^{86}Sr$ (0.704975), possibly the result of seawater alteration. Therefore, the Sr-isotope result of this sample will be not used in the discussion.

3.5.2 Lead

Some representative lava flows were also analysed for Pb isotopes and display a wide range of compositions ($^{206}Pb/^{204}Pb$: 16.62-18.04; $^{207}Pb/^{204}Pb$: 14.63-15.50; $^{208}Pb/^{204}Pb$: 36.11-37.76). The lava flows show a negative correlation on a plot $^{208}Pb/^{204}Pb$ versus $^{206}Pb/^{204}Pb$, several trends for $^{207}Pb/^{204}Pb$ versus $^{206}Pb/^{204}Pb$, but no clear correlation for $^{208}Pb/^{204}Pb$ versus $^{207}Pb/^{204}Pb$ (Fig. 3.14). The distinct geochemical groups on Baffin Island, as defined by trace elements and Sr- and Nd-isotopes (section 3.4.2 and 3.5.1), are not recognisable in Pb-isotope ratios, neither is any systematic relationship apparent between Pb isotopes and either $^{87}Sr/^{86}Sr$ or $^{143}Nd/^{144}Nd$ (Fig. 3.15).

3.5.3 Hafnium

Fifteen representative samples were analysed for $^{176}Hf/^{177}Hf$ isotopes. In a $^{176}Hf/^{177}Hf$ versus $^{143}Nd/^{144}Nd$ plot (Fig. 3.16), the lava flows and dykes define two parallel trends. The high-Nb/Zr lavas of Durban Island and Padloping Island have the lowest ratios of both $^{143}Nd/^{144}Nd$ (0.51287-0.51292) and $^{176}Hf/^{177}Hf$ (0.28307-0.28311), while the

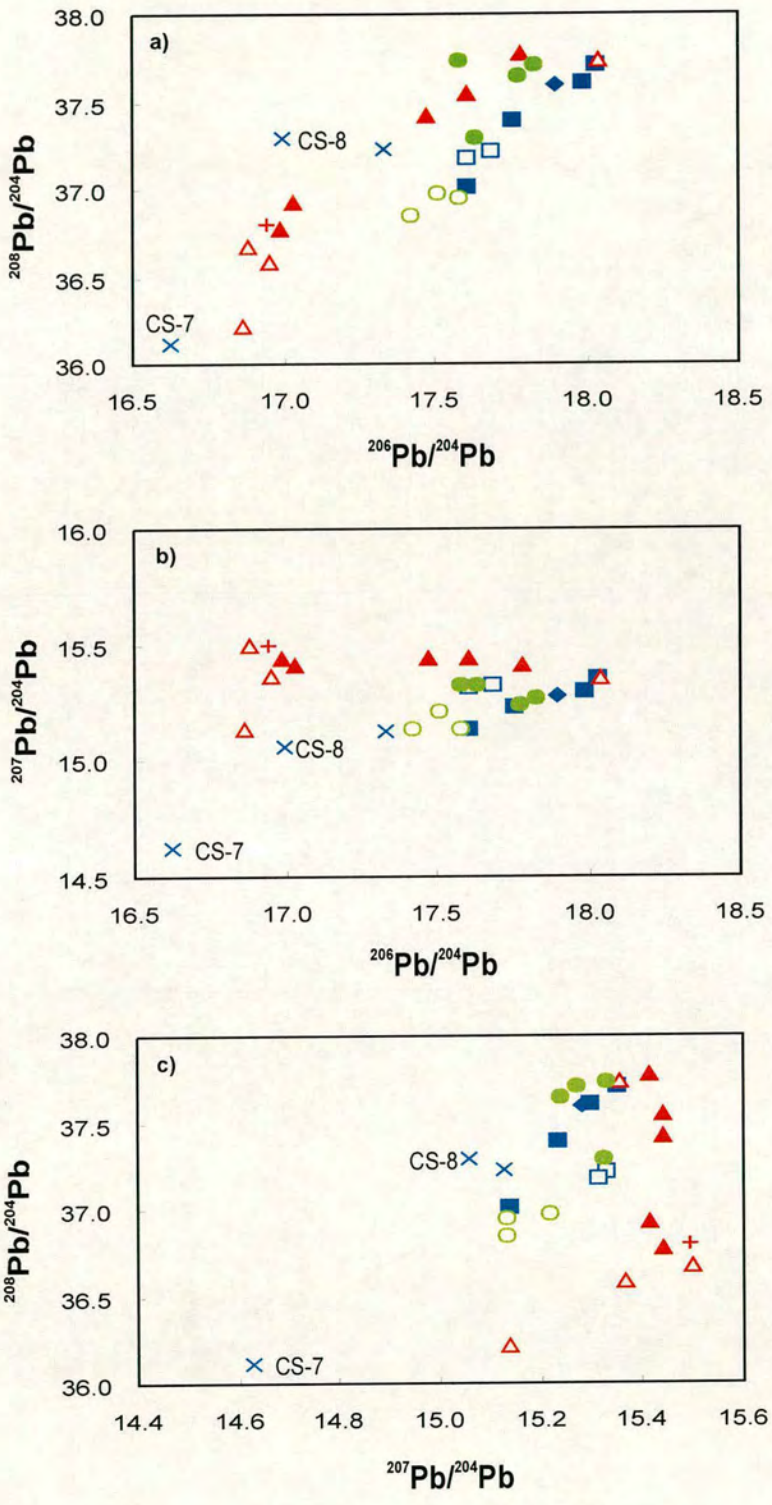

Fig. 3.14. (a) $^{208}Pb/^{204}Pb$ versus $^{206}Pb/^{204}Pb$, (b) $^{207}Pb/^{204}Pb$ versus $^{206}Pb/^{204}Pb$ and (c) $^{208}Pb/^{204}Pb$ versus $^{207}Pb/^{204}Pb$ for the Baffin Island samples. Symbols as in Fig. 3.13.

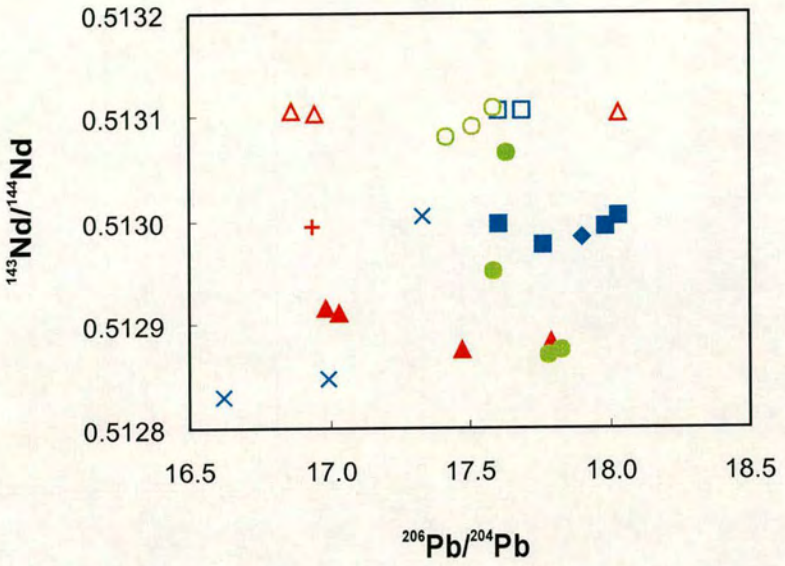

Fig. 3.15. Plot of $^{206}Pb/^{204}Pb$ versus $^{143}Nd/^{144}Nd$. Symbols as in Fig. 3.13.

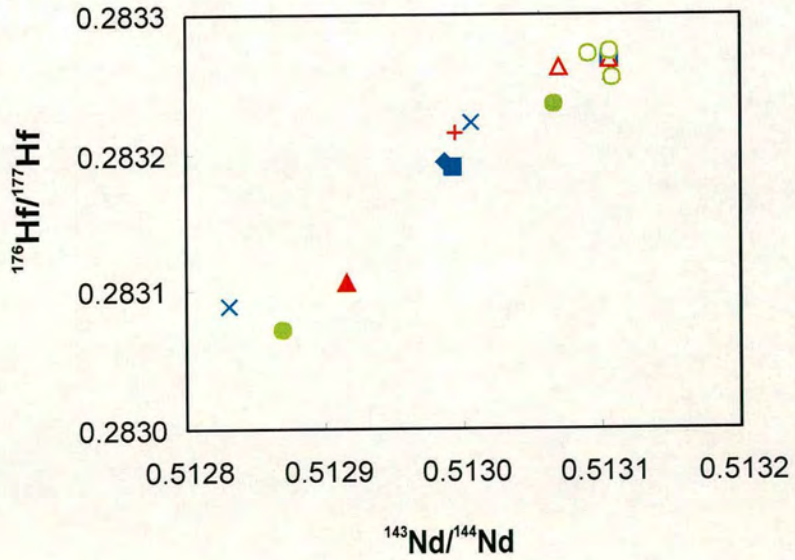

Fig. 3.16. $^{176}Hf/^{177}Hf$ versus $^{143}Nd/^{144}Nd$ for selected Baffin Island lava flows and dykes. Symbols as in Fig. 3.13.

highest ratios (0.51307-0.51311 and 0.28326-0.28327, respectively) are shown by the low-Nb/Zr lava flows on Padloping Island and Durban Island. The hyaloclastites of Cape Searle have isotope compositions intermediate between these two groups. Note that dyke (CS-7) has low Nb/Zr and $(La/Sm)_n<1$ (chapter 3.4.2 and figures within), but shows very low $^{143}Nd/^{144}Nd$ (0.51283) and $^{176}Hf/^{177}Hf$ (0.28309).

3.5.4 Helium

Eleven samples with well-preserved olivine crystals were chosen for He-isotope analyses. In Fig. 3.17, the He-isotope composition of the olivines is plotted against whole-rock Sr- and Nd isotope ratios. The stratigraphically lower lavas of both Padloping Island and Durban Island (low Nb/Zr) differ from the high-Nb/Zr lava flows of Cape Searle and Durban Island in terms of $^{87}Sr/^{86}Sr$ - $^{3}He/^{4}He$ variations. These trends are parallel and correlate negatively. The first group also shows higher $^{3}He/^{4}He$ (37.5-49.5 R_a) than the second group of samples (14.5-26.5 R_a), while the $^{87}Sr/^{86}Sr$ of both groups overlap (0.7032-0.7036 and 0.7033-0.7040, respectively). However, the Baffin Island lavas define a positive linear trend on a plot of $^{143}Nd/^{144}Nd$ versus $^{3}He/^{4}He$, with the low-Nb/Zr lavas of both Padloping Island and Durban Island having consistently higher $^{3}He/^{4}He$ (37.5-49.5 R_a) and $^{143}Nd/^{144}Nd$ (0.51306-0.51311) than the high-Nb/Zr lavas of both Cape Searle and Durban Island (14.5-26.5 R_a and 0.51291-0.51301, respectively). Note that dyke CS-7 lies off the lava flows trend in Sr-He and Nd-He plots having high $^{87}Sr/^{86}Sr$, low $^{143}Nd/^{144}Nd$ but also high $^{3}He/^{4}He$ values. The samples analysed for lead show only a small variation in He-isotope ratios (38 to 44 R_a), but a larger range for example in $^{206}Pb/^{204}Pb$ isotopes (16.6 to 18) (Fig. 3.17).

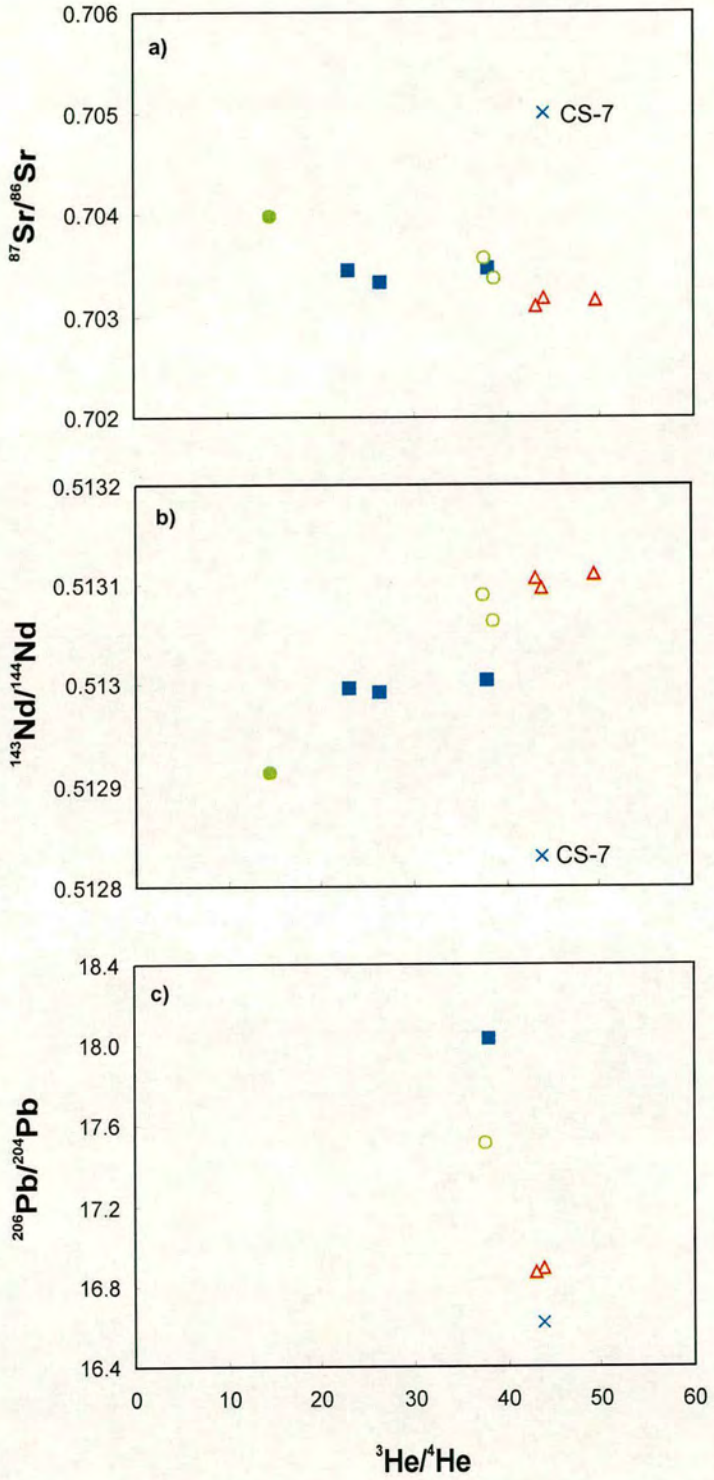

Fig. 3.17. (a) $^{87}Sr/^{86}Sr$-$^{3}He/^{4}He$, (b) $^{143}Nd/^{144}Nd$-$^{3}He/^{4}He$ and (c) $^{206}Pb/^{204}Pb$-$^{3}He/^{4}He$ plots for selected lava flows and dykes on Baffin Island. Symbols as in Fig. 7.13.

III Discussion

4 Olivine-liquid equilibrium

4.1 Introduction

The use of the terms "picrite" and "komatiite" and the distinction between these two definitions has led to scientific debate over the nomenclature of ultramafic rocks. According to the petrographic definition, a picrite is a mafic volcanic rock with abundant olivine crystals, while the second definition is based on chemical criteria proposed by the International Union of Geological Sciences (IUGS) Subcommission on the Systematics of Igneous Rocks (Le Maitre, 1989). This definition describes a picrite as a volcanic rock with SiO_2 <47 wt. %, total alkalis <2 wt. % and MgO >18 wt. %. The 1998 IUGS classification has been revised for high-Mg and picritic volcanic rocks (Le Bas, 2000) and as a result, the 18 wt. % minimum MgO now applies only to komatiites and meimechites, while the minimum MgO for picrites is reduced to 12 wt. %. Discussion over the merits of the new IUGS chemical classification continues (Kerr & Arndt, 2001; Le Bas, 2001), because the terms "komatiite" and "picrite" are only used in a purely chemical sense. The chemical classification still ignores their distinctive textural features, according to which komatiites are characterised by crystalline quench textures (Viljoen & Viljoen, 1969), also called spinifex textures (Nesbitt, 1971), whereas picrites lack these features. In order to avoid confusion, the term "picrite" should be used in a clear and specific sense, and an objective definition that incorporates both textural and chemical criteria might be best (Kerr & Arndt, 2001). However, the chemical classification has to be used with caution if the volcanic rock contains accumulated olivines (e.g. Le Maitre, 1989; Le Bas, 2001). Neither the petrographic nor the chemical definition for picrites take into account the origin of the rock. Commonly, it is thought that picrites form from MgO-rich magmas. However, a rock, defined by both the petrographic and chemical classifications as a picrite, could also have been produced by the accumulation of olivines from a liquid with basaltic composition.

Furthermore, the accumulated olivines could be either phenocrysts, which crystallised from the host magma, or xenocrysts originating from a foreign source. It is therefore essential, when studying high-MgO lavas, to establish by independent means the origin of the olivine crystals and the composition of the host/parental magma. Such parental melts of highly magnesian rocks could be close to that of primary mantle-derived melts and therefore their identification might help to understand mantle compositions and conditions at which volcanic rocks were formed.

The West Greenland/Baffin Island lavas contain up to 30 wt. % MgO and these high-magnesium volcanic rocks have been a focal point of controversy over the MgO contents of primary magmas in general. The higher values of this range might represent either primary liquids rising from the mantle (Clarke, 1970; Clarke & O'Hara, 1979; Francis, 1985) or reflect the mechanical accumulation of olivine phenocrysts (Hart & Davies, 1978, 1979). Previous authors have disagreed about the MgO concentrations in primary magmas erupted in the Baffin Bay volcanic province. While Clarke (1970) and Clarke & O'Hara (1979) argued for primary liquids with 19-20 wt. % MgO, Hart & Davies (1978, 1979) claimed, on the basis of Ni-partitioning between olivine and liquid, that rocks with more than 11-13 wt. % MgO contain accumulated olivine. Pedersen (1985) measured olivines with up to $Fo_{92.5}$ in Tertiary picrites from West Greenland and calculated liquid MgO contents of 18-19 wt. %. Francis (1985) regarded olivines with forsterite contents up to 93 mol. % of the Padloping Island suite as xenocrysts. However, if these forsteritic olivines represent early cumulates (not xenocrysts), then the existence of liquids with more than 18 wt. % MgO is likely. On the other hand, if the less forsteritic phenocryst compositions (Fo_{86-89}) are only taken into account, Francis (1985) argued for primary compositions with 11-13 wt. % MgO, similar to the estimates of Hart & Davies (1978, 1979). More recent publications, however, showed that primary high-Mg liquids (20-21 wt. % MgO) did exist at depth in West Greenland, but only liquids with lower MgO contents (10-14 wt. % MgO) actually erupted on the surface (L.M.Larsen & Pedersen, 2000). In contrast to Francis (1985), who defined the MgO-

rich olivines as xenocrysts on Baffin Island, L.M.Larsen & Pedersen (2000) suggested that these olivines were integral parts of the cognate mineral assemblage of the West Greenland picrites. Herzberg & O'Hara (2002) used a new method for constraining the composition of primary magmas. Their model does not use olivine compositions and FeO-MgO exchange coefficients (e.g. Albarede, 1992; Langmuir et al., 1992; L.M.Larsen & Pedersen, 2000; Thompson & Gibson, 2000) to calculate primary magmas. Instead, they developed a method that involves a parameterisation of large experimental database, providing forward modelling of potential primary magma compositions that exit in the melting regime in the mantle (represented in CMAS projections and FeO-MgO plots). For Baffin Island, they used a sample of Robillard et al. (1992) and estimated primary magmas with MgO contents of 17-20 wt. %. Furthermore, they concluded that high Mg-olivines (Fo_{93}) in Icelandic plume lavas may be either wall-rock xenocrysts from refractory plume mantle or phenocrysts from perfect fractional melts, which exited the melting regime and mixed with other melts before eruption.

4.2 Origin of the Baffin Island lavas

4.2.1 Classification of the lavas

The samples from Baffin Island are MgO-rich (Chapter 3) and contain a large proportion of olivine crystals. According to the new 1998 IUGS classification for high-Mg and picritic volcanic rocks (Le Bas, 2000), around 40 % of all analysed samples could be classified as komatiites (Fig. 3.7). However, the lavas do not show any spinifex textures and also contain accumulated olivines (see the following discussion). The chemical classification, therefore, has to be used with caution and consequently, the lavas with more than 12 wt. % MgO are called "picrites" and the term "komatiites" will not be used in this study.

4.2.2 Olivine control lines

In order to establish the nature of the picrites on Baffin Island and to help resolve the controversy about the MgO contents of the primary magmas, a detailed analysis of olivine compositions from Durban Island was carried out. As Padloping Island olivine compositions have already been analysed by Francis (1985, 1986), only some representative olivine compositions for the different magma types (section 3.4 and 3.5) and the dyke(s) on Padloping Island and Cape Searle were measured. One test to establish whether an olivine-rich magma represents a primary liquid is to compare the Fo contents of the phenocrysts with the calculated liquidus olivine for this rock. If the calculated composition of the liquidus olivine matches the observed olivine composition in the rock, then the lava may represent a primary liquid composition. In contrast, if the calculated liquidus olivine is more magnesian than the observed olivine composition, then the lava probably contains accumulated olivines. The liquidus olivine in equilibrium with the bulk-rock composition can be calculated from the Fe/Mg partition coefficient ($K_D = 0.3 \pm 0.03$) between olivine and liquid (Roeder & Emslie, 1970). Fig. 4.1 shows the Fo contents of the measured olivines from a) Durban Island and (b) combined Padloping Island and Cape Searle, respectively, as a function of the Mg-number (Mg# = atomic $Mg/(Mg+Fe^{2+})$) of their host rock. In order to calculate the Mg# of the rock, it is necessary to estimate the Fe_2O_3/FeO ratio. By considering only the true amount of FeO exchangeable with olivine, Herzberg & O'Hara (2002) used FeO and Fe_2O_3 values ($Fe^{3+}/\Sigma Fe=0.1$) for Baffin Island that have been determined by wet chemistry on Padloping Island rocks (Robillard et al., 1992). Until additional data are available, it seems that a $Fe^{3+}/\Sigma Fe$ ratio of 0.1 is the most reasonable estimate for Baffin Island.

The Fo content of the olivine phenocrysts will depend on the MgO/FeO ratio of the melt, and as this decreases with cooling and crystallisation, the most forsteritic olivines in

individual lavas will indicate the MgO content of their initial bulk composition. For Durban Island (Fig. 4.1a) most of the analysed olivines are clearly out of equilibrium with their host magma. They also plot to the right of the equilibrium field, indicating that the samples might contain excess olivine. However, olivines of DI-20 ($Fo_{84.7}$) and high-forsterite olivines from DI-27 (up to $Fo_{91.8}$) were in equilibrium with their host rock. The occurrence of such highly forsteritic olivines in Durban Island suggests that high-magnesium melts with MgO contents up to 17.5 wt. % (calculated assuming $K_D^{Ol/L}{}_{FeO/MgO} = 0.3$) were available in the formation of the Baffin Island picrites. Whether these high forsteritic olivines in the lava flows represent phenocrysts or xenocrysts in the rocks in which they are now found, will be discussed in more detail later in this chapter. As well as the Durban Island lavas, the few analysed olivine crystals from Padloping Island and Cape Searle (Fig. 4.1b) are also not in equilibrium with the whole rock of their hosts and contain accumulated olivines. However, the dykes from Cape Searle (CS-7) and Padloping Island (PI-16) contain very magnesian olivines (up to $Fo_{92.9}$), which were in equilibrium with liquids with 19.64 wt. % MgO. If these olivines are not xenocrysts (and it seems very likely, see discussion below), but part of the whole magma evolution history of Baffin Island, then the liquid composition in equilibrium with these highly magnesian olivines actually might represent or be close to the liquid primary composition. The olivines of DI-13 have very low forsterite contents (64.36 - 71.89 mol.%). This may be either because not enough olivine grains were analysed in order to sample the most Fo-rich olivine, or because more evolved, groundmass olivines were analysed instead of phenocrysts.

The bulk composition of magnesian rocks can also help to determine whether the suite of lavas represent primary liquids or if they were formed by the accumulation of olivines. If the rocks are cumulates, they will plot in many geochemical variation diagrams on tight linear trends that project back to the cumulus olivine composition (e.g. Krishnamurthy & Cox, 1977). The Baffin Island samples do define such olivine control

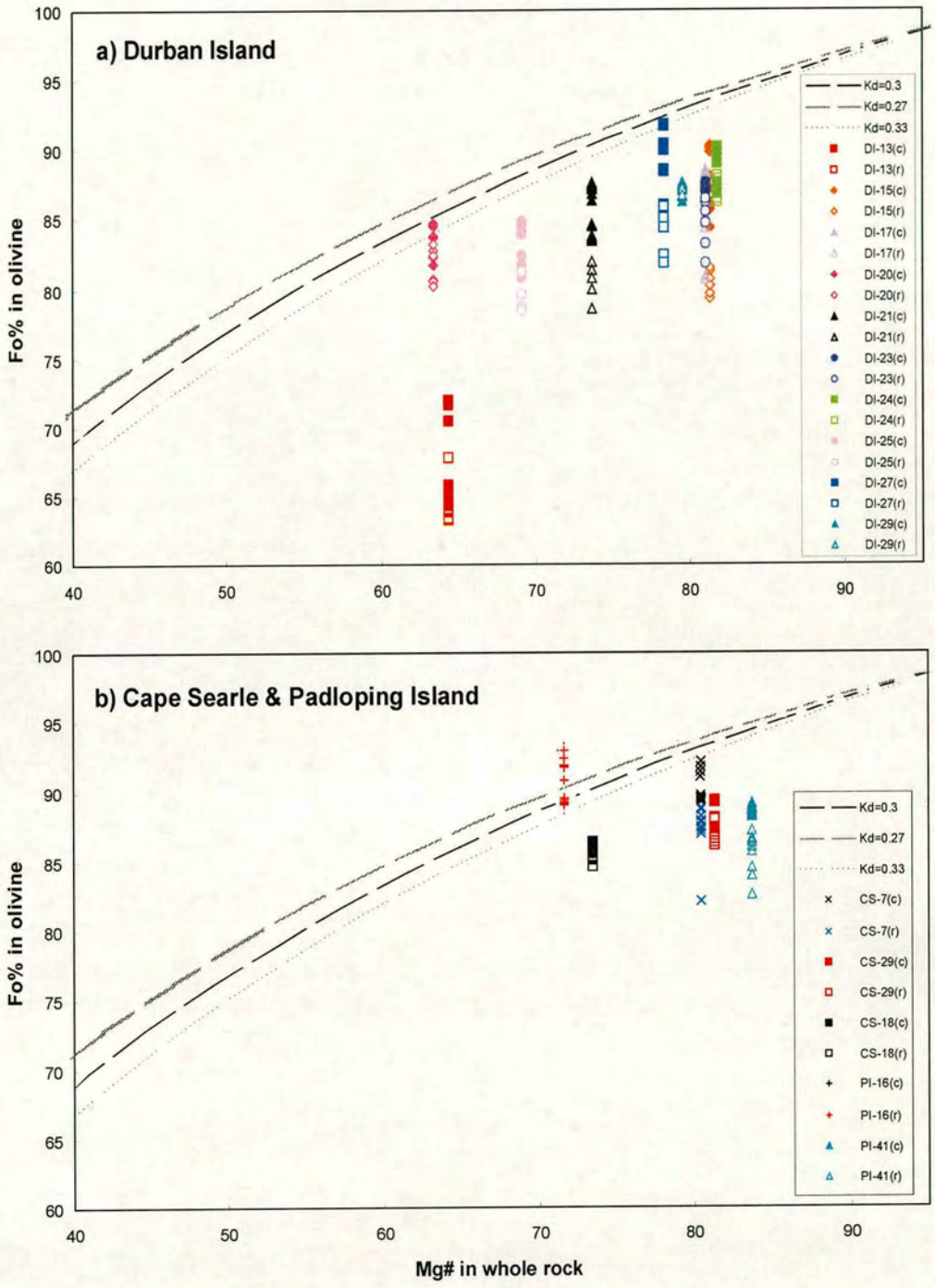

Fig. 4.1. Plot of whole-rock Mg-number (atomic 100*(Mg/(Mg+Fe^{2+})) assuming 10 % Fe^{3+} (see text for discussion of this estimate) vs. forsterite in olivine phenocrysts of (a) Durban Island and (b) Cape Searle and Padloping Island. The equilibrium field is based on Fe/Mg between olivine and whole rock (K_d = 0.3 ±0.03) after Roeder & Emslie (1970).

trends in MgO-oxide variation diagrams (see also chapter 3), suggesting that they do not represent primary liquids, but instead might be mixtures between melt(s) and either, (1) varying proportion of accumulated olivine, (2) olivines picked up on the way to the surface or (3) xenocrysts. By using the diagram Al/(Mg + Fe) versus Mg/(Mg + Fe) (Fig. 4.2), the intersection of the olivine-control trend with the abscissa provides an estimate of the olivine composition dominating the trend (Irvine, 1979). The regression line gives an estimated olivine composition of ~Fo_{90} for all analysed samples on Baffin Island. Considering the three locations individually, Durban Island and Cape Searle data extrapolate to an olivine composition of ~Fo_{89}, while data from Padloping Island lava flows and Cape Searle dykes trend towards more-forsteritic olivines (~Fo_{91} and ~$Fo_{92.5}$, respectively).

Linear variations between bulk-rock MgO and FeO show similar estimated compositions for the average cumulus olivine of all analysed samples and for each of the three locations considered individually (Fig. 4.3 and Table 4.1). However, the olivine control lines provide a different picture if the lava flows are separated by their geochemical signatures (see section 3.4 and 3.5), which are summarised in Table 4.1. Note that in all three locations the stratigraphically lower samples point towards more magnesian olivines (~Fo_{90}) than do the middle and upper samples (Fo_{87-89}), independent of their geochemical signature. Fig. 4.3 also shows a frequency histogram. According to this, the majority of measured olivine composition of the lava flows is less magnesian (Fo_{87-89}) than predicted by the olivine control lines (Fo_{90}). In more detail, only ~10 % of the analysed olivines in the lava flows have forsterite contents of 90 mol. % or higher, while ~58 % have compositions of Fo_{87-89}. Because the magnesian olivines (>Fo_{90}) are also rare in West Greenland, L.M.Larsen & Pedersen (2000) suggested that these olivines might remain in the conduit system during magma ascent and only the more iron-rich olivines erupted on the surface. This interpretation is a plausible explanation for the less frequent occurrence of high-forsterite olivines in Baffin Island lavas. However, the abundance (%) of olivine compositions of the dykes on Padloping Island and Cape

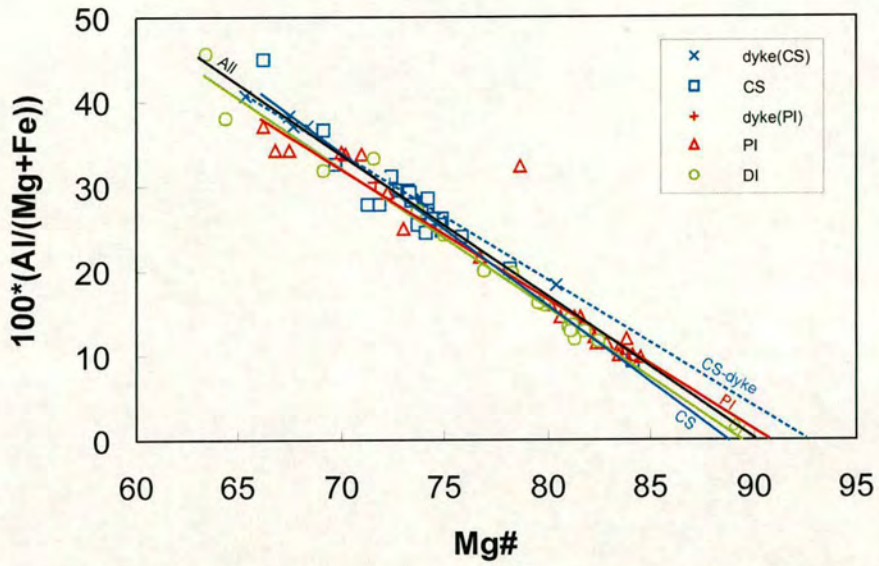

Fig. 4.2. Atomic (100* [Al / (Mg+Fe)]) versus Mg# for lavas from Baffin Island. FeO is calculated assuming Fe^{3+} / Σ(Fe) = 0.1 (see text for discussion). Regression lines are shown for all analysed Baffin Island samples and for Padloping Island (PI), Durban Island (DI), Cape Searle (CS) and Cape Searle dykes (CS-dyke). The intersection with the abscissa is for BI: Fo_{90}; DI+CS: $Fo_{\sim 89}$; PI: Fo_{91} and CS-dyke: $Fo_{92.5}$.

Table 4.1. Summary of the graphically estimated olivine compositions in Fig. 4.2 and 4.3

Olivine control lines		
	estimated Fo-content of olivine after plot:	
	MgO vs. FeO	100 (Al/(Mg+Fe))
All samples	89.7	90
Durban Island		
all	90.0	89.2
top (low Nb/Zr)	89.6	89.5
middle (high Nb/Zr)	87.6	87.0
low (low Nb/Zr)	90.2	90.4
Padloping Island		
all	90.4	91.0
top (high Nb/Zr)	87.0	86.0
low (low Nb/Zr)	90.0	91.0
Cape Searle		
all	89.8	89.0
dyke (low Nb/Zr)	92.8	92.5
top (low Nb/Zr)	89.2	88.5
low (high Nb/Zr)	90.2	92.0

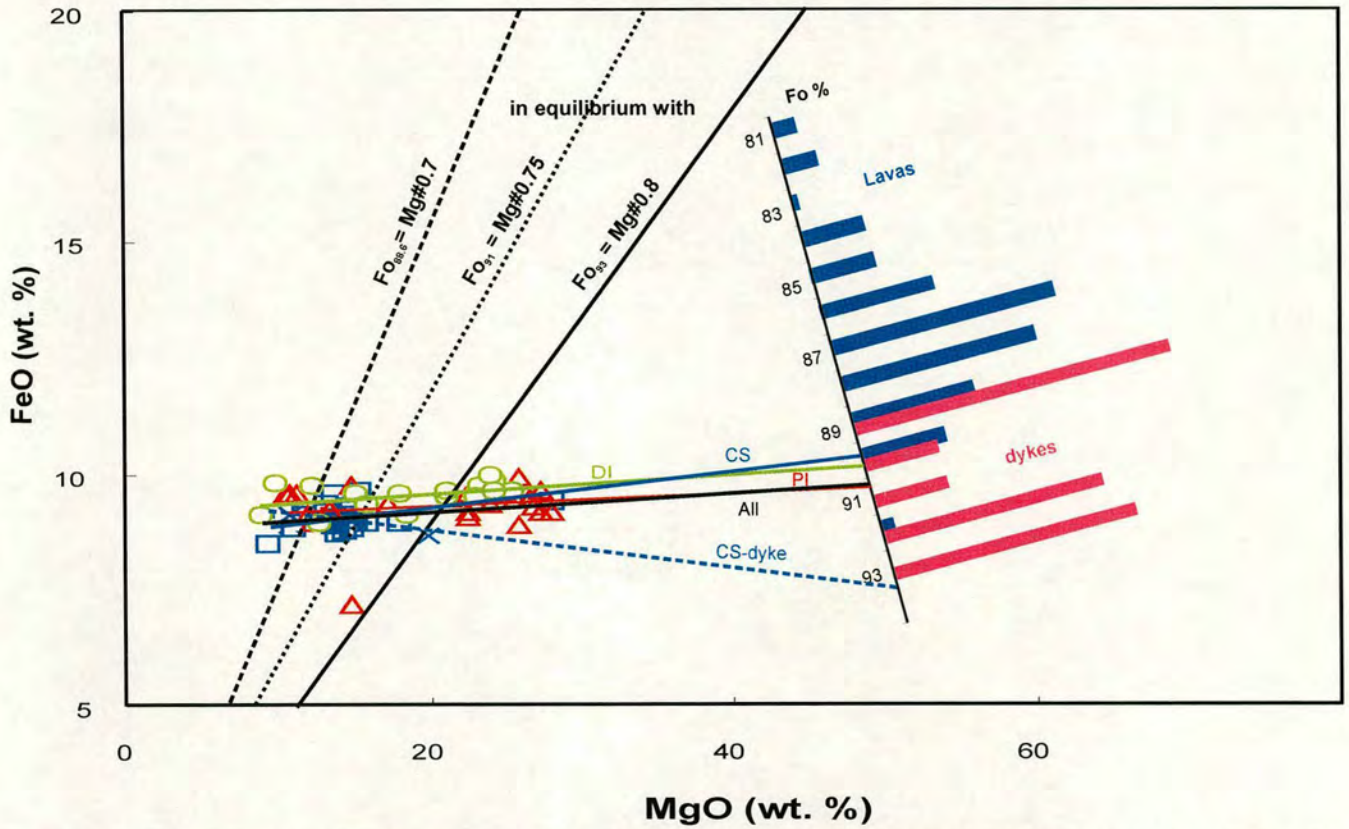

Fig. 4.3. Whole-rock FeO vs. MgO. The near-horizontal lines indicate the least-square regression line to the whole-rock FeO-MgO contents (i.e. olivine control line). Regression lines are shown for all analysed Baffin Island lava flows, for Durban Island (DI), Padloping Island (PI), Cape Searle lavas (CS) and dykes (CS-dyke). The intersection of the olivine control line with the olivine composition line (Fo %) defines the average accumulated olivine composition of Fo_{90}, $Fo_{\sim 90}$, $Fo_{90.4}$, $Fo_{89.8}$ and $Fo_{92.8}$, respectively. The frequency histogram illustrates the volume % of the olivine core composition of the lava flows and dykes. The oblique lines reflect the FeO/MgO of melts in equilibrium (assuming K_D = 0.3 (Roeder & Emslie, 1970) with the most forsteritic olivines. The liquids with constant Mg# of 0.7, 0.75 and 0.8 are in equilibrium with the olivine composition of $Fo_{88.6}$, Fo_{91} and Fo_{93}, respectively. The intersection of these lines with the olivine control lines provides an estimate of the composition of the liquid from which their olivines crystallised. Symbols as in Fig. 4.2.

Searle are fundamentally different from the lava flows. First, no olivines with less than Fo_{89} were measured in the dykes. Second, only 34 % of the analysed olivines of the dykes have Fo_{89}, while ~66 % are more magnesian than Fo_{90}, of which 26.3 % are Fo_{93}. This observation suggests that the explanation, that most of the highly magnesian olivines were left at depth, might apply to the lava flows but not to the dykes. Moreover it demonstrates that the highly magnesian olivines have been an integral part of the cognate mineral assemblage, but that they erupted, probably at higher ascent velocities, only in the dykes, and not so abundantly in the lava flows.

Because some of the most Mg-rich olivines (>Fo_{90}) show kink-bands, Francis (1985, 1986) classified them as xenocrysts (from magmatic and not mantle sources), but also mentioned that they could represent early (dunitic) cumulates which had failed to reach the surface. However, the presence or absence of kink-bands did not distinguish xenocrysts from phenocrysts in this study. For example, PI-16 contains the most forsteritic olivine (Fo_{93}) analysed (chapter 3). This olivine not only lacks any kink-bands, but also forms a perfect euhedral crystal. It is difficult to imagine how it could have survived prolonged transport as a xenocryst and therefore it is more likely that it was precipitated from an ultramafic magma as a phenocryst. Furthermore, even through some of the complex-textured olivines on Baffin Island do occasionally show kink-bands, the source of these deformed olivines is more likely within this magmatic system rather than in the underlying mantle. The CaO (0.25-0.32 wt. %) and Cr_2O_3 (0.10-0.20 wt. %) contents of the Baffin Island olivines with >Fo_{90} (see section 3.2. and Fig. 3.5) are far above the values for mantle olivines (<0.1 wt. % CaO and <0.01 wt. % Cr_2O_3 for spinel- and <0.04 wt. % Cr_2O_3 for garnet lherzolite; e.g. Hervig et al., 1986; Bernstein et al., 1998). The crystals also contain glass inclusions indicating that these highly magnesian olivines crystallised from melts and are thus unlikely to be mantle xenocrysts.

4.2.3 Calculation of the parental liquid composition and temperature

It has been shown above that most of the olivines in the lava flows, and to a lesser extent the dykes, on Baffin Island are not in equilibrium with their host rock. The bulk composition of the rocks appears to have been compromised by a significant accumulation of olivine phenocrysts and therefore the whole-rock compositions should not be used as direct indicators of their primary or parental liquid composition. The process of olivine accumulation can be corrected for, and the procedure for an olivine addition/subtraction method (similar to that of Green et al., 2001) is outlined below. As mentioned above (section 4.2.2), the equilibrium liquidus olivine for a particular bulk-rock composition can be calculated (assuming $K_{D\,FeO/MgO}^{Ol/L} = 0.3$; Roeder & Emslie, 1970). This composition is compared to the analysed olivine composition in the rock. If the most magnesian observed olivine composition is lower than the calculated parental liquid one, then the analysed olivine composition is incrementally subtracted from the bulk rock to obtain a new composition (the inferred parental liquid composition), for which the calculated liquidus olivine matches the observed olivine composition. In contrast, if the most magnesian observed olivine composition is higher than the calculated liquid one, then the analysed olivine composition is incrementally added to the bulk rock. Table 4.2 summarises the procedure and Fig. 4.4 illustrates the method graphically. The parental liquid composition for DI-13 has not been calculated, because the analysed olivines are likely to represent either microphenocrysts with lower forsterite contents, or groundmass olivines.

For example, the liquidus olivine composition of the whole-rock composition of DI-24 (MgO = 24.59 wt. %) is calculated to be $Fo_{93.71}$, but the most magnesian olivine (ol7c1) measured has only $Fo_{90.15}$. By subtracting 32.27 % of the observed olivine composition from the bulk-rock, the calculated olivine composition matches the analysed one

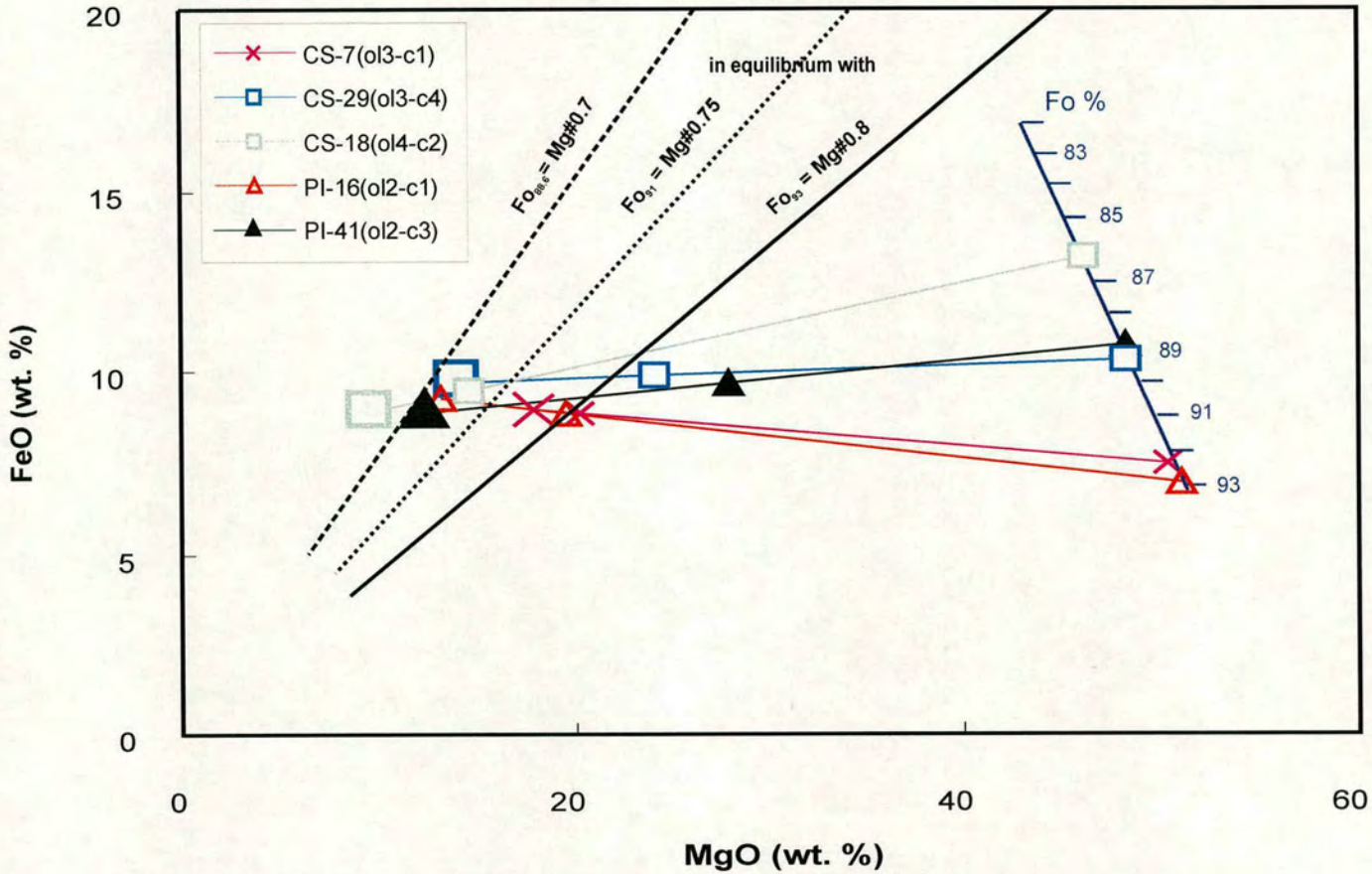

Fig. 4.4.b. The addition/subtraction method displayed graphically for Cape Searle and Padloping Island. For explanation see Fig. 4.4a.

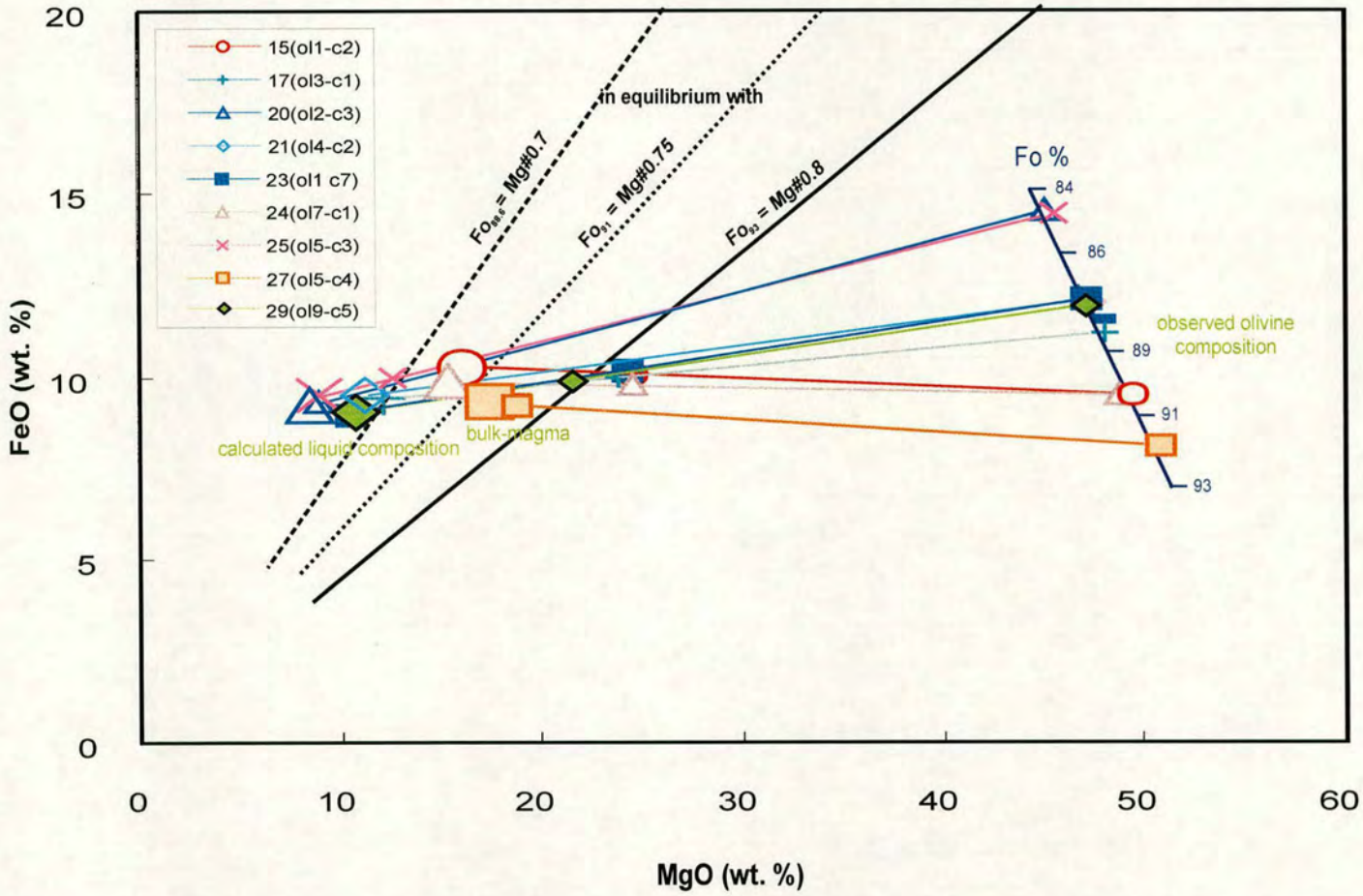

Fig. 4.4a. The addition/subtraction method displayed graphically for Durban Island. For the outline of the diagram see Fig. 4.3. The observed olivine composition is subtracted from or added to the bulk-magma, until the composition matches the calculated olivine composition (assuming $K_D^{ol/L}{}_{FeO/MgO}$ = 0.3, Roeder & Emslie, 1970). The new composition presents the calculated liquid composition (bigger symbol). This method is shown for sample DI-29 in more detail.

Table 4.2. Summary of the accumulation/fractionation correction of the Baffin Island lava flows and dykes

Sample	olivine	MgO-rock	Fo(cal)	Fo(real)	method	inferred parental MgO	% add/sub ol
DI-15	ol1 c2	24.54	93.55	90.28	sub	16.01	29.2
DI-17	ol 3c1	23.85	93.42	88.50	sub	12.22	39.1
DI-20	ol2 c3	9.03	85.23	84.65	sub	8.57	1.3
DI-21	ol4 c2	15.27	90.30	87.55	sub	11.20	11.9
DI-23	ol1c7	24.28	93.44	87.59	sub	10.74	45.9
DI-24	ol7 c1	24.59	93.71	90.15	sub	15.28	32.3
DI-25	ol5 c3	12.52	88.16	84.86	sub	8.96	10.2
DI-27	ol5 c4	18.73	92.32	91.78	sub	17.48	3.8
DI-29	ol9 c5	21.58	92.82	87.54	sub	10.69	35.4
CS-7	ol3 c1	20.28	93.18	92.28	sub	17.94	7.5
CS-29	ol3 c4	24.12	93.54	89.32	sub	13.69	35.8
CS-18	ol4 c2	14.71	90.19	86.20	sub	9.33	15.8
PI-16	ol1 c2	13.14	89.37	92.97	add	19.67	18.9
PI-41	ol2 c3	27.89	94.48	88.91	sub	11.95	57.6

Column 1: analysed samples
Column 2: olivine used for calulation
Column 3: MgO-content of bulk rock (recalculated to 100% volatile-free)
Column 4: calculated forsterite (mol. %) for olivine in equilibrium with bulk-rock, assuming $K_D^{ol/L}{}_{Fe/MgO} = 0.3$ (Roeder & Emslie, 1970)
Column 5: observed most magnesian olivine
Column 6: correceted method (add/subtract observed olivine until in equilibrium with calculated olivine composition)
Column 7: inferred MgO (wt. %) of calculated parental liquid
Column 8: % olivine added/subtracted

($Fo_{90.15}$) and the new inferred parental liquid composition now contains 15.28 wt. % MgO. Calculations for Durban Island lavas give a wide range of parental liquid compositions with 8.6-17.48 wt. % MgO (Table 4.2). However, if the lava flows are divided by their geochemical characteristics (chapter 7) then the depleted lavas generally show more magnesian liquid composition estimates (12.22-17.48 wt. % MgO) than the enriched middle series lava flows (8.6-11.2 wt. % MgO). The same picture can be seen in Padloping Island and Cape Searle (Table 4.3) where the depleted lava flows display liquid compositions of 11.6-13.7 wt. % MgO, while the enriched flows contain only 9.33 wt. % MgO. The dykes on Padloping Island and Cape Searle have more magnesian calculated liquid compositions than the lava flows (19.6 wt. % and 17.9 wt. % MgO, respectively). The observed olivine compositions ($Fo_{92.28}$) of the dyke CS-7 had, like all lava flows, to be subtracted from the bulk-rock (20.28 wt. % MgO). In contrast, the Padloping dyke bulk-rock MgO content is quite low (13.14 wt. %), but contains phenocrysts (not xenocrysts, see discussion above) with $Fo_{92.9}$, which had to be added to the bulk-rock composition in order to account for the estimated liquid composition (19.6 wt. % MgO).

The wide range of olivine compositions suggests that the olivines could not have been in equilibrium with a single magma. Instead, it seems more likely that a complex magmatic system was available in Baffin Island leading to several batches of magmas in equilibrium with olivines of various compositions, all mixing on the way to the surface.

As the bulk-rocks on Baffin Island do not represent primary liquid compositions, but contain accumulated olivines, the inferred calculated parental liquid composition was used to estimate the temperature (Table 4.3). By using the Ford et al. (1983) geothermometer the liquidus temperatures at 1 atm were calculated for the Baffin Island lavas and dykes. Depending on the method used, the temperatures are 1339-1358° C (T_{Fe}) and 1211-1332° C (T_{Mg}) for the lava flows and 1414-1430° C (T_{Fe}) and 1339-1358° C (T_{Mg}) for the dykes. Segregation temperatures, calculated for the (magmas segregated

from their source peridotite) parental liquid compositions by the method of Albarede (1992), range between 1288 and 1500° C for the lava flows and between 1389 and 1552° C for the dykes. The temperatures calculated using the method of Albarede (1992) are higher, because this method calculates the temperature of primary magmas at the depth of segregation, while the temperatures calculated after Ford et al. (1983) are of parental magmas at the time the olivines started to crystallise.

With their forward model of a depleted peridotite source, Herzberg & O'Hara (2002) calculated primary magmas with 18-20 wt. % MgO for Baffin Island. These magmas have eruption temperatures of about 1400-1440 °C, intersecting the solidus for fertile peridotite at 3.8-4.7 GPa, and have potential temperatures of 1520-1570° C. This interpretation is in good agreement with the results of this study.

Table 4.3. Summary of calculated liquid compositions and temperatures of the Baffin Island rocks

Sample	DI-15	DI-17	DI-20	DI-21	DI-23	DI-24	DI-25	DI-27
olivine	ol1 c2	ol3 c1	ol2 c3	ol4 c2	ol1 c7	ol7 c1	ol5 c3	ol5 c4
SiO_2	48.11	49.48	49.60	48.51	49.68	48.22	49.17	48.08
Al_2O_3	12.12	14.46	16.46	15.91	15.41	13.52	16.04	12.29
$FeO_{(0.1)}$	10.23	9.42	9.22	9.44	9.03	9.90	9.49	9.29
MgO	16.01	12.22	8.57	11.20	10.74	15.28	8.96	17.48
CaO	10.55	11.67	13.07	11.88	11.72	10.68	13.48	10.29
Na_2O	1.45	1.26	1.70	1.58	1.66	1.18	1.50	1.33
K_2O	0.04	0.04	0.06	0.06	0.11	0.04	0.02	0.04
TiO_2	0.87	1.01	1.07	1.10	1.12	0.88	1.03	0.74
MnO	0.19	0.19	0.18	0.17	0.19	0.18	0.18	0.17
NiO	0.04	0.08	0.02	0.03	0.00	0.03	0.01	0.08
CrO	0.31	0.27	0.06	0.14	0.40	0.31	0.09	0.19
Total	100	100	100	100	100	100	100	100
Mg#(liquid)	73.63	69.82	62.37	67.89	67.95	73.34	62.74	77.04
Mg#(rock)	81.33	81.00	63.42	73.67	81.05	81.73	69.12	78.32
T_{Mg}[1]	1317	1263	1209	1252	1245	1307	1211	1332
T_{Fe}[1]	1392	1340	1280	1322	1319	1383	1283	1405
T[2]	1468	1365	1264	1344	1324	1450	1277	1502

Sample	DI-29	CS-7	CS-29	CS-18	PI-16	PI-41
olivine	ol9 c5	ol3 c1	ol3 c4	ol4 c2	ol1 c2	ol2 c3
SiO_2	49.27	48.26	48.81	49.17	47.70	49.36
Al_2O_3	15.63	12.45	14.22	16.67	11.57	15.39
$FeO_{(0.1)}$	9.03	8.91	9.71	8.86	8.87	8.85
MgO	10.69	17.94	13.69	9.33	19.67	11.95
CaO	12.60	10.46	10.73	12.95	10.07	11.83
Na_2O	1.38	1.00	1.40	1.65	1.14	0.97
K_2O	0.03	0.05	0.06	0.04	0.04	0.12
TiO_2	1.11	0.51	1.06	1.05	0.52	1.02
MnO	0.18	0.17	0.19	0.18	0.16	0.17
NiO	0.02	0.08	0.02	0.01	0.12	0.00
CrO	0.28	0.23	0.28	0.13	0.12	0.38
Total	100	100	100	100	100	100
Mg#(liquid)	67.85	78.22	71.54	65.24	79.78	70.66
Mg#(rock)	79.53	80.41	81.31	73.42	71.63	83.71
T_{Mg}[1]	1241	1339	1289	1222	1358	1263
T_{Fe}[1]	1314	1414	1365	1291	1430	1341
T[2]	1326	1511	1407	1288	1552	1370

For details of calculation methods, see text and Fig. 4.1 and 4.2.

[1]Ford et al. (1983); temperatures of parental magmas at the time the olivines started to crystallise

[2]Albarede (1992); temperatures of primary magmas at the depth of segregation

4.3 Summary

The Baffin Island samples are MgO-rich (8.9-28.1 wt. %, mean 17.6 wt. %) and contain a large proportion of olivine crystals. In order to investigate whether the lava flows and dykes represent liquid compositions or if they were formed by olivine accumulation, olivine compositions were analysed, in detail from Durban Island and less comprehensively from Padloping Island and Cape Searle. Comparisons of the most magnesian olivine phenocrysts in each of the analysed flows with the liquidus olivine composition calculated for these rocks, indicate that most of the lavas are not in equilibrium with their host rock. The average analysed olivine composition (Fo_{87-89}) suggests that lavas with >14 wt. % MgO have accumulated olivines in various proportions. However, the rare occurrence (~10 %) of olivines with forsterite contents up to 91.8 mol. % demonstrate that magnesian melts with MgO contents up to 17.5 wt. % were also available in the formation of the Baffin Island lava flows. The dykes on Padloping Island and Cape Searle contain much higher proportions (58 %) of Fo-rich olivines (highest measured value $Fo_{92.9}$), which were in equilibrium with liquids with 19.6 wt. % MgO. It has been demonstrated that these magnesian olivines do not represent xenocrysts, but were instead part of the cognate mineral assemblage on Baffin Island. L.M.Larsen & Pedersen (2000) concluded that most of the high magnesian olivines in the West Greenland picrites stayed behind in the conduit system, and only the more iron-rich olivines erupted at the surface. This conclusion applies to the lava flows but not to the dykes on Baffin Island. A different process (e.g. higher ascent velocities, turbulent flow) must have taken place during the dykes' eruption, leading to the large quantity of highly magnesian olivines.

To correct for the olivine accumulation process and to determine the parental liquid composition in equilibrium with the most Fo-rich observed olivine in each sample, an olivine-addition/subtraction method was used. The results show parental liquid compositions with MgO contents of 8.6-17.5 wt. % for the lava flows and 17.9-19.6 wt.

% for the dykes. The wide range of the olivine compositions, which led to the large variety of the calculated parental liquid compositions, demonstrates that the olivines cannot have been in equilibrium with a single magma type. They probably reflect the history of a complex magmatic system, in which several batches of magmas have been mixed, and only a small proportion of these mixtures actually reached the surface. Estimates for the parental liquidus temperature at the time that the olivines started to crystallise range from 1211 to 1358° C for the lava flows and from 1339 to 1430° C for the dykes (depending on the calculation method used).

5 Crustal contamination

5.1 Introduction

Before either the mantle source characteristics or the melting regime of the Tertiary rocks on Baffin Island can be investigated (see chapter 6 and 7), it is necessary to determine whether or not the lavas interacted with continental crust. Various workers have shown the effects of crustal contamination on lava compositions from several locations in the NAIP, such as West Greenland (section 2.2.1), East Greenland (Holm, 1988; Fram & Lesher, 1997; Hansen & Nielsen, 1999; Fitton et al., 1998, 2000; Saunders et al., 1999) and the British Isles (Dickin, 1981; Thompson et al., 1982, 1986). Studies in the British Tertiary Igneous Province (BTIP) have identified contaminants of metasediments and of both amphibolitic and granulitic continental crust (Carter et al., 1978; Dickin, 1981; Thompson, 1982). Similar contamination processes have been recorded in East Greenland. The Ocean Drilling Program (ODP) Leg 152 data at the SE Greenland margin shows that the early lavas have been contaminated with granulite-facies gneiss (probably lower crust), while the composition of later lava flows have isotopic characteristics typical of upper crustal amphibolite-facies gneiss (Fitton et al., 1998). In contrast, the isotopic composition of the stratigraphically lower basalts around the Kangerlussuaq Fjord in central East Greenland have been affected by crustal contamination with amphibolite, whereas at higher stratigraphic levels lavas show inputs of granulite-facies gneiss (Hansen & Nielsen, 1999). Holm (1988), however, suggested minor influence from crustal contamination. Instead, he explained the variation of the Sr, Nd and Pb isotopes of East Greenland lavas as a result of interaction between four mantle-derived components: (1) an enriched old lithospheric mantle, (2) an ocean island basalt (OIB)-type mantle, (3) a typical Icelandic source and (4) a less enriched, lithospheric mantle.

Evidence of crustal contamination processes has been also recorded in West Greenland, where both a sediment and a felsitic continental crust contaminant have been identified (Pedersen, 1985b; Pedersen & Pedersen, 1987; Goodrich & Patchett, 1991; Pedersen et al., 1996; Lightfoot et al., 1997; Schäfer et al., 2000). A more detailed summary of West Greenland contamination is given in section 2.2.1. On Baffin Island, magmas rose through Archaean and Proterozoic crust, as well as Tertiary sedimentary sequences (e.g. Jackson & Taylor, 1972; Burden & Langille, 1990; Jackson & Berham, 2000) and contamination during their ascent is a distinct possibility and has to be taken into account.

5.2 Modelling contamination processes

Some incompatible trace element ratios, such as Ba/Zr, Ba/Nb, La/Nb and Th/Nb, are increased and distinctive in crustal material (see Table 5.1 for average continental crust, MORB and primitive mantle compositions). Higher values of such ratios, combined with higher SiO_2 and K_2O, as well as disturbed isotope ratios, could be the result of crustal contamination. Some Baffin Island rocks are more extreme (higher $^{87}Sr/^{86}Sr$ and lower $^{143}Nd/^{144}Nd$) than any rocks analysed from Iceland and such ratios could have been influenced by crustal material. However, the Baffin Island rocks do not show clear correlations between isotope ratios ($^{87}Sr/^{86}Sr$ and $^{143}Nd/^{144}Nd$) and indices of either differentiation (e.g. SiO_2 content) or contamination (e.g. incompatible trace elements).

Fig. 5.1a shows a plot of Ba/Zr versus SiO_2. The Baffin Island samples show, firstly, not very high Ba/Zr (<1.6) and SiO_2 (<50 wt. %) values and, secondly, no positive correlation (which would be expected if the samples have been stored, differentiated and crustally contaminated in crustal magma reservoirs). Similar patterns can be seen in plots like Ba/Nb versus $^{143}Nd/^{144}Nd$ (Fig. 5.1.b), Th/Nb versus SiO_2 (Fig. 5.1.c) and

Table 5.1. Average values of SiO_2, TiO_2, K_2O, Ba/Zr, Ba/Nb, La/Nb, Th/Nb for primitive mantle, N-MORB and continental crust

	Primitive mantle	**N-MORB**	**Continental crust**
SiO_2 (wt. %)	44.93	50.45 (b)	59.10
TiO_2 (wt. %)	0.20	1.27 (a)	0.70
K_2O (wt. %)	0.03	0.07 (a)	1.88
Ba/Zr	0.63	0.085 (a)	3.17
Ba/Nb	10.03	2.70 (a)	32.50
La/Nb	0.98	1.07 (a)	1.50
Th/Nb	0.12	0.05 (a)	0.47

References: Primitive mantle, McDonough & Sun (1995);
N-MORB, (a) Sun & McDonough (1989), (b) Hofmann (1988);
Continental crust, Rudnick & Fountain (1995).

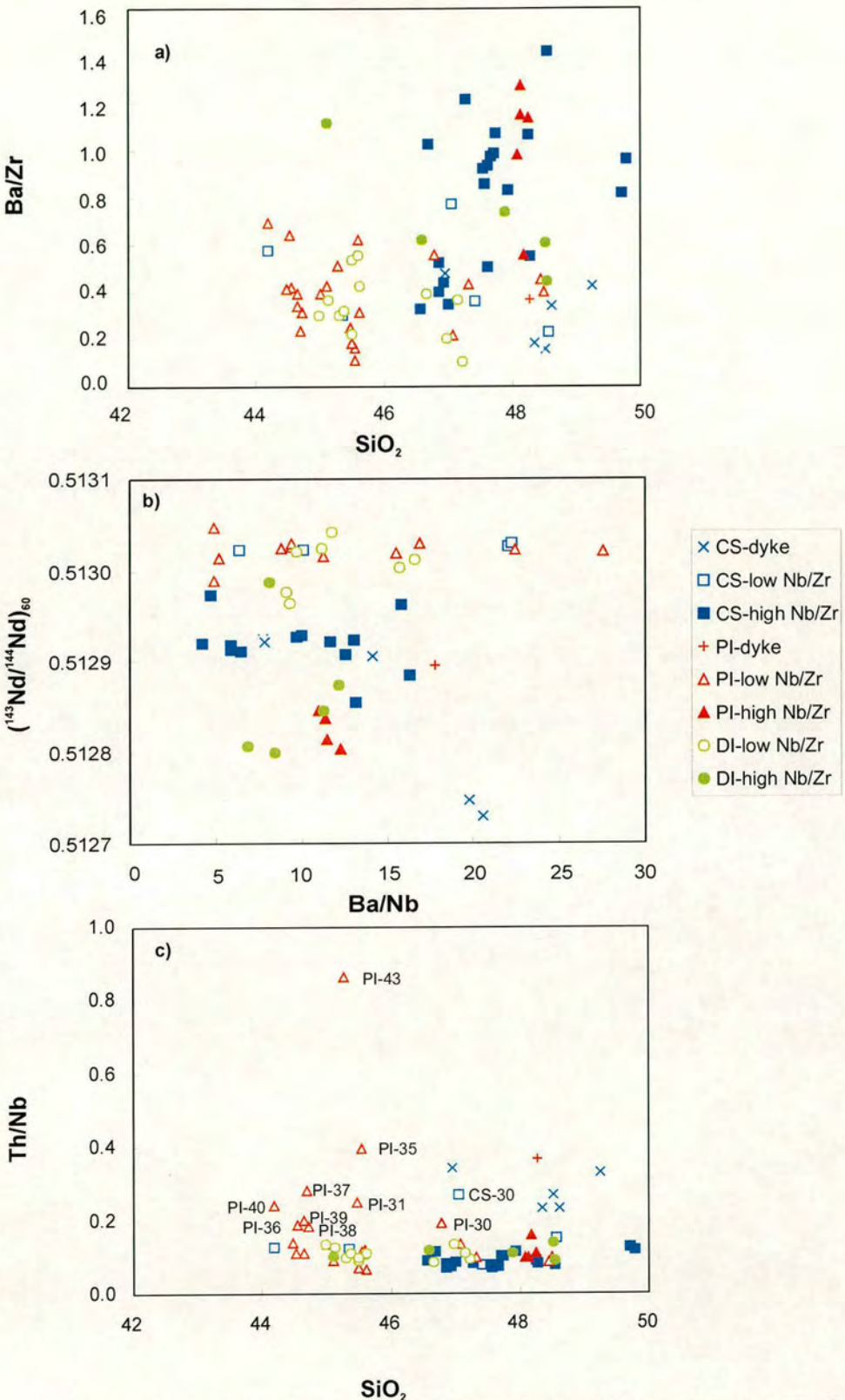

Fig. 5.1. Example plots to show that crustal contamination processes had no significant influence on the incompatible trace element ratios and Sr- and Nd isotope systems; (a) Ba/Zr versus SiO_2, (b) Ba/Nb versus $(^{143}Nd/^{144}Nd)_{60}$, (c) Th/Nb versus SiO_2 and (d) $(^{87}Sr/^{86}Sr)_{60}$ versus SiO_2. SiO_2 has been recalculated to 100% on a volatile-free basis. For each group (in d), REE patterns are also shown. For explanation see text.

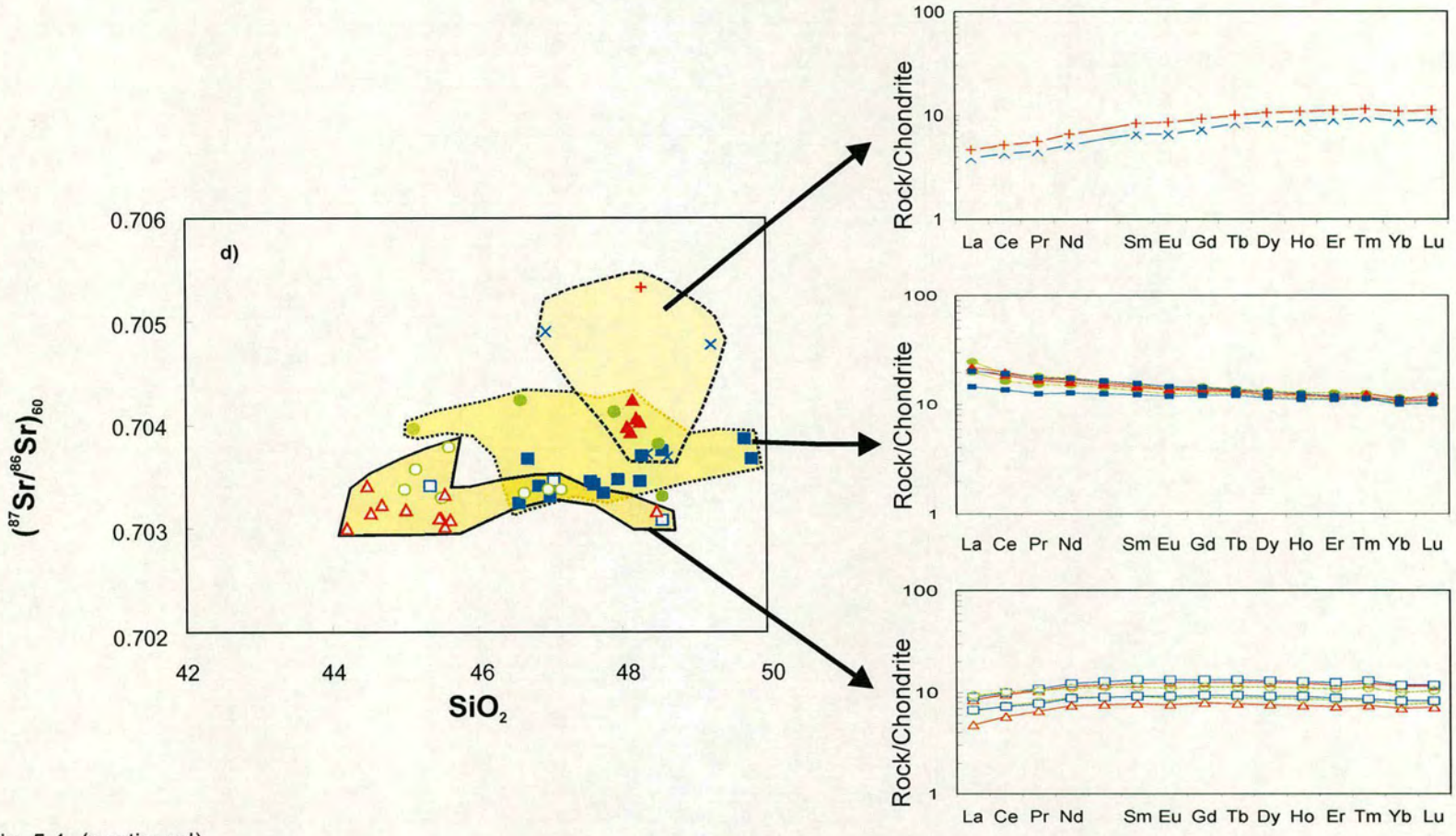

Fig. 5.1. (continued)

$^{87}Sr/^{86}Sr$ versus SiO_2 (Fig. 5.1.d). Contamination processes in these plots would lead to higher Ba/Zr, Ba/Nb, Th/Nb, SiO_2, $^{87}Sr/^{86}Sr$ and lower $^{143}Nd/^{144}Nd$ values. Contamination with sediments (e.g. shales) leads to higher Th/Nb values. Most of the Baffin Island rocks (Fig. 5.1c) have very low Th/Nb values (<0.2), with the exception of the dykes on Padloping Island and Cape Searle and interestingly, a single lava flow (PI-36 to PI-40) on Padloping Island. CS-43, PI-35, PI-30/31 and CS-30 also have higher values (Fig. 5.1c), suggesting that sediments could have interacted with these magmas.

In Fig. 5.1d, three different groups can be distinguished: (1) low-Nb/Zr samples (2) high-Nb/Zr samples and (3) the dyke samples (for definition of the low- or high-Nb/Zr groups, see chapter 3). Representative REE patterns of each group are also shown. If crustal contamination has affected the magmas on Baffin Island, one would expect a positive correlation between $^{87}Sr/^{86}Sr$ and SiO_2. However, the different groups show nearly constant $^{87}Sr/^{86}Sr$ ratios with increasing SiO_2 contents. Also, the samples that are relatively more enriched in incompatible elements (high-Nb/Zr group) are not those that have higher $^{87}Sr/^{86}Sr$ ratios and SiO_2 contents. Instead, the dykes, which have low Nb/Zr and the most depleted REE pattern of the Baffin Island samples, show the highest $^{87}Sr/^{86}Sr$ ratios and SiO_2 contents. Most likely the incompatible element-poor nature of the dyke parental magma rendered them most sensitive to any interaction with continental crust. Because there is no systematic relationship between any index of contamination and either $^{87}Sr/^{86}Sr$ or $^{143}Nd/^{144}Nd$, these variations are not due to crustal contamination processes. Overall, crustal contamination is highly unlikely to have been the cause for either the relative incompatible enrichment or the high $^{87}Sr/^{86}Sr$ and low $^{143}Nd/^{144}Nd$ ratios, and smaller degrees of melting or a relatively more enriched source are more likely explanations for the compositions of these magmas (chapter 6).

For most of the North Atlantic Igneous Province, the Archaean and Proterozoic rocks, which form the basement, are characterised by distinctively unradiogenic Pb (e.g. Dickin, 1981; Kalsbeek et al., 1993; Taylor et al., 1992; Whithouse et al., 1998). These

signatures are so extreme compared to mantle compositions, that Pb isotope ratios are a powerful tool in studies of potential crustal contamination in this region. Some Baffin Island lavas have Pb ratios similar to Icelandic and North Atlantic rocks, but others trend towards less radiogenic Pb (Fig. 5.3), which could be the result of interaction with the Archaean and Proterozoic basement rocks. However, note that co-variations between Pb-isotope ratios and either $^{87}Sr/^{86}Sr$, $^{143}Nd/^{144}Nd$ and incompatible-element ratios sensitive to crustal contamination (e.g. Ba/Zr, La/Nb) are absent (Fig. 5.2). This supports the result above, that is, that the $^{87}Sr/^{86}Sr$, $^{143}Nd/^{144}Nd$, and incompatible element ratios have not been significantly affected by crustal contamination, while the Pb-isotope ratios possibly show interaction of the Baffin Island magmas with their Precambrian basement rocks. Also, as shown by Kalsbeek & Taylor (1985) in West Greenland, the magmatic Pb isotopes of basaltic rocks with low Pb concentrations may be totally exchanged with crustal Pb, while the isotope systems of Sr or Nd might not have been significantly affected. Some of the Tertiary volcanic rocks on Skye also contain a significant proportion of crustal Pb, but still show no other evidence for contamination, which, according to Dickin (1981) could be the result of the greater mobility of the element Pb.

To identify the potential contaminants, several end-members have been classified. Unfortunately, Pb isotope ratios and Pb concentrations from the Baffin Island basement of the studied area are not available yet. Instead, different rock compositions were chosen as possible contaminants from the Nagssugtoquidian mobile belt on West Greenland, to which the basement rocks of the studied lava flows and dykes belong (e.g. Jackson et al., 1990). In Fig. 5.3, the lava flows and dykes of Baffin Island define several straight lines extending from Icelandic and North Atlantic MORB to more unradiogenic Pb compositions. Note that the analysed samples show a large variation in $^{207}Pb/^{204}Pb$ ratio (14.63 to 15.50). Due to the almost complete decay of the ^{235}U parent to ^{207}Pb at the present day, this variation in the $^{207}Pb/^{204}Pb$ ratios must be a long-lived signature. The scatter of $^{207}Pb/^{204}Pb$ for a given $^{206}Pb/^{204}Pb$ would have been generated

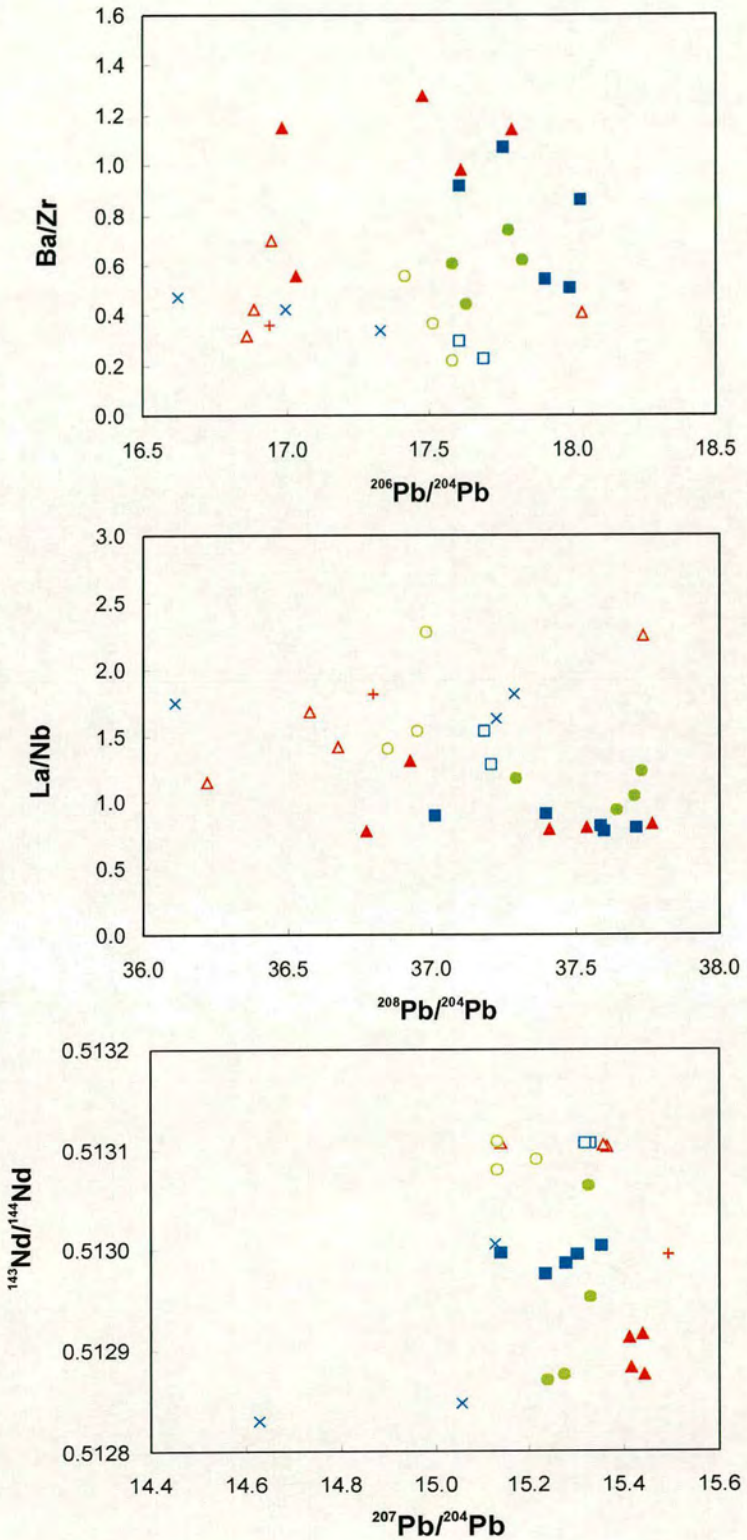

Fig. 5.2. (a) Ba/Zr versus $^{206}Pb/^{204}Pb$, (b) La/Nb versus $^{208}Pb/^{204}Pb$ and (c) $^{143}Nd/^{144}Nd$ versus $^{207}Pb/^{204}Pb$. Symbols for Baffin Island samples as in Fig. 5.1.

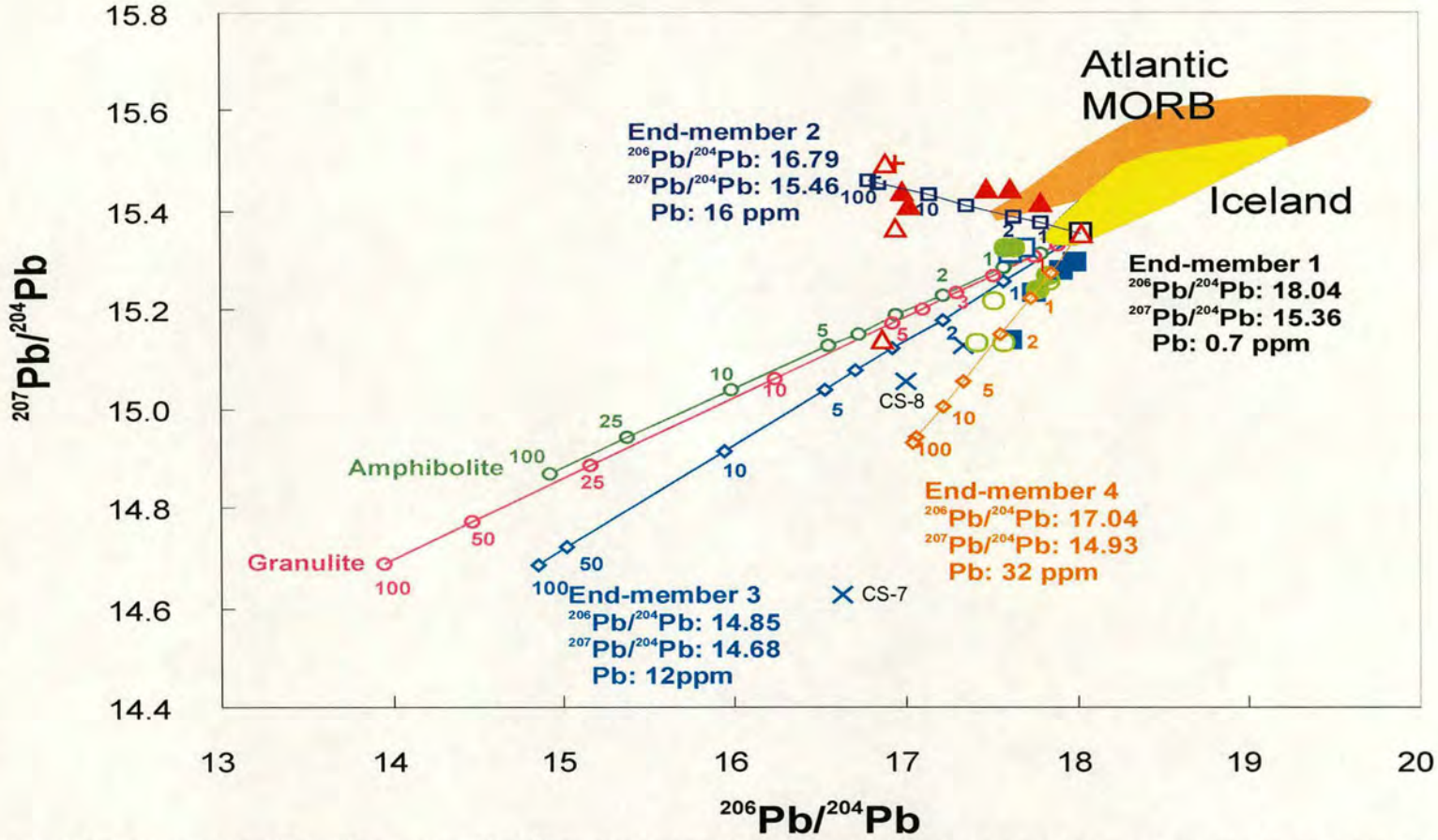

Fig. 5.3. Binary mixing for $^{207}Pb/^{204}Pb$ versus $^{206}Pb/^{204}Pb$. The mixing lines are calculated by mixing the most primitive Baffin Island sample (PI-41) with three different end-members of the Nagssugtoquidian mobile belt on West Greenland as well as with the average composition of both amphibolite and granulite gneiss of Dickin (1981). Mixing curves are labeled with wt. % of contaminant. End-member 1 corresponds to PI-41 of Baffin Island; end-member 2 to Arfersiorfik quartz diorite (sample 298617; Karlsbeek et al., 1987); end-member 3 to Egedesminde gneiss (isotope ratios:sample 298617, Pb (ppm): sample 298616; Kalsbeek et al., 1987); end-member 4 to Akungdlit pink gneiss (isotope ratios: sample 298696, Pb (ppm):sample 298686; Kalsbeek et al., 1987). Iceland isotope composition are from Sun & Jahn, 1975; Cohen & O'Nions, 1982a; Furman et al., 1991; Hards et al., 1995; Hanan & Schilling, 1997; Breddam et al., 2000 and Prestvik et al., 2001. North Atlantic MORB compositions are from Cohen et al., 1980; Dupre & Allegre, 1980; Ito et al., 1987 and Dosso et al., 1991, 1993. Symbols for Baffin Island samples as in Fig. 5.1.

in the Archaean, when the production of ^{207}Pb was still substantial, suggesting that contamination of the Baffin Island rocks with the Archaean basement is quite likely. Several end-members have been chosen in order to explain these different trends in Fig. 5.3 (see Table 5.2). Some of the analysed crustal rocks of Kalsbeek et al. (1987) have Pb-isotope ratios, that are similarly or more radiogenic (higher $^{207}Pb/^{204}Pb$ and $^{206}Pb/^{204}Pb$ ratios) than the volcanic rocks of Baffin Island. Therefore, the most unradiogenic rocks of the three different locations within the Nagssugtoquidian mobile belt were chosen as potential end-members. Unfortunately, the Pb content was not measured in some of these rocks analysed by Kalsbeek et al. (1987) and thus the Pb content for the mixing calculations had to be taken from another sample of this formation. The most primitive Baffin Island sample (PI-41) represents end-member 1 (Table 5.2). This sample was mixed with three different end-members of the Nagssugtoquidian mobile belt on West Greenland (Table 5.2). End-member 2 corresponds to the Proterozoic Arfersiorfik quartz diorite. End-member 3 represents the Archaean Egedesminde gneiss and end-member 4 the Archaean Akugdlit pink gneiss.

The Padloping Island lava flows and dyke (high- and low-Nb/Zr groups) could have been contaminated with the Arfersiorfik quartz diorite, leading to slightly increasing $^{207}Pb/^{204}Pb$ ratios with decreasing $^{206}Pb/^{204}Pb$ ratios. The assimilation ranges from 1% to nearly 50%. The stratigraphically higher lavas of Cape Searle (low-Nb/Zr-group), as well as DI-13 and DI-20 (high-Nb/Zr group) plot between the Arfersiorfik quartz diorite and the Egedesminde gneiss mixing lines; and their contaminant could be a hybrid composition between these two extremes. In either case, the amount of contamination for these samples does not exceed 2 %. The lower series lavas of Cape Searle (high-Nb/Zr group) and the middle series lavas of Durban Island (high-Nb/Zr group) can be formed by mixing the basaltic end-member (PI-41) with up to 2 % of the Akungdlit pink gneiss.

Table 5.2. Pb isotopic compositions and Pb (ppm) contents of the proposed end-members (from Karlsbeek et al., 1987)

End-member (Fig. 5.3)	Sample Formation	Sample name	$^{206}Pb/^{204}Pb$	$^{207}Pb/^{204}Pb$	Pb (ppm)
1	Padloping Island	PI-41	18.04	15.36	0.7
2	Arfersiorfik quartz diorite	298645	16.79	15.46	16
3	Egedesminde gneiss	298617 298616	14.85	14.68	 12
4	Akungdlit pink gneiss	298696 298686	17.04	14.93	 32

End-member (Fig. 5.4)	Sample Formation	Sample name	$^{206}Pb/^{204}Pb$	$^{208}Pb/^{204}Pb$	Pb (ppm)
1	Padloping Island	PI-41	18.04	37.73	0.7
2	Arfersiorfik quartz diorite	298640 298645	16.00	35.32	 16
3	Egedesminde gneiss	298617 298616	14.85	14.68	 12
4	Akungdlit pink gneiss	298692 298686	16.80	35.69	 32

Because the Lewsian complex of NW Scotland and the Nagssugtoquidian mobile belt of West Greenland are very similar in their history and isotopic compositions (e.g. Kalsbeek et al., 1993), the average compositions of amphibolite-facies gneiss ($^{206}Pb/^{204}Pb$: 14.91; $^{207}Pb/^{204}Pb$: 14.87; Pb= 12 ppm) and granulite-facies gneiss ($^{206}Pb/^{204}Pb$: 13.95; $^{207}Pb/^{204}Pb$: 14.69; Pb= 5 ppm) of Scotland (Dickin, 1981) are also included in Fig. 5.3. These crustal compositions do not satisfy the disturbed Pb-isotope ratios (particularly not the $^{207}Pb/^{204}Pb$ ratio). Even though the compositions of the Precambrian basement of the studied lava flows and dykes are not available, the three end-members of the Nagssugtoquidian mobile belt of West Greenland could represent the crustal contamination material. However, accurate estimates of the degree of crustal contamination are difficult, because for some of the crustal rocks, the Pb concentrations had not been analysed and therefore have had to be estimated (see above). Obviously, precise modelling of crustal contamination will only be possible when data from the actual Baffin Island basement are available.

By using $^{208}Pb/^{204}Pb$ and $^{206}Pb/^{204}Pb$ ratios in conjunction, it is possible to locate the depth of the crustal contaminant, because the crust may develop a stratified signature of these isotopes in response to high-grade metamorphism (e.g. Dickin, 1981). In Fig. 5.4, the mixing lines between sample PI-41 and the same local basement end-members used in Fig. 5.3 as well as the average amphibolite (probably upper crust) and the granulite-facies gneiss (probably lower crust) composition of Dickin (1981) are shown. For end-member 3 (Archaean Egedesminde gneiss), the same sample as in Fig. 5.3 has been used. However, because the compositions of the end-member 2 (Proterozoic Arfersiorfik quartz diorite) and end-member 4 (Archaean Akugdlit pink gneiss) in Fig. 5.3 do not have the most unradiogenic compositions of the formation, different rock samples have been chosen for the mixing-calculation in Fig. 5.4.

According to the $^{207}Pb/^{204}Pb$ - $^{206}Pb/^{204}Pb$ diagram (Fig. 5.3) the Padloping Island lava flows and dykes could have been contaminated by mainly the Arfersiorfik quartz diorite

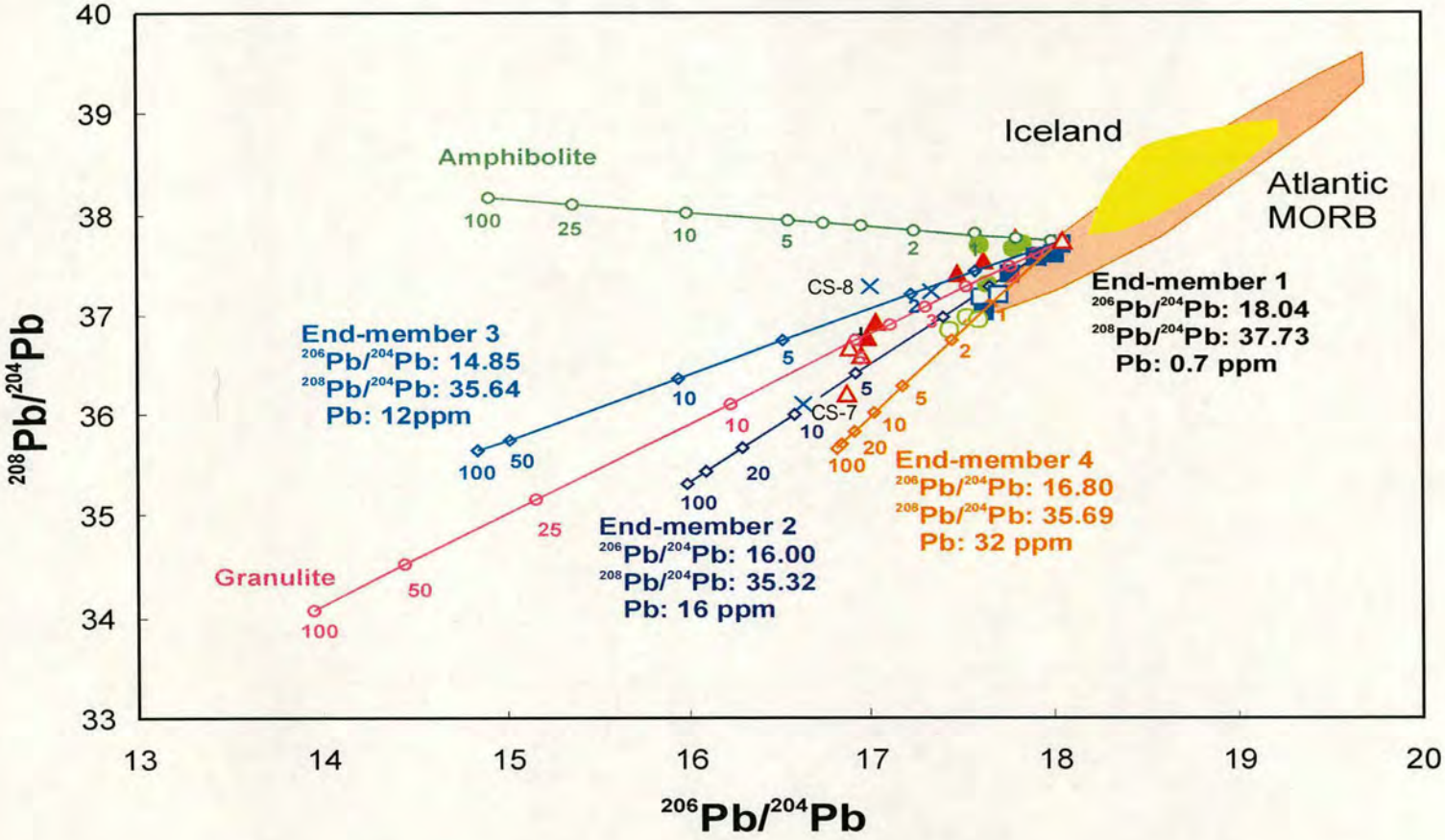

Fig. 5.4. $^{208}Pb/^{204}Pb$ versus $^{206}Pb/^{204}Pb$ for the Baffin Island lava flows and dykes. The mixing lines were calculated by mixing the most primitive Baffin Island sample (PI-41) with three different end-members of the Nagssogtoquidian mobile belt on West Greenland. The mixing curves are labeled with wt. % of contaminant. Average composition of granulite- and amphibolite-facies Lewsian gneiss ($^{06}Pb/^{204}Pb$, 13.95; $^{208}Pb/^{204}Pb$, 34.08; Pb = 5 ppm and $^{06}Pb/^{204}Pb$, 14.91; $^{208}Pb/^{204}Pb$, 38.18; Pb = 12 ppm, respectively) are from Dickin (1981). End-member 1 corresponds to PI-41 of Baffin Island, end-member 2 to Arfersiorfik quartz diorite (isotope ratios: sample 298640, Pb (ppm): sample 298645; Karlsbeek et al., 1987), end-member 3 to Egedesminde gneiss (isotope ratios: sample 298617, Pb (ppm): sample 298616; Karlsbeek et al., 1987) and end-member 4 to Akungdlit pink gneiss (isotope ratios: sample 298692, Pb (ppm): sample 298686; Karlsbeek et al., 1987). References for Icelandic and Atlantic MORB isotope data as in Fig. 5.3. Symbols for Baffin Island samples as in Fig. 5.1.

(except for sample PI-27, in which the contaminant was more likely the Egedesminde gneiss). However, in the $^{208}Pb/^{204}Pb$ - $^{206}Pb/^{204}Pb$ plot, the influence of the Egedesminde gneiss contaminant on the Padloping Island lava flows is more obvious, and therefore a potential contaminant with a hybrid composition between Arfersiorfik quartz diorite and Egedesminde gneiss is most likely for these samples (assimilation less than 7 %). The high-Nb/Zr samples of Durban Island show in the $^{206}Pb/^{204}Pb$ -$^{208}Pb/^{204}Pb$ plot an assimilation of 1 % with the Egedesminde gneiss, while the low-Nb/Zr group of Durban Island and the Cape Searle lava flows (high- and low-Nb/Zr group) could have been contaminated (less than 2 %) with the Akugdlit pink gneiss. The average composition of the amphibolite- and granulite-facies gneiss composition of Dickin (1981) are also included in Fig. 5.4. According to this, contamination with granulite-facies gneiss (up to 7 % assimilation) could explain the trend towards more unradiogenic Pb. None of the Baffin Island samples show clear evidence for contamination with amphibolite-facies crustal material (Fig. 5.4).

By modelling the most basic Baffin Island lava flow (PI-41) with several possible end-members of the Nagssugtoquidian mobile belt of West Greenland, it has been shown that the Pb isotope ratios of the Baffin Island lava flows could be explained by crustal contamination with a wide range of basement rock compositions. However, the lack of any systematic relationship between Pb isotope ratios and either Sr- or Nd-isotopes suggests that Sr- and Nd-isotope ratios were not significantly affected by crustal contamination processes. Moreover, by assuming a basic Baffin Island sample (PI-41 with Pb: 0.7 ppm, Sr: 148.8 ppm, Nd: 3.24 ppm), the effect of 7 % crustal assimilation (average continental crust with Pb: 12.6 ppm; Sr: 325 ppm; Nd: 20 ppm; McLennan & Taylor, 1995) is more visible in the Pb contents than it is in the Sr and Nd contents. By adding 7 % of crustal material to the basic Baffin Island lava flow, the mixture will contain 56 % crustal Pb, but less crustal Nd and Sr compositions (29 % and 13%, respectively). Therefore, although it cannot be completely excluded that some of the Sr

and Nd isotope ratios have been affected by crustal contamination processes, the effects of crustal contamination appear negligible.

5.3 Summary

Magmas passing through continental crust have the potential to modify their composition by assimilation of crustal material. In order to determine the genesis and evolution of lavas, it is necessary to consider whether or not the basic magmas assimilated, equilibrated or otherwise interacted with continental crust during their uprise from the mantle. The Baffin Island lava flows and dykes erupted through Archaean and Proterozoic crust as well as Tertiary sedimentary sequences (e.g. Burden & Langille, 1990; Jackson et al., 2000) and contamination of the magmas is a distinct possibility in such an environment.

Some Baffin Island rocks are isotopically more extreme (higher $^{87}Sr/^{86}Sr$ and lower $^{143}Nd/^{144}Nd$) than any rocks analysed from Iceland and it is essential to test whether these isotope ratios were affected by crustal contamination. The Sr- and Nd-isotope systems lack any clear correlation with indices of either crustal contamination (e.g. incompatible trace element ratios such as Ba/Zr, Ba/Nb, La/Nb, Th/Nb) or differentiation (e.g. SiO_2 content). These observations suggest that these isotope and trace element ratios were not affected by crustal material. However, the lava and dyke compositions of Baffin Island show disturbed Pb-isotope ratios, trending in general towards more unradiogenic Pb. Several studies have demonstrated that the Precambrian basement of most parts of the NAIP has low $^{206}Pb/^{204}Pb$ (e.g. Dickin, 1981; Kalsbeek et al., 1993; Whitehouse et al., 1998) and therefore any crustal contamination processes might be more apparent in Pb isotope compositions. The absence of any co-variation between Pb-isotope ratios and either other isotope ratios (Sr and Nd) or indices of crustal

contamination confirms the suggestion above that the incompatible trace elements and Sr- and Nd-isotope ratios of the lava flows have not been changed by crustal material. However, the dykes show an interaction with crustal material.

Small amounts of contamination are indicated by modelling the most basic Baffin Island lava flow (PI-41) with several possible end-members of the Nagssugtoquidian mobile belt of West Greenland in $^{207}Pb/^{204}Pb$- $^{206}Pb/^{204}Pb$ and $^{208}Pb/^{204}Pb$- $^{206}Pb/^{204}Pb$ diagrams. The Padloping Island rocks could have been contaminated with the Arfersiorfik quartz diorite, while addition of either Egedesminde gneiss or Akungdlit pink gneiss to the basic lava flow could have produced the observed Pb-isotope ratios of Cape Searle and Durban Island. Even through assimilation with any local basement rock does not exceed 2 %, the crustal contamination models show that a wide range of basement rocks have disturbed the Pb isotope ratios. By using the average Hebridean amphibolite-and granulite-facies gneiss composition of Dickin (1981), the mixing-lines with the basaltic end-member show that granulite-facies gneiss has possibly affected the Pb-isotope compositions (up to 7 % assimilation), while amphibolite-facies gneiss seems unlikely to have been involved in the crustal contamination processes.

6 Mantle melting

6.1 Introduction

The source composition and mineralogy, as well as the temperatures and depths at which melts form, have a significant impact on the geochemical variations of volcanic rocks (e.g. Klein & Langmuir, 1987; Kinzler & Grove, 1992). In order to examine such geochemical variations due to partial melting processes, different models have been developed that relate incompatible element concentrations in residual solids and derived liquids to the type and degree of melting. The two fundamental end-member models for the creation of partial melt in the mantle are equilibrium (batch) and fractional melting processes. The former generates a melt that is in equilibrium with the crystalline residue throughout the entire melting interval, while in the latter the melt is immediately isolated from the crystalline residue. Several refinements of these end-member processes have been proposed, including non-modal melting and pooling melts from different sources (e.g. Elliot et al., 1991; Sobolev et al., 1994; Gurenko & Chaussidon, 1995). The important input parameters in the partial melting models are: the starting bulk composition of the source, the partition coefficient between the mantle phases and melt, and the proportions of minerals in the bulk solid and those contributing to the liquid.

6.2 Mantle melting processes

Modelling the partial melting processes of erupted rocks is problematic, because of the large number of unknown parameters, so that any calculated melting curves are highly sensitive to the assumed parameters used in the particular model. However, by using both major element and trace element contents and ratios in different models, and by

comparing the results, it is still possible to estimate the depth and degree of partial melting.

Herzberg (1995) and Herzberg & Zhang (1996) developed a model using bulk Al_2O_3 content versus CaO/Al_2O_3 ratio that is based on experimental work on the anhydrous phase equilibrium relations of komatiite and peridotite. The liquids on the solidus reported in this model are based on experimental data in the system CaO-MgO-Al_2O_3-SiO_2 (e.g. Presnall et al., 1979; Bertka & Holloway, 1988; Herzberg, 1992). The compositions of liquids on the solidus are difficult to determine experimentally at any pressure (Herzberg, 1992; Hirose & Kushiro, 1993; Baker & Stolper, 1994) because the segregation of small melts from a peridotite source is difficult and also because the liquids can be modified by quench crystallisation at the termination of an experiment (Herzberg, 1995). This problem, according to Herzberg (1995) can be avoided by the adoption of the "shotgun" experimental method (O'Hara, 1968), where liquid compositions on the solidus (L+Ol+Opx+Cpx+Gt) have been bracketed by examining the nature of the liquidus phase for a wide range of komatiite compositions. Herzberg (1995) and Herzberg & Zhang (1996) demonstrated that the wide range of Al_2O_3 and CaO/Al_2O_3 contents in picrites and komatiites can be explained by melt segregation at upper mantle pressures ranging from 3 to ~10 GPa. This model is very useful, because CaO/Al_2O_3 is insensitive to compositional and modal variations in olivine. According to this model, the West Greenland picrites were generated at 3-4 GPa (Herzberg, 1995). In later work, using experimental phase equilibrium studies, Herzberg & O'Hara (1998, 2002) calculated eruption temperatures for West Greenland and Baffin Island primary magmas of about 1400-1440° C (see also chapter 4) and pressures of initial melting on the anhydrous solidus of 3.8-4.7 GPa. Fig. 6.1a shows the model developed by Herzberg (1995) and Herzberg & Zhang (1996) using the bulk Al_2O_3 versus CaO/Al_2O_3 ratio for the Baffin Island rocks analysed in this study. Al_2O_3 is a good indicator of depth in the garnet peridotite field, because its concentration in initial melts drops considerably with increasing pressure (Herzberg, 1992, 1995), while CaO does not change as much, and

thus the ratio CaO/Al_2O_3 in magmas on the solidus will also change with increasing pressure (Herzberg & Zhang, 1996). However, the Al_2O_3 content in a magma can also depend on the source composition, the degree of melting and the amount of olivine fractionation, but, according to Herzberg (1992, 1995), for liquids on or close to the solidus these factors have only a small effect on the CaO/Al_2O_3 ratio. In Fig. 6.1a, the Baffin Island lava flows cluster between 8 and 16 wt. % Al_2O_3 and between 0.6-0.9 CaO/Al_2O_3. The wide range of the Al_2O_3 content at nearly constant CaO/Al_2O_3 can be explained by variable amounts of olivine addition and subtraction (Herzberg, 1995). Most of the low-Nb/Zr group of Padloping Island, Durban Island and Cape Searle cluster next to the solidus line at higher pressures (around 3-4 GPa) compared with the high-Nb/Zr group, which is clustered at lower pressures (2-3 GPa). This observation is consistent with the higher temperatures of the low-Nb/Zr group (calculated in chapter 4), because deeper melting occurs at higher temperatures in anhydrous systems (e.g. Herzberg, 1995). Note that the Baffin Island volcanic rocks plot to the left (low CaO/Al_2O_3) of the solidus line. Since primary magmas can only plot on or to the right of this line (Herzberg, 1995), none of the Baffin Island samples is primary in composition (see also chapter 4).

As demonstrated in chapter 4, most of the Baffin Island rocks contain accumulated olivines which will reduce their Al_2O_3 content and lead to higher calculated segregation pressures in this model. Therefore, this effect has been removed by normalising the whole data set to 14 wt. % MgO by addition or subtraction of olivine with Fo_{89} (composition of sample PI-41; olivine 4, core 4). This method is described in chapter 4. The value of 14 wt. % for MgO was chosen because the average analysed olivine composition (Fo_{87-89}) suggests that Baffin Island lavas with >14 wt. % MgO might contain accumulated olivines (see chapter 4). Fig. 6.1b shows the Herzberg (1995) and Herzberg & Zhang (1996) model using the data set normalised to 14 wt. % MgO. Both the low- and the high-Nb/Zr group now cluster between 12.4 wt. % and 14.3 wt. % Al_2O_3 (except PI-42 with 15.9 wt. % Al_2O_3) and between 0.7 wt. % and 0.9 CaO/Al_2O_3

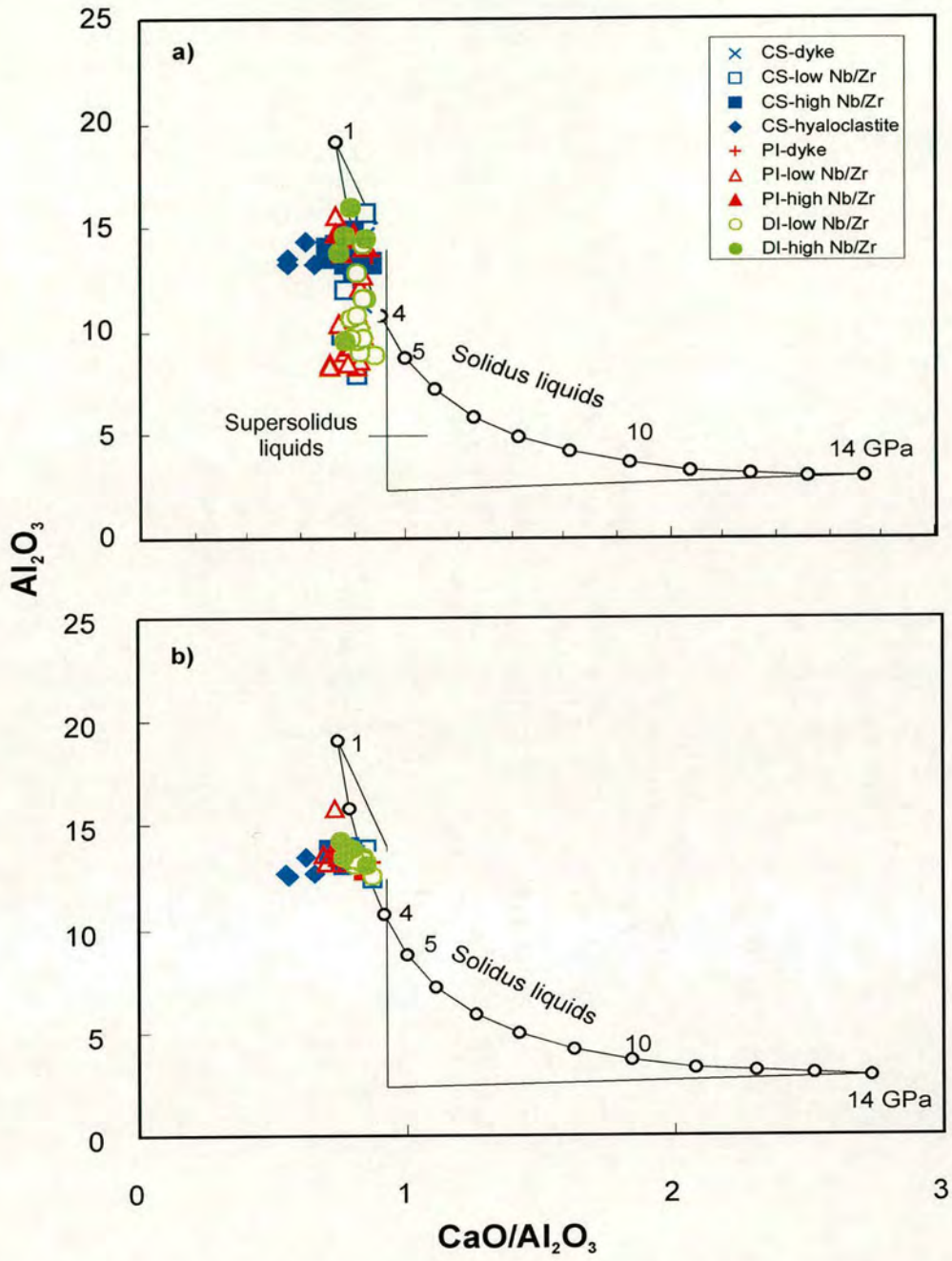

Fig. 6.1. Al_2O_3 (wt. %) versus CaO/Al_2O_3 for the Baffin Island volcanic rocks using the model developed by Herzberg (1995) and Herzberg & Zhang (1996). For liquids on the solidus (Ol+Opx+Cpx+Gt+L), variations in CaO/Al_2O_3 can be retrieved from the empirical equations: CaO (wt. %) = $16.0811-2.0724P+0.1355P^2-0.0018P^3$ and Al_2O_3 (wt. %) = $22.8581-4.0110P+0.2703P^2-0.0061P^3$ (Herzberg, 1995). Numbers refer to pressures (GPa) along the solidus. In the 2.5-4 GPa pressure range, garnet is the first phase to melt and with increasing melting involve [Ol+Opx+Cpx+L]→[Ol+Opx+L]→[Ol+L]→[L]; in the 4-9 GPa range progressive melting will exhaust Cpx first, and involve [Ol+Opx+Gt+L]→[[Ol+Opx+L]→[Ol+L] →[L] (Herzberg, 1995). The effect of olivine addition or subtraction is to decrease and increase Al_2O_3, respectively, without changing CaO/Al_2O_3. (a) Analysed data set recalculated to 100% on a volatile-free basis, (b) corrected data set generated by normalising the data to 14 wt. % MgO by addition or subtraction of an olivine crystal (olivine 4, core 4 of PI-41) with Fo_{89}.

(except hyaloclastic rocks of Cape Searle with ~0.6 CaO/Al_2O_3) implying segregation pressures of ~3 GPa.

Similar estimates for segregation pressures for the Baffin Island samples are obtained by using the simple equation obtained from linear regression of experimental data of Scarrow and co-workers (Scarrow & Cox, 1995; Scarrow et al., 2000). Accumulation of olivine could reduce the SiO_2 values (used in the formula) towards lower values, which would result in higher calculated segregation pressures using this model. Therefore, the corrected data set was also used in this model. The estimated pressures for Cape Searle range between 1.7 and 3.2 GPa, for Padloping Island between 2.0 and 3.1 GPa and for Durban Island between 1.8 and 2.5 GPa (Fig. 6.2). However, note that the two single flows (PI-36-40 and PI-41/42) on Padloping Island show segregation pressures between 2.2-3.1 GPa. Such wide ranges for single flows are unexpected: possible explanations might be either that the method used to determine segregation pressures is unreliable, or that the samples collected as single flows do not in fact represent single flows; but neither is satisfactory. Scarrow et al. (2000) calculated segregation pressures for the West Greenland lava flows between 2.2 and 3 GPa, within the range of the estimated pressures of the Baffin Island suite. Robinson & Wood (1998) placed the garnet-spinel transition zone at ~2.6 GPa, suggesting that at least some of the Baffin Island rocks could have been formed within the garnet-lherzolite field.

By choosing incompatible trace element ratios for modelling partial melting processes, the problem of olivine accumulation can be solved, because these ratios are not influenced significantly by the addition of olivine crystals. However, before examining geochemical variations due to mantle melting, the effect of shallow level fractionation has to be taken into account. Since olivine is normally crystallised at shallower depths, MgO is a good indicator of fractionation for basaltic rocks (Putirka, 1999). One method of testing whether the trace element variation is due to olivine fractionation is to compare the trace element ratios with the MgO content (Fig. 6.3). The trace element

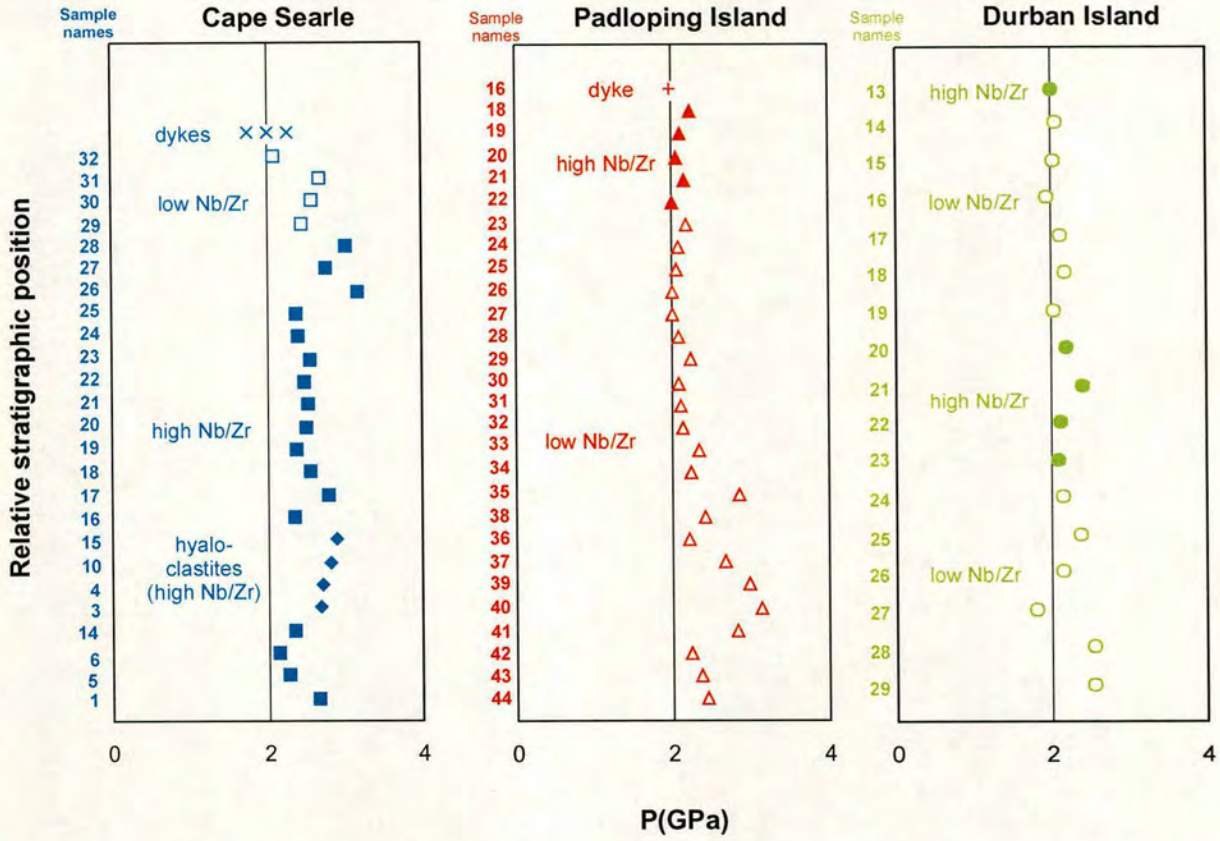

Fig. 6.2. Stratigraphic profiles of the calculated segregation pressures after Scarrow & Cox (1995) and Scarrow et al. (2000) for Cape Searle Padloping Island and Durban Island. The data set was normalised to 14 wt. % MgO by the addition/subtraction method (described in chapter 4) of an olivine with Fo_{89}. The linear regression of experimental data for the variation of pressure with SiO_2 in HK-66 melt gives: P(GPa) = (213.6-4.05 SiO_2)/10 (Scarrow & Cox, 1995).

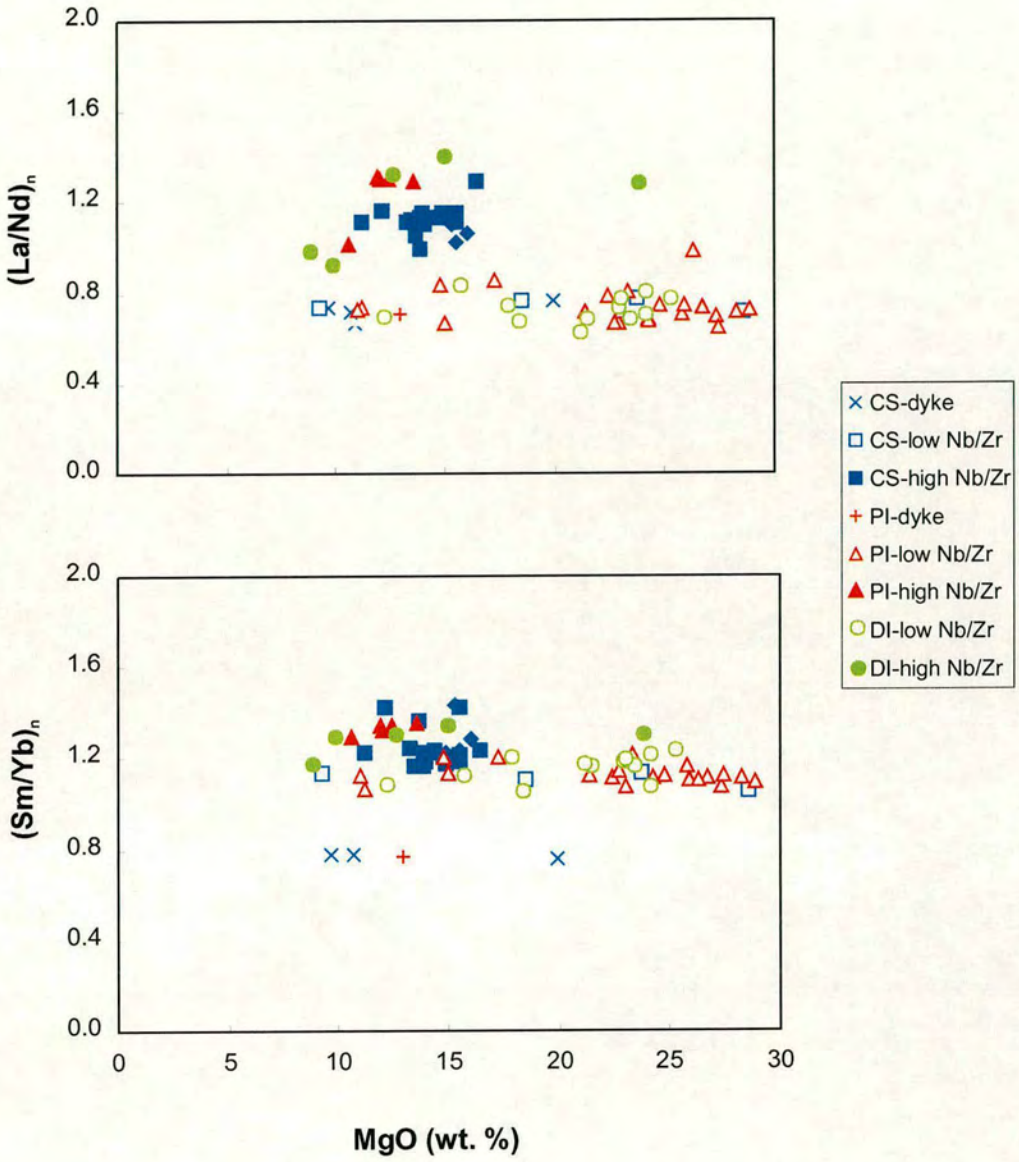

Fig. 6.3. (a) $(La/Nd)_n$ and (b) $(Sm/Yb)_n$ versus MgO (wt. %).

ratios used in the following calculation ($(La/Nd)_n$ and $(Sm/Yb)_n$) show no clear correlation with the MgO content (Fig. 6.3), and therefore these ratios seem to be unaffected by shallow fractionation of olivine and seem more likely to be the result of other processes (e.g. source composition, partial melting).

A non-modal fractional melting equation (Shaw, 1979) is used to calculate the trace element concentrations of the liquids produced by partial melting of spinel and mixtures of garnet and spinel lherzolites (Fig. 6.4). A N-MORB source (Sun & McDonough, 1989) depleted in incompatible elements and a primitive mantle source (McDonough & Sun, 1995) were chosen as starting bulk compositions. The initial mantle mineral modes in spinel and garnet lherzolite and the trace element partition coefficient values are from McKenzie & O'Nions (1991). The mantle phase proportions contributing to the liquid are taken from Johnson et al. (1990). The equations and input parameters used in the partial melting model are summarised in Table 6.1.

For the trace element model presented here, the ratios $(La/Nd)_n$ and $(Sm/Yb)_n$ ($_n$=chondrite normalised) were chosen, as each ratio has the potential to yield information about either the chemistry or mineralogy of the source region and both have isotopic implications (see chapter 7). While $(La/Nd)_n$ is a good indicator for the mantle source composition and the extent of melting, $(Sm/Yb)_n$ provides information on the modal mineralogy of the source. Because Nd is more compatible than La during peridotite melting, the $(La/Nd)_n$ ratio decreases as the extent of melting increases. However, as the degree of melting increases, the $(La/Nd)_n$ ratio very quickly approaches a constant value (the starting mantle value), because the incompatible elements La and Nd can only be fractionated from each other at small degrees of melting. The concentration of Yb, on the other hand, is very low in basaltic rocks formed by small degrees of melting at high pressures, because Yb is highly compatible in garnet. Therefore, melts produced at high pressures will have high $(Sm/Yb)_n$ values. As melting increases and proceeds to shallower depths, the Yb concentration in basaltic rocks

Table 6.1.Equations and input parameters for the partial melting calculations

Non-modal accumulated fractional melting equation:

$C_L/C_o=1/F(1-(1-FP/D_o)^{1/P})$

$D_o=\Sigma x_i D_i$

$P=\Sigma p_i D_i$

Key

C_L:	element in the liquid
C_o:	source (bulk) composition
D_o:	bulk mineral-liquid distribution coefficient
F:	degree of melting
P:	bulk partition coefficient for melt
D:	mineral-liquid partition coefficient
p_i:	mineral proportion by mass of element i
x_i:	mantle phase proportions of element i
D_i:	D value for element i

Source composition(C_o)

Partition coefficient(D_i)[3]

	N-MORB[1]	PM[2]	ol	opx	cpx	sp	gt
La_n	10.55	2.73	0.0004	0.003	0.054	0.01	0.01
Nd_n	15.63	2.90	0.001	0.0068	0.21	0.01	0.087
Sm_n	17.19	2.90	0.0013	0.01	0.26	0.01	0.217
Yb_n	17.94	2.90	0.0015	0.049	0.28	0.01	4.03

Mantle phase proportions[4]

	ol	opx	cpx	sp	gt
x(sp-Lher.)	0.578	0.27	0.119	0.033	
x(gt-Lher.)	0.598	0.211	0.076		0.115

Proportions phases will contribute during melting[5]

	ol	opx	cpx	sp	gt
p(sp-Lher.)	0.1	0.2	0.68	0.02	
p(gt-Lher.)	0.03	0.03	0.44		0.5

1: N-MORB and chondrite value (Sun & McDonough, 1989)
2: primitive mantle (McDounough & Sun, 1995); chondrite value (Sun & McDonough, 1989)
3: McKenzie & O'Nions (1991)
4. McKenzie & O'Nions (1991)
5: Johnson et al. (1990)

increases progressively, because garnet is not the residual aluminious phase any more. This process is illustrated in Fig. 6.4 using a non-modal fractional melting equation.

By assuming a N-MORB source (Fig. 6.4a), some of the low-Nb/Zr group of Padloping Island and Durban Island could be produced either by 5-10 % melting of a spinel-lherzolite source, or by 7-10 % % melting of a source mainly composed of spinel lherzolite (96-99 wt. %) with small amounts of garnet (1-4 wt.%). The low-Nb/Zr samples of Cape Searle may be explained by 5-8% melting of a spinel-lherzolite source. The high-Nb/Zr group plot between the melting curves of a spinel lherzolite and a mixture of spinel and garnet lherzolite (98:2) source and could have been produced by 2-5 % of partial melting. The high-Nb/Zr group of Padloping Island and Durban Island could be produced by melting of a spinel lherzolite source (99%) with a very small amount of garnet (1%). However, part of the high-Nb/Zr group plots to the left of the spinel-lherzolite curve and melting of a N-MORB source appears not to be consistent with the trace element compositions of these samples. Calculated melting curves of a slightly more enriched source (primitive mantle) give a better fit with the observed trace element compositions of the high-Nb/Zr samples (Fig. 6.4b). In this case, the high-Nb/Zr samples of Cape Searle can be successfully modelled by a source either composed of pure spinel lherzolite (6-8 % melting) or by a mix of 96 % spinel and 4 % garnet lherzolite (5-6 % melting). The high Nb/Zr group of Padloping Island and Durban Island could be produced by 3-7% melting of a mainly spinel-lherzolite source (98%) with small amounts of garnet (2%).

Modelling the dyke compositions with a source composed of spinel or garnet lherzolite appears more problematic. The measured trace element ratios of the dykes have similar $(La/Nd)_n$, but display lower $(Sm/Yb)_n$ ratios compared with the low-Nb/Zr group. It was not possible to extend the melting curves to such low $(Sm/Yb)_n$ ratios, but it is suggested that the dykes were also produced from a N-MORB source. According to their lower

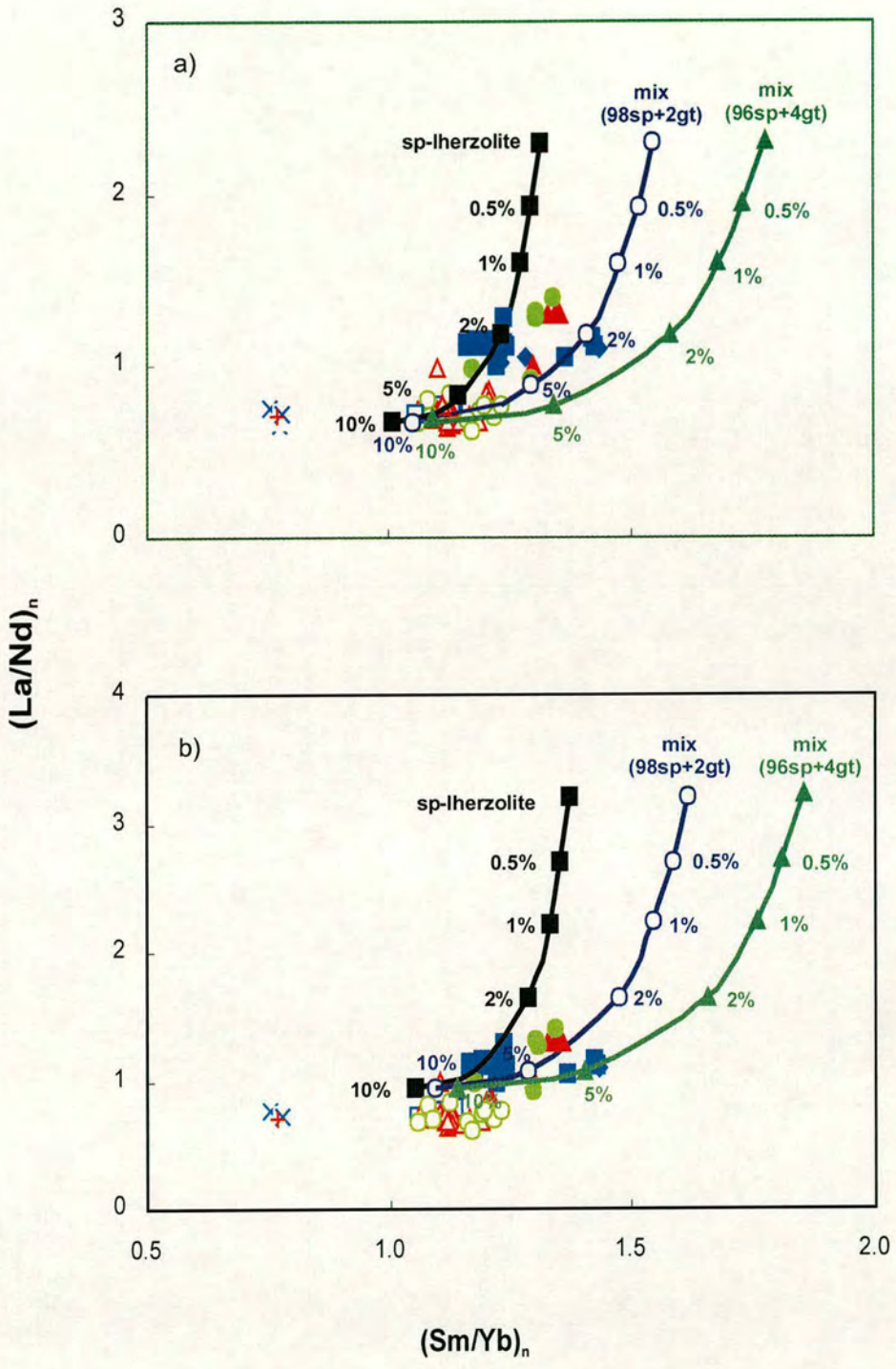

Fig. 6.4. $(La/Nd)_n$ versus $(Sm/Yb)_n$ for calculated melting curves of spinel and mixtures of spinel and garnet lherzolites of (a) a N-MORB source (Sun & McDonough, 1989) and (b) primitive mantle (McDonough & Sun, 1995). The equations and parameters used for these calculations are summarised in Table 6.2. Symbols for Baffin Island samples as in Fig. 6.3. For explanation see text.

$(Sm/Yb)_n$ ratios, the calculated depth of melting seems to have been shallower for the dykes than for the lava flows.

The partial melting model presented here indicates that the low-Nb/Zr group and the high-Nb/Zr group of Baffin Island were generated mainly from sources composed of spinel lherzolite or mixtures of spinel and garnet lherzolite, suggesting deriviation of magmas from melt columns which could have extended across the garnet-spinel transition zone. The low-Nb/Zr group of all three locations on Baffin Island appears to be the result of melting of a trace element depleted source (N-MORB). Some of the high-Nb/Zr group could also be obtained from a mantle source with a N-MORB composition but the observed trace element ratios are more consistent with a source slightly more enriched in incompatible elements (primitive mantle).

There is a clear correlation between trace element and isotope ratios (chapter 7), implying that the range of trace element patterns cannot be produced by partial melting processes of a single homogeneous mantle source. Because trace element variations in part reflect source composition and because the high-Nb/Zr samples tend to fit the melting curves characteristic of a primitive mantle source, the high-Nb/Zr group would appear to have a source composition slightly less depleted in incompatible elements than the N-MORB source. It also has lower degrees of melting than the low-Nb/Zr group, consistent with its higher concentrations of incompatible elements. This result will be confirmed in the next chapter using isotope ratios, which demonstrate that the low- and high-Nb/Zr groups appear to have been produced by different source compositions.

The melting conditions calculated in this study are similar to those suggested previously for West Greenland and Baffin Island. Earlier work on the Baffin Island picrites (Clarke, 1970) showed that they could be the product of high degrees of melting at 3 GPa and depths of ~100 km. Later work on the basis of Al-Si systematics (Francis, 1985) suggested that the Padloping Island primary magmas could represent 15-20 % partial

melting of a spinel-lherzolite mantle at ~2.5 GPa. Francis (1985) added that the MORB-related picrite suites appear to have had primary magmas that equilibrated with the mantle at even greater depths. Robillard et al. (1991) proposed that the Baffin Island mantle source was a mixture of enriched plume mantle and depleted entrained mantle in the head of the plume. Because they were unable to reproduce the composition of both the N-MORB and E-MORB-types from a common homogeneous source, they concluded that the differences between N-MORB-type and E-MORB-type magmas require two compositionally distinct mantle sources. The West Greenland picrites represent high degrees of melting (24-28 %) constrained at depths of 60-90 km, corresponding to 2-3 GPa (Gill et al., 1992). A likely scenario for these picrites is that they reflect melting which initiated in the garnet-lherzolite field and continued in the spinel-lherzolite field (Schäfer et al., 2000).

6.3 Summary

In order to examine the geochemical variations of the Baffin Island volcanic rocks due to partial melting processes, different models comparing results achieved from major element contents and trace element ratios were developed. By using bulk Al_2O_3 content versus CaO/Al_2O_3 ratios after the model of Herzberg (1995) and Herzberg & Zhang (1996), it has been demonstrated that the high-Nb/Zr lavas of Baffin Island can be explained by melt segregation pressures of 2-3 GPa. The melting that led to the low-Nb/Zr lavas may have taken place at higher pressures ranging between 3 and 4 GPa. However, the accumulation of olivine crystals can change the Al_2O_3 content towards lower values, which would lead to higher calculated segregation pressures. To correct for the process of olivine accumulation, a modified data set recalculated to 14 wt. % MgO has been created by an olivine (Fo_{89}) addition/subtraction method. In this case, using the model of Herzberg (1995) and Herzberg & Zhang (1996), both the low- and the high-Nb/Zr groups imply segregation pressures of ~3 GPa.

Similar segregation pressures are obtained by using the method of Scarrow & Cox (1995). The estimated pressures with the recalculated data set to 14 wt. % MgO range for Cape Searle between 1.7 and 3.2 GPa, for Padloping Island between 2.0 and 3.1 GPa and for Durban Island between 1.8 and 2.5 GPa.

A non-modal fractional melting model was developed in order to calculate the trace element concentrations of the liquids produced by partial melting of spinel and mixtures of garnet and spinel lherzolites. $(La/Nd)_n$ and $(Sm/Yb)_n$ ratios are particularly useful, because each ratio provided different information about either the chemistry or the mineralogy of the source region. This model uses a source depleted in incompatible elements (N-MORB) and a slightly more enriched source (primitive mantle). Part of the low-Nb/Zr group of Padloping Island and Durban Island can be modelled by melt generation occurring within the spinel-lherzolite facies (5-10 %), while the other part was modelled by 7-10 % melting of a source mainly composed of spinel lherzolite (96-99 wt. %) with small amounts of garnet (1-4 wt. %). The low- Nb/Zr lavas of Cape Searle could be produced by 5-8 % melting of a spinel-lherzolite source. While the low-Nb/Zr groups of all three locations on Baffin Island can be successfully modelled using a N-MORB source, these calculated melting curves do not satisfy fully the trace element concentrations of the high-Nb/Zr lava flows. Because the Baffin Island lavas show a clear correlation between trace element and isotope ratios, the trace element patterns cannot be produced by partial melting processes alone. As confirmed in the next chapter, it seems more likely that the source of the low- Nb/Zr group was slightly more enriched in incompatible elements. In this case, the high- Nb/Zr samples of Cape Searle can be modelled by a source composed either of pure spinel lherzolite (6-8 % melting) or by a mix of 96 % spinel and 4 % garnet lherzolite (5-10 % melting). The high Nb/Zr group of Padloping Island and Durban Island could be explained by 3-7% melting of a mixture of spinel- and garnet-lherzolite source (98:2).

7 Mantle sources

7.1 Introduction

The NAIP provides an ideal natural laboratory in which to study the structure, origin and composition of a mantle plume and its evolution through time. Volcanic rocks from Iceland and the individual volcanic areas within the NAIP provide material not only from the entire width of the plume head, but also from the Palaeogene to the present day. Although the NAIP is one of the best-studied areas, with a large amount of data from Iceland itself and from other parts of the NAIP, there are still several gaps in our knowledge and further work is necessary and of fundamental significance for better understanding plume dynamics. In particular, representative data from the periphery of the NAIP is required in order to allow a direct comparison between Iceland and the 61 Ma plume axis. The most extreme western margin of the province (Baffin Island) is relatively little studied and the history of this volcanic event poorly understood. Previous Baffin Island studies were based on a relatively old and small collection and have not used the latest geochemical techniques (section 2.2.2). A detailed chemical and isotopic study of Baffin Island should help to establish (1) whether the geochemical signature of the Iceland plume was present in the outer edge of the province and (2) if so whether its compositional signature was the same at the time of the break-up or instead (3) if the Baffin Island Tertiary lavas were only the result of a local volcanic eruption event, fed by small magma chambers, and unrelated to the NAIP formation.

In order to establish the compositional characteristics of the Iceland mantle plume, it is necessary to distinguish the chemical signature generated by the plume itself from that arising from the plume's interaction with the shallower mantle on its way to the surface. Numerous geochemical studies on Icelandic lavas have emphasised that the Iceland plume must be heterogeneous and compositional variation in Icelandic basalts require

contributions from different mantle reservoirs or components (e.g. Elliot et al., 1991; Hémond et al., 1993). The Icelandic lavas have higher abundances of incompatible elements, high $^{87}Sr/^{86}Sr$, low $^{143}Nd/^{144}Nd$ and radiogenic Pb compared with North Atlantic MORB (e.g. Hart et al., 1973; Sun & Jahn, 1975; Zindler et al., 1979). The geochemical variations in basalts from Iceland have been attributed since the 1970s to mixing between depleted MORB asthenosphere source and an enriched Iceland plume (e.g. Schilling, 1973; Hart et al., 1973; Sun et al., 1975). However, Thirlwall et al. (1994) and Thirlwall (1995) noted that the analysed Icelandic basalts have distinctly higher $^{208}Pb/^{204}Pb$ at a given $^{207}Pb/^{204}Pb$ than North Atlantic MORB. Because the Icelandic data and Atlantic MORB define separate Pb-isotope trends, these authors suggested that the depleted component is not the MORB source, but instead, is a distinct component of the plume itself. Several authors support this hypothesis on the basis of Pb isotopes, Nb-Zr-Y systematics and Hf-Nd isotope relationships (Hards et al., 1995, Kerr, 1995a; Fitton et al., 1997, 2003; Hardarson et al., 1997; Kempton et al., 1998, 2000; Nowell et al., 1998, Chauvel & Hémond, 1999), while others propose that a depleted Iceland plume component is not required and that the presence of a depleted asthenospheric MORB source for some Icelandic basalts should not be excluded (e.g. Hanan & Schilling, 1997; Hanan et al., 2000). In particular, Hanan and co-authors questioned the arguments for a depleted plume component based on Nb-Zr-Y systematics and Hf-Nd relationships. Instead, they suggested that the apparent distinction between Iceland and the North Atlantic can be accounted for by a three-component mixing model, involving two incompatible trace element enriched components (one with relatively high, the other with low $^{206}Pb/^{204}Pb$ ratios) and the depleted MORB source as the third component. However, Fitton et al. (2003), in their response to Hanan et al. (2000), demonstrated that firstly, the trace element data of Hanan et al. (2000) excluded data from depleted Icelandic basalts, and secondly, that their argument against a depleted component on the basis of Hf-Nd relationships is based only on one sample. New Hf data presented by Fitton et al. (2003) still supports the distinction between N-MORB and a depleted component of the Iceland plume.

7.2. $^{87}Sr/^{86}Sr$-$^{143}Nd/^{144}Nd$ relationship

The previous chapters show that the Baffin Island lava flows and dykes can be divided into two different groups, defined by low Nb/Zr and high Nb/Zr, respectively. Lava flows of the low-Nb/Zr group are generally more magnesium-rich, contain more-forsteritic olivines, represent higher-magnesium liquid compositions, and were produced at higher temperatures than the high-Nb/Zr rocks. The differences in their petrology, trace element composition and melting conditions are also reflected in $^{87}Sr/^{86}Sr$ and $^{143}Nd/^{144}Nd$ isotope ratios. The Baffin Island lavas display well-defined trends on both Nb/Zr versus $^{87}Sr/^{86}Sr$ (Fig. 7.1a) and $(La/Sm)_n$ versus $^{143}Nd/^{144}Nd$ (Fig. 7.1b), with the low-Nb/Zr group having consistently higher $^{143}Nd/^{144}Nd$ and lower $^{87}Sr/^{86}Sr$ values. The correlation between the incompatible trace element abundances and isotopes cannot be produced by mantle melting processes alone, and can be better explained by the availability of at least two different mantle sources at the time of the formation of the Baffin Island lavas. The low-Nb/Zr group of the Baffin Island lavas at all three locations show similar trace element and isotope ratios, while in the high-Nb/Zr group, the Cape Searle lava flows can be distinguished by their geochemical signature (slightly lower $^{87}Sr/^{86}Sr$ and higher $^{143}Nd/^{144}Nd$) from the Padloping Island and Durban Island samples (Fig. 7.1). Note that the dykes do not follow the general trends of the lava flows in Fig. 7.1 and instead show higher $^{87}Sr/^{86}Sr$ and lower $^{143}Nd/^{144}Nd$ ratios than do lava flows with similar Nb/Zr values. As explained in chapter 5, the dykes have the lowest contents of incompatible elements and the most depleted REE patterns of the Baffin Island samples; it is suggested that their incompatible-element-poor nature rendered them most sensitive to the interaction with continental crust, leading to higher $^{87}Sr/^{86}Sr$ and lower $^{143}Nd/^{144}Nd$ ratios.

By comparing the Baffin Island lava flows with Icelandic basalts and North Atlantic MORB (Fig. 7.2a), the low-Nb/Zr group of Baffin Island samples plot within the field of

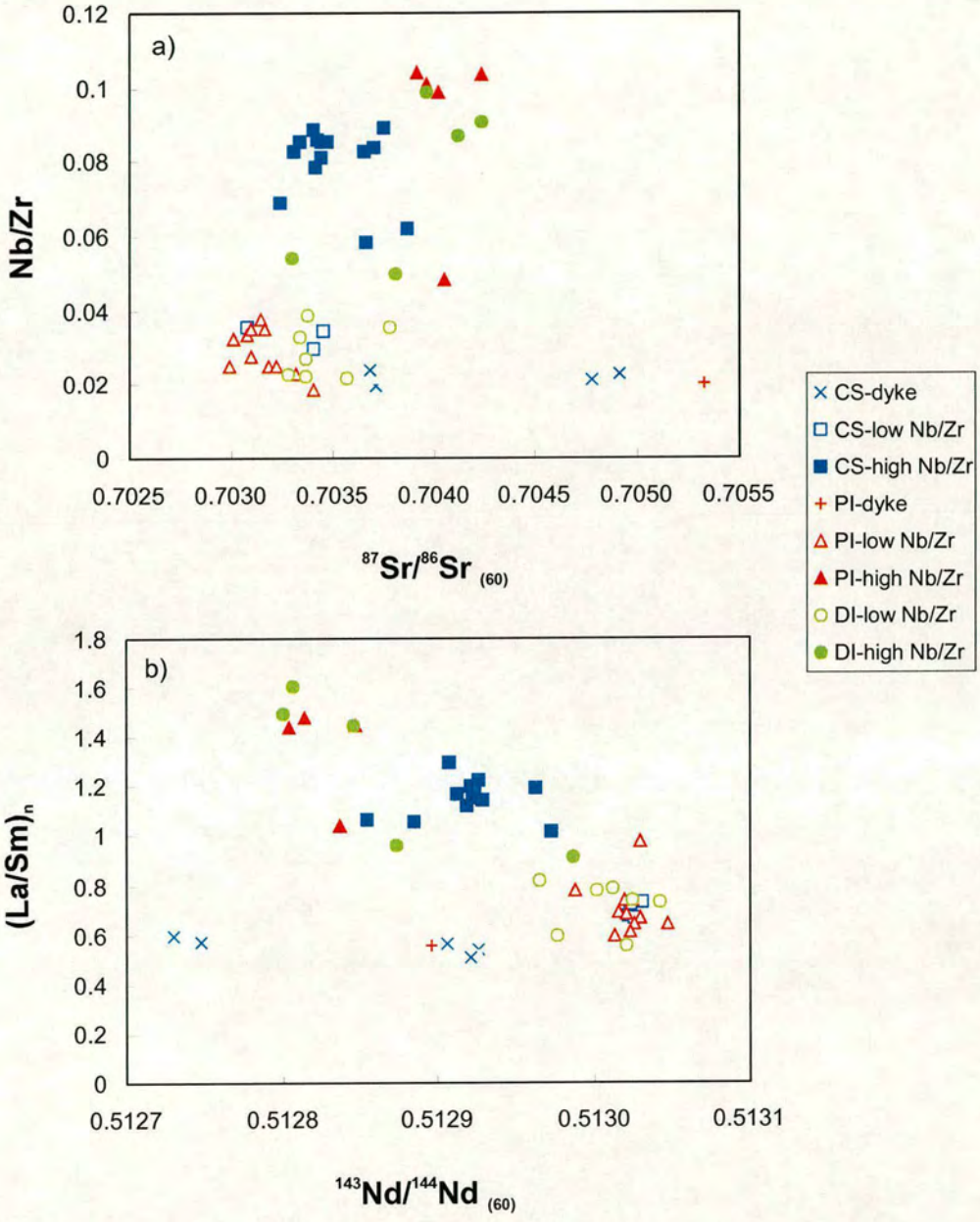

Fig. 7.1. (a) Nb/Zr versus $(^{87}Sr/^{86}Sr)_{60}$ and (b) $(La/Sm)_n$ versus $(^{143}Nd/^{144}Nd)_{60}$

both North Atlantic MORB and Iceland. In contrast, the high-Nb/Zr lavas of Cape Searle have Sr- and Nd-isotope ratios that fall at the lower end of the Iceland field, while the high-Nb/Zr lavas of Padloping Island and Durban Island are more extreme than basalts from Iceland, plotting towards even higher $^{87}Sr/^{86}Sr$ and lower $^{143}Nd/^{144}Nd$ ratios.

The Baffin Island lava flows and dykes have a wider range of Sr- and Nd-isotope ratios than values observed in West Greenland (Fig. 7.2b), although most of the low-Nb/Zr group of Padloping Island fall within the fields of the Naujanquit member and Ordlingassoq member of the Vaigat Formation of Disko Island (for location and lithostratigraphy see Fig. 2.6 and 2.7). However, the low-Nb/Zr group of Cape Searle and Durban Island have similar $^{143}Nd/^{144}Nd$ ratios to the Padloping Island rocks, but slightly higher $^{87}Sr/^{86}Sr$ ratios, plotting to the right of these fields. For the high-Nb/Zr group, only the Cape Searle rocks show similar isotope ratios to West Greenland rocks, clustering in the field of the Vaigat Formation of Nuussuaq, while the low-Nb/Zr group of Padloping Island and Durban Island do not correlate with West Greenland rocks at all, having markedly higher Sr- and lower Nd-isotope ratios (Fig. 7.2b). The Baffin Island lava succession is normally magnetised (Deutsch et al., 1971) and is most likely a time equivalent to the Anaanaa Member of the Vaigat Formation (Pedersen et al., 2002). Unfortunately, only one sample of the Anaanaa member has been analysed so far (Graham et al., 1998), and this sample has slightly higher $^{143}Nd/^{144}Nd$ but similar $^{87}Sr/^{86}Sr$ ratios to the low-Nb/Zr group of Baffin Island.

To summarise, according to trace element patterns and Sr- and Nd-isotope ratios, it seems most likely that at least two isotopically different sources were available during the formation of the Baffin Island volcanic rocks: (1) a relatively depleted source with $^{87}Sr/^{86}Sr = 0.7030\text{-}0.7034$ and $^{143}Nd/^{144}Nd = 0.5130$; and (2) a relatively enriched mantle source with $^{87}Sr/^{86}Sr = 0.7039\text{-}0.7042$ and $^{143}Nd/^{144}Nd = 0.51280\text{-}0.51284$. Most of the Baffin Island rocks plot within the field of Icelandic basalts, suggesting that the geochemical signature of the Iceland mantle plume was present at the most westerly

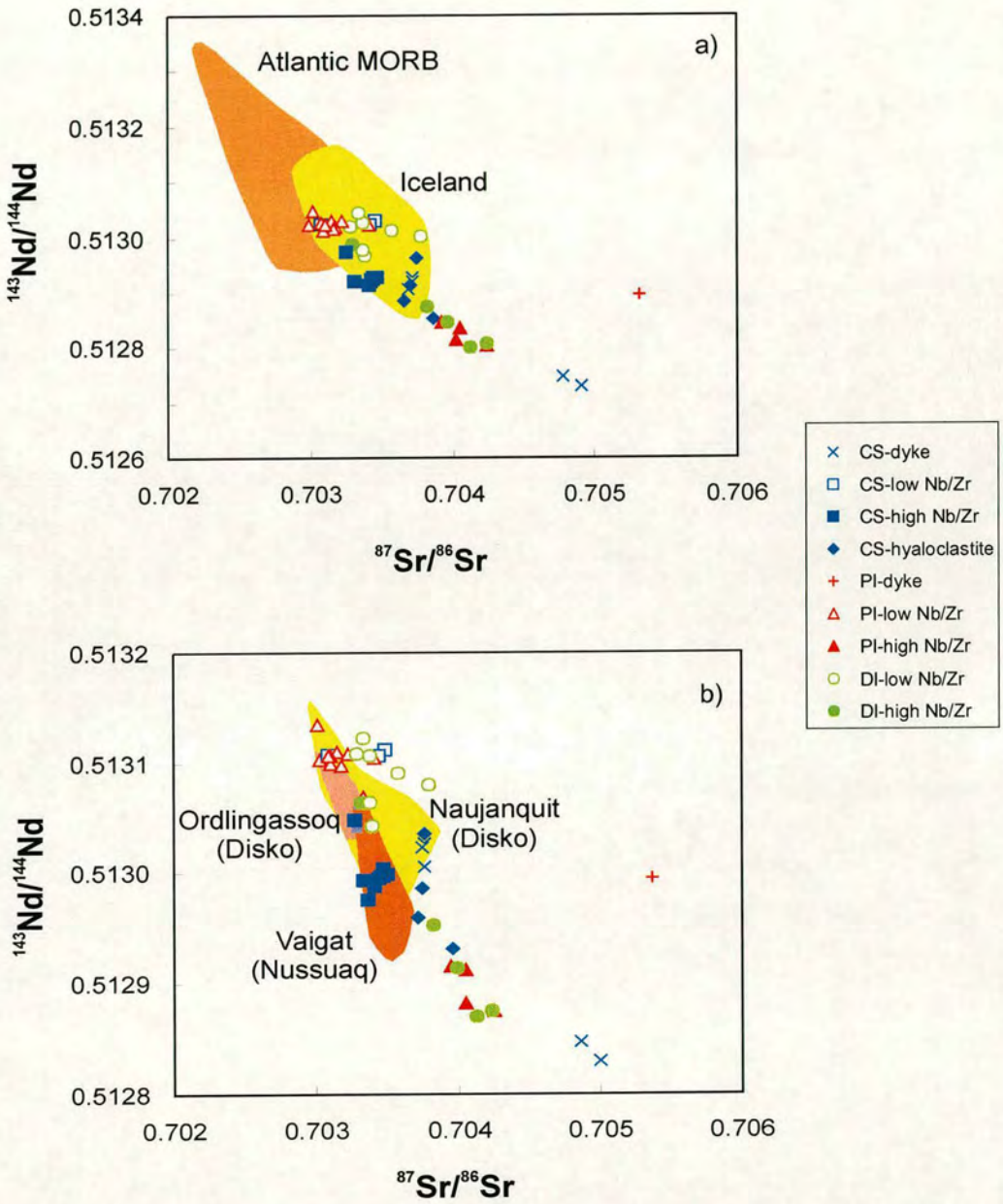

Fig. 7.2. Correlation between $^{143}Nd/^{144}Nd$ versus $^{87}Sr/^{86}Sr$ of the Baffin Island lavas compared to (a) Atlantic MORB and Icelandic basalts and (b) West Greenland. The Sr- and Nd data are age-corrected (60 Ma) in (a) and the measured values in (b). Data sources: Atlantic N-MORB (Cohen et al., 1980; Ito et al., 1987; Dosso et al., 1991, 1993); Iceland (Zindler et al., 1979; Condomines et al., 1983; Hemond et al., 1991; Furman et al., 1991; Hards et al., 1995; Stecher et al., 1999; Prestvik et al., 2001; Breddam et al., 2002); West Greenland (Holm et al., 1993; Lightfoot et al., 1997; Graham et al., 1998).

edge of the NAIP. Because the Baffin Island lava flows show evidence for only very low levels of crustal contamination, the high-$^{87}Sr/^{86}Sr$ and low-$^{143}Nd/^{144}Nd$ lavas of Padloping Island and Durban Island could represent the most enriched end-member of the ancestral Iceland plume. This extreme end-member might have been present at the initiation of the Iceland plume but its geochemical signatures are not evident in the plume today. The existence of enriched mantle material within the proto-Icelandic mantle plume has been also suggested by Bernstein et al. (2001), who sampled melilitites with similar Sr- and Nd-isotope signatures in East Greenland.

7.3. Nb-Zr-Y systematics

Icelandic basalts have diverse compositions, covering a wide range of geochemical signatures from very depleted picrites to enriched alkaline rocks. To test whether these depleted volcanic rocks represent N-MORB or a distinct depleted component of the plume, Fitton et al. (1997) developed a useful discriminant to distinguish between these two components. They demonstrated that in a logarithmic plot of Nb/Y versus Zr/Y, Icelandic basalts and N-MORB define separate and parallel linear arrays. Lavas from the neovolcanic zones of Iceland, covering the whole range from depleted picrites from the Reykjanes Peninsula (low Zr/Y) to the most enriched off-axis alkali basalts from Snaefellsjökull (high Zr/Y), have relative higher Nb abundances (and therefore higher Nb/Y ratios) than N-MORB. To characterise the mantle source of an individual sample, Fitton et al. (1997) defined the lower bound of the Iceland array as a reference line that expresses the excess or deficiency in Nb. This parameter (ΔNb) provides a useful discriminant between Icelandic basalts and N-MORB, such that basalts originating from an Icelandic mantle source have positive ΔNb values, while basalts formed in the depleted upper mantle have negative ΔNb values. Fitton et al. (1997) showed that ΔNb is insensitive (1) to low-pressure fractional crystallisation, (2) to processes due to the

effects of variable degrees of melting and source depletion through melt extraction (as they result in variations along the representative N- MORB linear arrays) and (3) to crustal contamination (since estimated crustal compositions plot on or slightly below the reference line and therefore crustal contamination processes could not produce the positive ΔNb values).

The Nb/Y and Zr/Y variation of the lava flows and dykes of Baffin Island are presented in Fig. 7.3. All of the relatively enriched lava flows (defined in section 7.2.) plot within the Iceland array, while the depleted lava flows and dykes (defined in section 7.2) plot below the reference line within the N-MORB field. None of the depleted samples plot within the Iceland array, suggesting that the depleted component of the Iceland plume either was not available at the time of eruption in the most westerly margin of the NAIP, or was not sampled by the melting process. Instead, the depleted lava flows and dykes appear to have their origin in the upper mantle. According to ΔNb, both Icelandic and N-MORB sources were available at the western periphery of the ancestral Iceland plume. However, as shown in section 7.2, the enriched lavas of Cape Searle have similar Sr- and Nd isotopes to Icelandic lavas, while the enriched lavas of Padloping Island and Durban Island are more extreme and therefore distinct from the geochemical signature of the Iceland plume.

7.4. Hf-Nd isotope systematics

The pioneering work of Patchett and co-workers (Patchett & Tatsumoto, 1980, 1981a,b; Patchett et al., 1984; Patchett, 1983a,b) provided much of our current understanding of the Lu-Hf system. The correlation between Hf- and Nd-isotopic compositions in OIB indicates that the two isotope systems Lu-Hf and Sm-Nd are mainly coupled. However, some processes, such as erosion and sedimentation may decouple them (e.g. Patchett et

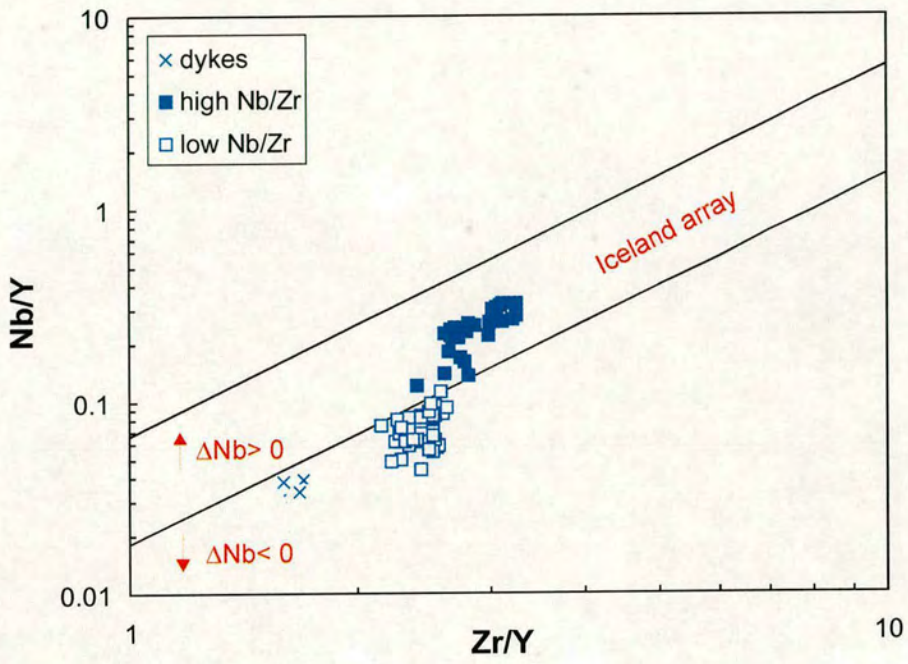

Fig. 7.3. The Nb/Y versus Zr/Y variation of the Baffin Island lava flows and dykes. The lower bound of the Iceland array represents a reference line with respect to which an excess or deficienty in Nb can be expressed ($\Delta Nb = 1.74 + \log (Nb/Y) - 1.92 \log(Zr/Y)$ after Fitton et al. (1997). For explanation see text.

al., 1984). Zircon is a refractory mineral with high contents of Hf that is concentrated in sandstones and turbidites. Red clays, however, lack zircons and have higher Lu/Hf ratios; thus the presence of ancient pelagic sediment in the source of basalts will result in higher $^{176}Hf/^{177}Hf$ ratios for a given $^{143}Nd/^{144}Nd$ ratio (e.g. Patchett et al., 1984).

While $^{176}Hf/^{177}Hf$ and $^{143}Nd/^{144}Nd$ correlate in OIB, MORB samples display a proportionally greater degree of spread of $^{176}Hf/^{177}Hf$ compared with $^{143}Nd/^{144}Nd$, showing almost the whole range of $^{176}Hf/^{177}Hf$ at nearly constant $^{143}Nd/^{144}Nd$. Salters & Hart (1991) and Salters (1996) demonstrated that the Lu/Hf ratios are not coupled with the Hf-isotope ratios in the MORB source. MORB have Lu/Hf ratios lower than primitive mantle, whereas values higher than primitive mantle are required to account for the high $^{176}Hf/^{177}Hf$. Salters & Hart (1989) attributed this hafnium paradox to residual garnet in the MORB source. Hf is not a rare earth element and its chemistry is not coherent with the HREE. If garnet is present in the residue, melting develops high Lu/Hf ratios (Lu is compatible in garnet) and, over time, a radiogenic Hf isotope signature. However, Chauvel & Blichert-Toft, 2001) concluded that the Hf paradox does not require that garnet was a residual phase during melting and instead, the composition of MORB could be explained by melting entirely in the spinel stability field. According to them, it is possible that melting starts in the garnet field, but it is not required by the Lu-Hf system. Patchett & Tatsumoto (1980) explained the decoupling of the Hf and Nd isotope system as a result of stronger fractionation of Lu/Hf than Sm/Nd in very trace element depleted source regions, such as the MORB source, due to the greater incompatibility of Hf relative to Lu compared with Nd and Sm.

The high precision analysis of Hf-isotope ratios has been a problem for many years, as the element Hf has a high first ionization potential and is difficult to separate from other elements in its pure form as well. Some of the pre-1997 Hf-isotope data analysed (TIMS and hot-SIMS) had large analytical errors (e.g. Fitton et al., 2003). Only recent analytical techniques have made it possible to produce very high precision Hf-isotope

analysis. Because high precision data (plasma ionisation multi-collector mass spectrometry [PIMMS]) of North Atlantic N-MORB from the Goban Spur and the Hatton Bank show less variation in $^{176}Hf/^{177}Hf$ and correlate positively with $^{143}Nd/^{144}Nd$, Kempton et al. (2000) argued that the $^{176}Hf/^{177}Hf$ and $^{143}Nd/^{144}Nd$ isotope system might not be decoupled in MORB as previously thought (e.g. Patchett & Tatsumoto, 1980; Salters & White, 1998). However, new high precision data (PIMMS) of MORB samples from the Atlantic, Pacific and Indian ocean still show, particularly in the Atlantic, large variation in $^{176}Hf/^{177}Hf$ with only minor changes in $^{143}Nd/^{144}Nd$ (Chauvel & Blichert-Toft, 2001),

The Hf-isotope compositions of the fifteen analysed samples of Baffin Island range from $\varepsilon Hf = 11.2$ to 17.81 and correlate positively with εNd (Fig. 7.4). They form a linear array, which can be described by a regression line $\varepsilon Hf = 1.26\ \varepsilon Nd + 6.32$. The Baffin Island slope in Hf-Nd isotope space is slightly shallower than the 'mantle array' ($\varepsilon Hf = 1.33\ \varepsilon Nd + 3.19$; Vervoort et al., 1999). Nowell et al. (1998) showed that Icelandic basalts define a much steeper trend than the mantle array ($\varepsilon Hf = 3.34\ \varepsilon Nd + 10.69$). However, new, more precise data of Kempton et al. (2000) and Stracke et al. (2003) show that the regression line of the Icelandic basalts is much shallower ($\varepsilon Hf = 1.77\ \varepsilon Nd + 0.97$) than predicted by Nowell et al. (1998) and is not much distinguishable from the 'mantle array' regression line (Stracke et al., 2003). Note that the Baffin Island lavas all plot above the mantle array regression line with positive $\Delta\varepsilon Hf$ (Fig. 7.4). $\Delta\varepsilon Hf$ is the vertical deviation of a given sample value from the mantle array regression line in Hf-Nd isotope space ($\Delta\varepsilon Hf = \varepsilon Hf - 1.33\ \varepsilon Nd - 3.19$). Several possible processes have been suggested for the generation of a source isotope signature with positive $\Delta\varepsilon Hf$: (1) presence of ancient pelagic sediments in the source region (since pelagic sediments have relatively high Lu/Hf ratio for a given Sm/Nd ratio [e.g. Blichert-Toft et al., 1999]), (2) material from the subcontinental mantle lithosphere (SCML) (e.g. Schmidberger et al., 2002), (3) isolation of a significant amount of basalts from the mantle for several billions

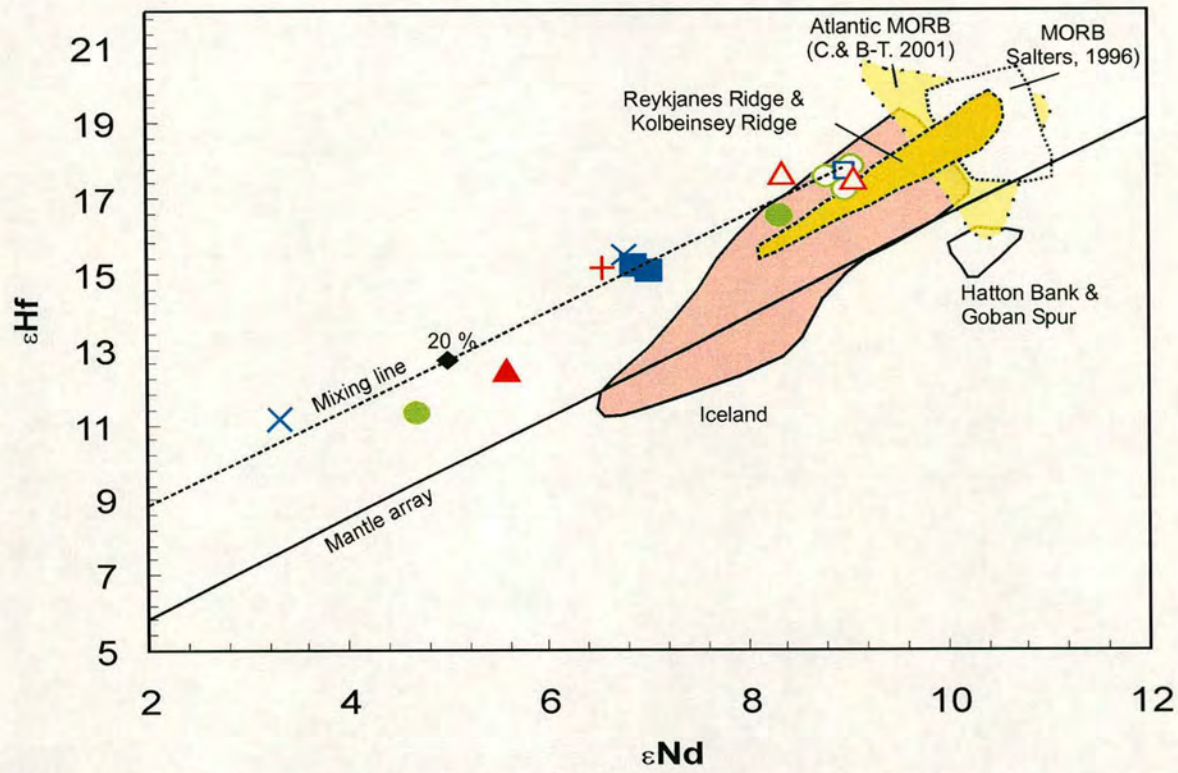

Fig. 7.4. εHf versus εNd of the Baffin Island lava flows and dykes compared with literature data: (1) PIMMS analyses: Iceland (Kempton et al., 2000; Stracke et al., 2003); Atlantic MORB (Chauvel & Blichert-Toft, 2001); Hatton Bank and Goban Spur (Kempton et al., 2000); Reykjanes Ridge and Kolbeinsey Ridge (Kempton et al., 2000), (2) Hot-SIMS analysis: MORB (Salter, 1996). Mantle regression line (εHf = 1.33 εNd - 3.19) from Vervoort et al. (1999). The mixing line is calculated by mixing Baffin Island sample PI-41 (εNd = 9, εHf = 17.79) with a mixture of ancient sediment composed of 90% mud (εNd = -11, εHf = -6) and 10% sand (εNd = -11, εHf = -22). Compositions of 1.5 Ga mud and sand components are from Eisele et al. (2002). Only the mixing line, not the endmember of the ancient sediment, is shown in the diagram. Symbols as in Fig. 7.1.

of years (e.g. Salters & Hart, 1991; Salters & White, 1998), or (4) by fractionation and isolation of small amounts (<1 %) of perovskite during the early stages of Earth's history (e.g. Salters & Hart, 1991; Salters & White, 1998). Kempton et al. (2000) suggested that the high $^{176}Hf/^{177}Hf$ ratio of some Iceland basalts is a long-lived feature of the plume and represents the residue of an ancient melting event in which a mineral (such as garnet) with a high Lu/Hf ratio is a residual phase.

As shown in chapter 5, the Pb-isotope ratios of the Baffin Island lava flows and dykes have been affected by crustal contamination processes and thus are not suitable for defining mantle sources. However, the trace element ratios have not been affected and could help to constrain the processes that generated the high εHf values of the Baffin Island lavas. Eisele et al. (2002) estimated the compositions of 1.5 Ga-old mud and sand components in εHf versus εNd space (present day εNd for mud and sand: -11; present day εHf for mud and sand: -6 and –22, respectively). These estimated compositions have been chosen to test whether ancient sediments were present in the Baffin Island source. The Baffin Island trend in the εHf versus εNd plot can be achieved by mixing the most primitive sample PI-41 (εNd: -9, εHf: -17.79) with a sediment mixture composed of 90 % mud and 10 % sand. According to this calculation, the relatively isotopically depleted lava flows (defined as the low-Nb/Zr group in previous chapters) could contain around 10 % of ancient sediment in their source, while the relatively isotopically enriched lava flows (defined as the high-Nb/Zr group) could contain much more (up to 30 %). Such high contents of sedimentary material in the source should be also evident in trace element ratios enriched in sediments (e.g. La/Nb and Th/Nb). However, as shown in Fig. 7.5, no correlation between La/Nb and Th/Nb versus εHf is observed. The enriched lava flows do not have higher contents of La/Nb and Th/Nb (as expected if they contain higher pelagic sediments in their source), but instead, have similar or even lower values than the depleted lava flows. Therefore, even though it is possible to construct a

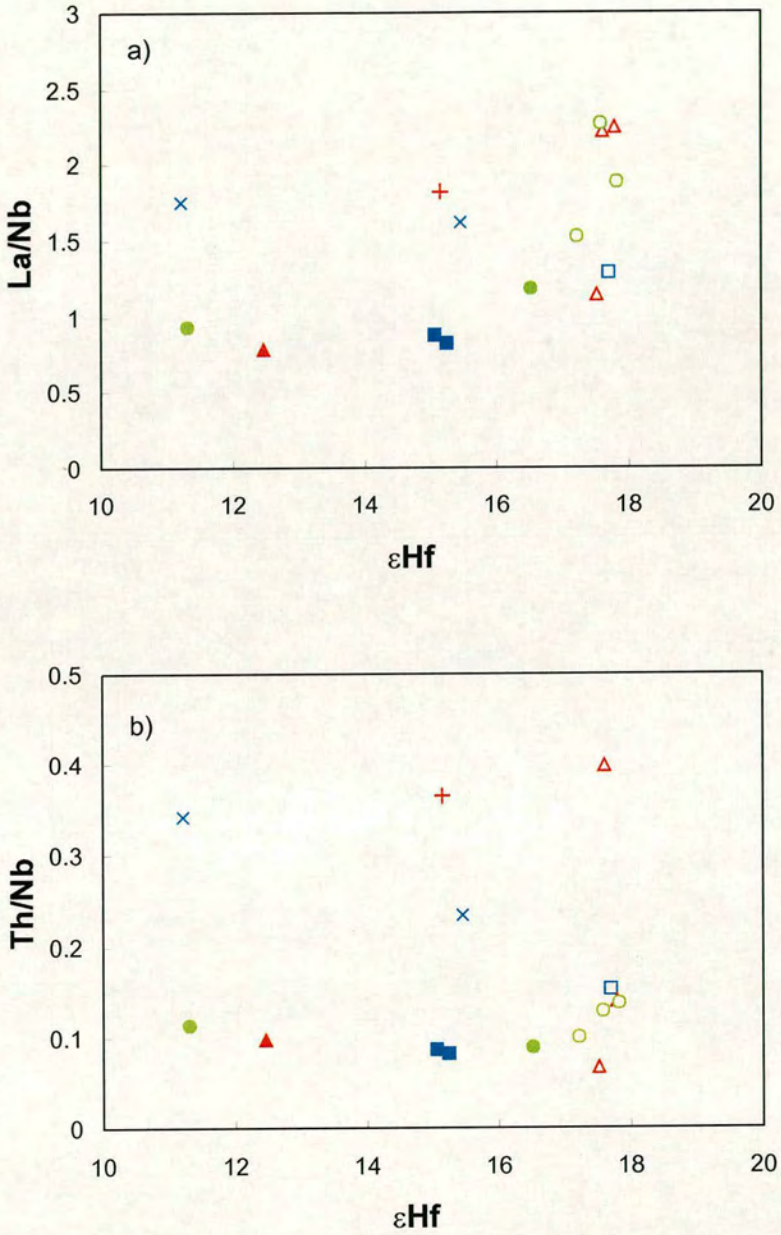

Fig. 7.5. (a) La/Nb and (b) Th/Nb versus εHf. Symbols as in Fig. 7.1.

mixing curve between the Baffin Island lava flows and ancient pelagic sediments, it seems very unlikely that such sedimentary components were responsible for the high εHf values.

The geochemical composition of "typical" subcontinental mantle lithosphere is difficult to evaluate, because its composition can only be determined by studying mantle xenoliths. Evidence from the subcontinental mantle of the study area is available, because Schmidberger and co-authors et al. (Schmidberger & Francis, 1999, 2001; Schmidberger et al., 2001, 2002) carried out a comprehensive study (Sr-Nd-Pb-Hf isotopes and trace element ratios) on mantle xenoliths of the northern Canadian craton. The analysed kimberlites, garnet peridotite nodules and garnets are characterised by strong enrichments in incompatible elements (e.g. large ion lithosphile elements (LILE) and LREE) relative to chondrites and primitive mantle composition. The Sr- and Pb-isotopic signatures and incompatible trace element ratios of the peridotites correlate with temperature and pressure, and have been divided into (1) low-temperature ($^{87}Sr/^{86}Sr_{(0.1Ga)}$: 0.7038-0.7066; $^{143}Nd/^{144}Nd_{(0.1Ga)}$: 0.51255-0.51276; $^{206}Pb/^{204}Pb_{(0.1Ga)}$: 17.82-19.03) and (2) high-temperature ($^{87}Sr/^{86}Sr_{(0.1Ga)}$: 0.7052-0.7095; $^{143}Nd/^{144}Nd_{(0.1Ga)}$: 0.51242-0.51262; $^{206}Pb/^{204}Pb_{(0.1Ga)}$: 17.18-18.30) peridotites (e.g. Schmidberger et al., 2001). Schmidberger et al. (2001) concluded that the shallow low- and deep high-temperature peridotites represent chemically distinct mantle reservoirs that do not share a common petrogenetic history. These differences are also displayed by Hf-isotope signatures, as the low-temperature peridotites are characterised by highly radiogenic Hf-isotope compositions ($^{176}Hf/^{177}Hf_{(0.1Ga)}$: 0.28296-0.28419) compared to the high-temperature peridotites ($^{176}Hf/^{177}Hf_{(0.1Ga)}$: 0.28265-0.28333). According to Schmidberger et al. (2002), long-term growth (billions of years) is required to produce these highly depleted Hf-isotope signatures. The strong fractionation of the Lu/Hf ratios during the generation of the melt-depleted peridotites can be interpreted as evidence that, firstly, garnet was present as a residual phase during partial melting and, secondly, for an

ancient (Archaean) depletion event that resulted in the stabilisation of the mantle root beneath the northern Canadian craton to depths of about 150 km.

As the subcontinental mantle lithosphere (SCML) beneath the Canadian craton is characterised by high $^{176}Hf/^{177}Hf$ relative to $^{143}Nd/^{144}Nd$, this could account for the Hf-isotope signature of the Baffin Island lava flows. However, the strong incompatible trace element enrichment of the mantle xenoliths of this area argue against the SCML as a candidate for the origin of the Baffin Island mantle sources. Even small amounts of SCML would change the trace element concentration of the lava flows, and as shown in the previous chapters, some of the Baffin Island lavas show very depleted characteristics which are inconsistent with a source origin in the subcontinental lithosphere. Therefore, the SCML does not explain the high $\Delta\varepsilon Hf$ values of the Baffin Island volcanic rocks and other processes must account for the generation of the source isotope signature.

As shown in chapter 6, the Baffin Island lava flows were generated over a wide range of depths, and for some of the lavas melt generation could have started within the garnet-lherzolite facies. Ancient melt extraction at a depth where the garnet/clinopyroxene ratio was relatively high could create a residue with an unusual (Lu/Hf)/(Sm/Nd) ratio (e.g. Salters & Hart, 1991; Blichert-Toft & White, 2001). Melting in the presence of garnet would lead to higher Hf-isotope ratios in the residue with time: such process could account for the high εHf relative to εNd of the Baffin Island source.

The parameter ΔNb is a useful discriminant between N-MORB and Icelandic lavas, but it cannot distinguish whether Icelandic rocks have enriched or depleted geochemical signatures (e.g. Kempton et al., 2000). By combining ΔNb with $\Delta\varepsilon Hf$, Kempton et al. (2000) argued that it is possible to distinguish not only between N-MORB and Icelandic basalts, but also the enriched and depleted components of the Iceland plume. In this diagram (Fig. 7.6), most of the Icelandic basalts cluster in the upper right quadrant

(positive ΔNb and positive ΔεHf), and Kempton et al. (2000) suggested that they may be indicative of an 'average' Iceland composition. However, the most incompatible element enriched samples analysed by Kempton et al. (2000) have slightly negative ΔεHf and plot in the lower right quadrant. Their North Atlantic N-MORB data from Goban Spur and Hatton Bank plot in the lower left quadrant (negative ΔNb and negative ΔεHf), and can be distinguished from the depleted end of the Reykjanes-Kolbeinsey (RR-KR) array, which has negative ΔNb, but positive ΔεHf values (upper left quadrant). Kempton et al. (2000) concluded that the RR-KR represents an additional depleted component, distinct from both N-MORB and Iceland, and could represent the depleted plume sheath derived from the upper mantle, but from deeper than N-MORB source asthenosphere.

The Baffin Island lava flows and dykes are similar to basalts from the Reykjanes Ridge and Kolbeinsey Ridge, having positive ΔεHf and forming an elongate, subhorizontal array. The depleted (low-Nb/Zr group) lava flows and dykes plot in the upper left quadrant (negative ΔNb and positive ΔεHf), while the enriched lava flows (high-Nb/Zr group) plot in the upper right quadrant (positive ΔNb and positive ΔεHf). According to the model of Kempton et al. (2000), the depleted Baffin Island lava flows would not represent N-MORB, but instead might have been derived from the plume sheath. The enriched Baffin Island lava flows, however, have Nd-Hf isotope signatures of average Icelandic basalts.

In the diagram ΔεHf versus ΔNb, Kempton et al. (2000) made the distinction between the depleted (positive ΔNb and positive ΔεHf) and the enriched (positive ΔNb and negative ΔεHf) component of the Iceland plume. However, with new precise data from the Theistareykir area in northern Iceland (Stracke et al., 2003), this distinction is not replicated. The Theistareykir basalts are depleted to enriched in incompatible elements

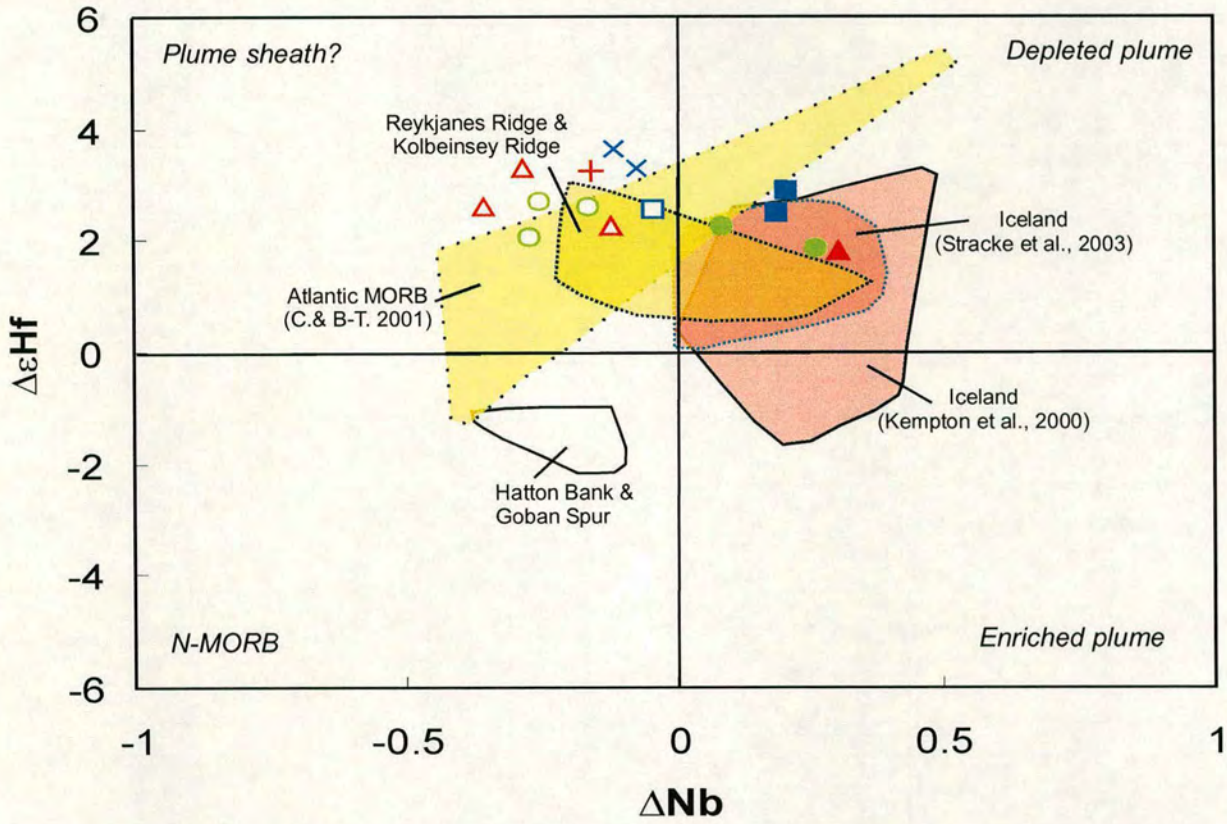

Fig. 7.6. ΔεHf versus ΔNb (after Kempton et al., 2000) for the Baffin Island lava flows and dykes compared with literature data; (1) Iceland (Kempton et al., 2000; Stracke et al., 2003); Atlantic MORB (Chauvel & Blichert-Toft, 2001); Hatton Bank and Globan Spur (Kempton et al., 2000); Reykjanes Ridge and Kolbeinsey Ridge (Kempton et al., 2000). For explanation see text. Symbols for Baffin Island rocks as in Fig. 7.1.

(e.g. $(La/Sm)_n$: 0.33-1.27), but have only positive ΔεH values. As shown in section 7.2, the enriched Baffin Island samples show the most extreme Sr-Nd-isotope ratios and might represent the most enriched end-member of the ancestral Iceland plume. These very enriched Baffin Island samples also have positive ΔNb and positive ΔεHf, plotting in the upper right quadrant in the ΔεHf versus ΔNb plot (defined by Kempton et al. (2000) as the field for the depleted component of the Iceland plume). Thus, neither the Theistareykir nor the Baffin Island basalts confirm the distinction between depleted and enriched Iceland plume components using Hf-Nd isotopes.

Kempton et al. (2000) used samples from the Goban Spur and the Hatton Bank to define the Hf-Nd isotope characteristics of North Atlantic N-MORB. With these data, they suggested, it is possible to distinguish samples with an upper mantle source (negative ΔεHf) from samples derived from a different source in the upper mantle asthenosphere, e.g. plume sheath (positive ΔεHf). However, with new precise data for North Atlantic MORB (Chauvel & Blichert-Toft, 2001), this distinction cannot be so clearly confirmed, as the new samples show a much wider range in Hf-isotope ratios than the samples analysed by Kempton et al. (2000). Therefore, at the time of writing, it is not clear whether it is possible to distinguish between Icelandic basalts and N-MORB as well as between the depleted and enriched components of the plume using Hf-Nd isotopes. More precise Hf data from the North Atlantic, Iceland and other locations within the NAIP are required to confirm this hypothesis. Note also that to date no Hf-isotopic compositions are available for the most enriched off-axis volcanic rocks of Iceland. If these rocks follow the general Iceland trend (towards lower Hf-isotope ratios relative to their Nd isotope ratios), the Baffin Island samples might plot within this trend or just off it (because of their slightly lower Nd isotope ratios than Icelandic basalts [section 7.2]) and thus their Hf-isotope ratios might be not so distinct from Icelandic basalts.

To date, it seems that basaltic rocks from the NAIP show a wide range of Hf-isotope ratios. The high $^{176}Hf/^{177}Hf$ relative to $^{143}Nd/^{144}Nd$ ratios might be a long-lived feature of the Iceland plume (Kempton et al., 2000). Ancient melt extraction at a depth where the garnet/clinopyroxene ratio was relatively high, could create a residue with an unusual (Lu/Hf)/(Sm/Nd) ratio (e.g. Salters & Hart, 1989, 1991; Blichert-Toft & White, 2001). Melting in the presence of garnet would lead to higher Hf-isotope ratios in the residue, which seems to be the most plausible explanation for the positive ΔεHf of the Baffin Island lava flows and dykes.

7.5 $^{3}He/^{4}He$ isotope ratios

Helium isotope studies have provided important indicators of processes such as mantle convection and have been used to trace the origin of mantle-derived magmas. MORBs have relatively low and uniform $^{3}He/^{4}He$ ratios of 8 ±1 R_a ($^{3}He/^{4}He$ ratio of the sample normalised to the atmospheric ratio (R_a) of 1.39 x 10^{-6}), and are thought to derive from a relatively degassed, shallow mantle source. In contrast, the $^{3}He/^{4}He$ ratios of OIBs vary from low ratios in, for example, San Miguel Island (Azores) ($^{3}He/^{4}He$ = 4 R_a; Moreira et al., 1999) to very high ratios in Iceland ($^{3}He/^{4}He$ = 37.7 R_a; Hilton et al., 1999). The high $^{3}He/^{4}He$ ratios of some OIBs have been interpreted as indicators of a mantle source that has maintained a high $^{3}He/(U+Th)$ ratio through time. Such a source might indicate the existence of a primordial, undegassed mantle reservoir isolated at depth in the lower mantle (e.g. Kurz et al., 1982, 1985). In this interpretation, the He-isotope signature provides geochemical evidence for large-scale stratification of the mantle, with a relatively degassed upper mantle and the presence of an undegassed, primordial lower mantle reservoir. OIBs with high $^{3}He/^{4}He$ ratios are attributed to upwelling mantle plumes, which are thought to derive from such an undegassed, isolated reservoir.

Samples from the NAIP with $^3He/^4He$ >8 R_a have been recorded from (a) West Greenland: 30.6 R_a (Graham et al., 1998), (b) Hold with Hope, NE Greenland: 21.7 R_a (Marty et al., 1998), (c) Isle of Skye: 22.1 R_a (Stuart et al., 2000) (d) Prince of Wales Mountains, East Greenland: 10.5 R_a (Ellam & Stuart, 2000) and (e) from Iceland itself: 37.7 R_a (Hilton et al., 1999).

The Helium isotope compositions of basalts from Baffin Island, carried out in this study on eleven olivine phenocryst samples, have the highest $^3He/^4He$ ratio yet recorded from any terrestrial rocks, ranging from 14.5- 49.5 R_a. It is necessary to demonstrate that these high $^3He/^4He$ ratios represent magmatic helium and not nucleogenic and/or cosmogenic ^3He. Nucleogenic ^3He may be produced within crystals by thermal neutron capture by ^6Li (e.g. Aldrich & Nier, 1948). As demonstrated in other parts of the NAIP, however, nucleogenic ^3He production plays no significant role in Palaeocene basalts and can be ruled out as a contaminant and thus as an explanation for the high $^3He/^4He$ ratios (Graham et al., 1998; Marty et al., 1998; Stuart et al., 2000).

Cosmogenic ^3He could be produced through spallation reactions involving cosmic ray secondary particles with target nuclides of Si, O and Mg (Kurz, 1986). These particles are strongly attenuated in the atmosphere, and the ^3He-production rate increases nearly exponentially with atmospheric height. However, the Baffin Island lava flows and dykes have been sampled from seacliffs, which have not been on the Earth's surface for a long enough period of time to accumulate a significant component of cosmogenic helium.

Magmatic helium was extracted from the olivine phenocrysts using *in vacuo* crush release techniques. This method is designed to release magmatic helium from CO_2 bubbles associated with melt inclusions and minimises the contribution from radiogenic and cosmogenic He (^4He and ^3He, respectively) hosted in the crystal lattice (e.g. Kurz, 1986). However, it is possible that diffuse exchange between cosmogenic He produced in the glassy melt inclusions and the original He trapped in fluid inclusions might lead to

an enhancement of cosmogenic ^{3}He in the fluid phase. If this were the case, one would expect an inverse relationship between ^{4}He contents and $^{3}He/^{4}He$ ratios, because the cosmogenic (high ^{3}He) component would be relatively more abundant if He levels trapped (high ^{4}He) were low. The Baffin Island olivine phenocrysts do not display such a relationship (Fig. 7.7), suggesting that cosmogenic He was not the cause of the high $^{3}He/^{4}He$ ratios and that the crushing method has only released magmatic helium. In order to examine the potential accumulation of cosmogenic He in more detail, the olivine powders remaining from the crushing process were transferred to a high-temperature vacuum furnace for the determination of $^{3}He/^{4}He$ and He contents within the olivine lattice. If, as it was the case for the Baffin Island lava flows and dykes, the fusion yields much lower $^{3}He/^{4}He$ than the crushed $^{3}He/^{4}He$ ratios (Fig. 7.8), then the lattice contains predominately radiogenic post-eruptive He (from in situ decay of U and Th, or by α- particle implantation from the surrounding host rock), and it can be concluded that cosmogenic He was not the cause of the high $^{3}He/^{4}He$ ratios. Based on these observations it seems that the high $^{3}He/^{4}He$ ratios of the Baffin Island rocks have not accumulated either nucleogenic or cosmogenic ^{3}He and represent magmatic helium.

Contamination with ancient crustal rocks (which have high values of radiogenic He) would lower the magmatic $^{3}He/^{4}He$ ratio signature. As shown in chapter 5, the disturbed Pb-isotope ratios of the Baffin Island lava flows and dykes could have been affected by amphibolite- and granulite-facies basement rocks. However, the Pb-isotope ratios do not correlate with any other isotope ratios (e.g. Sr, Nd, Hf and He), nor with trace element ratios sensitive to crustal contamination processes. Thus, while the Pb-isotope ratios may indicate interaction with the crustal basement rocks, incompatible trace elements and Sr- and Nd-isotope ratios have not been changed by crustal material (see chapter 5). However, the Cape Searle dyke (CS-7) has high $^{3}He/^{4}He$, high $^{87}Sr/^{86}Sr$ and low $^{143}Nd/^{144}Nd$ ratios, but very low concentrations of incompatible trace elements. In this case, the incompatible-element-poor nature of the dyke parental magma rendered it most

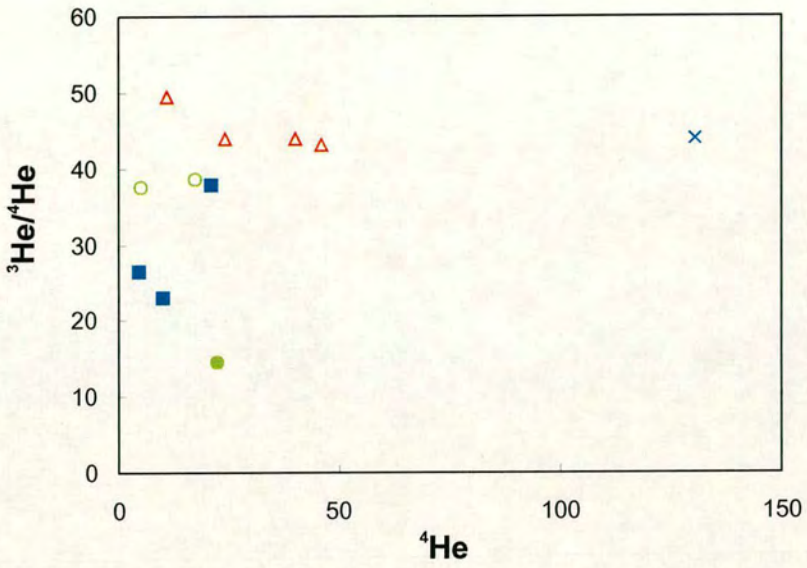

Fig. 7.7. $^3He/^4He$ versus ^4He.

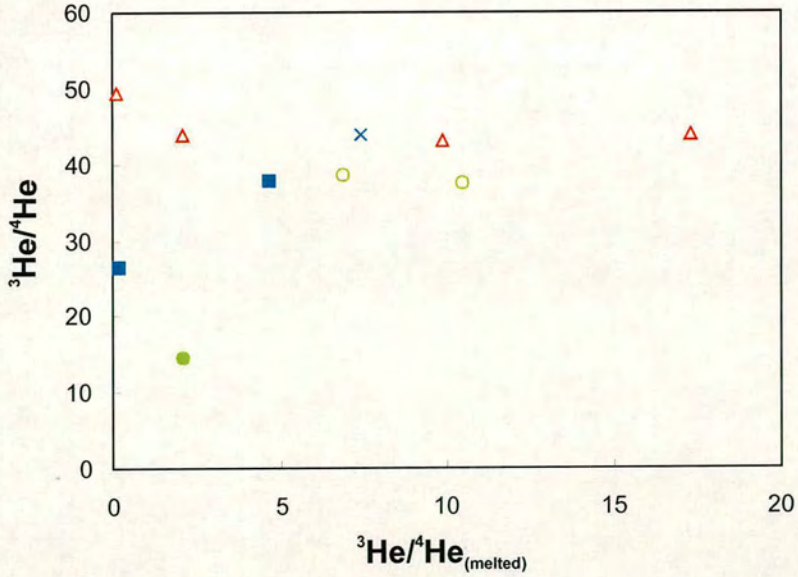

Fig. 7.8. $^3He/^4He$ versus $^3He/^4He_{(melted)}$. The first ratio represents the result using *in vacuo* crush release techniques, while for the second ratio, the olivine powders remaining from the crushing process were transferred to a high temperature vacuum furnace.

sensitive to interaction with the continental crust. Its high $^{3}He/^{4}He$ ratio (43.3 ± 0.6 R_a) suggests that the olivine crystals retained uncontaminated He, while the whole-rock Pb-isotope ratio (and in this case also the Sr- and Nd-isotope ratios) were influenced by crustal material. A possible explanation is, as suggested for Skye basalts, that the whole-rock Pb-isotope composition reflects contamination of the magma after the magmatic gases had been trapped in the olivine crystals (Stuart et al., 2000).

The $^{3}He/^{4}He$ of the Baffin Island olivines correlate strongly with other whole-rock isotope systems (e.g. negatively with $^{87}Sr/^{86}Sr$ (section 3.5.4; Fig. 3.17) and positively with $^{143}Nd/^{144}Nd$ (section 3.5.4; Fig. 3.17 and Fig. 7.9), as well as with incompatible trace element ratios (e.g. negatively with $(La/Sm)_n$ and Nb/Zr [Fig. 7.9]). The two different geochemical groups defined in the previous sections (i.e. high and low Nb/Zr), can be also be distinguished by their helium isotope signatures. The isotopically depleted lava flows have higher $^{3}He/^{4}He$ ratios (37.5-49.5 R_a) than do the isotopically enriched ones (14.5-37.9 R_a). This observation is inconsistent with the prevailing view that lavas with higher $^{3}He/^{4}He$ ratios than "typical" N-MORB contain an excess of the primitive, high ^{3}He, little-degassed component that is widely held to come from a source deeper than the upper mantle. However, the isotopically depleted lava flows of Baffin Island with high $^{3}He/^{4}He$ ratios are characterised by geochemical signatures of the upper mantle (e.g. partial melting [chapter 6] and derivation from a N-MORB mantle source [negative ΔNb - section 7.2]). As the $^{3}He/(U+Th)$ of the MORB reservoir is incapable of significantly changing $^{3}He/^{4}He$ ratios even over hundreds of millions of years, the He- Sr- and Nd- isotope composition of the isotopic depleted lava flows cannot represent N-MORB source mantle at 61 Ma (Stuart et al., 2003). It seems more likely that the high $^{3}He/^{4}He$ component is the product of mantle mixing. Stuart et al. (2003), using data from the present study, suggested that mixing between a small proportion of ^{3}He-rich mantle with depleted mantle (^{3}He: 1.2-4.6 x 10^{9} atoms g^{-1}; Porcelli & Wasserburg, 1995) will severely change the $^{3}He/^{4}He$ ratio without significantly altering Sr- and Nd- isotope

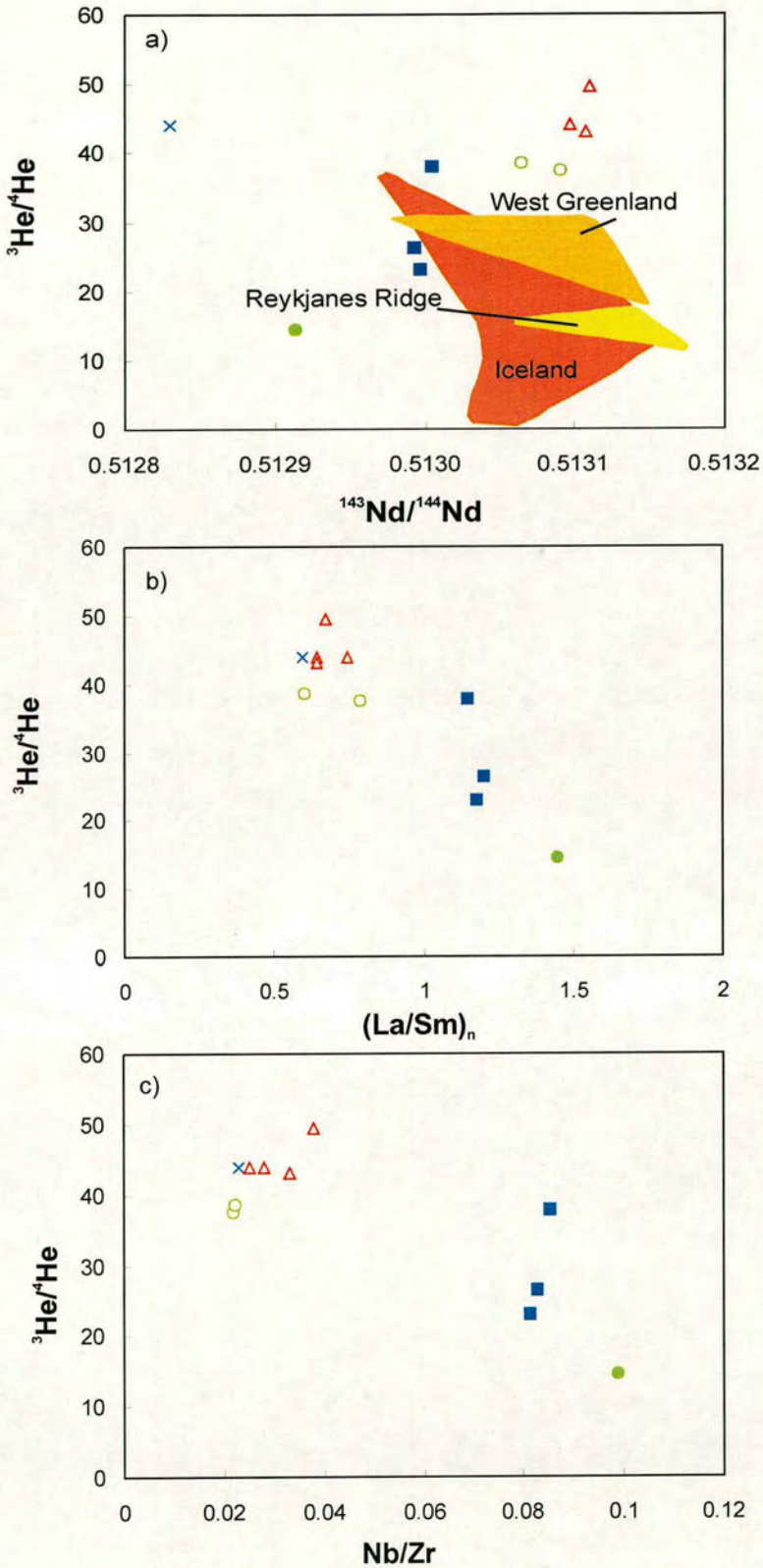

Fig. 7.9. (a) $^3He/^4He$ versus $^{143}Nd/^{144}Nd$ for the Baffin Island lava flows and dyke compared with literature data (West Greenland: Graham et al., 1998; Reykjanes Ridge: Taylor et al., 1997; Iceland: Condomines et al., 1983; Hilton et al., 1999; Breddam et al., 2000) and $^3He/^4He$ versus (b) $(La/Sm)_n$ and (c) Nb/Zr. Symbols as in Fig. 7.1.

ratios and trace element concentrations. They assumed that the moderately incompatible lithophile element concentration in the depleted mantle reservoir is less than a factor of two lower than undepleted mantle (e.g. McKenzie & O'Nions, 1995) and that an undegassed mantle reservoir (with $^{3}He/^{4}He = 50\ R_a$) has a ^{3}He concentration of 8×10^{10} atoms g^{-1} (initial $^{3}He/^{4}He = 120\ R_a$, bulk silicate Earth U = 21 ppb and U/Th = 3.8). This mixing event could have taken place either when the plume head dispersed into the upper mantle, or at the 670 km- boundary layer where both reservoirs (upper and lower mantle material) would have been available. If all geochemical results of this study are taken into account, the latter explanation seems to be more plausible for the Baffin Island lava flows. As shown in chapter 6, the Baffin Island lava flows were generated over a wide range of depths and most of the magmas derive from a melting column, which could have extended across the garnet-spinel transition zone. Note that these lavas also have the highest $^{3}He/^{4}He$ ratios, suggesting that they contain slightly more of the component from the lower, less-degassed mantle. Secondly, provided that the model of Kempton et al. (2000) can be confirmed (which requires additional Hf-isotope data), it would help explain further the generation of the Baffin Island volcanics. In this case, as discussed in the previous section, the isotopically depleted lava flows have not been derived from a N-MORB source, but instead from a source with a slightly deeper origin. The boundary zone between the upper and lower mantle region is maybe the best potential reservoir. This would account for (1) the depleted nature of some of the Baffin Island lava flows (upper mantle signature), (2) for the high Hf-isotope ratios (possibly sheath material with a long history of trace element depletion and isolation from the convecting upper mantle) and (3) high helium isotope ratios which represent a small contribution of the lower mantle.

The isotopically enriched lava flows of Baffin Island have $^{3}He/^{4}He$ ratios lower than the isotopically depleted ones. As shown in chapter 6, the depths of melting of the isotopically depleted and enriched lava flows are very similar even though they might have been derived from different sources (chapter 6). In contrast to the isotopically

depleted lava flows, which have characteristics of a N-MORB source, the isotopically enriched lava flows are more consistent with a source slightly more enriched in incompatible elements (primitive mantle). While some of the isotopically enriched lava flows have much lower $^{3}He/^{4}He$ ratios (e.g. DI-23: 14 R_a), others (e.g. CS-6: 37.9 R_a) are very similar to some depleted lava flows (e.g. DI-24: 37.5 R_a). The most extreme values require that the helium components of these sources were isolated prior to melting. However, some lava flows have similar helium isotope ratios, but otherwise very different trace element and isotopic characteristics. Although trace element and isotope characteristics indicate different mantle sources for these lavas, the helium ratios suggest a similar lower mantle origin for the helium component, which could have been part of the mantle source itself (enriched lava flows), or could be explained by mixing of a small quantity of lower mantle material with the upper mantle source (depleted lava flows).

7.6 Summary

In order to establish whether the geochemical signature of the Iceland plume was present in the westernmost margin of the NAIP, a detailed chemical and isotopic study of Baffin Island was carried out. The Baffin Island lavas display well-defined trends between incompatible trace element ratios (e.g. $(La/Sm)_n$ and Nb/Zr) and Sr- and Nd- isotopic compositions. These correlations cannot be produced by mantle melting processes alone, and are better explained by the availability of different sources at the time of the formation of the Baffin Island lavas: (1) a relatively depleted source with $^{87}Sr/^{86}Sr \approx$ 0.7030-0.7034 and $^{143}Nd/^{144}Nd \approx 0.5130$; and (2) a relatively enriched source with $^{87}Sr/^{86}Sr \approx 0.7039$-0.7042 and $^{143}Nd/^{144}Nd \approx 0.51280$-0.51284. The depleted lava flows are similar to North Atlantic MORB, while the enriched lava flows are similar to (Cape

Searle), or even more extreme than the most enriched basalts erupted on Iceland and across the NAIP (Padloping Island and Durban Island).

To test whether the depleted basalts on Iceland represent N-MORB or are a distinct depleted component of the plume, Fitton et al. (1997) developed a useful discriminant to distinguish between these components. In a logarithmic plot of Nb/Y versus Zr/Y, Icelandic and N-MORB define parallel and non-overlapping linear arrays. The parameter ΔNb expresses the excess or deficiency in Nb and provides a useful discriminant between Icelandic basalts (positive ΔNb) and N-MORB (negative ΔNb). The relatively enriched lava flows of Baffin Island have positive ΔNb values, while the relatively depleted lava flows have negative ΔNb. According to this parameter, both Icelandic and N-MORB sources were available at the western periphery of the ancestral Iceland plume. Kempton et al. (2000) argued that by combining ΔNb with Hf-isotope ratios, it is possible to determine if Icelandic rocks have depleted or enriched signatures. The Baffin Island lava flows have Hf-isotope ratios that range from εHf =11.2 to 17.81 and correlate positively with εNd. Even through the Baffin Island lava flows plot above the mantle array regression line, processes such as the presence of ancient pelagic sediments or material from the subcontinental mantle lithosphere are not responsible for the positive ΔεHf values of the Baffin Island rocks. Instead, it is suggested that an ancient melt extraction process, at a depth where the garnet/clinopyroxene ratio was relatively high, could have created a residue with an unusual (Lu/Hf)/(Sm/Nd) ratio and thus, melting in the presence of garnet would result in higher Hf- relative to Nd-isotope ratios.

Helium isotope studies have provided important indicators of processes such as mantle convection and have been used to trace the origin of mantle-derived magmas. While N-MORBs have relatively low and uniform $^{3}He/^{4}He$ ratios of 8 ±1 R_a, OIBs vary from lower to much higher ratios. The high $^{3}He/^{4}He$ ratios of some OIBs have been

interpreted as indicators of a mantle source that has maintained a high $^{3}He/(U+Th)$ ratio through time and indicates the existence of a primordial, undegassed mantle reservoir isolated at depth in the lower mantle. The Baffin Island lava flows have the highest $^{3}He/^{4}He$ ratios yet recorded in any terrestrial rocks, ranging from 14.5-49.5 R_a. The $^{3}He/^{4}He$ isotope ratios correlate strongly with other whole-rock isotope systems, as well as with incompatible trace element ratios. The two different geochemical groups can be also distinguished by their helium signatures (depleted lavas: 37.5-49.5 R_a, enriched lavas:14.5-37.9 R_a). Note that the high helium component is present in the depleted basalts that are derived from large-volume melts of the depleted upper mantle. This reservoir is the result of mixing between upper mantle and a small proportion of an undegassed lower mantle component, which possibly has taken place at the 670 km discontinuity where both reservoirs are available.

By combining the isotopic and trace element results, the Baffin Island isotopic signature can be described as followed: the high Nb/Zr lava flows of Cape Searle plot in a $^{143}Nd/^{144}Nd$-$^{87}Sr/^{86}Sr$-diagram within the field of Icelandic basalts, suggesting that the geochemical signature of the Iceland mantle plume was present at the most westerly margin of the NAIP. The isotopically extreme lava flows of Padloping Island and Durban Island (high $^{87}Sr/^{86}Sr$ and low $^{143}Nd/^{144}Nd$) could represent the most enriched end-member of the ancestral Iceland plume, which was present at the initiation of the plume but its geochemical signatures are not evident today. The low Nb/Zr lava flows of Baffin Island have similar Sr- and Nd isotope signatures to both depleted Icelandic and North Atlantic N-MORB. ΔNb reveals that these samples do not represent the depleted component of the Iceland plume, but instead show Nb/Y versus Zr/Y ratios of N-MORB. However, the He- and Hf-isotope ratios show that the depleted lava flows of Baffin Island might not have been derived from a N-MORB source, but rather from a source with a slightly deeper origin. This reservoir could represent the 'plume sheath', with a long history of trace element depletion and isolation from the convecting upper

mantle (high Hf-isotope signature). If its origin was at the 670 km boundary between the upper and lower mantle, mixing between a small proportion of primordial helium from the lower mantle with upper mantle material could have resulted in the high helium characteristics.

8 Summary and conclusions

(1) Baffin Island lava flows and dykes are very magnesium-rich (up to 28 wt. % MgO) and contain a large amount of olivine phenocrysts. Most of the analysed olivine phenocrysts are clearly out of equilibrium with their host magmas and the average olivine composition (Fo_{87-89}) suggests that most lavas with MgO > 14 wt. % contain accumulated olivines in various proportions. However, the rare occurrence (10 %) of olivines with forsterite contents up to 91.8 mol % demonstrates that lava flows with MgO contents up to 17.5 wt. % were occasionally available in the formation of the Baffin Island picrites. The small quantity of these highly magnesian olivines in the lava flows implies that in general only the most iron-rich olivines erupted at the surface, while the high magnesian olivines remained in the conduit system. Different processes (e.g. higher ascent velocities, turbulent flows) must have taken place during the eruption of the dykes in order to explain the much greater abundance of Fo-rich olivines (up to $Fo_{92.9}$).

The wide range of olivine compositions of both lava flows and dykes results in a large variety of calculated parental liquid compositions (8.6 – 17.5 wt. % MgO for lava flows and 17.9 – 19.6 wt. % MgO for dykes) and indicates a complex magmatic system, in which several batches of magma have been mixed and of which only a small proportion actually reached the surface.

The lava flows and dykes have estimated parental liquidus temperatures ranging from 1211 – 1358°C and 1339 – 1430°C respectively, at the time the olivines started to crystallise.

(2) The Baffin Island rocks display no clear correlation between isotope ratios (e.g. $^{87}Sr/^{86}Sr$ and $^{143}Nd/^{144}Nd$) and indices of either crustal contamination or differentiation. This demonstrates that neither the Sr- and Nd-isotope system, nor the trace element ratios of the lava flows, were significantly affected by crustal material, in contrast to the dykes, which do show interaction with crustal material.

However, the disturbed Pb-isotope ratios show interaction with continental crust. Possible sources of contamination may have been either a wide range of Archaean and Proterozoic basement rocks (up to 2 % assimilation), or an average Hebridean granulite-facies gneiss (up to 7 % assimilation).

(3) The Baffin Island lava flows and dykes can be divided into two groups, defined by low Nb/Zr and high Nb/Zr, respectively. Assuming a N-MORB source, the low-Nb/Zr samples of Cape Searle can be modelled by 5-8 % melting of a spinel-lherzolite source, while some of the low-Nb/Zr samples from Padloping Island and Durban Island would have been generated within the spinel-lherzolite facies (5-10 %), and others would have been produced from a source composed of a spinel-lherzolite mixture (1–4:96–99). Although the low-Nb/Zr groups of all three locations on Baffin Island can be successfully modelled using a N-MORB source, the calculated melting curves are not consistent with the trace element compositions of the high-Zr/Nb group. Instead, melting of a slightly more enriched source (primitive mantle) is suggested. In this case, the high-Nb/Zr samples of Cape Searle can be modelled by a source composed either of pure spinel lherzolite (6-8 % melting), or by a mix of 96 % spinel and 4 % garnet lherzolite (5-10 % melting). 3-7% melting of a source composed of a mixture of spinel- and garnet-lherzolite source (98:2) could have produced the high Nb/Zr group of Padloping Island and Durban Island.

Segregation pressures range between 1.7 and 3.1 GPa, confirming that the Baffin Island lavas were generated within the melting column over a wide range of depths, throughout the whole eruption event.

(4) In general, lava flows of the low-Nb/Zr group are more magnesium-rich, contain more forsteritic olivines, represent higher-magnesium parental liquid compositions and were produced at slightly higher degrees of melting, at greater depths and at greater temperatures than the high-Nb/Zr rocks. These differences are also reflected in isotope ratios, with the low-Nb/Zr group having consistently higher $^{143}Nd/^{144}Nd$ (ca.0.5130) and lower $^{87}Sr/^{86}Sr$ (0.7030 – 0.7034) than the high-Nb/Zr group ($^{143}Nd/^{144}Nd$: 0.51280 – 0.51284: $^{87}Sr/^{86}Sr$: 0.7039 – 7042).

The relatively enriched samples (e.g. high-Nb/Zr group) of Cape Searle have similar $^{87}Sr/^{86}Sr$ and $^{143}Nd/^{144}Nd$ isotope compositions to Icelandic lavas, while the relatively enriched lavas of Durban Island and Padloping Island are more extreme than Icelandic rocks. These high $^{87}Sr/^{86}Sr$, low $^{143}Nd/^{144}Nd$ lavas could represent the most enriched endmember of the ancestral Iceland plume, which has been present at 62, but of which the geochemical signatures are not evident today.

The relatively depleted lava flows and dykes (e.g. low-Nb/Zr group) have compositions similar to both North Atlantic and Icelandic rocks. Nb/Y and Zr/Y variations (ΔNb) indicate that these volcanics are derived from a N-MORB source and do not represent a distinct depleted component of the Iceland plume.

The high $^{176}Hf/^{177}Hf$ isotope ratios relative to $^{143}Nd/^{144}Nd$ (positive ΔεHf) are best explained by an ancient melt extraction process at depth, where the gt/cpx ratio was relatively high (creating a residue with unusual high (Lu/Hf)/(Sm/Nd) ratio); melting in the presence of garnet could result in such high $^{176}Hf/^{177}Hf$ ratios.

The $^{3}He/^{4}He$ isotope ratios of the olivine phenocrysts correlate strongly with other whole-rock isotope systems (e.g. negatively with $^{87}Sr/^{86}Sr$ and positively with $^{143}Nd/^{144}Nd$), as well with incompatible trace element ratios (e.g. negatively with $(La/Sm)_n$ and Nb/Zr). The high helium component (up to 49.5 R_a) is present in the depleted basalts that are derived from large-volume melts of the depleted upper mantle. This is not consistent with the view that lavas with higher $^{3}He/^{4}He$ ratios than typical N-MORB are derived from the lower, less degassed mantle reservoir. A process of mantle mixing between upper and lower mantle material best explains such a high $^{3}He/^{4}He$ signature. It is suggested that the depleted lava flows are not derived from a N-MORB source, but instead from a source slightly deeper in origin. Such a reservoir could represent a plume 'sheath', which originated at the 670-km thermal boundary. This reservoir could account for: (1) the depleted nature of the Baffin Island lavas (upper mantle signature); (2) the high Hf isotope ratios (long history of trace element depletion and isolation from the convecting upper mantle); and (3) high helium isotope signature (contribution of a small proportion of primordial helium from the lower mantle).

References

Albarède, F. 1992. How deep do common basaltic magmas form and differentiate? *J. Geophys. Res.* **97** (B), 10,997-11,009

Aldrich, L.T. & Nier, A.O. 1948. The occurrence of ^{3}He in natural sources of helium. *Phys. Rev.* **71**, 1590-1594

Allen, R.M., Nolet, G., Morgan, W.J., Vogtfjörd, K., Bergsson, B.H., Erlendsson, P., Foulger, G.R., Jakobsdóttir, S., Julian, B.H., Pritchard, M., Ragnarsson, S. & Stefánsson, R. 1999. The thin hot plume beneath Iceland. *Geophys. J. Int.* **137**, 51-63

Anderson, D.L., Zhang, Y.-S. & Tanimoto, T. 1992. Plume heads, continental lithosphere, flood basalts and tomography. *In*: Storey, B.C., Alabaster, T.U. & Pankhurst, R.J. (eds). Magmatism and the causes of continental break-up. *Geological Society Special Publication* **68**, 99-124

Anderson, D.L. 1998. The Edges of the Mantle. *In*: Gurnis, M., Wysession, M.E. et al. 1998. The Core- Mantle- Boundary Region. *Geodynamics* **28**, American Geophysical Union. Washington, DC, 255-271

Baker, M.B. & Stolper, E.M. 1994. Determining the composition of high-pressure mantle melts using diamond aggregates. *Geochim. Cosmochim. Acta.* **58**, 2811-2827

Balkwill, H.R. 1987. Labrador Basin: structural and stratigraphic style. *In*: Beaumont, C. & Tankard, A.J. (eds.): Sedimentary Basins and basin-forming mechanism. *Can. Soc. of Petroleum Geologists, Memoir* **12**, 17-43

Balkwill, H.R., McMillan, N.J., MacLean, B., Williams, G.L. & Srivastava, S.P. 1990. Geology of the Labrador Shelf, Baffin Bay, and Davis Strait; chapter 7. *In*: Keen, M.J. & Williams, G.L. (eds.): Geology of the continental margin of eastern Canada, Geology of Canada, **2**, 31-85

Berggren, W.A., Kent, D.V., Swisher, C.C. & Aubry, M.-P. 1995. A revised Cenozoic geochronology and chronostratigraphy. *In*: Geochronology, time scales and global stratigraphic correlations. *Society for Sedimentary Geology Special Publication* **54**, 129-212

Bernstein, S., Kelemen, P.B. & Brooks, C.K. 1998. Depleted spinel harzburgite xenoliths in Tertiary dykes from East Greenland: Restites from high degree melting. *Earth Planet. Sci. Lett.* **154**, 221-235

Bertka, C. & Holloway, J.R. 1994. Anhydrous partial melting of an iron-rich mantle II: primary melt compositions at 15 kbar. *Contrib. Mineral. Petrol.* **115**, 323-338

Bijwaard, H. & Spakman, W. 1998. Tomographic evidence for a narrow whole mantle plume below Iceland. *Earth Planet. Sci. Lett.* **166**, 121-126

Blichert-Toft, J., Albarède, F., Rosing, M., Frei, R. & Bridgwater, D. 1999. The Nd and Hf isotopic evolution of the mantle through the Archean. Results from the Isua supracrustals, West Greenland, and from the Birimian terranes of West Africa. *Geochim. Cosmochim. Acta*. **63**, 3901-3014

Breddam, K., Kurz, M.D. & Storey, M. 2000. Mapping out the conduit of the Iceland mantle plume with helium isotopes. *Earth Planet. Sci. Lett.* **176**, 45-55

Breddam, K. 2002. Kistufell: Primitive melt from the Iceland mantle plume. *J. Petrol.* **43**, 345-373

Brooks, C.K. 1973. Rifting and doming in the southern east Greenland. *Nature* (London) **244**, 23-25

Burden, E.T. & Langille, A.B. 1990. Stratigraphy and sedimentology of Cretaceous and Palaeocene strata in half-grabens on the southeast coast of Baffin Island, Northwest Territories. *Bull. Can. Petroleum Geol.* **38**, 185-196

Campbell, I.H & Griffiths, R.W. 1990. Implications of mantle plume structure for the evolution of flood basalts. *Earth Planet. Sci. Lett.* **99**, 79-93

Cande, S.C. & Kent, D.V. 1995. Revised calibration of the geomagnetic polarity time scale for the late Cretaceous and Cenozoic. *J. Geophys. Res.* **100** (B), 6093-6095

Carter, S.R., Evensen, N.M., Hamilton, P.J. & O'Nions, R.K. 1978. Nd- and Sr-isotopic evidence for crustal contamination of continental volcanics. *Science* **202**, 743-747

Carter, S.R., Evensen, N.M., Hamilton, P.J. & O'Nions, R.K. 1979. Basalt magma sources during the opening of the North Atlantic. *Nature* **281**,28-30

Chalmers, J.A. 1991. New evidence on the structure of the Labrador Sea/Greenland continental margin. *J. Geol. Soc. London* **148**, 899-908

Chalmers, J.A., Pulvertaft, T.C.R., Christiansen, F.G., Larsen, H.C., Laursen, K.H. & Ottesen, T.G. 1993. The southern West Greenland continental margin: rifting history, basin development, and petroleum potential. *In*: J.R. Parker (ed.). Petroleum Geology of

Northwest Europe: Proceedings of the 4th Conference, Geological Society, London, 915-931

Chalmers, J.A. & Laursen, K.H. 1995. Labrador Sea: the extent of continental and oceanic crust and the timing of the onset of seafloor spreading. *Marine and Petroleum Geology* **12**, 205-217

Chalmers, J.A., Dahl-Jensen, T., Bate, K.L. & Whittaker, R.C. 1995a. Geology and petroleum prospectively of the region offshore southern West Greenland- a summary. *Rapp. Grønlands Geol. Unders* **165**, 13-21

Chalmers, J.A., Larsen, L.M. & Pedersen, A.K. 1995b. Widespread Palaeocene volcanism around the northern North Atlantic and Labrador Sea- evidence for a large, hot, early plume head. *J. Geol. Soc. London* **152**, 965-969

Chambers, L.M. & Pringle, M.S. 2001. Age and duration of activity at the Isle of Mull Tertiary igneous centre, Scotland, and confirmation of the existence of subchrons during Anomaly 26r. *Earth Planet. Sci. Lett.* **193**, 333-345

Chauvel, C. & Hémond, C. 2000. Melting of a complete section of recycled oceanic crust: trace element and Pb isotopic evidence from Iceland. *Geochem. Geophys. Geosyst.* **1**, 1999GC000002

Chauvel, C. & Blichert-Toft, J. 2001. A hafnium isotope and trace element perspective on melting of the depleted mantle. *Earth. Planet. Sci. Lett.* **190**, 137-151

Chian, D. & Louden, K.E. 1994. The continent-ocean crustal transition across the southwest Greenland margin. *J. Geophys. Res.* **99** (B5), 9117-9135

Chian, D., Keen, C., Reid, I. & Louden, K.E. 1995. Evolution of nonvolcanic rifted margins: New results from the conjugate margins of the Labrador Sea. *Geology* **23**, 589-592

Clarke, D.B. 1967. Tertiary basalts from Baffin Island and West Greenland. *Proc. Geol. Soc. London* **No. 1637**, 50-51

Clarke, D.B. 1968a. Tertiary basalts of the Baffin Bay area. Unpublished Ph.D. thesis. University of Edinburgh.

Clarke, D.B. 1968b. The basalts of Svartenhuk Peninsula, progress report. *Rapp. Greenland Geol. Unders* **15**, 15-17

Clarke, D.B. 1970. Tertiary basalts of Baffin Bay: possible primary magma from the mantle. *Contrib. Mineral. Petrol.* **25**, 203-224

Clarke, D.B. & Upton, B.G.J. 1971. Tertiary basalts of Baffin Island. *Can. J. Earth. Sci.* **8**, 248- 258

Clarke, D.B. 1975. Tertiary basalts dredged from Baffin Bay. *Can. J. Earth. Sci.* **12**, 1396-4105

Clarke, D.B. & Pedersen, A.K. 1976. Tertiary volcanic province of West Greenland. *In*: Escher, A. & Watts, W.S. (eds.). Geology of Greenland. Geological Survey Of Greenland, Copenhagen, 365-385

Clarke, D.B. & O'Hara, M.J. 1979. Nickel and the existence of high- MgO liquids in nature. *Earth Planet. Sci. Lett.* **44**, 153-158

Clarke, D.B., Cameron, B.I., Muecke, G.K. & Bates, J.L. 1988. Early Tertiary basalts from the Labrador Sea floor and Davis Strait region. *Can. J. Earth. Sci.* **26**, 956-968

Coffin, M.F. & Eldholm, O. 1992. Volcanism and continental break-up: a global compilation of large igneous provinces. *In*: Storey, B.C., Alabaster, T.U. & Pankhurst, R.J. (eds). Magmatism and the causes of continental break-up. *Geological Society Special Publication* **68**, 17-30

Coffin, M.F. & Eldholm, O. 1993. Scratching the surface: estimating dimensions of large igneous provinces. *Geology* **21**, 515-518

Cohen, R.S., Evensen, N.M., Hamilton, P.J. & O'Nions, R.K. 1980. U-Pb, Sm-Nd and Rb-Sr systematics of mid-ocean ridge basalt glasses. *Nature* **283**, 149-152

Cohen, R.S. & O'Nions, R.K. 1982. The lead, neodymium and strontium isotopic structure of ocean ridge basalts. *J. Petrol.* **23**, 299-324

Condomines, M., Grönvold, K., Hooker, P.J., Muehlenbachs, K., O'Nions, R.K., Óskatsson, N. & Oxburgh, E.R. 1983. Helium, oxygen, strontium and neodymium isotopic relationships in Icelandic volcanics. *Earth Planet. Sci. Lett.* **66**, 125-136

Courtney, R.C. & White, R.S. 1986. Anomalous heat flow and geoid across the Cape Verde Rise: Evidence for dynamic support from a thermal plume in the mantle. *Royal Astronomical Society Geophysical Journal* **87**, 815-967

Cserepes, L. & Yuen, D.A. 2000. On the possibility of a second kind of mantle plume. *Earth. Planet. Sci. Lett.* **183**, 61-71

Dam, G., Larsen, M. & Sønderholm, M. 1998. Sedimentary response to mantle plumes: Implications from Palaeocene onshore successions, West and East Greenland. *Geology* **26**, 207-210

Davies, G.F. 1988. Ocean bathymetry and mantle convection 1. large-scale flow and hotspots. *J. Geophys. Res.* **93**, 467-480

Dawes, P.R. & Kerr, J.W. 1982. The case against major displacement along Nares Strait. *In*: P.R. Dawes & J.W. Kerr (eds.). Nares Strait and the drift of Greenland: A conflict in plate tectonics. *Medd. Groenl. Geosci.* **8,** 392 pp.

Deutsch, E.R., Kristjansson, L.G. & May, B.T. 1971. Remanent magnetism of lower Tertiary lavas on Baffin Island. *Can. J. Earth. Sci.* **8**, 1542-1552

Dickin, A.P. 1981. Isotope geochemistry of Tertiary Igneous rocks from the Isle of Skye, N.W. Scotland. *J. Petrol.* **22**, 155-189

Dosso, L., Hanan, B.B., Bougault, H., Schilling, J.G. & Joron, J.-L. 1991. Sr-Nd-Pb geochemical morphology between 10° and 17° N on the Mid-Atlantic Ridge: a new MORB isotope signature. *Earth. Planet. Sci. Lett.* **106**, 29-43

Dosso, L., Bougault, H. & Joron, J.-L. 1993. Geochemical morphology of the North Mid-Atlantic Ridge, 10°-24°N: Trace element-isotope complementarily. *Earth Planet. Sci. Lett.* **120**, 443-462

Dupré, B. & Allègre, C.J. 1980. Pb-Sr-Nd isotopic correlation and chemistry of the North Atlantic mantle. *Nature* **286**, 17-22

Eisele, J., Sharma, M., Galer, S.J.G., Blichert-Toft, J., Devey, C.W. & Hofmann, A.W. 2002. The role of sediment recycling in EM-1 inferred from Os, Pb, Hf, Nd, Sr isotope and trace element systematics of the Pitcairn hotspot. *Earth Planet. Sci. Lett.* **196**, 197-212

Ellam, R.M. & Stuart, F.M. 2000. The sub-lithospheric source of North Atlantic Basalts: evidence for, and significance of, a common end-member. *J. Petrol.* **41**, 919-932

Elliot, T.R., Hawkesworth, C.J. & Grönvold, k. 1991. Dynamic melting of the Iceland Plume. *Nature* **351**, 201-206

Elthon, D. & Ridley, W.I. 1979. Comments on: "The partitioning of Nickel between olivine and silicate melt" by S.R. Hart & K.E. Davis. *Earth Planet. Sci. Lett.* **44**, 162-164

Fitton, J.G., Saunders, A.D., Norry, M.J., Hardarson, B.S. & Taylor, R.N. 1997. Thermal and chemical structure of the Iceland plume. *Earth Planet. Sci. Lett.* **153**, 197-208

Fitton, J.G., Hardarson, B.S., Ellam, R.M. & Rogers, G. 1998. Sr-, Nd-, and Pb-isotope composition of volcanic rocks from the southeast Greenalnd margin at 63°N: temporal variation in crustal contamination during continental breakup. *Proceedings of the Ocean Drilling Program, Scientific results*. **152**, 351-357

Fitton, J.G., Larsen, L.M., Saunders, A.D., Hardarson, B.S. & Kempton, P.D. 2000. Palaeogene Continental to Oceanic Magmatism on the SE Greenland Continental Margin at 63°N: a Review of the Results of Ocean Drilling Program Legs 152 and 163. *J. Petrol.* **41**, 951-966

Fitton, J.G., Saunders, A.D., Kempton, P.D. & Hardarson, B.S. 2003. Does depleted mantle form an intrinsic part of the Iceland plume? Geochem. Geophys. Geosyst., 4, Paper number 2002GC000424, (Available at http://www.g-cubed.org)

Ford, C.E., Russell, D.G., Craven, J.A. & Fisk, M.R. 1983. Olivine-liquid equilibria: Temperature, pressure and composition dependence of the crystal/liquid cation partion coefficients for Mg, Fe^{2+}, Ca and Mn. *J. Petrol.* **24**, 256-265

Foulger, G.R., Pritchard, M.J., Julian, B.R., Evans, J.R., Allen, R.M., Nolet, G., Morgan, W.J., Bergsson, B.H., Erlendsson, P., Jakobsdóttir, S., Ragnarsson, S., Stefansson, R. & Vogtfjörd, K. 2000. The seismic anomaly beneath Iceland extends down to the mantle transition zone and no deeper. *Geophys. J. Int.* **142**, F1-F5

Foulger, G.R. & Pearson, D.G. 2001. Is Iceland underlain by a plume in the lower mantle? Seismology and helium isotopes. *Geophys. J. Int.* **145**, F1-F5

Fram, M.S. & Lesher, C.E. 1997. Generation and polybaric differentiation of East Greenland Early Tertiary Flood Basalts. *J. Petrol.* **38**, 231-275

Fram, M.S., Lesher, C.E. & Volpe, A.M. 1998. Mantle melting systematics: transition from continental to oceanic volcanism on the southeast Greenland margin. *Proceedings of the Ocean Drilling Program, Scientific results*. **152**, 373-386

Francis, D. 1985. The Baffin Bay lavas and the value of picrites as analogues of primary magmas. *Contrib. Mineral. Petrol.* **89**, 144-155

Francis, D. 1986. The pyroxene paradox in MORB glasses- a signature of picritic parental magmas? *Nature* **319**, 586-589

Frisch, T. & Dawies, P.R. 1994. A seismic reflection study of northern Baffin Bay: implication for tectonic evolution: Discussion. *Can. J. Earth. Sci.* **31**, 219-220

Furman, T., Frey, F.A. & Park, K.-H. 1991. Chemical constraints on the petrogenesis of mildly alkaline lavas from Vestmannaeyjar, Iceland: the Eldfell (1973) and Surtsey (1963-1967) eruptions. *Contrib. Mineral. Petrol.* **109**, 19-37

Furman, T., Frey, F. & Park, K.-H. 1995. The scale of source heterogeneity beneath the Eastern neovolcanic zone, Iceland. *J. Geol. Soc. London* **152**, 997-2000

Geoffroy, L., Gelard, J.P., Lepvrier, C. & Oliver, P. 1998. The coastal flexure of Disko (West Greenland), onshore expression of the 'oblique reflectors'. *J. Geol. Soc. London* **155**, 463-473

Geoffroy, L., Callot, J.-P., Scaillet, S., Skuce, A., Gélard, J.P., Ravilly, M., Angelier, J., Bonin, B., Cayet, C., Perrot, K. & Lepvrier, C. 2001. Southeast Baffin volcanic margin and the North-American-Greenland plate separation. *Tectonics* **20**, 566-584

Gill, R.C.O., Nielsen, T.F.D., Brooks, C.K. & Ingram, G.A. 1988. Tertiary volcanism in the Kangerdlugssuaq region, E Greenland: trace-element geochemistry of the Lower Basalts and tholeiitic dyke swarms. *In*: Morton, A.C. & Parson, L.M. (eds). Early Tertiary volcanism and the opening of the NE Atlantic. *Geological Society Special Publication* **39**, 161-179

Gill, R.C.O., Pedersen, A.K. & Larsen, J.G. 1992. Tertiary picrites in West Greenland : melting of the periphery of a plume? *In*: Storey, B.C., Alabaster, T.U. & Pankhurst, R.J. (eds). Magmatism and the causes of continental break-up. *Geological Society Special Publication* **68**, 335-348

Goodrich, C.A. & Patchett, P.J. 1991. Nd and Sr isotope chemistry of metallic iron-bearing, sediment-contaminated Tertiary volcanics from Disko Island, Greenland. *Lithos* **27**, 13-27

Govindaraju, K. 1994. 1994 compilation of working values and sample description for 383 standards. Geostandards Newsletter, 18 (Special issue), 158pp

Graham, D.W., Larsen, L.M., Hanan, B.B., Pedersen, A.K. & Lupton, J.E. 1998. Helium isotope composition of the early Iceland mantle plume inferred from the Tertiary picrites of West Greenland. *Earth Planet. Sci. Lett.* **160**, 241-255

Grant, A.C. 1975. Geophysical results from the continental margin off southern Baffin Island. *In*: C.J. Yorath, E.R. Parker & D.J. Glass (eds). Canada's continental margins and offshore petroleum exploration. *Canadian Society of Petroleum Geologists, Memoir* **4**, 411-431

Grant, A.C. 1980. Problems with plate tectonics: the Labrador Sea. *Bulletin of Canadian Petroleum Geology* **28,** 252-278

Grant, A.C. 1982. Problems with plate tectonic models for Baffin Bay-Nares Strait; evidence from the Labrador Sea. *In*: P.R. Dawes & J.W. Kerr (eds.). Nares Strait and the drift of Greenland; a conflict in plate tectonics. *Meddeleser om Grønland, Geoscience* **8**, 313-326

Green, D.H., Falloon, T.J., Eggins, S.M. & Yaxley, G.M. 2001. Primary magmas and mantle temperatures. *Eur. J. Mineral.* **13**, 437-451

Griffiths, R.W. & Campbell, I.H. 1990. Stirring and structure in mantle starting plumes. *Earth Planet. Sci. Lett* **99**, 66-78

Gurenko, A.A. & Chaussidon, M. 1995. Enriched and depleted primitive melts included in olivine from Icelandic tholeiites: origin by continuous melting of a single mantle column. *Geochim. Cosmochim. Acta*. **59**, 2,905-2,917

Hald, N. & Pedersen, A.K. 1975. Lithostratigraphy of the early Tertiary volcanic rocks of central West Greenland. *Rapp. Grønlands Geol. Unders*. **69**, 17-24

Hanan, B.B. & Schilling, J.-G. 1997. The dynamic evolution of the Iceland mantle plume: the lead isotope perspective. *Earth Planet. Sci. Lett*. **151**, 43-60

Hanan, B.B., Blichert-Toft, J., Kingsley, R. & Schilling, J.-G. 2000. Depleted Iceland mantle plume geochemical signature: Artifact of multicomponent mixing? *Geochem. Geophys. Geosyst*. **1**, 1999GC000009

Hansen, H. & Nielsen, T.F.D. 1999. Crustal contamination in Palaeogene East Greenland flood basalts: plumbing system evolution during continental rifting. *Chem. Geol*. **157**, 89-118

Hardarson, B.S. & Fitton, J.G., Ellam, R.M. & Pringle, M.S. 1997. Rift relocation- a geochemical and geochronical investigation of a palaeo-rift in northwest Iceland. *Earth Planet. Sci. Lett*. **153**, 181-198

Hards, V.L., Kempton, P.D. & Thompson, R.N. 1995. The heterogeneous Iceland plume: new insights from the alkaline basalts of the Snaelfell volcanic centre. *J. Geol. Soc. London* **152**, 1003-1009

Harland, W.B., Armstrong, R.L., Craig, L.E., Smith, A.G. & Smith, D.G. 1990. A Geologic Time Scale. *Cambridge Univ. Press, New York.*

Hart, S.R., Schilling, J.-G., Powell, J.L. 1973. Basalts from Iceland and along the Reykjanes Ridge: Sr isotope geochemistry. *Nature Phys. Sci.* **246**(155), 104-107

Hart, S.R. & Davies, K.E. 1978. Nickel partitioning between olivine and silicate melt. *Earth Planet. Sci. Lett.* **40**, 203-219

Hart, S.R. & Davis, K.E. 1979. Reply to D.B. Clarke and M.J. O'Hara, "Nickel, and the existence of high-MgO liquids in nature". *Earth Planet. Sci. Lett.* **44**, 159-161

Helmberger, D.V., Wen, L. & Ding, X. 1998. Seismic evidence that the source of the Iceland hotspot lies at the core-mantle boundary. *Nature* **396**, 251-255

Hemond. C., Arndt, N.T., Lichtenstein, U. & Hofmann, A.W. 1993. The heterogeneous Iceland plume: Nd-Sr-O isotopes and trace element constraints. *J. Geophys. Res.* **98**, (B), 15,833-15,850

Henderson, G., Rosenkrantz, A. & Schiener, E.J. 1976. Cretaceous-Tertiary sedimentary rocks of West Greenland. *In*: Escher, A. & Watt, W.S (eds). Geology of Greenland. Geological Survey of Greenland, 340-362

Hervig, R.L., Smith, J.V. & Dawson, J.B. 1986. Lherzolite xenoliths in kimberlites and basalts: petrogenetic and crystallochemical significance of some minor and trace elements in olivine, pyroxenes, garnet and spinel. *Trans. R. Soc. Edinburgh, Earth Sci.* **77**, 181-201

Herzberg, C. 1992. Depth and degree of melting of komatiites. *J. Geophys. Res.* **97**, 4521-4540

Herzberg, C. 1995. Generation of plume through time: an experimental perspective. *Chem. Geol.* **126**, 1-16

Herzberg, C. & O'Hara, M.J. 1998. Phase equilibrium constraints on the origin of basalts, picrites and komatiites. *Earth-Science Rewiews* **44**, 39-79

Herzberg, C. & O'Hara, M.J. 2002. Plume-associated ultramafic magmas of phanerozoic age. *J. Petrol.* **43**, 1857-1883

Herzberg, C. & Zhang, J. 1996. Melting experiments on anhydrous peridotite KLB-1: Composition of magmas in the upper mantle and transition zone. *J. Geophys. Res.* **101**, B4, 8271-8295

Hill, R.I. 1991. Starting plumes and continental break- up. *Earth Planet. Sci. Lett* **104**, 398-416

Hilton, D.R., Grönvold, K., Macpherson, C.G. & Castillo, P.R. 1999. Extreme $^{3}He/^{4}He$ ratios in northwest Iceland: constraining the common component in mantle plumes. *Earth Planet. Sci. Lett.* **173**, 53-60

Hirose, E. & Kushiro, I. 1993. Partial melting of dry peridoties at high pressures: determination of compositions of melts segregated from peridotite using aggregates of diamond. *Earth Planet. Sci. Lett.* **114**, 477-489

Hofmann, A.W. 1988. Chemical differentiation of the Earth: the relationship between mantle, continental crust, and oceanic crust. *Earth Planet. Sci. Lett.* **90**, 297-314

Holm, P.M. 1988. Nd, Sr and Pb isotope geochemistry of the Lower Lavas, E Greenland Tertiary Igneous Province. *In*: Morton, A.C. & Parson, L.M. (eds). Early Tertiary

volcanism and the opening of the NE Atlantic. *Geological Society Special Publication* **39**, 181-195

Holm, P.M., Gill, R.C.O., Pedersen, A.K., Larsen, J.G., Hald, N., Nielsen, T.F.D. & Thirlwall, M.F. 1993. The Tertiary picrites of West Greenland: contributions from 'Icelandic' and other sources. *Earth Planet. Sci. Lett* **115**, 227-244

Irvine, T.N. 1979. Rocks whose composition is determined by crystal accumulation and sorting. *In*: The evolution of the igneous rocks: Fiftieth Anniversary Perspectives. Princeton University Press, 245-306

Ito, G., White, W.M. & Göpel, C. 1987. The O, Sr, Nd and Pb isotope geochemistry of MORB. *Chem. Geol.* **62**, 157-176

Jackson, G.D. & Taylor, F.C. 1972. Correlation of major Aphebian rock units in the northeastern Canadian Shield. *Can. J. Earth. Sci.* **9**, 1650-1669

Jackson, G.D., Hunt, P.A., Loveridge, W.D. & Parrish, R.R. 1990. Reconnaissance geochronology of Baffin Island, N.W.T. *In:* Radiogenic Age and isotopic studies: Report 3, Geological Survey of Canada, Paper 89-2, 123-148

Jackson, G.D. & Berham, R.G. 2000. Precambrian metamorphic and tectonic evolution of northern Baffin Island, Nunavut, Canada. *Canadian Mineralogist* **38**, 399-421

Jackson, H.R., Keen, C.E. & Falconer, R.K.H. 1979. New geophysical evidence for sea-floor spreading in central Baffin Bay. *Can. J. Earth. Sci.* **16**, 2122-2135

Jackson, H.R., Dickie, K. & Marillier, F. 1992. A seismic reflection study of northern Baffin Bay: implication for tectonic evolution. *Can. J. Earth. Sci.* **29**, 2353-2369

Jackson, H.R. & Marillier, F. 1994. A seismic reflection study of northern Baffin Bay: implication for tectonic evolution: Reply. *Can. J. Earth. Sci.* **31**, 221-222

Johnston, K.T.M., Dick, H.J.B & Shimizu, N. 1990. Melting in the oceanic upper mantle: An ion microprobe study of diopsides in abyssal peridotites. *J. Geophys. Res.* **95**(B), 2661-2678

Johnston, S.T. & Thorkelson, D.J. 2000. Continental flood basalts: episodic magmatism above long-lived hotspots. *Earth Planet. Sci. Lett.* **175**, 247-256

Kalsbeek, F. & Taylor, P.N. 1985. Age and origin of early Proterozoic dolerite dykes in South-West Greenland. *Contrib. Mineral Petrol.* **89**, 307-316

Kalsbeek, F., Pidgeon, R.T. & Taylor, P.N. 1987. Nagssugtoqidian mobile belt of West Greenland: a cryptic 1850Ma suture between two Archean continents- chemical and isotopic evidence. *Earth. Planet. Sci. Lett.* **85**, 365-385

Kalsbeek, F., Austrheim, H., Bridgwater, D., Hansen, B.T., Pedersen, S. & Taylor, P.N. 1993. Geochronology of Archean and Proterozoic events in the Ammassalik area, south-east Greenland, and comparisons with the Lewsian of Scotland and the Nagssugtoqidian of West Greenland. *Precam. Research* **62**, 239-270

Keen, M.J. & Clarke, D.B. 1974. Tertiary basalts of Baffin Bay: geochemical evidence for a fossil hot-spot. *In*: Kristjansson (ed.): Geodynamics of Iceland and the North Atlantic area. *Proceedings of the NATO Advanced study institute*, 127-137

Kempton, P.D., Nowell, G.M., Fitton, J.G., Saunders, A.D. & Taylor, R.N. 1998. The Iceland plume in space and time: a Sr-Nd-Pb-Hf study of the North Atlantic rifted margin. *Mineralogical magazine* **62A**, 759-760

Kempton, P.D., Fitton, J.G., Saunders, A.D., Nowell, G.M., Taylor, R.N., Hardarson, B.S. & Pearson, G. 2000. The Iceland plume in space and time: a Sr-Nd-Pb-Hf study of the North Atlantic rifted margin. *Earth. Planet. Sci. Lett.* **177**, 255-271

Kempton, P.D. Nowell, G.M. & Barry, T.L. 2001. Procedure for High Precision Isotopic Analysis of hafnium in silicate rocks and minerals by plasma ionisation multi-collector mass spectrometry (PIMMS) and an Assessment of data quality at the NERC Isotope Geosciences Laboratory. NIGL Rep. Ser:171, NERC Isotope Geosci. Lab., Keyworth, U.K.

Kennet, B.L.N. & Engdahl, E.R. 1991. Travel times for global earthquake location and phase identification. *Geophys. J. Int.* **105**, 429-466

Kent, A.J.R., Stolper, E.M., Woodhead, J., Hutcheon, L.D. & Francis, D. 1998. Using glass inclusions to investigate a heterogeneous mantle: an example from N- and EMORB-like lavas from Baffin Island. *Min. Mag.* **62A** (Goldschmidt Conference), 765-766

Kent, D.V. & Gradstein, F.M. 1986. A Jurassic to recent chronology. *In*: Vogt, P.R. & Tucholke, B.E. (eds.) The western North Atlantic region: Boulder, Colorado. Geological Society of America, The Geology of North America, v.M, 351-378

Kent, R.W., Storey, M. & Saunders, A.D. 1992. Large igneous provinces: sites of plume impact or plume incubation? *Geology* **20**, 891-894

Kent, R.W. 1995. Magnesian basalts from the Hebrides, Scotland: Chemical composition and relationship to the Iceland plume. *J. Geol. Soc. London* **152**, 979-983

Kerr, A.C. 1995a. The melting processes and composition of the North Atlantic (Iceland) plume: geochemical evidence from the early Tertiary basalts. *J. Geol. Soc. London* **152**, 975-978

Kerr, A.C. 1995b. The geochemistry of the Mull-Morvern Tertiary lava succession, NW Scotland: an assessment of mantle sources during plume-related volcanism. *Chem. Geol.* **122**, 43-58

Kerr, A.C., Saunders, A.D., Tarney, J., Berry, N.H. & Hards, V.L. 1995. Depleted mantle-plume geochemical signatures: No paradox for plume theories. *Geology* **23**, 843-846

Kerr, A.C. & Arndt, N.T. 2001. A note on the IUGS Reclassification of the high-Mg and picritic volcanic rocks. *J. Petrol.* **42**, 2169-2171

Kerr, J.W. 1967. A submerged continental remnant beneath the Labrador Sea. *Earth Plant. Sci. Lett.* **2,** 283-289

Kinzler, R.J. & Grove, T.L. 1992. Primary magmas of mid-ocean ridge basalts 2. Applications. *J. Geophys. Res.* **97** (B), 6907-6926

Klein, E.M. & Langmuir, C.H. 1987. Global correlations of ocean ridge basalt chemistry with axial depth and crustal thickness. *J. Geophys. Res.* **92** (B), 8089-8115

Klose, G.W., Malterre, E., McMillan, N.J. & Zinkan, C.G. 1982. Petroleum exploration offshore southern Baffin Island, northern Labrador Sea, Canada. *In*: Embry, A.F. &

Balkwill, H.R. (eds.): Arctic geology and geophysics, Proceedings of the Third International Symposium on Arctic geology. *Can. Soc. of Petroleum Geologists. Memoir* **8**, 233-244

Krishnamurthy, P. & Cox, K.G. 1977. Picrite basalts and related lavas from the Deccan Traps of Western India. *Contrib. Mineral. Petrol.* **62**, 53-75

Kristoffersen, Y. & Talwani, M. 1977. Extinct triple junction south of Greenland and the Tertiary motion of Greenland relative to North America. *Geol. Soc. Am. Bull.* **88**, 1037-1949

Kurz, M.D. 1986. Cosmogenic helium in a terrestrial igneous rock. *Nature* **320**, 435-439

Kurz, M.D., Jenkins, W.J., Schilling, J.-G. & Hart, S.R. 1982. Helium isotopic variation in the mantle beneath the central North Atlantic Ocean. *Earth Plant. Sci. Lett.* **58**, 1-14

Kurz, M.D., Meyer, P.S. & Sigurdsson, H. 1985. Helium isotopic systematics within the neovolcanic zones of Iceland. *Earth Planet. Sci. Lett.* **74**, 291-305

Langmuir, C.H., Klein, E.M. & Plank, T.1992. Petrological systematics of mid-ocean ridge basalts: constraints on melt generation beneath ocean ridges. *In*: Morgan, J.P., Blackman, D.K. & Sinton, J.M. (eds.). Mantle flow and melt generation at mid-ocean ridges. *Geophys. Monogr. Ser.* **71**, 183-280, AGU, Washington, D.C.

Larsen, H.C., Saunders, A.D., Clift, P.D. & Shipboard Scientific Party. 1994. 1. Introduction: Breakup of the southeast Greenland margin and the formation of the Irminger Basin: Background and scientific objectives. *Proc. Ocean Drill. Prog., Init. Repts.* **152**, 5-16

Larsen, H.C. & Saunders, A.D. 1998. 41. Tectonism and volcanism at the Southeast Greenland rifted margin: a record of plume impact and later continental rupture. *Proceedings of the Ocean Drilling Program, Scientific results*. **152**, 503-533

Larsen, L.M., Pedersen, G.K. & Piasecki, S. 1992. Timing and duration of Early Tertiary vulcanism in the North Atlantic: new evidence from West Greenland. *In*: Storey, B.C., Alabaster, T.U. & Pankhurst, R.J. (eds): Magmatism and the causes of continental break-up. *Geological Society Special Publication* **68**, 321-333

Larsen, L.M., Fitton, J.G. & Fram, M.S. 1998.Volcanic rocks of the southeast Greenland margin in comparison with other parts of the North Atlantic Tertiary Igneous province. *Proceedings of the Ocean Drilling Program, Scientific results*. **152**, 315-330

Larsen, L.M., Fitton, J.G. & Saunders, A.D. 1999. Composition of volcanic rocks from the southeast Greenland margin, Leg163: major and trace element geochemistry. *Proceedings of the Ocean Drilling program, Scientific results* **163**, 63-75

Larsen, L.M. & Pedersen, A.K. 2000. Processes in high-Mg, high-T magmas: evidence from olivine, chromite and glass in Palaeogene picrites from West Greenland. *J. Petrol.* **41**, 1071-1098

Larsen, L.M., Pedersen, A.K., Sundvoll, B. & Frei, R. 2003. Alkali picrites formed by melting of old metasomatized lithospheric mantle: Manîtdlat member, Vaigat formation, Palaeocene of West Greenland. *J. Petrol.* **44**, 3-38

Larsen, T.B., Yuen, D.A., Malevsky, A.V. & Smedsmo, J.L. 1996. Dynamics of strongly time-dependent convection with non-Newtonian temperature-dependent viscosity. *Phys. Earth Planet. Inter.* **94**, 75-703

Larsen, T.B. & Yuen, D.A. 1997. Ultrafast upwelling bursting through the upper mantle. *Earth Planet. Sci. Lett.* **146**, 393-399

Larsen, T.B., Yuen, D.A. & Storey, M. 1999. Ultrafast mantle plumes and implications for flood basalt volcanism in the Northern Atlantic Region. *Tectonophysics* **311**, 31-43

Lawver, L.A. & Müller, R.D. 1994. Iceland hotspot track. *Geology* **22**, 311-314

Le Bas, M.J. & Streckeisen, A.L. 1991. The IUGS systematics of igneous rocks. *J. Geol. Soc. London* **148**, 825-833

Le Bas, M.J. 2000. IUGS Reclassification of the high-Mg and picritic volcanic rocks. *J. Petrol.* **41**, 1467-1470

LeBas, M.J. 2001. Reply to comment by Kerr and Arndt. *J. Petrol.* **42**, 2173-2174

Le Maitre, R.W., Bateman, P., Dudek, A., Keller, J. Lameyre, J., Le Bas, M.J., Sabine, P.A., Schmid, R., Sorensen, H., Streckeisen, A., Woolley, A,R. & Zanettin, B. 1989. A classification of igneous rocks and glossary of terms: recommendations of the International Union of Geological Sciences Subcommision on the Systematics of Igneous Rocks. *Blackwell Scientific Publications*, Oxford.

Lightfoot, P.C., Hawkesworth, C.J., Olshefsky, K., Green, T., Doherty, W. & Keays, R.R. 1997. Geochemistry of Tertiary tholeiites and picrites from Qeqertarssuaq (Disko Island) and Nuussuaq, West Greenland with implications for the mineral potential of comagmatic intrusions. *Contrib. Mineral. Petrol.* **128**, 139-163

Manhes, C., Minster, C. & Allègre, C.J. 1978. Comparative uranium-thorium-lead and rubidium-strontium study of the Saint Severin amphoterite: consequences of early Solar System chronology. *Earth Planet. Sci. Lett.* **39**, 14-24

Marty, B., Upton, B.G.J. & Ellam, R.M. 1998. Helium isotopes in early Tertiary basalts, northeast Greenland: Evidence for 58 Ma plume activity in the North Atlantic-Iceland volcanic province. *Geology* **26**, 407-410

McDonough, W.F. & Sun, S.-s. 1995. The composition of the Earth. *Chem. Geol.* **120**, 223-253

McKenzie, D. & Bickle, M.J. 1988. The volume and composition of melt generated by extension of the lithosphere. *J. Petrol.* **29**, 625-679

McKenzie, D. & O'Nions, R.K. 1991. Partial melt distributions from inversion of rare earth element concentrations. *J. Petrol.* **32**, 1021-1091

McKenzie, D. & O'Nions, R.K. 1995. The source regions of ocean island basalts. *J. Petrol.* **36**, 133-159

McMillan, J.G. 1910. Report on the Dominion of Canada Government Expedition to the Arctic Islands and Hudson Strait on Board the D.G.S. "Arctic". (In report by J.E. Bernier) Government Printing Bureau, Ottawa

McWhae, J.R.H. 1981. Structure and spreading history of the northwestern Atlantic region from the Scotian Shelf to Baffin Bay. *In*: Kerr, J.W. & Fergusson, A.J. (eds.): Geology of the North Atlantic Borderlands. *Can. Soc. of Petroleum Geol. Memoir* **7**, 299-332

Mégnin, C. & Romanowicz, B. 2000. The three-dimensional shear velocity structure of the mantle from the inversion of body, surface and higher-mode waveforms. *Geophys. J. Int.* **143**, 709-728

Moreira, M., Doucelance, R., Dupré, B., Kurz, M., Allegrè, C.J. 1999. Helium and lead isotope geochemistry in the Azores archipelago. *Earth Planet. Sci. Lett.* **169**, 189-205

Morgan, W.J. 1971. Convection plumes in the lower mantle. *Nature* **230**, 42-43

Mutter, J.C., Buck, W.R. & Zehnder, C.M. 1988. Convective partial melting, 1, A model for the formation of thick basaltic sequences during the initiation of spreading. *J. Geophys. Res.* **93**, 1031-1048

Nadin, P.A., Kusznir, N.J. & Toth, J. 1995. Transient regional uplift in the early Tertiary of the northern North Sea and the development of the Iceland plume. *J. Geol. Soc. London* **152**, 953-958

Nataf, H.-C. & VanDecar, J. 1993. Seismological detection of a mantle plume? *Nature* **364**, 115-120

Nielsen, T.F.D., Soper, N.J., Brooks, C.K., Faller, A.M., Higgins, A.C. & Matthews, D.W. 1981. The pre-basaltic sediments and the lower basalts at Kangerdlugssuaq, East Greenland: their stratigraphy, lithology, palaeomagnetism and petrology. *Medd. Grøn. Geosci.* **6**, 25 pp

Nowell, G.M., Kempton, P.D., Noble, S.R., Fitton, J.G., Saunders, A.D., Mahoney, J.J. & Taylor, R.N. 1998. High precision Hf isotope measurements of MORB and OIB by thermal ionisation mass spectrometry: insights into the depleted mantle. *Chem. Geol.* **149**, 211-233

O'Connor, J.M., Stoffers, P., Wijbrans, J.R., Shannon, P.M. & Morrissey, T. 2000. Evidence from episodic seamount volcanism for pulsing of the Iceland plume in the past 70 Myr. *Nature* **408**, 954-958

O'Hara, M.J. 1968. The bearing of phase equilibria studies on the origin and evolution of igneous rocks. *Earth Sci. Rev.* **4**, 69-133

Olive, V., Ellam, R.M. & Wilson, L. 2001. A protocol for the determination of the rare earth elements at picomole levels in rocks by ICP-MS: results on geological reference materials USGS PCC-1 and DTS-1. Geostand. Newsl.J.Geostand.Geoanal. 25, 219-228.

O'Nions, R.K. & Clarke, D.B. 1972. Comparative trace element geochemistry of Tertiary Basalts from Baffin Bay. *Earth Planet. Sci. Lett.* **15**, 436-446

O'Nions, R.K. & Pankhurst, R.J. 1973. Secular variation in the Sr-isotope composition of Icelandic volcanic rocks. *Earth Planet. Sci. Lett.* **21**, 197-409

Patchett, P.J. & Tatsumoto, M. 1980. Hafnium isotope variations in oceanic basalts. *Geophys. Res. Lett.* **7,** 1077-1080

Patchett, P.J. & Tatsumoto, 1981a. The hafnium isotopic evolution of lunar basalts. *Lunar Planet. Sci.* **12**, 819-821

Patchett, P.J. & Tatsumoto, 1981b. Lu/Hf in chondrites and definition of a chondritic hafnium growth curve. *Lunar Planet. Sci.* **12**, 822-824

Patchett, P.J. 1983a. Hafnium isotope results from mid-ocean ridges and Kerguelen. *Lithos* **16**, 47-51

Patchett, P.J. 1983b. Importance of the Lu-Hf isotopic system in studies of planetary chronology and chemical evolution. *Geochim. Cosmochim. Acta* **47**, 81-91

Patchett, P.J., White, W.M., Feldmann, H., Kielinczuk, S. & Hofman, A.W. 1984. Hafnium/ rare earth element fractionation in the sedimentary system and crustal recycling into the Earth's mantle. *Earth. Planet. Sci. Lett.* **69**, 365-378

Pearson, D.G., Emeleus, C.H. & Kelly, S.P. 1996. Precise $^{40}Ar/^{39}Ar$ age of the initiation of Palaeogene vulcanism in the Inner Hebrides and its regional significance. *J. Geol. Soc. London* **153**, 815-818

Pedersen, A.K. 1985a. Lithostratigraphy of the Tertiary Vaigat Formation on Disko, central West Greenland. *Rapp. Grønlands Geol. Unders.* **124,** 1-30

Pedersen, A.K. 1985b. Reaction between picritic magma and continental crust: early Tertiary silicic basalts and magnesian andesites from Disco, central West Greenland. *Bull. Grønlands Geol. Unders.* **152**, 126 pp

Pedersen, A.K. & Pedersen, S. 1987. Sr isotope chemistry of contaminated Tertiary volcanic rocks from Disko, central West Greenland. *Bull. geol. Soc. Denmark* **36**, 315-336

Pedersen, A.K., Larsen, L.M., Pedersen, G.K. & Dueholm, K.S. 1996. Filling and plugging of a marine basin by volcanic rocks: the Tunoqqu Member of the Lower Tertiary Vaigat Formation on Nuussuaq, central West Greenland. *Bull. Grønlands Geol. Unders.* **171**, 5-28

Pedersen, A.K., Larsen, L.M., Riisager, P. & Dueholm, K.S. 2002. Rates of volcanic deposition, facies changes and movements in a dynamic basin: Nuussuaq Basin, West Greenland, around the C27n-C26r transition. *In*: Jolley, D.W. & Bell, B.R. (eds). The North Atlantic Igneous Province: stratigraphy, tectonic, volcanic and magmatic processes. *Geol. Soc. London, Spec. Publ.* **197**, 157-181

Peterson, T.D., Van Breemen, O., Sandeman, H. & Cousens, B. 2002. Proterozoic (1.85-1.75 Ga) igneous suites of the western Churchill Province: granitoid and ultrapotassic magmatism in a reworked Archean hinterland. *Precambrian Research* **119**, 73-100

Piasecki, S., Larsen, L.M., Pedersen, A.K. & Pedersen, G.K. 1992. Palynostratigraphy of the Lower Tertiary volcanics and marine clastic sediments in the southern part of the West Greenland Basin: implications for the timing and duration of the volcanism. *Rapp. Grønlands Geol. Unders* **154**, 13-31

Pierce, J.W. 1982. The evolution of the Nares Strait lineament and its relation to the Eurekan orrogeny. *In*: Dawes, P.R. & Kerr, J.W. (eds.). Nares Strait and the drift of Greenland: a conflict in plate tectonics. *Meddelelser om Grønland, Geoscience* **8**, 237-252

Porcelli, D. & Wasserburg, G.J. 1995. Mass transfer of helium, neon, argon and xenon through a steady-state upper mantle. *Geochim. Cosmochim. Acta.* **59**, 4921-4937.

Pouchou, L. & Pichoir, F. 1984. A new model for quantitative X-ray microanalysis. *Reserche Aerospatiale*, **3**, 167-192.

Presnall, D.C., Dixon, J.R., O'Donnell, T.H., Dixon, S.A. 1979. Generation of mid-ocean ridge tholeiites. *J. Petrol.* **20**, 3-35

Prestvik, T., Goldberg, S., Karlsson, H. & Grönvold, K. 2001. Anomalous strontium and lead isotope signatures in the off-rift Öræfajökull central volcano in south-east Iceland. Evidence for enriched endmember(s) of the Iceland mantle plume? *Earth. Planet. Sci. Lett.* **190**, 211-220

Pulvertaft, T.C.R. & Clarke, D.B. 1966. New mapping on Svartenhuk Peninsula. *Greenland Geol. Surv. Report* **11**, 15-17

Putirka, K. 1999. Melting depths and mantle heterogeneity beneath Hawaii and the East Pacific Rise: Constraints from Na/Ti and rare earth element ratios. *J. Geophys. Res.* **101** (B), 2817-2829

Reid, I. & Jackson, H.R. 1997. Crustal structure of northern Baffin Bay: seismic refraction results and tectonic implications. *J. Geophys. Res.* **102** (B), 523-542

Rice, P.D. & Shade, B.D. 1982. Reflection seismic interpretation and seafloor spreading history of Baffin Bay. *In*: Embry, A.F. & Balkwill, H.R. (eds.): Arctic geology and geophysics, Proceedings of the Third International Symposium on Arctic geology. *Can. Soc. of Petroleum Geologists. Memoir* **8**, 245-265

Richards, M.A., Duncan, R.A. & Courtillot, V.E. 1989. Flood basalts and hot-spot tracks: plume heads and tails. *Science* **246,** 103-107

Riisager, J. Riisager, P. & Perrin, M. 1999. Paleodirectional and palaeointensity results of Paleocene and Eocene basalts from West Greenland. *Bull. Geol. Soc. Denmark* **46**, 69-78

Riisager, P. & Abrahamsen, N. 1999. Magnetostratigraphy of Palaeocene basalts from the Vaigat formation of West Greenland. *Geophys. J. Int.* **134**, 774-782

Ritsema, J., van Heijst, H.J. & Woodhouse, J.H. 1999. Complex shear wave velocity structure imaged beneath Africa and Iceland. *Science* **286**, 1925-1928

Robillard, I., Francis, D. & Ludden, J.N. 1992. The relationship between E- and N-type magmas in the Baffin Bay lavas. *Contrib. Mineral.Petrol.* **112**, 230-241

Robinson, J.A.C. & Wood, B.J. 1998. The depth of the spinel to garnet transition at the peridotite solidus. *Earth Planet. Sci. Lett.* **164**, 277-284

Roeder, P.L. & Emslie, R.F. 1970. Olivine-liquid equilibrium. *Contrib. Mineral. Petrol.* **29**, 275-289

Roest, W.R. & Srivastava, S.P. 1989. Sea-floor spreading in the Labrador Sea: A new reconstruction. *Geology* **17**, 1000-1003

Rolle, F. 1985. Late Cretaceous-tertiary sediments offshore central West Greenland: lithostratigraphy, sedimentary evolution, and petroleum potential. *Can. J. Earth. Sci.* **22**, 1001-1019

Rudrick, R.L. & Foundain, D.M. 1995. Nature and composition of the continental crust: a lower crustal perspective. *Reviews of Geophysics* **33,** 267-309

Salters, V.J.M. 1996. The generation of mid-ocean ridge basalts from Hf and Nd isotope perspective. *Earth Planet. Sci. Lett.* **141**, 109-123

Salters, V.J.M. & Hart, S.R. 1991. The mantle sources of ocean ridges, islands and arcs: the Hf- isotope connection. *Earth Planet. Sci. Lett.* **104**, 364-380

Salters, V.J.M. & White, W.M. 1998. Hf isotope constraints on mantle evolution. *Chem. Geol.* **145**, 447-460

Saunders, A.D., Fitton, J.G., Norry, M.J. & Kent, R.W. 1997. The North Atlantic Igneous Province. *In*: Mahoney, J.J. & Coffin, M.F. (eds). Large Igneous Provinces. *Am. Geophys. Union Monogr.* **100**, 45-93

Saunders, A.D., Larsen, H.C. & Fitton, J.G. 1998. Magmatic development of the southeast Greenland margin and evolution of the Iceland plume: geochemical constraints from Leg 152. *Proceedings of the Ocean Drilling program, Scientific results* **152**, 479-501

Saunders, A.D., Kempton, P.D., Fitton, J.G. & Larsen, L.M. 1999. Sr, Nd, and Pb isotopes and trace element geochemistry of basalts from the southeast Greenland margin. *Proceedings of the Ocean Drilling program, Scientific results* **163**, 77-93

Scarrow, J.H. & Cox, K.G. 1995. Basalts generated by decompressive adiabatic melting of a mantle plume: a case study from the Isle of Skye, NW Scotland. *J. Petrol.* **36**, 3-22

Scarrow, J.H., Curran, J.M. & Kerr, A.C. 2000. Major element records of variable plume involvement in the North Atlantic Province Teriary flood basalts. *J. Petrol.* **41**, 1155-1176

Schäfer, B.F., Parkinson, I.J. & Hawkesworth, C.J. 2000. Deep mantle plume osmium isotope signature from West Greenland Tertiary picrites. *Earth. Planet. Sci. Lett.* **175**, 105-118

Schilling, J.-G. 1973. Iceland mantle plume: geochemical evidence along the Reykjanes Ridge. *Nature* **242**, 565-571

Schilling, J.-G., Zajac, M., Evans, R., Johnston, T., White, W., Devine, J.D. & Kingsley, R. 1983. Along the Mid-Atlantic Ridge from 29°N to 73°N. *Am. J. Sci.* **283**, 510-586

Schmidberger, S.S. & Francis, D. 1999. Nature of the mantle roots beneath the North American craton: mantle xenolith evidence from Somerset Island kimberlites. *Lithos* **48,** 195-216

Schmidberger, S.S. & Francis, D. 2001. Constraints on the trace element composition of the Archean mantle root beneath Somerset Island, Arctic Canada. *J. Petrol.* **42**, 1095-1117

Schmidberger, S.S., Simonetti, A. & Francis, D. 2001. Sr-Nd-Pb isotope systematics of mantle xenoliths from Somerset Island kimberlites: evidence for lithosphere stratification beneath Arctic Canada. *Geochim. Cosmochim. Acta*, **65**, 4243-4255

Schmidberger, S.S., Simonetti, A., Francis, D. & Gariépy, C. 2002. Probing Archean lithosphere using the Lu-Hf isotope systematics of peridotite xenoliths from Somerset Island kimberlites, Canada. *Earth Planet. Sci. Lett.* **197**, 245-259

Shaw, D.M. 1979. Trace element fractionation during anatexis. *Geochim. Cosmochim. Acta.* **34**, 237-243

Shen, Y., Solomon, S.C., Bjarnason, I.T. & Wolfe, C.J. 1998. Seismic evidence for a lower-mantle origin of the Iceland plume. *Nature* **395**, 62-65

Sinton, C.W. & Duncan, R.A. 1998. ^{40}Ar-^{39}Ar ages of lavas from the southeast Greenland margin, ODP152, and the Rockall Plateau, DSDP Leg81. *Proceedings of the Ocean Drilling program, Scientific results* **152**, 387-402

Sleep, N.H. 1990. Hotspots and mantle plumes: some phenomenology. *J. Geophys. Res* **95**, 6715-6736

Sobolev, A.V., Gurenko, A.A. & Shimizu, N. 1994. Ultra-depleted melts from Iceland: data from melt inclusion studies. *Mineral. Mag.* **58A**, 860-861

Srivastava, S.P. 1978. Evolution of the Labrador Sea and its bearing on the early evolution of the North Atlantic. *Geophys. J.Royal.Astronomical. Soc.* **52**, 313-357

Srivastava, S.P., Falconer, R.K.H. & Maclean, B. 1981. Labrador Sea, Davis Strait, Baffin Bay: geology and geophysics- a review. *In*: Kerr, J.W. & Fergusson, A.J. (eds.). Geology of the North Atlantic Borderlands. *Can. Soc. of Petroleum Geol. Memoir* **7**, 333-398

Srivastava, S.P., Arthur, M. & Clement, B. et al. 1987. Site 645:Proceedings, initial Report (Part A), Ocean Drilling Program 105, 917p

Srivastava, S.P. & Roest, W.R. 1999. Extent of oceanic crust in the Labrador Sea. *Marine and Petroleum Geology* **16**, 65-84

Stecher, O., Carlson, R.W. & and Gunnarsson, B. 1999. Torfajökull: a radiogenic end-member of the Iceland Pb-isotopic array. *Earth Planet Sci. Lett.* **165**, 117-127

Storey, M., Duncan, R.A., Pedersen, A.K., Larsen, L.M. & Larsen, H.C. 1998. $^{40}Ar/^{39}Ar$ geochronology of the West Greenland volcanic province. *Earth Planet Sci. Lett.* **160**, 569-586

Stracke, A., Zindler, A., Salters, V.J.M., McKenzie, D., Blichert-Toft, J., Albarède, F. & Grönvold, K. 2003. Theistareykir revisited. Geochemistry Geophysics Geosystems, 4(2), 8507, doi:10.1029/2001GC000201

Stuart, F.M., Turner, G. & Taylor, R.P. 1994. He-Ar systematics of ancient hydrothermal fluids: resolving mantle, crustal contributions. *Noble Gas Isotope Geochemistry, Cosmochemistry, Terra Publ. Japan*, 261-278

Stuart, F.M., Ellam, R.M., Harrop. P.J., Fitton, J.G. & Bell, B.R. 2000. Constraints on mantle plumes from helium isotopic composition of basalts from the British Tertiary Igneous province. *Earth Planet. Sci. Lett.* **177**, 273-285

Stuart, F.M., Lass-Evans, S., Fitton, J.G. & Ellam R.M. 2003. High $^{3}He/^{4}He$ ratios in picritic basalts from Baffin Island and the role of a mixed reservoir in mantle plumes. *Nature* **424**, 57-59.

Sun, S.-S. & Jahn, B. 1975. Lead and strontium isotopes in post-glacial basalts from Iceland. *Nature* **255**, 527-530

Sun, S.-s. & McDonough, W.F. 1989. Chemical and isotopic systematics of ocean basalts: implications for mantle composition and processes. *In*: Saunders, A.D. & Norry, M.J. (eds). Magmatism in the ocean basins. *Geological Society Special Publication* **42**, 313-345

Sutherland, P.C. 1853. On the geological and glacial phenomena on the coast of Davies Strait and Baffin Bay. *Quart. J. Geol. Soc. London* **9**, 296-312

Tackley, P.J., Stevenson, D.J., Glatzmaier, G.A. & Schubert, G. 1993. Effects on an endothermic phase transition at 670 km depth in a spherical model of convection in the Earth's mantle. *Nature* **361**, 699-704

Taylor, F.C. 1971. A revision of Precambrian structural provinces in northeastern Quebec and northern Labrador. *Can. J. Earth. Sci.* **8**, 579-589

Taylor, F.C. 1981. Precambrian geology of the Canadian North Atlantic Borderlands. *In*: Kerr, J.W. & Fergusson, A.J. (eds.): Geology of the North Atlantic Borderlands. *Can. Soc. of Petroleum Geol. Memoir* **7**, 11-30

Taylor, P.N., Kalsbeek, F. & Bridgwater, D. 1992. Discrepancies between neodynium, lead and strontium model ages from Precambrian of southern East Greenland: Evidence for a Proterozoic granulite-facies event affecting Archaean gneisses. *Chem. Geol. (Isoptope Geoscience Sectio)* **94**,281-291

Tegner, C., Lesher, C.E., Larsen, L.M. & Watt, W.S. 1998. Evidence from the rare-earth-element record of mantle melting for cooling of the Tertiary Iceland plume. *Nature* **395**, 591-594

Thirlwall, M.F., Upton, B.G.J. & Jenkins, C. 1994. Interaction between continental lithosphere and the Iceland plume- Sr-Nd-Pb isotope geochemistry of Tertiary basalts, NE Greenland. *J. Petrol.* **35**, 839-879

Thirlwall, M.F. 1995. Generation of the Pb isotopic characteristics of the Iceland plume. *J. geol. Soc. London* **152**, 991-996

Thompson, R.N. 1982. Magmatism of the British Tertiary Volcanic Province. *Scott. J. Geol.* **18**, 49-107

Thompson, R.N. & Gibson, S.A. 1991. Subcontinental mantle plumes, hotspots and pre-existing thinspots. *J. Geol. Soc. London* **148**, 973-977

Thompson, R.N. & Gibson, S.A. 2000. Transient high temperatures in mantle plume heads inferred from magnesian olivines in Phanerozoic picrites. *Nature* **407**, 502-506

Thy, P., Lesher, C.E. & Fram, M.S. 1998. Low pressure experimental constraints on the evolution of basaltic lavas from site 917, southeast Greenland continental margin. *Proceedings of the Ocean Drilling Program, Scientific results*. **152**, 359-372

Tucholke, B.E. & Frey, V.A. 1985. Basement structure and sediment distribution in northwest Atlantic Ocean. *Am. Assoc. Petrol. Geol. Bull.* **69**, 2077-2097

van Keken, P. 1997. Evolution of starting mantle plumes: a comparison between numerical and laboratory models. *Earth Planet. Sci. Lett.* **148**, 1-11

Vervoot, J.D., Patchett, B.J., Blichert-Toft, J. & Albarède, F. (1999). Relationship between Lu-Hf and Sm-Nd isotopic systems in the global sedimentary system. *Earth Planet. Sci. Lett*. **168**, 79-99

Viljoen, M.J. & Viljoen, R.P. 1969. The geology and geochemistry of the Lower Ultramafic Unit on the Onverwacht Group and a proposed new class of igneous rocks. *In*: *Upper Mantle Project. Geological Society of South Africa, Special Publication* **2**, 55-85

White, N. & Lovell, B. 1997. Measuring the pulse of a plume with the sedimentary record. *Nature* **387**, 888-891

White, R.S., Spence, G.D., Fowler, S.R., McKenzie, D.P., Westbrook, G.K. & Bowen, A.N. 1987. Magmatism at rifted continental margins. *Nature* **330**, 439-444

White, R.S. 1988. A hot-spot model for the early Tertiary volcanism in the N Atlantic. *In*: Morton, A.C. & Parson, L.M. 1988. Early Tertiary volcanism and the opening of the NE Atlantic. *Geological Society Special Publication* **39**, 3-13

White, R.S & McKenzie, D. 1989. Magmatism at rift zones: the generation of volcanic continental margins and flood basalts. *J. Geophys. Res.* **100**, 17,543-17,585

Whitehouse, M.J., Kalsbeek, F. & Nutman, A.P. 1998. Crustal growth and crustal recycling in the Nugssugtoqidian orogen of West Greenland: constraints from radiogenic isotope systematics and U-Pb zircon geochronology. *Precambrian research* **91**, 365-381

Whittaker, R.C., Hamann, N.E., Pulvertaft, T.C.R. 1997. A new frontier province offshore Northwest Greenland: structure, basin development, and petroleum potential of the Melville Bay area. *American Association of Petroleum Geologists* (AAPG) *Bulletin*, **81,** 978-998

Williams, A.J., Day, S.J., Stuart, F.M. & Phillips, W.M. Timing and rates of landscape development in central Gran Canaria, eastern Atlantic Ocean, from cosmogenic ^{3}He concentrations in pyroxene microphenocrysts. *In preparation*

Wilson, J.T. & Clarke, D.B. 1965. Geological expedition to Cape Dyer and Searle, Baffin Island, Canada. *Nature* **205**, 349-350

Wolfe, C.J., Bjarnason, I.T., VanDecar, J.C. & Solomon, S.C. 1997. Seismic structure of the Iceland mantle plume. *Nature* **385**, 247-247

Ziegler, P.A. 1988. Evolution of the Arctic-North Atlantic and the Western Tethys. *Am. Assoc. Petrol. Geol. Mem.* **43**, 198 pp

Zindler, A., Hart, S.R. & Frey, F.A. 1979. Nd and Sr isotope ratios and rare element abundances in Reykjanes basalts: evidence for mantle heterogeneity beneath Iceland. *Earth. Planet. Sci. Lett.* **45**, 249-262

IV Appendix

Appendix A1: Analytical methods

A1.1 Olivine compositions

The olivine compositions were analysed using a Cameca Camebax Microbeam Electron Probe at Edinburgh University, operating at an accelerating voltage of 20kV. The beam current was 25nA and the beam width 1μm. Data were processed using PAP data reduction software supplied by the manufacturer and described by Pouchou and Pichoir (1984). The samples were analysed together with well-established standards (e.g. andradite, wollastonite, pyroxene and olivine in this study). The precision has been calculated according to the following equation: $1\sigma = \frac{1}{\sqrt{T}(\sqrt{Rp} - \sqrt{Rb})}$,

where: σ = relative standard deviation;

T = counting time;

R = count rate;

p = peak;

b = background.

The precision for all analysed elements is less than 0.1% (see three example olivine analyses with different forsterite contents in Table A1.1.1).

A1.2. Major elements

Major element analyses of all Baffin Island samples were performed on glass disks using a Philips PW 1480 automatic XRF spectrometer at Edinburgh University.

Table A1.1.1: Precision estimates for the electron probe analyses (shown for three example samples)

	PI-16 (Ol1 C2) 92.97 Fo%					**PI-41 (OL2 C3)** 88.91 Fo%					**DI-21 (Ol5 C1)** 83.39 Fo%				
	wt.%	T	Rp	Rb	1σ	wt.%	T	Rp	Rb	1σ	wt.%	T	Rp	Rb	1σ
SiO_2	40.62	30	9770	45.00	0.08	39.94	30	9656	45.60	0.08	38.63	30	9531	47.14	0.08
Al_2O_3	0.12	30	42.00	18.33	0.01	0.07	30	31.67	18.07	0.01	0.06	30	32.80	19.33	0.01
FeO	6.91	30	658.6	12.80	0.06	10.73	30	1020	11.93	0.07	15.82	30	1527	14.27	0.08
MgO	51.24	30	11835	22.47	0.09	48.24	30	10709	19.67	0.09	44.52	30	9502	21.27	0.09
CaO	0.29	30	89.08	20.87	0.01	0.32	30	96.55	20.40	0.01	0.33	30	99.85	19.47	0.01
MnO	0.12	30	18.00	8.33	0.02	0.17	30	21.93	7.47	0.02	0.26	30	30.24	8.40	0.02
NiO	0.48	30	63.44	14.73	0.02	0.39	30	54.67	11.80	0.02	0.26	30	45.70	18.67	0.02
Cr_2O_3	0.18	30	16.80	5.67	0.02	0.09	30	11.40	5.67	0.02	0.08	30	11.87	6.33	0.02
Total	99.94					99.96					99.97				

1σ: standard devition in wt. %

T: counting time

Rp: count rate (peak)

Rb: count rate (background)

$$1\sigma = \frac{1}{\sqrt{T}(\sqrt{Rp} - \sqrt{Rb})}$$

Approximately 1 g rock powder was dried overnight in an oven at 110°C, placed in platinum capsules and ignited at 1100°C in a furnace for 20 min. The capsules were re-weighed to calculate the percent-weight of loss on ignition (LOI). The residue was then mixed with approximately 5 g of lithium borate flux (Johnson Matthey Spectroflux 105) and fused at 1100°C. The crucible was re-weighed and any flux weight loss was made up with extra flux. The sample-flux mix was re-melted on a Bunsen burner to prepare the glass disks.

The major element oxide abundances (SiO_2, Al_2O_3, Fe_2O_3, MgO, CaO, Na_2O, K_2O, TiO_2, MnO, P_2O_5) were analysed along with the international standards BHVO1, BCR1 and BIR1. The calibration lines for the major elements are very good, so accuracy and precision are closely similar (Fitton et al., 1998). Typical precision estimates are given in table A1.2.1. More details of the analytical techniques are given by Fitton et al. (1998).

A1.3. Trace elements

The trace element concentrations of Nb, Zr, Y, Sr, Rb, Th, Pb, La, Ce, Nd, Zn, Cu, Ni, Cr, V, Ba and Sc for all Baffin Island samples were analysed on a Philips PW 1480 automatic XRF spectrometer at the University of Edinburgh before the start of this project. Around 6 g of whole-rock powder was used to produce pressed-powder pellets. Very long count times were used to determine Nb, Zr and Y abundances, while some other elements (e.g. Nb, Th, Pb) were analysed at least three times and the results averaged. Trace element precision was estimated by analysing international standards (BHVO1, BCR1 and BIRI) repeatedly during the analyses of the Baffin Island samples. Typical trace element precisions are given in Table A1.3.1. The accuracy is difficult to quantify, but may be assessed by comparing the average standard concentration in Edinburgh with those given by e.g. Govindaraju (1994). The mean concentrations of

Table A1.2.1 Typical precision estimates for the major element analysis (Fitton et al., 1998)

Element	Peak and background count times (s)	Typical $1\sigma^*$
Si	50	0.1
Al	50	0.05
Fe	10	0.03
Mg	50	0.05
Ca	20	0.03
Na	50	0.05
K	20	0.005
Ti	20	0.006
Mn	10	0.007
P	50	0.003

Notes: *: standard deviation in wt. %

Table A1.3.1: Typical precision estimates for the trace elements analysed by XRF (Fitton et al., 1998)

Element	Peak and background count times (s)	Typical $1\sigma^*$
Nb	500	0.1
Zr	100	0.4
Y	100	0.4
Sr	40	0.5
Rb	100	0.3
Th	500	0.4
Pb	500	0.4
La	500	1.0
Ce	500	1.5
Nd	500	1.0
Zn	40	0.5
Cu	40	0.5
Ni	40	1.0
Cr	40	1.0
V	40	2.0
Ba	200	5.0
Sc	100	0.5

Notes: *: standard deviation in ppm

Table A1.3.2: XRF trace element data (ppm) for international standards typical for Edinburgh analyses (Fitton et al., 1998)

	BCR-1			BIR-1			BHVO-1		
Element	Mean	1s*	n	Mean	1s*	n	Mean	1s*	n
Nb	13.3	0.1	3	0.6	0.2	3	20.1	0.1	3
Zr	190.8	0.4	3	13.4	0.3	3	177.7	0.4	3
Y	37.2	0.2	3	16.4	0.6	3	28.1	0.4	3
Sr	333.7	0.4	3	110.6	0.4	3	403.0	0.9	3
Rb	48.1	0.6	3	0.2	0.3	3	9.6	0.3	3
Th	6.1	0.4	15				1.4	0.5	15
Pb	14.0	0.4	15				2.5	0.5	15
La	24.9	0.7	15	0.9	1.1	15	14.7	2.1	3
Ce	53.7	1.3	15	1.0	1.8	15	39.2	0.6	3
Nd	28.6	1.0	15	2.0	1.0	15	26.4	0.8	3
Zn	126.3	0.5	3	69.6	0.2	3	105.1	0.6	3
Cu	26.6	0.5	3	118.0	0.5	3	132.3	3.0	3
Ni	14.2	0.2	3	152.8	1.0	3	114.3	1.2	3
Cr	28.0	1.0	3	375.0	2.0	3	287.7	0.5	3
V	390.2	1.4	3	313.7	2.8	3	308.1	1.5	3
Ba	682.3	6.1	3	17.3	2.0	3	133.6	3.1	3
Sc	31.7	0.9	3	39.5	0.3	3	29.8	0.4	3

Table A1.3.3: Trace element concentration and precision for two housestandars (PI-16 and CS-22), for BHVO-1 and BCR-1 (measured during this study[1] and over a two years period[2])

Element	PI-16[1]		CS-22[1]		BHVO-1[1]		BCR-1[1]		BCR-1[2]	
	Mean (n=8)	1s*	Mean (n=10)	1s*	Mean (n=6)	1s*	Mean (n=15)	1s*	Mean (n=30)	1s*
La	1.11	1.94	3.16	4.04	15.49	1.87	25.02	1.21	24.9	0.40
Ce	3.17	2.10	7.72	3.72	38.68	1.88	53.65	1.10	53.9	1.00
Pr	0.53	1.66	1.12	4.07	5.39	1.86	6.78	1.14	6.78	0.10
Nd	3.08	1.84	5.57	3.66	24.80	2.11	28.71	1.09	28.7	0.40
Sm	1.30	2.49	1.77	3.31	6.15	2.29	6.61	1.58	6.58	0.10
Eu	0.49	2.18	0.65	3.20	1.98	2.03	1.99	2.35	1.95	0.03
Gd	1.98	1.98	2.30	2.21	6.21	3.36	6.80	1.70	6.66	0.11
Tb	0.38	2.84	0.42	2.50	0.95	4.73	1.08	3.04	1.05	0.02
Dy	2.72	2.06	2.73	2.36	5.21	1.69	6.34	0.97	6.32	0.10
Ho	0.62	2.01	0.61	3.17	0.97	3.52	1.30	2.44	1.25	0.02
Er	1.85	1.81	1.70	1.95	2.52	2.71	3.64	1.29	3.61	0.07
Tm	0.30	1.98	0.27	2.54	0.36	2.32	0.56	1.36	0.56	0.01
Yb	1.85	1.79	1.63	1.90	2.03	1.75	3.40	1.17	3.37	0.07
Lu	0.28	1.91	0.25	1.55	0.29	1.75	0.51	1.20	0.51	0.01
	Mean (n=10)		Mean (n=9)				Mean (n=7)			
Hf	0.87	2.30	1.48	1.12			4.87	3.27		
Pb	3.06	2.61	0.75	13.22			13.07	1.34		
Th	0.24	4.60	0.28	2.97			6.10	3.08		
U	0.24	2.99	0.08	2.36			1.78	2.31		

[1]: analysed during this study

[2]: routinely analysed over a two years period (Olive et al., 2001)

BCR-1, BIR-1 and BHVO-1 are given in Table A1.3.2. Details of the analytical methods are given by Fitton et al. (1998).

The REE, Hf, Pb, Th and U were determined by inductively coupled plasma-mass spectrometry (ICP-MS) at the Scottish University Environmental and Research Centre (SUERC) in East Kilbride. 0.1g of whole-rock powder was accurately weighed and dissolved in a PFA teflon screw-top beaker using a HF-HNO_3- HCl-digestion. For determining the REE, the samples were diluted by the factor of 5000 using 5 % HNO_3. and 10ml of each sample was spiked with 0.1ml (1 ppm solution) of In, Ru and Re. For determining Pb, Th, U and Hf, the sample were diluted by a factor of 1000 using 5 % HNO_3 and 10 ml of each sample was spiked with 0.1ml (1ppm solution) of In, Re and Bi. Each run consists of a series of two blanks, an Icelandic standards of know concentration, which has been diluted to different levels, three geostandards (BCR and BHVO and a house standard), and six samples. The result of BCR-1 routinely analysed over 2 years at SUERC (Olive et al., 2001) is compared to that given by Govindaraju (1994) in Table A1.3.3 and demonstrate a precision of around 2% (1s). A very detailed description of the analytical procedure is given by Olive et al. (2001).

A1.4 Isotope ratios

A1.4.1 Strontium and Neodymium

$^{87}Sr/^{86}Sr$ and $^{143}Nd/^{144}Nd$ were measured using a VG 54E thermal ionisation mass spectrometer at the Scottish Universities Environmental and Research Centre (SUERC). Samples of between 0.1 and 0.2g were accurately weighed in a PFA teflon beaker and dissolved using a HF-HNO_3-HCl digestion. Sr and REE were separated using cation exchange chromatography. The samples were loaded onto columns using 10ml Bio-Rad AG50W x 8,200-400 mesh resin, and the collection of Sr was carried out in 2.5M HCl.

The Sr fraction was dried, then dissolved in 1µl 1M H_3PO_4 and loaded onto a single outgassed Ta filament. The $^{87}Sr/^{86}Sr$ ratio was corrected for mass fractionation using $^{86}Sr/^{88}Sr = 0.1194$. According to repeated analysis of NBS987, uncertainties (2 sd) of the $^{87}Sr/^{86}Sr$ ratios are in the last decimal place.

The REE fraction was further eluted in 2.5M HCl and collected in 3M HNO_3. For some of the samples, Ba was removed through Eichrom Indusries Spec® resin, but some samples did not need this procedure, as the resin had been changed and Ba was not interfering with the REEs. Nd and Sm were separated in a mixture of acetic acid, methanol and nitric acid using Bio-Rad AG1x8 200-400 mesh anion exchange resin. The samples were dried, and in preparation for the mass spectrometer dissolved in 1µl H_2O and loaded on the Ta side filament of triple Ta-Re-Ta filaments. $^{143}Nd/^{144}Nd$ were corrected for mass fractionation using $^{146}Nd/^{144}Nd = 0.7219$. The SUERC Johnson Matthey Nd standard gave $^{143}Nd/^{144}Nd = 0.511500 \pm 10$ (2 sd) during the analysis of the Baffin Island samples.

A1.4.2 Lead isotopes

Pb-isotope ratios were measured at SUERC, using multi-collector inductively coupled plasma-mass spectrometry (MC-ICP-MS). 0.1g rock sample was digested using successive HF/HNO_3-6 M HCl-1 M HBr anion exchange method similar to Manhes et al. (1978). After the column procedure, each sample was dried and dissolved in HNO_3. According to the Pb content of the sample, the dilution for each sample was calculated (i.e. for 1 ppm Pb = add 1ml of 5 % HNO_3 to dried sample). 5 ppb of the standard NIST 997 (TI) were also added to each sample. They were left on a hot plate overnight and the following day, the sample solution was transferred to tubes and measured with the MC-ICP-MS along with the standard NBS 981.

A1.4.3 Hafnium isotopes

The Hf-isotope ratios were determined at the NERC Isotope Geosciences Laboratory in Keyworth, using plasma ionisation multi-collector mass spectrometry (PIMMS). Samples of between 1.5 and 3 g (the amount of sample depends on the amount of Hf in the sample and was calculated as: amount of sample (g) x conc. of Hf in sample (µg/g) x column efficiency [85 %] = yield (µg)) were weighed into Savillex bombs ensuring that ~1 µg Hf was recovered. The samples were dissolved in 16 M HNO_3- 29M HF, dried down and further leached with 4N HF. The separation of Ti-Zr-Hf from major and other trace elements was carried out using BioRad® AG1-X8 anion exchange resin. The Ti-Zr-Hf fraction was collected with 1N HF-1N HCL. 36.6N H_2SO_4 was added to the solution and dried down. Ti was separated from Zr and Hf using BioRad® AG1-X8 anion exchange resin. The dried samples were diluted in 0.52N H_2SO_4- 5% H_2O_2, loaded onto the columns and the Hf-fraction was collected with 1N HF-2N HCL. The dried samples were dissolved in a dilute solution of nitric acid (2%) and 0.1M HF for running by PIMMS. Sample solutions for running with PIMMS require concentrations of 200-500 ppb Hf (i.e. calculated as: number of ng of Hf separated = Hf (ppm) in sample x sample weight (mg)). The data were corrected for mass fractionation during the run by normalisation to $^{179}Hf/^{177}Hf$ of 0.7325 and reported relative to an accepted value of JMC 475 of 0.282160. A very detailed description of the analytical techniques is given by Kempton et al. (2001).

A1.4.4 Helium isotopes

Helium isotope ratios and concentrations were analysed at SUERC, using an all metal MAP 215-50 mass spectrometer. Olivine crystals were extracted from crushed whole rocks by heavy liquid separation. The olivine concentrates were cleaned in dilute HNO_3

at 80°C and then washed in distilled water. Olivine crystals were handpicked under a binocular microscope, then washed in 5% HCl, followed by distilled water. The olivine separate was repicked, then ultrasonically cleaned in deionised water, followed by acetone, prior to loading into the crushing apparatus. The gases were extracted by *in vacuo* crushing of ~1 g olivine. The olivine powders remaining after crushing were wrapped in Al foil and fused in a double-walled resistance furnace at 1850°C. $^{3}He/^{4}He$ and helium concentrations were calculated by peak height comparison to pipettes of 2.9 x 1012 atoms He from an artificially prepared He-Ar standard ($^{3}He/^{4}He = 5.95 \times 10^{-5}$; $^{4}He/^{22}Ne$ >6000). $^{3}He/^{4}He$ were normalised to the atmospheric ratio (1.39×10^{-6} R_a). ^{4}He blanks averaged 4×10^{-11} cm^3 STP and ^{3}He blanks (5×10^{-15} cm^3 STP) were less than 5% of the measured ^{3}He. A detailed description of the analytical technique is given by Stuart et al. (1994, 2000) and Williams et al. (in prep.).

A2 Petrology of Baffin Island samples

Sample	Texture		Phenocrysts		
			shape	size	vol. %
Cape Searle					
CS-13	porphyritic	ol	eu/sub	< 0.5 mm	1%
CS-11	porphyritic	ol	eu/sub	< 0.3 mm	2-5 %
CS-8	porphyritic,ophitic	ol	sub/lg	< 2.0 mm	<1%
CS-7	porphyritic, ophitic, subophitic	ol	eu/sub/an	< 3.5 mm	10%
CS-12	non-porphyritic, ophitic	ol	sub	< 0.4 mm	2%
CS-32	non-porphyritic, (sub)ophitic, intergranular	ol	sub	< 0.4 mm	1%
		plg	sub	< 1.0 mm	20%
CS-31	non-porphyritic	ol	sub	< 1.2 mm	15%
CS-30	non-porphyritic, (sub)ophitic, intergranular	ol	sub	< 1.0 mm	10-15%
		plg	sub	< 2.0 mm	10-15%
CS-29	non-porphyritic,ophitic	ol	eu/sub/an/sk/lg	< 3.0 mm	25-30%
		plg	an	< 2.0 mm	10%
CS-28	porphyritic,ophitic	ol	eu/sub/an/sk/lg	< 2.0 mm	10%
CS-27	non-porphyritic,ophitic, glomeroporphyric(ol)	ol	eu/sub/an/sk/lg	< 1.0 mm	5%
CS-26	non-porphyritic,ophitic, poikilophitic	ol	eu/sub/an	< 1.0 mm	10%
CS-25	porphyritic,ophitic, glomeroporphyritic((ol)	ol	eu/sub	< 1.0 mm	10%
CS-24	non-porphyritic,ophitic, glomeroporphyric(plg)	ol	sub/an	< 1.0 mm	3-5%
CS-23	non-porphyritic,ophitic	ol	sub/an	< 0.7 mm	7%
CS-22	non-porphyritic,(sub)ophitic	ol	sub	< 0.8 mm	3%
CS-21	non-porphyritic, (sub)ophitic	ol	sub/an	< 1.0 mm	3%
CS-20	non-porphyritic,(sub)ophitic, glomeroporphyric(ol)	ol	eu/sub/an/sk	< 1.0 mm	10-15%
CS-19	non-porphyritic,(sub)ophitic, glomeroporphyric(ol)	ol	eu/sub/an	< 1.0 mm	7%
CS-18	porphyritic,ophitic, glomeroporphyritic(ol+plg)	ol	eu/sub	< 1.0 mm	15-20%
		plg	eu/sub	< 0.5 mm	2%
CS-17	porphyritic, glomeroporphyritic(ol+plg)	ol	eu/sub	< 2.0 mm	15%
		plg	sub	< 0.5 mm	15%
CS-16	porphyritic,ophitic, glomeroporphyritic(ol+plg)	ol	eu/sub	< 1.0 mm	10-15%
		plg	sub	< 0.5 mm	3%
CS-15	vitrophyritic, glomeroporphyritic(ol)	ol	eu/sub	< 1.0 mm	10-15%
		plg	eu/sub	< 1.0 mm	2%
CS-10	vitrophyritic, glomeroporphyritic(ol)	ol	eu/sub/sk/lg	< 1.5 mm	10-15%
		plg	sub	< 0.5 mm	2%
CS-4	vitrophyritic	ol	eu/sub/an/sk/lg	< 1.5 mm	10%
CS-3	vitrophyritic	ol	eu/sub/an/sk/lg	< 1.0 mm	5-7%
CS-14	porphyritic, glomeroporphyritic(ol+plg)	ol	eu/sub	< 0.7 mm	10-15%
		plg	sub	< 1.0 mm	3%
CS-6	non-porphyritic,(sub)ophitic, glomeroporphyric(ol+plg)	ol	eu/sub/lg	< 1.0 mm	10-15%
		plg	sub	< 0.5 mm	3-5%
CS-5	porphyritic, glomeroporphyritic(ol+plg)	ol	eu/sub/sk/lg	< 1.5 mm	15-20%
		plg	sub	< 1.5 mm	5%
CS-1	porphyritic, glomeroporphyritic(ol+plg)	ol	eu/sub/sk/lg	< 2.0 mm	10-15%

The abundance of minerals was estimated from thin sections
(ol: olivine; plg: plagioclase; eu: euhedral; sub: subhedral; an: anhedral; sk: skeletal; lg: long-growth)

A2 (continued) Petrology of Baffin Island samples

Sample	Texture	Phenocrysts			
			shape	size	vol. %
Padloping Island					
PI-16	porphyritic	ol	eu/sub	< 1.5 mm	5%
PI-18	non-porphyritic, subophitic	ol	eu/sub	< 0.7 mm	10%
PI-19	non-porphyritic, subophitic	ol	eu/sub	< 2.0 mm	10%
PI-20	non-porphyritic, subophitic	ol	eu/sub	< 1.3 mm	10%
PI-21	non-porphyritic, subophitic	ol	eu/sub	< 1.2 mm	15%
PI-22	porphyritic, glomeroporphyritic	ol	eu/sub/an/sk	< 2.0 mm	10-15%
PI-23	non-porphyritic, subophitic	ol	sub/an/sk/lg	< 3.0 mm	25%
PI-24	non-porphyritic, subophitic	ol	sub/sk/lg	< 3.0 mm	25%
PI-25	non-porphyritic, subophitic	ol	sub/an/sk/lg	< 3.5 mm	25%
PI-26	porphyritic, subophitic	ol	eu/sub/an/sk/lg	< 2.0 mm	20%
PI-27	porphyritic, subophitic	ol	eu/sub/sk/lg	< 3.5 mm	25%
PI-28	porphyritic, glomeroporphyritic (ol)	ol	eu/sub	< 1.0 mm	30-40%
PI-29	porphyritic, glomeroporphyritic (ol)	ol	eu/sub	< 1.0 mm	30-40%
PI-30	non-porphyritic, subophitic	ol	eu/sub/sk/lg	< 2.0 mm	10%
PI-31	non-porphyritic, subophitic	ol	eu/sub/an/sk	< 1.5 mm	20-25%
PI-32	non-porphyritic, subophitic, glomeroporphyritic(ol)	ol	eu/sub/an	< 3.0 mm	30%
PI-33	porphyritic, glomeroporphyritic (plg)	ol	eu/sub/an/sk	< 2.0 mm	5-10%
PI-34	porphyritic, subophitic	ol	eu/sub/an/sk	< 3.0 mm	20%
PI-35	porphyritic, subophitic	ol	eu/sub/an/lg	< 1.5 mm	20-25%
PI-38	non-porphyritic, subophitic	ol	eu/sub/an/sk	< 1.5 mm	< 50 %
PI-36	non-porphyritic, ophitic	ol	sub/an	< 2.3 mm	25-30%
PI-37	non-porphyritic, subophitic	ol	eu/sub/an	< 2.0 mm	15-20%
PI-39	non-porphyritic, ophitic	ol	sub/an	< 1.0 mm	30%
PI-40	non-porphyritic	ol	eu/sub	< 2.0 mm	35-40%
PI-41	non-porphyritic	ol	eu/sub	< 2.0 mm	40-50 %
PI-42	non-porphyritic	ol	eu/sub/an/sk/lg	< 1.0 mm	< 50 %
PI-43	non-porphyritic, subophitic	ol	eu/sub/sk/lg	< 2.0 mm	15-20%
PI-44	vitrophyric	ol	eu/sub/sk/lg	< 2.0 mm	30%
Durban Island					
DI-13	porphyritic, glomeroporphyritic (ol+plg)	ol	eu/sub	< 0.5 mm	5%
		plg	eu/sub	< 0.8mm	1%
DI-14	non-porphyritic	ol	eu/sub	< 2.5 mm	30%
DI-15	non-porphyritic, intergranular	ol	eu/sub	< 2.0 mm	40%
DI-16	non-porphyritic	ol	eu/sub/an/sk/lg	< 1.5 mm	30%
DI-17	subophitic	ol	eu/sub/sk	< 1.5 mm	10-20%
DI-18	subophitic	ol	eu/sub/sk	< 1.5 mm	15%
DI-19	subophitic	ol	eu/sub/sk	< 1.5 mm	10-20%
DI-20	non-porphyritic, subophitic	ol	sub	< 0.3 mm	10%
DI-21	subophitic, glomeroporphyritic (ol)	ol	eu/sub	< 1.5 mm	20%
DI-22	porphyritic, subophitic, glomeroporphyritic (plg)	ol	eu/sub	< 1.0 mm	10%
		plg	sub	< 0.3 mm	< 7 %
DI-23	subophitic, glomeroporphyritic (ol)	ol	eu/sub	< 2.0 mm	20%
DI-24	porphyritic, ophiomottled, glomeroporphyritic (ol)	ol	eu/sub/sk/lg	< 2.0 mm	25-30%
DI-25	porphyritic	ol	eu/sub	< 0.8 mm	<10%
DI-26	subophitic	ol	eu/sub/sk	< 2.0 mm	10%
DI-27	porphyritic	ol	eu/sub/sk/lg	< 2.5 mm	20-25%
DI-28	subophitic	ol	eu/sub/an/sk	< 2.5 mm	20%
DI-29	vitrophyric	ol	eu/sub/sk/lg	< 1.0 mm	15%

A3 Microprobe analyses (in wt. %) of olivine crystals

sample	DI-13										
	ol1 c1	ol1 c2	ol1 c3	ol1 r1	ol1 r2	ol1 r3	ol2 c1	ol2 c2	ol2 c3	ol2 r1	ol2 r2
SiO_2	35.81	35.70	35.64	35.53	35.64	35.48	36.00	35.79	36.01	35.41	35.96
Al_2O_3	0.05	0.04	0.04	0.43	0.03	0.03	0.06	0.04	0.05	0.05	0.04
FeO	30.78	30.92	31.11	31.04	31.50	31.83	30.72	30.86	30.85	31.92	30.42
MgO	31.71	31.55	31.58	31.38	31.11	30.92	31.81	31.64	31.47	30.88	31.96
CaO	0.26	0.26	0.26	0.24	0.25	0.23	0.25	0.28	0.27	0.23	0.26
Na_2O	0.02	0.03	0.00	0.01	0.03	0.01	0.02	0.02	0.01	0.02	0.00
K_2O	0.00	0.00	0.01	0.01	0.00	0.01	0.01	0.00	0.00	0.01	0.00
TiO_2	0.04	0.01	0.02	0.03	0.03	0.03	0.02	0.02	0.02	0.03	0.04
MnO	0.42	0.43	0.45	0.40	0.46	0.44	0.43	0.43	0.41	0.48	0.44
NiO	0.06	0.07	0.08	0.06	0.08	0.09	0.06	0.07	0.08	0.09	0.08
Cr_2O_3	0.00	0.03	0.00	0.04	0.00	0.02	0.03	0.02	0.02	0.02	0.01
Total	99.15	99.02	99.20	99.16	99.12	99.09	99.39	99.16	99.17	99.14	99.21
Fo%	64.75	64.53	64.41	64.32	63.77	63.39	64.87	64.64	64.53	63.30	65.19

sample	DI-13									
	ol2 r3	ol3 c1	ol4 c1	ol4 c2	ol4 r1	ol4 r2	ol5 c1	ol5 c2	ol5 c3	ol5 r2
SiO_2	35.82	35.87	36.17	36.08	35.94	35.85	36.77	36.68	36.68	36.26
Al_2O_3	0.03	0.05	0.05	0.05	0.04	0.03	0.06	0.06	0.06	0.04
FeO	31.28	30.88	29.87	30.18	30.43	31.14	25.33	26.35	25.49	28.54
MgO	31.02	31.28	32.20	32.11	31.84	31.45	36.33	35.11	36.11	33.59
CaO	0.25	0.24	0.29	0.29	0.26	0.24	0.30	0.28	0.30	0.25
Na_2O	0.00	0.02	0.02	0.01	0.00	0.03	0.02	0.00	0.00	0.02
K_2O	0.00	0.00	0.01	0.00	0.01	0.01	0.00	0.00	0.00	0.00
TiO_2	0.04	0.03	0.03	0.03	0.03	0.05	0.03	0.03	0.01	0.03
MnO	0.41	0.44	0.41	0.42	0.43	0.46	0.36	0.38	0.36	0.40
NiO	0.10	0.10	0.06	0.06	0.04	0.05	0.09	0.08	0.08	0.08
Cr_2O_3	0.01	0.03	0.03	0.04	0.00	0.02	0.02	0.05	0.02	0.02
Total	98.97	98.93	99.14	99.26	99.02	99.31	99.31	99.02	99.12	99.23
Fo%	63.87	64.36	65.78	65.48	65.10	64.30	71.89	70.38	71.63	67.73

sample	DI-15										
	ol1 c1	ol1 c2	ol1 c3	ol1 c3	ol1 r1	ol1 r2	ol2 c1	ol2 c2	ol2 c3	ol2 c4	ol2 r1
SiO_2	40.15	40.21	40.34	40.16	38.67	38.85	39.67	39.35	39.38	39.63	38.63
Al_2O_3	0.07	0.05	0.06	0.09	0.04	0.06	0.06	0.05	0.08	0.08	0.03
FeO	9.82	9.50	9.70	9.97	17.65	17.56	13.37	13.57	13.53	13.78	19.26
MgO	49.53	49.51	49.64	49.22	42.95	43.28	46.53	46.30	46.51	46.01	41.18
CaO	0.30	0.30	0.29	0.26	0.30	0.26	0.31	0.31	0.32	0.31	0.27
Na_2O											
K_2O											
TiO_2											
MnO	0.14	0.16	0.13	0.16	0.24	0.30	0.23	0.19	0.19	0.20	0.29
NiO	0.40	0.44	0.44	0.40	0.29	0.33	0.37	0.36	0.36	0.32	0.30
Cr_2O_3	0.14	0.12	0.13	0.12	0.06	0.08	0.06	0.08	0.11	0.11	0.05
Total	100.55	100.28	100.72	100.38	100.20	100.72	100.61	100.20	100.47	100.45	100.02
Fo%	89.99	90.28	90.12	89.79	81.27	81.46	86.12	85.88	85.97	85.62	79.22

sample	DI-15							
	ol2 r2	ol3 c1	ol3 c2	ol3 c3	ol3 c4	ol3 r2	ol3 r3	ol3 r4
SiO_2	38.43	39.87	39.62	40.09	39.14	38.69	39.66	38.72
Al_2O_3	0.02	0.06	0.06	0.07	0.07	0.04	0.06	0.04
FeO	18.98	12.41	12.33	11.49	14.82	17.97	12.80	18.41
MgO	41.59	47.08	46.86	47.72	44.77	42.02	46.48	41.73
CaO	0.29	0.29	0.28	0.30	0.31	0.27	0.31	0.28
Na_2O								
K_2O								
TiO_2								
MnO	0.28	0.18	0.18	0.20	0.22	0.27	0.18	0.30
NiO	0.29	0.34	0.35	0.38	0.34	0.33	0.37	0.27
Cr_2O_3	0.03	0.09	0.04	0.08	0.12	0.02	0.08	0.04
Total	99.89	100.32	99.73	100.32	99.80	99.60	99.95	99.78
Fo%	79.62	87.12	87.14	88.10	84.34	80.65	86.62	80.17

(ol: olivine; c: core; r: rim)

A3 (continued) Microprobe analyses (in wt. %) of olivine crystals

sample	DI-17										
	ol1 c1	ol1 c2	ol1 c3	ol1 r1	ol1 r2	ol1 r3	ol2 c1	ol2 c2	ol2 r1	ol2 r2	ol3 c1
SiO_2	39.43	39.30	39.69	39.15	38.44	39.08	39.76	39.63	39.42	39.40	39.75
Al_2O_3	0.05	0.06	0.05	0.06	0.06	0.06	0.06	0.06	0.06	0.07	0.05
FeO	12.16	12.49	11.39	14.46	18.13	14.89	11.41	11.27	12.76	13.02	11.13
MgO	47.07	46.60	47.62	45.04	42.25	44.91	47.96	47.58	46.72	46.46	48.05
CaO	0.34	0.35	0.34	0.34	0.32	0.31	0.34	0.60	0.34	0.35	0.32
Na_2O	0.00	0.01	0.01	0.02	0.00	0.02	0.00	0.00	0.02	0.00	0.02
K_2O	0.01	0.01	0.01	0.00	0.00	0.00	0.01	0.01	0.01	0.01	0.00
TiO_2	0.02	0.02	0.02	0.02	0.02	0.01	0.02	0.02	0.03	0.03	0.02
MnO	0.17	0.17	0.16	0.20	0.24	0.20	0.18	0.18	0.20	0.20	0.16
NiO	0.28	0.31	0.28	0.29	0.20	0.25	0.28	0.27	0.28	0.21	0.26
Cr_2O_3	0.13	0.10	0.08	0.06	0.08	0.03	0.05	0.09	0.09	0.11	0.04
Total	99.66	99.42	99.64	99.63	99.75	99.75	100.06	99.70	99.93	99.83	99.80
Fo%	87.35	86.94	88.17	84.74	80.60	84.32	88.23	88.27	86.71	86.42	88.50

sample	DI-17									
	ol3 c2	ol3 c3	ol3 c4	ol3 r1	ol3 r2	ol3 r3	ol4 c1	ol4 c2	ol4 c3	ol4 r2
SiO_2	39.65	39.76	39.73	39.32	39.67	39.24	39.12	38.95	39.10	38.77
Al_2O_3	0.06	0.06	0.06	0.07	0.07	0.06	0.07	0.05	0.05	0.08
FeO	11.18	11.22	11.30	13.24	11.86	14.07	14.10	14.35	14.31	17.92
MgO	48.13	47.87	47.91	46.42	47.58	45.58	45.38	45.24	45.61	42.52
CaO	0.33	0.30	0.32	0.32	0.32	0.31	0.33	0.32	0.32	0.32
Na_2O	0.01	0.01	0.01	0.00	0.03	0.00	0.02	0.01	0.02	0.01
K_2O	0.01	0.00	0.00	0.00	0.01	0.01	0.01	0.01	0.00	0.00
TiO_2	0.01	0.01	0.02	0.01	0.04	0.04	0.01	0.02	0.03	0.03
MnO	0.18	0.17	0.17	0.19	0.17	0.22	0.18	0.18	0.18	0.26
NiO	0.25	0.26	0.26	0.22	0.24	0.24	0.22	0.21	0.21	0.18
Cr_2O_3	0.05	0.07	0.08	0.07	0.08	0.07	0.07	0.07	0.07	0.05
Total	99.87	99.72	99.86	99.85	100.06	99.85	99.50	99.41	99.88	100.13
Fo%	88.475	88.386	88.316	86.210	87.734	85.240	85.16	84.89	85.04	80.88

sample	DI-20										
	ol1 c1	ol1 c2	ol1 c3	ol1 r1	ol1 r2	ol1 r3	ol2 c1	ol2 c2	ol2 c3	ol2 r3	ol2 r4
SiO_2	38.94	39.01	38.61	38.42	38.73	38.12	39.22	39.31	39.09	39.01	38.82
Al_2O_3	0.06	0.08	0.05	0.05	0.06	0.04	0.05	0.07	0.08	0.03	0.06
FeO	15.39	15.27	16.69	18.06	16.15	18.59	14.56	14.66	14.57	15.94	16.57
MgO	44.22	44.37	43.29	41.75	43.39	42.04	44.63	44.85	45.09	44.22	43.47
CaO	0.35	0.33	0.34	0.34	0.35	0.31	0.35	0.32	0.33	0.34	0.35
Na_2O	0.00	0.01	0.02	0.01	0.02	0.03	0.01	0.02	0.02	0.01	0.02
K_2O	0.00	0.00	0.01	0.00	0.01	0.01	0.01	0.01	0.00	0.00	0.01
TiO_2	0.02	0.02	0.01	0.02	0.02	0.04	0.02	0.03	0.02	0.01	0.01
MnO	0.20	0.24	0.25	0.24	0.22	0.28	0.21	0.20	0.20	0.23	0.24
NiO	0.13	0.18	0.15	0.12	0.14	0.10	0.16	0.19	0.18	0.11	0.13
Cr_2O_3	0.05	0.05	0.06	0.04	0.07	0.05	0.04	0.07	0.07	0.06	0.05
Total	99.37	99.55	99.47	99.07	99.17	99.60	99.24	99.74	99.66	99.97	99.73
Fo%	83.67	83.82	82.22	80.47	82.73	80.13	84.54	84.50	84.65	83.19	82.39

sample	DI-20				DI-21						
	ol4 c1	ol4 c2	ol4 c3		ol1 c4	ol1 c5	ol1 c6	ol1 c7	ol1 r4	ol1 r5	ol4 c1
SiO_2	38.65	38.43	38.65		39.57	39.31	39.61	39.45	39.09	37.91	39.46
Al_2O_3	0.06	0.05	0.06		0.04	0.05	0.06	0.07	0.05	0.07	0.06
FeO	16.63	18.16	17.28		12.17	12.46	12.39	12.36	14.75	19.96	12.16
MgO	43.59	42.45	43.18		47.26	47.28	47.17	47.16	45.10	40.97	47.45
CaO	0.34	0.36	0.36		0.31	0.32	0.34	0.31	0.29	0.29	0.29
Na_2O	0.02	0.02	0.02								
K_2O	0.01	0.01	0.00								
TiO_2	0.02	0.03	0.01								
MnO	0.23	0.25	0.24		0.22	0.20	0.21	0.18	0.23	0.29	0.23
NiO	0.11	0.13	0.12		0.31	0.34	0.36	0.33	0.28	0.25	0.34
Cr_2O_3	0.09	0.04	0.05		0.05	0.04	0.08	0.05	0.06	0.07	0.07
Total	99.75	99.91	99.97		99.92	99.98	100.21	99.92	99.85	99.82	100.05
Fo%	82.38	80.65	81.67		87.38	87.12	87.16	87.19	84.50	78.54	87.44

(ol: olivine; c: core; r: rim)

A3 (continued) Microprobe analyses (in wt. %) of olivine crystals

sample	DI-21										
	ol4 c2	ol4 c3	ol4 c4	ol4 r1	ol4 r2	ol4 r3	ol4 c5	ol4 c6	ol5 c1	ol5 c2	ol5 c3
SiO_2	39.59	39.60	39.43	38.50	38.83	38.37	39.56	39.61	38.63	38.93	38.81
Al_2O_3	0.06	0.06	0.07	0.05	0.06	0.06	0.08	0.04	0.06	0.04	0.06
FeO	12.00	12.11	12.31	17.48	15.54	17.04	13.10	12.73	15.82	15.45	15.67
MgO	47.36	47.14	47.19	42.84	44.62	43.41	46.53	47.10	44.52	44.63	44.75
CaO	0.31	0.32	0.29	0.29	0.31	0.29	0.31	0.30	0.33	0.33	0.30
Na_2O											
K_2O											
TiO_2											
MnO	0.19	0.21	0.21	0.27	0.25	0.26	0.21	0.19	0.26	0.22	0.26
NiO	0.32	0.31	0.34	0.29	0.31	0.27	0.36	0.34	0.26	0.26	0.27
Cr_2O_3	0.07	0.09	0.08	0.06	0.09	0.09	0.08	0.07	0.08	0.09	0.08
Total	99.90	99.83	99.91	99.76	100.00	99.78	100.23	100.38	99.97	99.95	100.20
Fo%	87.55	87.40	87.23	81.38	83.66	81.96	86.36	86.83	83.39	83.74	83.58

sample	DI-21						DI-23			
	ol6 c1	ol6 c2	ol6 c3	ol6 r1	ol6 r2	ol6 r3	ol1a c1	ol1a c2	ol1a c3	ol1b c4
SiO_2	39.02	38.99	39.06	38.30	38.84	38.41	39.41	39.64	39.44	39.61
Al_2O_3	0.05	0.06	0.06	0.04	0.06	0.05	0.08	0.04	0.05	0.05
FeO	14.77	14.72	15.49	18.79	15.71	17.92	12.58	12.46	12.46	12.03
MgO	45.47	45.28	44.69	42.14	44.34	42.26	46.74	46.88	47.21	47.27
CaO	0.31	0.31	0.31	0.31	0.33	0.36	0.32	0.34	0.30	0.33
Na_2O										
K_2O										
TiO_2										
MnO	0.21	0.23	0.20	0.28	0.26	0.28	0.20	0.17	0.19	0.19
NiO	0.28	0.27	0.25	0.20	0.25	0.24	0.35	0.35	0.36	0.35
Cr_2O_3	0.07	0.08	0.04	0.05	0.06	0.07	0.11	0.07	0.04	0.06
Total	100.18	99.94	100.10	100.12	99.85	99.58	99.78	99.93	100.05	99.89
Fo%	84.58	84.57	83.72	79.99	83.42	80.79	86.88	87.03	87.10	87.51

sample	DI-23										
	ol1b c5	ol1b c6	ol1c c7	ol1c c8	ol1d c9	ol1d c10	ol1d r1	ol1c r2	ol1e r3	ol2 c1	ol2 c2
SiO_2	39.66	39.70	39.51	39.38	39.50	39.24	38.46	39.21	38.94	39.46	39.40
Al_2O_3	0.04	0.07	0.06	0.07	0.06	0.06	0.05	0.04	0.06	0.09	0.05
FeO	12.01	11.95	11.98	11.97	11.89	12.24	17.21	13.31	15.92	12.51	12.42
MgO	47.25	47.18	47.42	47.40	47.06	47.74	43.23	46.63	44.28	47.22	47.41
CaO	0.33	0.32	0.32	0.31	0.30	0.31	0.30	0.32	0.29	0.30	0.31
Na_2O											
K_2O											
TiO_2											
MnO	0.21	0.20	0.18	0.19	0.19	0.20	0.25	0.20	0.24	0.21	0.21
NiO	0.35	0.36	0.38	0.37	0.32	0.37	0.30	0.35	0.35	0.34	0.34
Cr_2O_3	0.07	0.09	0.07	0.06	0.04	0.06	0.06	0.08	0.10	0.07	0.04
Total	99.93	99.85	99.92	99.75	99.36	100.23	99.85	100.14	100.17	100.21	100.17
Fo%	87.52017	87.56408	87.58769	87.59308	87.58499	87.42563	81.74575	86.19782	83.22223	87.06095	87.19101

sample	DI-23								
	ol2 c3	ol2 r1	ol2 Rr3	ol2 r3	ol3 c1	ol3 c2	ol3 c3	ol3 r2	ol3 r3
SiO_2	39.48	38.86	39.13	39.13	39.49	39.62	39.57	39.60	38.91
Al_2O_3	0.07	0.06	0.05	0.05	0.06	0.06	0.07	0.07	0.03
FeO	12.31	15.89	13.88	13.88	12.11	12.27	12.18	13.02	14.63
MgO	47.23	44.06	46.08	46.08	47.24	47.10	47.10	46.53	45.45
CaO	0.31	0.31	0.30	0.30	0.34	0.33	0.32	0.31	0.31
Na_2O									
K_2O									
TiO_2									
MnO	0.17	0.26	0.20	0.20	0.18	0.19	0.19	0.18	0.23
NiO	0.37	0.29	0.33	0.33	0.37	0.33	0.36	0.35	0.28
Cr_2O_3	0.08	0.07	0.06	0.06	0.08	0.06	0.07	0.07	0.05
Total	100.00	99.80	100.02	100.02	99.85	99.96	99.86	100.13	99.90
Fo%	87.25	83.18	85.54	85.54	87.43	87.25	87.33	86.43	84.71

(ol: olivine; c: core; r: rim)

A3 (continued) Microprobe analyses (in wt. %) of olivine crystals

sample	DI-24										
	ol5 c1	ol5 c2	ol5 c3	ol5 r1	ol5 r2	ol5 r3	ol3 c12	ol3 c14	ol3 c15	ol3 c16	ol3 c17
SiO_2	39.49	39.33	39.47	39.30	39.39	39.52	39.61	39.66	39.91	39.77	39.87
Al_2O_3	0.06	0.06	0.04	0.07	0.06	0.07	0.10	0.08	0.10	0.10	0.08
FeO	11.79	11.86	11.90	12.27	13.17	12.47	9.52	9.66	10.07	9.94	9.56
MgO	46.89	46.97	46.85	46.52	46.20	46.75	48.75	48.52	48.14	48.41	48.74
CaO	0.35	0.33	0.34	0.35	0.35	0.34	0.29	0.30	0.31	0.28	0.29
Na_2O											
K_2O											
TiO_2											
MnO	0.18	0.19	0.20	0.19	0.20	0.22	0.15	0.17	0.17	0.16	0.16
NiO	0.34	0.38	0.36	0.33	0.36	0.30	0.43	0.41	0.40	0.45	0.45
Cr_2O_3	0.10	0.07	0.06	0.07	0.06	0.08	0.10	0.14	0.15	0.15	0.13
Total	99.19	99.19	99.23	99.10	99.79	99.75	98.95	98.94	99.25	99.26	99.27
Fo%	87.64	87.60	87.53	87.11	86.21	86.99	90.13	89.95	89.50	89.67	90.09

sample	DI-24										
	ol3 r5	ol3 r6	ol3 r7	ol6 c1	ol6 c2	ol6 c4	ol6 c5	ol6 r1	ol6 r2	ol7 c1	ol7 c2
SiO_2	39.46	39.38	39.50	39.40	39.11	39.45	39.39	39.44	39.27	39.90	39.80
Al_2O_3	0.10	0.07	0.08	0.06	0.05	0.08	0.08	0.08	0.07	0.08	0.09
FeO	11.40	11.69	11.43	12.21	11.99	11.88	11.84	12.90	12.59	9.52	10.62
MgO	47.35	47.23	47.21	46.66	46.88	46.84	46.97	46.26	46.53	48.88	48.04
CaO	0.34	0.34	0.33	0.36	0.34	0.34	0.36	0.36	0.33	0.29	0.30
Na_2O											
K_2O											
TiO_2											
MnO	0.17	0.18	0.18	0.19	0.19	0.18	0.20	0.21	0.24	0.17	0.17
NiO	0.36	0.35	0.33	0.39	0.38	0.38	0.36	0.36	0.33	0.45	0.42
Cr_2O_3	0.09	0.08	0.07	0.06	0.08	0.06	0.07	0.06	0.06	0.13	0.13
Total	99.27	99.31	99.14	99.33	99.03	99.21	99.25	99.66	99.40	99.42	99.56
Fo%	88.10	87.81	88.04	87.20	87.45	87.54	87.62	86.47	86.82	90.15	88.97

sample	DI-24				DI-25						
	ol7 c4	ol7 c6	ol7 r2		ol3 c1	ol3 c2	ol3 c3	ol3 c4	ol3 r2	ol4 c3	ol4 c4
SiO_2	39.70	39.83	39.56		39.1	39.0	39.1	39.0	38.5	38.6	38.6
Al_2O_3	0.10	0.10	0.10		0.1	0.1	0.1	0.1	0.1	0.1	0.1
FeO	10.14	9.83	11.90		15.0	15.3	15.1	15.3	17.7	18.1	17.6
MgO	48.17	48.49	46.89		45.1	44.8	45.1	44.9	42.8	42.4	43.1
CaO	0.32	0.29	0.33		0.3	0.3	0.3	0.3	0.3	0.3	0.3
Na_2O											
K_2O											
TiO_2											
MnO	0.14	0.15	0.20		0.2	0.2	0.2	0.2	0.3	0.3	0.3
NiO	0.42	0.43	0.38		0.3	0.3	0.3	0.3	0.2	0.2	0.2
Cr_2O_3	0.12	0.14	0.05		0.1	0.0	0.1	0.0	0.0	0.0	0.1
Total	99.09	99.27	99.41		100.2	100.0	100.3	100.2	100.0	99.8	100.2
Fo%	89.44	89.79	87.54		84.27	83.93	84.14	83.92	81.16	80.72	81.32

sample	DI-25								
	ol4 r1	ol5 c1	ol5 c2	ol5 c3	ol5 c4	ol5 r1	ol5 r2	ol6 c1	ol6 c2
SiO_2	38.3	39.1	39.4	39.3	39.4	38.2	38.4	38.6	38.9
Al_2O_3	0.1	0.1	0.1	0.0	0.1	0.1	0.1	0.1	0.1
FeO	19.7	14.9	14.6	14.5	14.5	20.1	19.0	17.2	16.7
MgO	40.8	45.0	45.4	45.6	45.5	41.0	41.6	43.1	43.7
CaO	0.3	0.3	0.3	0.3	0.3	0.3	0.3	0.3	0.3
Na_2O									
K_2O									
TiO_2									
MnO	0.3	0.2	0.2	0.2	0.2	0.3	0.3	0.3	0.3
NiO	0.2	0.3	0.3	0.3	0.3	0.2	0.2	0.2	0.2
Cr_2O_3	0.0	0.0	0.1	0.1	0.1	0.1	0.0	0.0	0.0
Total	99.7	99.8	100.3	100.3	100.4	100.2	100.0	99.8	100.2
Fo%	78.69	84.33	84.73	84.86	84.83	78.43	79.61	81.73	82.39

(ol: olivine; c: core; r: rim)

A3 (continued) Microprobe analyses (in wt. %) of olivine crystals

sample	DI-27										
	ol1 c8	ol1 c9	ol1 c10	ol1 c11	ol1 r6	ol1 r7	ol5 c1	ol5 c2	ol5 c4	ol5 c5	ol5 c6
SiO_2	39.87	39.89	39.97	39.88	39.55	39.51	40.13	40.29	40.48	40.43	40.26
Al_2O_3	0.09	0.10	0.08	0.08	0.04	0.05	0.08	0.10	0.08	0.08	0.10
FeO	11.20	11.23	11.29	11.15	13.60	13.41	9.46	9.42	8.10	8.23	9.58
MgO	48.07	48.13	48.25	48.05	46.44	46.26	49.63	49.55	50.77	50.49	49.52
CaO	0.31	0.31	0.29	0.29	0.32	0.32	0.30	0.28	0.31	0.29	0.30
Na_2O											
K_2O											
TiO_2											
MnO	0.20	0.18	0.19	0.19	0.16	0.19	0.16	0.13	0.12	0.14	0.17
NiO	0.36	0.40	0.38	0.39	0.33	0.34	0.43	0.41	0.46	0.47	0.45
Cr_2O_3	0.08	0.09	0.12	0.08	0.07	0.06	0.14	0.12	0.10	0.11	0.14
Total	100.17	100.33	100.57	100.10	100.52	100.15	100.32	100.30	100.41	100.23	100.52
Fo%	88.45	88.42	88.40	88.48	85.89	86.01	90.34	90.36	91.78	91.62	90.22

sample	DI-27									
	ol5 c7	ol5 r1	ol5 r2	ol5 r3	ol6 c1	ol6 c2	ol6 c3	ol6 c4	ol6 r1	ol6 r2
SiO_2	40.07	39.28	38.62	39.02	39.88	39.81	39.86	39.68	39.21	38.64
Al_2O_3	0.10	0.04	0.06	0.09	0.06	0.06	0.06	0.05	0.06	0.06
FeO	9.87	13.56	16.49	14.27	11.22	11.21	11.22	11.11	14.86	17.03
MgO	49.13	46.14	43.12	45.38	48.02	47.90	47.98	47.65	45.04	43.05
CaO	0.29	0.32	0.28	0.32	0.29	0.30	0.31	0.30	0.34	0.32
Na_2O										
K_2O										
TiO_2										
MnO	0.18	0.25	0.26	0.23	0.16	0.19	0.14	0.17	0.20	0.26
NiO	0.39	0.34	0.30	0.31	0.39	0.38	0.39	0.37	0.30	0.26
Cr_2O_3	0.12	0.07	0.06	0.07	0.06	0.07	0.08	0.07	0.07	0.04
Total	100.14	100.00	99.20	99.68	100.07	99.91	100.04	99.40	100.07	99.65
Fo%	89.87	85.84	82.34	85.00	88.42	88.40	88.40	88.43	84.38	81.84

sample	DI-29										
	ol6 c1	ol7 c1	ol7 c6	ol7 c7	ol7 c9	ol7 r1	ol7 r2	ol8 c1	ol8 c3	ol8 c5	ol8 r1
SiO_2	39.45	39.56	39.71	39.42	39.30	39.57	39.50	39.48	39.43	39.37	39.40
Al_2O_3	0.12	0.06	0.07	0.05	0.07	0.06	0.05	0.06	0.04	0.07	0.08
FeO	12.17	12.16	12.13	12.24	12.10	12.10	12.24	12.09	12.06	11.95	12.38
MgO	46.52	46.55	47.71	47.18	47.48	47.30	47.35	47.44	46.85	46.68	46.48
CaO	0.32	0.35	0.35	0.35	0.33	0.34	0.34	0.34	0.36	0.35	0.34
Na_2O											
K_2O											
TiO_2											
MnO	0.17	0.21	0.20	0.21	0.16	0.21	0.20	0.21	0.21	0.19	0.21
NiO	0.36	0.37	0.34	0.37	0.36	0.34	0.36	0.32	0.37	0.35	0.31
Cr_2O_3	0.12	0.06	0.07	0.07	0.06	0.12	0.06	0.07	0.07	0.05	0.06
Total	99.23	99.33	100.57	99.88	99.86	100.05	100.09	100.01	99.39	99.00	99.26
Fo%	87.21	87.22	87.52	87.30	87.49	87.45	87.34	87.49	87.39	87.44	87.00

sample	DI-29										
	ol8 r2	ol8 r3	ol9 c1	ol9 c2	ol9 c3	ol9 r1	ol9 c5	ol9 c6	ol10 c1	ol10 c2	ol10 c3
SiO_2	39.33	39.35	39.27	39.36	39.50	39.32	39.45	39.55	39.49	39.36	39.39
Al_2O_3	0.06	0.09	0.05	0.07	0.06	0.07	0.05	0.07	0.04	0.07	0.07
FeO	12.67	12.39	12.76	13.14	11.90	12.76	11.95	12.07	12.24	12.41	12.39
MgO	46.06	46.86	46.21	46.12	46.76	46.71	47.09	46.83	46.67	46.45	46.52
CaO	0.35	0.35	0.33	0.34	0.35	0.35	0.34	0.34	0.36	0.35	0.34
Na_2O											
K_2O											
TiO_2											
MnO	0.18	0.20	0.20	0.18	0.19	0.23	0.17	0.20	0.20	0.20	0.20
NiO	0.33	0.35	0.31	0.31	0.39	0.35	0.34	0.33	0.33	0.35	0.34
Cr_2O_3	0.07	0.06	0.08	0.08	0.06	0.09	0.07	0.05	0.04	0.07	0.06
Total	99.05	99.65	99.22	99.59	99.20	99.86	99.47	99.44	99.38	99.24	99.29
Fo%	86.63	87.08	86.59	86.22	87.51	86.71	87.54	87.37	87.18	86.97	87.01

(ol: olivine; c: core; r: rim)

A3 (continued) Microprobe analyses (in wt. %) of olivine crystals

sample	CS-7										
	ol1 c1	ol1 c2	ol1 c3	ol1 c4	ol1 c5	ol1 c6	ol1 r1	ol1 r2	ol1 r3	ol2 c1	ol2 c2
SiO_2	40.45	40.44	40.01	40.31	40.55	40.50	39.76	40.02	39.82	39.78	39.85
Al_2O_3	0.09	0.11	0.08	0.09	0.08	0.08	0.10	0.09	0.09	0.09	0.13
FeO	7.67	7.80	10.10	8.19	8.05	8.00	12.16	10.78	11.40	10.03	10.23
MgO	49.96	50.33	48.67	49.97	50.26	50.20	47.07	48.10	47.65	48.35	48.46
CaO	0.31	0.31	0.32	0.32	0.31	0.30	0.32	0.31	0.31	0.29	0.30
Na_2O											
K_2O											
TiO_2											
MnO	0.13	0.14	0.19	0.12	0.12	0.15	0.19	0.15	0.17	0.16	0.15
NiO	0.43	0.45	0.38	0.46	0.43	0.43	0.33	0.39	0.37	0.38	0.40
Cr_2O_3	0.13	0.13	0.08	0.12	0.12	0.13	0.07	0.10	0.09	0.13	0.14
Total	99.18	99.71	99.82	99.57	99.91	99.80	100.00	99.94	99.89	99.21	99.65
Fo%	92.07	92.00	89.57	91.58	91.76	91.80	87.34	88.84	88.17	89.58	89.41

sample	CS-7										
	ol2 c3	ol2 c5	ol2 r2	ol2 r3	ol3 c1	ol3 c2	ol3 c3	ol3cC4	ol3 r1	ol3 r2	ol3 r3
SiO_2	39.73	39.97	39.59	39.75	40.37	40.52	40.40	40.51	39.43	39.95	39.97
Al_2O_3	0.11	0.11	0.10	0.10	0.09	0.08	0.07	0.08	0.09	0.08	0.11
FeO	10.19	10.09	11.67	12.21	7.50	7.54	7.60	7.63	12.36	10.91	10.96
MgO	48.32	48.29	47.06	46.72	50.24	50.47	50.10	50.22	46.34	47.71	48.06
CaO	0.30	0.29	0.33	0.33	0.31	0.30	0.32	0.32	0.34	0.33	0.31
Na_2O											
K_2O											
TiO_2											
MnO	0.13	0.17	0.19	0.20	0.12	0.12	0.13	0.12	0.23	0.18	0.16
NiO	0.41	0.42	0.33	0.34	0.42	0.45	0.41	0.44	0.34	0.38	0.37
Cr_2O_3	0.12	0.13	0.09	0.12	0.17	0.15	0.15	0.15	0.11	0.11	0.11
Total	99.31	99.47	99.36	99.77	99.20	99.63	99.18	99.45	99.24	99.65	100.05
Fo%	89.42	89.51	87.79	87.21	92.28	92.27	92.16	92.15	86.98	88.63	88.66

sample	CS-7						
	ol4 c1	ol4 c2	ol4 c3	ol4 c4	ol4 r1	ol4 r2	ol4 r3
SiO_2	40.24	40.13	39.97	40.25	39.65	38.61	39.67
Al_2O_3	0.07	0.07	0.08	0.08	0.06	0.05	0.07
FeO	10.33	10.50	10.35	10.37	12.29	16.87	11.58
MgO	48.36	48.49	48.42	48.49	47.06	43.20	47.14
CaO	0.32	0.32	0.33	0.32	0.33	0.34	0.31
Na_2O							
K_2O							
TiO_2							
MnO	0.16	0.16	0.17	0.18	0.24	0.26	0.18
NiO	0.32	0.36	0.34	0.39	0.30	0.24	0.31
Cr_2O_3	0.11	0.10	0.10	0.10	0.07	0.04	0.09
Total	99.90	100.13	99.76	100.17	100.00	99.60	99.35
Fo%	89.30	89.17	89.29	89.29	87.22	82.03	87.89

sample	CS-29										
	ol1 c1	ol1 c2	ol1 c3	ol2 c4	ol1 r1	ol1 r2	ol2 c1	ol2 c2	ol2 c3	ol2 c4	ol2 r1
SiO_2	39.80	39.85	39.73	39.87	39.62	39.78	40.21	40.18	40.18	40.12	39.88
Al_2O_3	0.09	0.11	0.08	0.10	0.09	0.09	0.08	0.14	0.06	0.08	0.05
FeO	12.15	12.09	12.16	12.20	12.88	12.76	10.41	10.45	10.44	10.43	11.58
MgO	47.00	47.06	46.70	47.03	45.81	46.36	48.42	48.52	48.61	48.87	47.37
CaO	0.32	0.33	0.30	0.32	0.34	0.31	0.31	0.31	0.32	0.31	0.33
Na_2O											
K_2O											
TiO_2											
MnO	0.18	0.18	0.20	0.20	0.20	0.20	0.15	0.15	0.16	0.18	0.17
NiO	0.35	0.37	0.35	0.34	0.32	0.36	0.40	0.41	0.40	0.40	0.35
Cr_2O_3	0.07	0.08	0.04	0.11	0.07	0.09	0.10	0.12	0.11	0.12	0.08
Total	99.94	100.06	99.55	100.17	99.32	99.95	100.07	100.27	100.29	100.51	99.82
Fo%	87.34	87.41	87.25	87.30	86.38	86.62	89.24	89.23	89.25	89.31	87.94

(ol: olivine; c: core; r: rim)

A3 (continued) Microprobe analyses (in wt. %) of olivine crystals

sample	CS-29					
	ol2 r2	ol3 c1	ol3 c2	ol3 c3	ol3 c4	ol3 r1
SiO_2	40.01	39.92	40.15	39.67	40.02	39.63
Al_2O_3	0.13	0.06	0.06	0.07	0.07	0.06
FeO	11.50	10.34	10.39	10.32	10.28	13.30
MgO	47.87	48.37	48.25	48.10	48.24	46.14
CaO	0.33	0.31	0.30	0.35	0.31	0.33
Na_2O						
K_2O						
TiO_2						
MnO	0.17	0.17	0.16	0.15	0.17	0.24
NiO	0.37	0.39	0.41	0.38	0.41	0.35
Cr_2O_3	0.11	0.13	0.10	0.10	0.11	0.09
Total	100.49	99.68	99.81	99.13	99.59	100.14
Fo%	88.13	89.29	89.23	89.26	89.32	86.08

sample	CS-18										
	ol1 c1	ol1 c2	ol1 c3	ol1 r1	ol1 r2	ol2 c1	ol2 c2	ol2 c3	ol2 r1	ol2 r2	ol3 c1
SiO_2	39.59	39.46	39.48	39.53	39.49	39.44	39.38	39.34	39.03	39.31	39.44
Al_2O_3	0.05	0.04	0.06	0.05	0.06	0.05	0.06	0.05	0.05	0.06	0.05
FeO	13.41	13.45	13.43	13.70	13.73	13.44	13.43	13.17	14.17	14.02	13.30
MgO	46.00	45.87	45.87	45.95	45.96	45.96	46.11	46.00	45.30	45.46	46.14
CaO	0.34	0.34	0.34	0.36	0.34	0.35	0.34	0.34	0.35	0.33	0.33
Na_2O											
K_2O											
TiO_2											
MnO	0.20	0.19	0.17	0.21	0.20	0.21	0.20	0.23	0.24	0.22	0.20
NiO	0.28	0.26	0.24	0.25	0.25	0.26	0.24	0.27	0.26	0.24	0.29
Cr_2O_3	0.06	0.04	0.08	0.08	0.08	0.04	0.07	0.07	0.06	0.09	0.09
Total	99.94	99.65	99.66	100.12	100.10	99.75	99.83	99.45	99.46	99.73	99.83
Fo%	85.94	85.88	85.90	85.67	85.65	85.91	85.96	86.16	85.08	85.25	86.09

sample	CS-18										
	ol3 c2	ol3 c3	ol3 c4	ol3 r1	ol3 r2	ol4 c1	ol4 c2	ol4 c3	ol4 c4	ol4 r1	ol4 r2
SiO_2	39.41	39.40	39.42	39.08	39.50	39.61	39.54	39.59	39.53	39.20	39.37
Al_2O_3	0.06	0.05	0.05	0.06	0.07	0.06	0.06	0.05	0.09	0.07	0.05
FeO	13.37	13.32	13.23	14.57	13.46	13.23	13.16	13.43	13.24	13.01	13.80
MgO	45.98	45.95	46.15	44.90	46.06	46.25	46.10	46.07	45.99	46.09	45.70
CaO	0.34	0.35	0.33	0.37	0.33	0.36	0.34	0.38	0.34	0.34	0.35
Na_2O											
K_2O											
TiO_2											
MnO	0.19	0.18	0.20	0.23	0.21	0.22	0.18	0.17	0.21	0.23	0.20
NiO	0.28	0.22	0.25	0.25	0.25	0.25	0.28	0.26	0.29	0.24	0.26
Cr_2O_3	0.05	0.03	0.07	0.06	0.11	0.06	0.05	0.04	0.09	0.08	0.07
Total	99.68	99.51	99.70	99.51	99.99	100.04	99.72	99.99	99.77	99.26	99.80
Fo%	85.98	86.02	86.15	84.60	85.92	86.17	86.20	85.95	86.10	86.33	85.52

sample	PI-16										
	ol1 c1	ol1 c2	ol1 c3	ol1 c4	ol1 c5	ol1 c6	ol1 r1	ol1 r2	ol1 r3	ol2 c1	ol2 c2
SiO_2	40.71	40.62	40.45	40.67	40.56	40.63	40.03	40.44	40.47	40.55	40.61
Al_2O_3	0.11	0.12	0.13	0.12	0.12	0.11	0.12	0.13	0.12	0.12	0.12
FeO	7.05	6.91	7.02	6.99	7.00	7.00	8.23	7.29	6.96	6.94	7.06
MgO	51.23	51.24	51.00	51.00	51.22	51.16	49.83	50.96	51.12	51.08	51.12
CaO	0.31	0.29	0.30	0.31	0.31	0.30	0.31	0.31	0.30	0.30	0.31
Na_2O											
K_2O											
TiO_2											
MnO	0.11	0.12	0.11	0.11	0.14	0.12	0.13	0.12	0.12	0.12	0.14
NiO	0.44	0.48	0.47	0.47	0.44	0.47	0.43	0.46	0.50	0.48	0.45
Cr_2O_3	0.18	0.18	0.18	0.18	0.17	0.17	0.14	0.18	0.15	0.15	0.15
Total	100.14	99.94	99.67	99.85	99.96	99.95	99.21	99.89	99.73	99.73	99.96
Fo%	92.84	92.97	92.83	92.86	92.88	92.87	91.52	92.57	92.90	92.92	92.81

(ol: olivine; c: core; r: rim)

A3 (continued) Microprobe analyses (in wt. %) of olivine crystals

sample	PI-16										
	ol2 c3	ol2 c4	ol2 c5	ol2 r1	ol2 r2	ol3 c1	ol3 c2	ol3 c3	ol3 c4	ol3 r1	ol3 r2
SiO_2	40.52	40.40	40.56	40.65	40.58	39.77	39.93	40.00	39.93	39.96	39.99
Al_2O_3	0.11	0.12	0.12	0.10	0.12	0.08	0.07	0.08	0.07	0.07	0.06
FeO	6.96	7.00	6.99	7.37	6.90	10.69	10.42	10.69	10.64	10.90	10.60
MgO	51.30	50.83	51.23	50.96	51.10	48.23	48.20	48.26	48.45	48.28	48.53
CaO	0.31	0.29	0.31	0.31	0.30	0.32	0.33	0.32	0.32	0.34	0.33
Na_2O											
K_2O											
TiO_2											
MnO	0.14	0.13	0.12	0.16	0.11	0.16	0.18	0.16	0.16	0.18	0.18
NiO	0.46	0.46	0.48	0.45	0.45	0.36	0.37	0.34	0.36	0.36	0.37
Cr_2O_3	0.18	0.16	0.19	0.17	0.20	0.08	0.08	0.07	0.08	0.07	0.08
Total	99.97	99.39	99.99	100.16	99.76	99.69	99.57	99.92	100.02	100.16	100.14
Fo%	92.93	92.83	92.90	92.50	92.96	88.94	89.18	88.95	89.03	88.76	89.09

sample	PI-16						PI-41				
	ol4 c1	ol4 c2	ol4 c3	ol4 r1	ol4 r2		ol1 c1	ol1 c2	ol1 c3	ol1 c4	ol1 r1
SiO_2	40.01	40.01	39.90	39.75	39.98		39.53	39.25	39.86	39.48	39.71
Al_2O_3	0.11	0.10	0.10	0.08	0.10		0.06	0.07	0.07	0.10	0.06
FeO	10.46	10.51	10.34	10.91	10.57		11.33	11.34	10.93	11.20	12.85
MgO	48.52	48.45	48.47	48.13	48.54		47.48	47.43	48.17	47.35	46.44
CaO	0.32	0.34	0.32	0.35	0.33		0.33	0.33	0.33	0.31	0.33
Na_2O											
K_2O											
TiO_2											
MnO	0.19	0.19	0.18	0.18	0.20		0.16	0.19	0.17	0.16	0.20
NiO	0.37	0.34	0.36	0.32	0.35		0.38	0.37	0.38	0.43	0.37
Cr_2O_3	0.08	0.08	0.10	0.08	0.09		0.09	0.08	0.11	0.09	0.07
Total	100.05	100.01	99.77	99.79	100.16		99.36	99.04	100.01	99.12	100.02
Fo%	89.22	89.15	89.31	88.72	89.12		88.19	88.18	88.71	88.29	86.57

sample	PI-41										
	ol1 r2	ol2 c1	ol2 c2	ol2 c3	ol2 c4	ol2 r1	ol2 r2	ol3 c2	ol3 c3	ol3 c4	ol3 c5
SiO_2	39.33	39.60	39.86	39.94	39.88	39.23	38.53	39.36	39.72	39.46	39.45
Al_2O_3	0.06	0.06	0.05	0.07	0.05	0.05	0.06	0.07	0.10	0.06	0.07
FeO	12.31	10.88	10.73	10.73	10.80	13.31	16.42	10.85	11.21	10.98	11.13
MgO	46.67	48.03	48.17	48.24	48.24	45.82	43.53	47.93	48.01	47.97	47.87
CaO	0.32	0.33	0.34	0.32	0.34	0.33	0.32	0.32	0.32	0.33	0.35
Na_2O											
K_2O											
TiO_2											
MnO	0.20	0.16	0.16	0.17	0.20	0.20	0.23	0.15	0.20	0.19	0.17
NiO	0.35	0.38	0.42	0.39	0.35	0.39	0.32	0.39	0.39	0.39	0.36
Cr_2O_3	0.09	0.10	0.09	0.09	0.05	0.08	0.07	0.11	0.12	0.09	0.08
Total	99.33	99.53	99.81	99.96	99.90	99.40	99.48	99.18	100.06	99.47	99.46
Fo%	87.12	88.73	88.90	88.91	88.85	85.99	82.53	88.73	88.42	88.62	88.46

sample	PI-41							
	ol4 r1	ol3 r2	ol4 c1	ol4 c2	ol4 c3	ol4 c4	ol4 r1	ol4 r2
SiO_2	38.96	38.88	39.50	39.52	39.53	39.89	39.16	39.35
Al_2O_3	0.07	0.07	0.05	0.06	0.07	0.05	0.06	0.07
FeO	14.60	15.09	10.55	10.90	11.03	10.75	13.08	13.73
MgO	44.80	44.33	48.35	48.06	47.97	48.33	46.28	46.03
CaO	0.32	0.32	0.32	0.33	0.34	0.32	0.35	0.33
Na_2O								
K_2O								
TiO_2								
MnO	0.22	0.24	0.15	0.18	0.18	0.15	0.22	0.20
NiO	0.33	0.31	0.39	0.36	0.43	0.38	0.31	0.38
Cr_2O_3	0.06	0.09	0.08	0.09	0.08	0.10	0.13	0.09
Total	99.35	99.32	99.39	99.50	99.62	99.97	99.59	100.17
Fo%	84.55	83.97	89.10	88.71	88.58	88.91	86.31	85.67

(ol: olivine; c: core; r: rim)

A4 Major element data (wt. %) from XRF analyses

Cape Searle								
sample	CS-13	CS-11	CS-8	CS-7	CS-12	CS-32	CS-31	CS-30
SiO_2	48.44	47.84	49.51	46.89	48.54	48.68	43.42	45.58
$Al2O_3$	14.86	14.61	15.01	11.36	14.62	15.78	7.82	11.60
Fe_2O_3	10.92	10.78	11.08	10.49	11.02	10.27	11.41	10.83
MgO	10.49	10.79	9.68	19.94	10.70	9.32	28.07	17.96
CaO	12.81	12.53	12.86	9.56	12.44	13.36	6.34	8.92
Na_2O	1.37	1.49	1.42	0.91	1.62	1.63	0.49	1.01
K_2O	0.05	0.04	0.07	0.05	0.05	0.03	0.05	0.14
TiO_2	0.66	0.65	0.68	0.46	0.65	0.93	0.47	0.65
MnO	0.17	0.17	0.18	0.16	0.18	0.17	0.16	0.17
P_2O_5	0.05	0.05	0.05	0.04	0.02	0.07	0.05	0.03
LOI	0.49	0.64	-0.05	0.18	0.35	-0.15	1.62	2.18
Total	100.31	99.60	100.49	100.05	100.19	100.09	99.89	99.06

Cape Searle								
sample	CS-29	CS-28	CS-27	CS-26	CS-25	CS-24	CS-23	CS-22
SiO_2	44.72	45.46	46.36	44.66	46.93	46.89	46.36	46.41
$Al2O_3$	9.64	12.71	13.76	12.43	13.82	13.84	13.68	13.26
Fe_2O_3	11.60	11.34	11.02	10.81	10.97	10.80	10.88	10.94
MgO	23.37	13.06	11.75	15.69	13.65	13.67	14.38	15.13
CaO	7.35	11.02	11.45	10.01	10.64	10.24	9.67	9.52
Na_2O	0.95	0.93	1.34	0.98	1.30	1.22	1.31	1.19
K_2O	0.04	0.08	0.12	0.08	0.08	0.08	0.09	0.11
TiO_2	0.72	1.00	1.04	0.75	0.83	0.84	0.79	0.80
MnO	0.18	0.17	0.17	0.17	0.17	0.17	0.17	0.16
P_2O_5	0.04	0.09	0.10	0.07	0.08	0.08	0.05	0.08
LOI	0.91	3.8	2.59	4.13	1.71	2.29	1.95	2.67
Total	99.51	99.66	99.69	99.78	100.19	100.12	99.33	100.27

Cape Searle								
sample	CS-21	CS-20	CS-19	CS-18	CS-17	CS-16	CS-15	CS-10
SiO_2	46.40	46.33	47.52	46.39	46.02	46.80	45.62	45.71
$Al2O_3$	13.41	12.95	14.70	13.83	14.29	13.54	13.49	12.55
Fe_2O_3	10.89	11.05	10.69	11.17	10.86	11.29	10.54	11.20
MgO	14.51	15.17	11.08	14.29	13.25	14.80	14.01	14.52
CaO	9.59	9.94	11.86	10.79	11.18	10.77	8.35	8.26
Na_2O	1.33	1.44	1.40	1.37	1.45	1.36	0.78	1.06
K_2O	0.11	0.11	0.07	0.04	0.05	0.05	0.10	0.15
TiO_2	0.81	0.81	0.94	0.87	0.87	0.86	0.85	0.98
MnO	0.17	0.17	0.17	0.17	0.17	0.17	0.16	0.17
P_2O_5	0.05	0.05	0.09	0.08	0.08	0.08	0.08	0.09
LOI	2.54	1.72	1.76	1.17	1.06	0.56	6.18	5.29
Total	99.81	99.74	100.27	100.17	99.28	100.27	100.15	99.97

A4 (continued) Major element data (wt. %) from XRF analyses

Cape Searle						
sample	CS-4	CS-3	CS-14	CS-6	CS-5	CS-1
SiO_2	45.88	46.04	47.00	47.62	46.79	46.20
$Al2O_3$	12.27	12.55	13.84	13.93	12.75	13.34
Fe_2O_3	10.72	10.62	10.89	11.09	11.67	11.62
MgO	14.80	14.30	13.85	13.25	15.43	13.74
CaO	6.86	6.93	10.76	11.15	10.39	11.66
Na_2O	0.57	0.82	1.20	1.84	1.23	1.38
K_2O	0.09	0.11	0.05	0.12	0.05	0.04
TiO_2	0.87	0.87	0.88	0.88	0.97	0.94
MnO	0.17	0.16	0.17	0.18	0.17	0.18
P_2O_5	0.08	0.08	0.08	0.06	0.10	0.08
LOI	7.47	7.55	1.48	-0.28	0.42	0.76
Total	99.78	100.02	100.19	99.83	99.96	99.95

Padloping Island								
sample	PI-16	PI-18	PI-19	PI-20	PI-21	PI-22	PI-23	PI-24
SiO_2	48.13	48.01	48.05	48.16	47.80	47.93	45.05	44.81
$Al2O_3$	13.65	14.74	14.47	14.51	14.70	13.68	9.61	8.99
Fe_2O_3	11.00	11.62	11.03	11.02	10.87	11.22	11.62	12.00
MgO	12.86	10.54	11.92	12.04	12.32	13.51	24.19	25.87
CaO	11.84	11.80	11.36	11.01	10.79	10.42	7.70	6.94
Na_2O	1.35	1.50	1.70	1.63	1.47	1.42	0.81	0.84
K_2O	0.05	0.07	0.12	0.15	0.12	0.15	0.02	0.03
TiO_2	0.62	1.09	1.03	1.02	0.96	1.01	0.62	0.63
MnO	0.17	0.18	0.17	0.18	0.17	0.17	0.17	0.18
P_2O_5	0.05	0.09	0.10	0.10	0.09	0.10	0.05	0.05
LOI	0.33	0.49	0.17	0.46	0.82	0.53	0.25	0.04
Total	100.04	100.12	100.12	100.27	100.12	100.14	100.10	100.37

Padloping Island								
sample	PI-25	PI-26	PI-27	PI-28	PI-29	PI-30	PI-31	PI-32
SiO_2	44.50	45.19	45.65	48.27	47.95	46.86	45.58	45.41
$Al2O_3$	8.29	9.32	9.80	14.11	13.94	12.24	10.16	10.27
Fe_2O_3	11.69	11.62	11.62	11.61	11.63	11.31	11.62	11.39
MgO	27.35	24.89	22.94	11.15	10.85	17.28	22.43	22.92
CaO	6.75	7.61	8.17	11.92	11.69	10.12	8.53	7.83
Na_2O	0.64	0.89	0.92	1.29	1.64	1.21	0.98	0.84
K_2O	0.02	0.02	0.02	0.06	0.07	0.03	0.02	0.03
TiO_2	0.49	0.61	0.69	0.90	0.94	0.86	0.69	0.66
MnO	0.17	0.17	0.17	0.18	0.18	0.17	0.17	0.17
P_2O_5	0.04	0.05	0.06	0.08	0.07	0.07	0.05	0.06
LOI	0.05	0.06	-0.01	0.47	0.46	0.17	0.06	0.54
Total	99.99	100.43	100.03	100.04	99.42	100.33	100.29	100.11

A4 (continued) Major element data (wt. %) from XRF analyses

Padloping Island								
sample	PI-33	PI-34	PI-35	PI-38	PI-36	PI-37	PI-39	PI-40
SiO_2	46.83	45.54	44.15	44.32	44.43	43.89	43.13	42.78
$Al2O_3$	12.64	10.68	10.09	8.83	8.55	9.14	8.14	8.11
Fe_2O_3	11.80	11.46	11.01	11.44	11.44	10.76	11.15	11.12
MgO	14.77	21.41	22.56	25.63	26.62	25.81	27.32	27.98
CaO	10.55	8.82	7.55	7.17	7.03	7.20	5.83	5.74
Na_2O	1.52	1.13	0.56	0.86	0.87	0.68	0.33	0.31
K_2O	0.03	0.02	0.09	0.04	0.02	0.04	0.02	0.02
TiO_2	1.08	0.70	0.69	0.60	0.56	0.48	0.48	0.53
MnO	0.18	0.17	0.16	0.17	0.17	0.16	0.16	0.16
P_2O_5	0.09	0.02	0.05	0.05	0.02	0.04	0.04	0.05
LOI	-0.33	0.11	3.31	0.65	0.05	1.66	3.77	3.12
Total	99.16	100.06	100.21	99.76	99.76	99.86	100.37	99.91

Padloping Island				
sample	PI-41	PI-42	PI-43	PI-44
SiO_2	43.45	47.00	44.76	44.96
$Al2O_3$	8.32	15.44	9.52	10.09
Fe_2O_3	11.26	8.72	11.36	11.15
MgO	26.80	14.91	24.01	22.40
CaO	6.51	11.35	7.55	8.27
Na_2O	0.52	1.09	0.72	1.00
K_2O	0.07	0.05	0.04	0.02
TiO_2	0.55	0.56	0.65	0.69
MnO	0.17	0.14	0.16	0.17
P_2O_5	0.05	0.05	0.06	0.06
LOI	2.49	0.84	1.54	0.48
Total	100.18	100.14	100.37	99.29

Durban Island								
sample	DI-13	DI-14	DI-15	DI-16	DI-17	DI-18	DI-19	DI-20
SiO_2	48.89	46.74	45.29	45.15	45.36	45.33	45.58	48.60
$Al2O_3$	14.64	11.69	8.89	9.06	9.58	10.05	9.75	15.97
Fe_2O_3	11.86	11.58	11.95	11.67	11.83	11.52	11.52	11.05
MgO	9.91	17.89	24.11	25.41	23.35	22.90	23.05	8.87
CaO	12.42	9.90	7.80	7.46	7.82	8.29	8.19	12.68
Na_2O	1.54	1.33	1.06	0.77	0.84	0.90	0.96	1.65
K_2O	0.09	0.02	0.03	0.03	0.02	0.03	0.03	0.06
TiO_2	1.09	0.81	0.64	0.59	0.67	0.65	0.66	1.04
MnO	0.18	0.18	0.18	0.16	0.17	0.17	0.17	0.18
P_2O_5	0.10	0.04	0.03	0.05	0.06	0.06	0.03	0.09
LOI	-0.32	0.28	0.15	-0.7	0.36	0.24	2.61	0.2
Total	100.39	100.46	100.13	99.64	100.07	100.14	102.55	100.38

A4 (continued) Major element data (wt. %) from XRF analyses

Durban Island								
sample	DI-21	DI-22	DI-23	DI-24	DI-25	DI-26	DI-27	DI-28
SiO_2	46.62	47.83	45.26	45.08	47.23	47.06	47.16	45.02
$Al2O_3$	13.86	14.64	9.60	9.62	14.19	12.81	11.67	10.57
Fe_2O_3	11.57	10.81	12.08	11.65	11.84	11.35	11.05	11.52
MgO	14.99	12.60	23.93	24.14	12.27	15.71	18.48	21.14
CaO	10.38	11.26	7.40	7.66	11.95	10.47	9.78	8.36
Na_2O	1.38	1.49	1.03	0.84	1.33	1.29	1.26	1.14
K_2O	0.05	0.06	0.07	0.03	0.02	0.04	0.04	0.02
TiO_2	0.96	0.94	0.70	0.62	0.91	0.83	0.70	0.71
MnO	0.17	0.17	0.18	0.17	0.18	0.17	0.17	0.17
P_2O_5	0.09	0.09	0.07	0.05	0.06	0.07	0.06	0.03
LOI	0.19	0.17	-0.12	0.09	0.17	0.33	-0.35	0.47
Total	100.26	100.07	100.20	99.95	100.15	100.13	100.02	99.15

Durban Island	
sample	DI-29
SiO_2	45.07
$Al2O_3$	10.67
Fe_2O_3	11.67
MgO	20.99
CaO	8.69
Na_2O	0.94
K_2O	0.02
TiO_2	0.76
MnO	0.17
P_2O_5	0.06
LOI	0.4
Total	99.44

A 5 Trace element data (ppm) from XRF analyses

Cape Searle								
sample	CS-13	CS-11	CS-8	CS-7	CS-12	CS-32	CS-31	CS-30
Nb	0.6	0.7	0.7	0.5	0.7	1.6	0.6	1.0
Zr	31.9	31.1	33.9	22.8	30.5	46.4	23.9	29.7
Y	19.5	19.4	20.8	13.4	19.1	20.5	9.9	13.8
Sr	51.7	51.6	52.2	36.8	52.3	107.4	37.8	207.3
Rb	0.9	0.8	1.9	1.3	1.6	0.5	0.7	1.8
Th	0.7	0.5	0.6	1.5	0.0	0.4	0.0	0.0
Pb	1.1	0.2	0.4	0.8	0.6	0.4	0.9	0.0
La	2.7	4.0	1.0	0.8	0.2	2.0	0.0	2.6
Ce	0.9	1.1	2.2	1.2	3.9	7.9	4.8	3.5
Nd	3.4	0.8	2.9	0.8	3.4	5.1	2.5	3.9
Zn	74.4	72.1	75.6	66.9	69.3	68.3	73.3	71.5
Cu	137.6	133.6	127.3	86.4	135.8	123.9	71.0	102.1
Ni	190.8	214.4	150.1	831.4	210.0	172.7	1372.5	668.1
Cr	522.1	546.6	491.6	1916.6	531.4	2075.1	2338.2	1376.5
V	299.7	296.0	295.2	220.5	284.4	303.6	154.4	210.1
Ba	4.9	5.7	14.4	10.8	10.3	10.5	13.8	22.9
Sc	53.0	52.5	51.1	40.4	43.6	46.8	24.3	35.1

Cape Searle								
sample	CS-29	CS-28	CS-27	CS-26	CS-25	CS-24	CS-23	CS-22
Nb	1.1	4.1	5.3	3.4	4.1	3.9	3.9	3.5
Zr	38.4	55.4	61.9	40.6	45.2	45.3	44.1	44.2
Y	15.8	18.6	19.0	14.9	17.0	17.3	16.6	16.2
Sr	61.3	107.8	137.0	103.9	93.5	91.4	86.7	85.3
Rb	0.9	0.7	1.5	0.6	1.1	1.1	1.3	1.9
Th	0.2	0.0	1.3	0.5	0.0	0.4	1.0	0.6
Pb	0.1	0.6	1.1	1.4	0.2	1.0	0.0	1.1
La	2.3	3.7	4.2	5.4	3.6	4.8	5.2	3.2
Ce	6.7	10.6	14.6	9.1	10.3	8.0	5.8	11.0
Nd	3.4	8.6	8.0	4.5	5.8	6.5	4.8	5.8
Zn	77.4	74.7	76.7	74.6	75.1	75.1	76.1	78.3
Cu	97.5	87.1	102.6	69.1	96.7	95.9	83.2	84.9
Ni	1039.7	395.6	289.0	465.3	343.9	350.8	385.3	406.5
Cr	1892.8	996.0	735.5	1120.3	890.5	852.3	915.4	980.2
V	204.0	276.5	262.9	215.9	238.7	238.6	237.7	227.6
Ba	11.5	20.0	66.4	41.6	44.1	37.7	41.3	40.6
Sc	27.4	39.4	39.6	31.9	37.1	38.1	36.7	33.6

A 5 (continued) Trace element data (ppm) from XRF analyses

Cape Searle								
sample	CS-21	CS-20	CS-19	CS-18	CS-17	CS-16	CS-15	CS-10
Nb	3.7	3.8	4.3	4.3	4.2	4.2	4.0	4.5
Zr	44.6	45.0	52.6	48.3	50.4	48.4	44.4	53.5
Y	16.8	16.6	19.6	18.0	18.1	18.4	16.5	17.2
Sr	85.5	105.7	124.1	100.5	108.1	103.3	257.0	100.1
Rb	2.3	1.3	0.7	0.3	0.9	0.3	1.5	1.6
Th	0.3	1.4	0.3	0.4	0.4	-0.2	0.4	0.5
Pb	0.6	1.3	1.4	7.0	1.5	7.0	2.3	0.0
La	4.0	3.2	5.3	3.1	4.5	5.3	3.3	5.3
Ce	7.0	8.5	9.6	8.8	10.1	10.6	8.4	10.2
Nd	7.1	7.1	5.6	4.6	6.9	4.3	7.1	7.8
Zn	77.0	78.6	79.3	82.5	83.8	84.7	80.9	73.2
Cu	86.8	94.3	105.5	105.9	106.7	105.6	106.8	117.9
Ni	371.9	398.6	227.2	364.3	347.1	378.0	338.4	430.7
Cr	880.1	1042.5	654.8	969.1	916.7	994.5	913.9	1053.4
V	233.8	237.2	274.0	265.3	272.4	262.5	267.9	300.0
Ba	43.9	54.6	56.0	25.1	20.2	21.1	63.0	29.2
Sc	34.1	36.1	37.7	39.9	41.0	43.0	51.5	52.0

Cape Searle						
sample	CS-4	CS-3	CS-14	CS-6	CS-5	CS-1
Nb	2.9	2.7	4.2	4.4	4.8	3.7
Zr	46.1	45.3	48.5	51.3	57.6	53.2
Y	16.8	16.3	18.2	18.6	17.9	20.1
Sr	64.3	115.0	97.2	119.2	120.4	103.3
Rb	2.4	2.5	1.0	1.4	0.7	0.8
Th	0.3	0.2	0.2	0.2	0.5	0.2
Pb	0.7	0.0	1.1	0.5	0.5	0.9
La	2.4	3.0	4.4	4.3	4.1	4.1
Ce	9.0	9.4	7.9	7.1	10.3	7.8
Nd	7.1	6.8	5.4	4.4	6.4	6.5
Zn	71.2	69.4	81.8	80.7	80.9	79.4
Cu	123.8	123.7	105.6	103.7	111.9	128.1
Ni	358.9	340.3	334.0	338.8	480.5	369.7
Cr	880.1	855.2	900.8	921.1	1125.8	968.4
V	193.9	199.0	269.8	260.9	275.0	302.6
Ba	37.6	43.4	24.5	44.0	20.0	17.4
Sc	52.2	53.3	46.0	38.4	42.1	46.3

A 5 (continued) Trace element data (ppm) from XRF analyses

Padloping Island								
sample	PI-16	PI-18	PI-19	PI-20	PI-21	PI-22	PI-23	PI-24
Nb	0.6	2.9	6.6	6.3	6.2	6.7	0.9	0.9
Zr	29.5	60.9	65.7	64.0	60.2	64.6	32.5	32.8
Y	17.6	21.7	21.5	21.2	19.5	20.8	13.4	13.0
Sr	50.1	135.3	125.2	125.3	125.1	120.0	67.8	66.8
Rb	1.1	0.6	0.9	1.4	0.8	1.3	0.5	0.2
Th	0.1	0.4	1.1	1.0	0.0	0.0	0.9	0.3
Pb	1.6	3.6	2.1	1.2	1.6	4.1	2.3	0.7
La	2.5	4.1	6.2	6.5	4.4	6.2	1.8	3.5
Ce	4.9	8.1	13.4	12.6	10.6	10.9	3.5	5.4
Nd	4.5	8.6	8.3	8.2	6.7	7.1	2.6	1.3
Zn	74.8	78.1	78.8	79.8	75.1	80.0	75.0	75.9
Cu	126.0	122.1	96.7	94.7	86.6	95.5	87.5	89.5
Ni	378.1	197.2	326.7	332.6	343.2	427.0	1126.9	1228.3
Cr	863.1	534.6	805.7	840.2	915.4	936.1	2031.7	2095.9
V	279.4	305.9	271.6	264.0	260.0	264.8	203.0	189.4
Ba	10.7	33.8	64.4	72.9	76.7	74.3	13.8	12.8
Sc	47.3	43.5	43.0	38.0	40.2	39.3	30.5	26.2

Padloping Island								
sample	PI-25	PI-26	PI-27	PI-28	PI-29	PI-30	PI-31	PI-32
Nb	0.9	0.8	1.2	1.6	1.7	2.0	1.0	1.0
Zr	24.0	32.0	36.5	46.0	48.9	46.3	36.3	34.0
Y	9.5	12.7	14.1	19.7	21.6	17.9	16.2	15.0
Sr	56.8	68.5	75.6	95.3	96.2	94.8	71.0	67.7
Rb	0.2	0.0	0.3	0.2	0.9	0.1	0.2	0.2
Th	0.0	0.6	0.0	0.0	1.1	0.3	0.0	0.0
Pb	0.4	14.2	2.0	0.7	2.0	1.5	1.5	1.7
La	2.3	4.2	0.9	2.2	0.9	2.9	1.6	1.8
Ce	5.4	4.4	1.5	8.7	6.6	6.2	4.2	2.5
Nd	2.9	1.9	3.5	6.0	4.7	4.1	3.3	1.8
Zn	74.1	74.9	75.0	79.6	81.3	78.6	75.6	75.1
Cu	64.8	87.3	87.1	121.1	125.0	116.3	90.1	89.3
Ni	1335.7	1190.0	1057.7	245.9	240.5	699.7	1027.1	1053.5
Cr	2289.9	2132.9	1964.1	670.4	653.4	1555.4	1876.2	1854.5
V	159.5	196.1	217.4	293.3	302.4	248.0	216.0	213.8
Ba	15.4	12.5	11.5	18.4	21.9	25.8	8.9	21.0
Sc	26.7	26.8	28.4	48.6	47.4	36.8	34.0	33.1

A 5 (continued) Trace element data (ppm) from XRF analyses

Padloping Island								
sample	PI-33	PI-34	PI-35	PI-38	PI-36	PI-37	PI-39	PI-40
Nb	2.2	1.2	0.8	0.7	1.0	0.6	0.5	0.7
Zr	59.3	37.3	35.5	30.8	29.2	24.1	23.1	27.9
Y	23.7	14.8	13.9	12.0	12.0	10.3	9.2	11.0
Sr	92.7	70.2	100.3	59.2	57.7	99.0	50.7	39.2
Rb	0.3	0.1	0.4	0.7	0.0	0.3	0.7	0.5
Th	0.3	0.8	0.0	0.0	0.5	0.8	0.7	0.6
Pb	3.3	1.2	0.9	0.0	1.0	1.6	0.5	0.5
La	2.7	1.9	1.6	3.7	3.5	2.8	1.4	1.7
Ce	8.5	2.1	4.7	5.3	1.9	6.3	2.9	2.5
Nd	7.1	2.5	4.4	2.0	2.3	2.6	1.1	3.2
Zn	84.4	76.4	71.9	73.1	75.4	70.0	69.7	72.6
Cu	152.0	97.6	73.7	89.0	83.1	67.5	68.2	73.6
Ni	540.4	936.9	959.3	1212.2	1253.6	1205.7	1323.2	1323.1
Cr	1050.4	1755.9	1575.2	2300.0	2302.5	2264.3	2352.9	2256.1
V	310.2	233.0	214.6	191.0	185.7	170.7	160.8	173.4
Ba	12.6	6.0	4.0	9.7	12.2	5.7	7.9	19.4
Sc	43.6	34.6	30.1	28.9	28.2	28.9	26.1	23.6

Padloping Island				
sample	PI-41	PI-42	PI-43	PI-44
Nb	0.5	0.7	1.1	1.3
Zr	27.2	27.7	32.5	37.3
Y	11.2	11.4	13.4	14.2
Sr	148.8	142.6	89.7	66.0
Rb	0.6	0.5	0.1	0.3
Th	0.6	0.8	0.6	0.1
Pb	0.1	0.9	0.6	0.7
La	2.3	0.8	1.8	2.6
Ce	2.5	5.7	4.3	2.6
Nd	3.6	3.5	2.7	4.1
Zn	74.2	57.8	73.8	77.2
Cu	71.5	73.9	80.2	90.9
Ni	1246.5	526.1	1080.5	991.3
Cr	2079.4	1300.1	1957.6	1863.3
V	185.5	191.7	204.8	227.7
Ba	11.2	12.0	16.6	6.8
Sc	23.5	29.4	28.9	40.4

A 5 (continued) Trace element data (ppm) from XRF analyses

Durban Island								
sample	DI-13	DI-14	DI-15	DI-16	DI-17	DI-18	DI-19	DI-20
Nb	3.2	1.4	1.1	0.8	0.9	0.9	1.2	2.7
Zr	58.3	42.8	33.3	29.8	34.0	34.4	34.3	54.8
Y	22.3	16.9	13.2	12.9	14.2	13.7	13.8	22.9
Sr	120.2	87.5	68.5	65.4	74.6	74.5	78.3	128.5
Rb	0.8	0.0	0.0	0.5	0.3	0.1	0.5	0.3
Th	0.0	0.3	0.2	0.0	0.0	0.0	0.6	0.4
Pb	0.3	1.9	0.2	0.5	0.4	0.4	0.2	1.4
La	2.5	1.3	2.5	2.6	1.5	3.3	2.1	3.2
Ce	10.1	6.4	2.1	4.4	4.0	7.9	3.1	4.6
Nd	9.3	5.2	3.2	4.0	5.1	4.9	4.1	6.9
Zn	80.4	77.7	79.5	76.1	76.2	73.1	74.5	73.6
Cu	136.1	110.4	87.8	83.4	85.2	87.5	87.3	120.8
Ni	157.1	709.0	1095.4	1220.9	1089.4	1043.2	1022.2	152.2
Cr	462.0	1480.6	2158.5	1927.2	1648.0	1712.6	1668.3	518.0
V	317.6	243.5	202.4	186.0	211.5	212.6	196.5	297.7
Ba	25.7	16.8	10.1	9.0	18.3	11.1	19.1	33.4
Sc	48.8	38.5	33.2	31.2	30.5	33.9	34.7	43.2

Durban Island								
sample	DI-21	DI-22	DI-23	DI-24	DI-25	DI-26	DI-27	DI-28
Nb	5.6	5.1	4.5	0.7	1.5	1.7	0.8	1.0
Zr	61.9	58.5	45.4	32.0	47.6	44.3	36.3	38.0
Y	22.1	20.5	14.0	14.0	20.8	17.7	16.4	16.0
Sr	120.7	124.6	83.0	71.8	95.1	101.1	72.0	82.3
Rb	0.1	0.4	0.8	0.2	0.4	0.4	0.3	0.2
Th	0.5	1.0	0.3	0.0	0.2	0.0	0.5	0.3
Pb	0.8	0.6	0.4	0.0	0.9	0.0	0.2	0.8
La	7.1	6.8	5.4	1.4	2.7	0.6	1.3	1.5
Ce	13.4	13.2	7.5	2.0	1.6	4.4	6.0	6.2
Nd	10.1	9.5	4.1	3.7	6.9	5.1	4.5	3.6
Zn	80.9	73.8	82.5	74.4	81.6	74.7	77.2	78.9
Cu	96.3	92.2	65.6	86.8	128.4	100.2	101.1	82.2
Ni	451.8	326.5	1034.7	1119.8	261.1	545.5	718.4	913.6
Cr	1083.1	843.1	2330.9	2192.8	693.8	1265.0	1590.8	1836.2
V	262.0	277.0	188.5	209.8	322.5	256.7	256.3	232.7
Ba	38.6	43.2	50.7	11.7	5.0	16.1	7.4	16.2
Sc	37.0	41.9	28.3	34.0	47.8	39.3	38.1	31.8

A 5 (continued) Trace element data (ppm) from XRF analyses

Durban Island	
sample	DI-29
Nb	0.9
Zr	40.0
Y	16.1
Sr	75.7
Rb	0.2
Th	0.4
Pb	0.8
La	1.8
Ce	2.7
Nd	3.3
Zn	84.3
Cu	86.7
Ni	892.2
Cr	1817.9
V	254.3
Ba	8.8
Sc	44.0

A 6 Trace element data (ppm) from ICP-MS analyses

Cape Searle								
sample	CS-13	CS-11	CS-8	CS-7	CS-12	CS-32	CS-31	CS-30
La	1.15	1.07	1.32	0.92	1.18	2.11	0.98	1.58
Ce	3.22	3.14	3.96	2.59	3.31	6.02	2.87	4.44
Pr	0.54	0.54	0.67	0.43	0.56	1.02	0.48	0.73
Nd	3.22	3.17	3.52	2.38	3.23	5.65	2.68	4.04
Sm	1.37	1.35	1.48	1.00	1.35	2.01	0.95	1.39
Eu	0.52	0.53	0.57	0.38	0.53	0.77	0.36	0.53
Gd	2.07	2.08	2.18	1.49	2.07	2.72	1.33	1.91
Tb	0.40	0.41	0.44	0.31	0.40	0.50	0.24	0.35
Dy	2.84	2.83	3.08	2.16	2.84	3.31	1.63	2.30
Ho	0.66	0.65	0.71	0.49	0.67	0.72	0.36	0.51
Er	1.91	1.92	2.10	1.48	1.97	2.06	1.02	1.44
Tm	0.31	0.31	0.34	0.24	0.31	0.33	0.16	0.22
Yb	1.96	1.94	2.12	1.47	1.93	1.97	1.00	1.40
Lu	0.30	0.30	0.32	0.23	0.30	0.30	0.16	0.21
Hf	0.87	1.11	1.04	0.96	0.94	1.43	1.34	1.13
Pb	0.93	1.80	0.60	0.60	2.50	1.30	1.00	1.10
Th	0.17	0.17	0.24	0.18	0.17	0.25	0.08	0.28
U	0.07	0.08	0.07	0.06	0.08		0.05	

Cape Searle								
sample	CS-29	CS-28	CS-27	CS-26	CS-25	CS-24	CS-23	CS-22
La	1.74	3.76	4.81	3.62	3.35	3.56	3.23	3.12
Ce	4.86	9.55	11.67	8.26	8.09	8.52	7.88	7.61
Pr	0.81	1.43	1.67	1.15	1.17	1.21	1.12	1.10
Nd	4.39	7.00	8.11	5.52	5.81	6.07	5.60	5.48
Sm	1.55	2.21	2.39	1.68	1.84	1.87	1.80	1.74
Eu	0.56	0.76	0.84	0.65	0.68	0.68	0.64	0.64
Gd	2.14	2.79	2.95	2.15	2.42	2.46	2.29	2.29
Tb	0.39	0.49	0.51	0.38	0.44	0.44	0.42	0.41
Dy	2.54	3.17	3.28	2.47	2.85	2.86	2.73	2.66
Ho	0.56	0.68	0.71	0.55	0.63	0.64	0.61	0.59
Er	1.61	1.92	1.97	1.54	1.79	1.75	1.74	1.68
Tm	0.25	0.29	0.29	0.24	0.28	0.27	0.27	0.26
Yb	1.52	1.80	1.87	1.51	1.76	1.75	1.66	1.63
Lu	0.24	0.28	0.28	0.23	0.26	0.26	0.25	0.25
Hf	2.06	2.41	1.60	1.24	2.05	1.26	2.02	1.48
Pb	0.43	0.56	1.10	2.00	1.00	2.15	0.70	0.70
Th	0.14	0.31	0.53	0.39	0.30	0.44	0.29	0.27
U	0.07	0.11		0.19	0.11		0.11	0.08

A 6 (continued) Trace element data (ppm) from ICP-MS analyses

Cape Searle								
sample	CS-21	CS-20	CS-19	CS-18	CS-17	CS-16	CS-15	CS-10
La	3.19	3.26	3.70	3.43	3.50	3.41	3.26	3.69
Ce	7.62	7.81	9.16	8.29	8.48	8.08	7.94	9.24
Pr	1.11	1.14	1.32	1.19	1.22	1.19	1.14	1.35
Nd	5.45	5.58	6.57	5.97	6.15	5.92	5.67	6.56
Sm	1.76	1.81	2.03	1.89	1.85	1.85	1.76	2.04
Eu	0.63	0.66	0.77	0.69	0.69	0.66	0.65	0.70
Gd	2.28	2.31	2.70	2.49	2.45	2.38	2.29	2.50
Tb	0.41	0.41	0.48	0.45	0.45	0.44	0.41	0.43
Dy	2.66	2.70	3.15	2.91	2.92	2.85	2.74	2.80
Ho	0.58	0.59	0.68	0.63	0.64	0.62	0.59	0.60
Er	1.71	1.71	1.94	1.82	1.84	1.77	1.70	1.67
Tm	0.26	0.26	0.31	0.29	0.29	0.28	0.26	0.25
Yb	1.66	1.65	1.84	1.70	1.77	1.71	1.60	1.58
Lu	0.25	0.24	0.29	0.26	0.27	0.26	0.24	0.24
Hf	2.92	1.14	1.35	1.38	1.86	1.42	1.17	1.38
Pb	1.70	0.70	2.30		1.10		2.15	2.00
Th	0.37	0.31	0.38	0.30	0.34	0.30	0.30	0.37
U	0.14	0.17		0.07	0.11	0.08	0.11	0.20

Cape Searle						
sample	CS-4	CS-3	CS-14	CS-6	CS-5	CS-1
La	3.08	3.00	3.23	3.55	4.21	3.19
Ce	7.81	7.74	8.16	8.74	10.51	8.25
Pr	1.15	1.13	1.18	1.26	1.51	1.24
Nd	5.72	5.75	5.74	6.25	7.44	6.29
Sm	1.87	1.83	1.86	2.00	2.26	2.02
Eu	0.65	0.66	0.65	0.73	0.77	0.72
Gd	2.35	2.35	2.40	2.49	2.72	2.61
Tb	0.42	0.42	0.43	0.45	0.48	0.47
Dy	2.75	2.77	2.80	2.98	3.13	3.09
Ho	0.62	0.61	0.63	0.65	0.66	0.67
Er	1.71	1.74	1.75	1.86	1.88	1.93
Tm	0.27	0.27	0.27	0.30	0.29	0.30
Yb	1.62	1.65	1.69	1.79	1.76	1.84
Lu	0.25	0.25	0.26	0.27	0.26	0.28
Hf	1.27	1.41	1.72	1.34	1.40	1.35
Pb	0.65	0.80	0.75	0.80	0.90	1.20
Th	0.36	0.31	0.31	0.31	0.41	0.33
U	0.11	0.10	0.08	0.09	0.18	0.16

A 6 (continued) Trace element data (ppm) from ICP-MS analyses

Padloping Island								
sample	PI-16	PI-18	PI-19	PI-20	PI-21	PI-22	PI-23	PI-24
La	1.09	3.85	5.30	5.23	4.90	5.24	1.28	1.36
Ce	3.14	9.63	12.20	12.10	11.30	12.10	3.88	4.06
Pr	0.53	1.46	1.67	1.66	1.58	1.67	0.66	0.70
Nd	3.02	7.49	7.94	7.90	7.41	7.97	3.67	3.79
Sm	1.26	2.38	2.34	2.28	2.20	2.33	1.28	1.33
Eu	0.49	0.85	0.83	0.81	0.79	0.81	0.46	0.48
Gd	1.91	3.05	2.93	2.87	2.75	2.93	1.74	1.75
Tb	0.37	0.54	0.53	0.50	0.49	0.51	0.32	0.31
Dy	2.67	3.48	3.36	3.27	3.13	3.29	2.09	2.09
Ho	0.61	0.76	0.73	0.70	0.68	0.70	0.46	0.46
Er	1.85	2.15	2.08	1.99	1.93	1.99	1.31	1.32
Tm	0.29	0.34	0.32	0.32	0.30	0.32	0.21	0.21
Yb	1.82	2.04	1.93	1.91	1.82	1.91	1.28	1.27
Lu	0.28	0.31	0.30	0.30	0.27	0.29	0.19	0.20
Hf	0.86	1.72	1.85	2.42	1.65	2.16	1.10	1.38
Pb	3.00	2.50	1.40	1.30	1.50	3.50	3.00	0.64
Th	0.22	0.47	0.65	0.69	0.62	0.65	0.08	0.10
U	0.23	0.11	0.15	0.17	0.14	0.16	0.04	0.05

Padloping Island								
sample	PI-25	PI-26	PI-27	PI-28	PI-29	PI-30	PI-31	PI-32
La	1.02	1.45	1.39	2.00	2.00	2.44	1.69	1.36
Ce	3.05	4.28	4.30	5.80	5.69	6.78	4.71	3.90
Pr	0.52	0.71	0.74	0.98	0.98	1.08	0.79	0.69
Nd	2.89	3.83	4.08	5.32	5.46	5.63	4.26	3.75
Sm	0.98	1.26	1.39	1.87	1.93	1.88	1.48	1.36
Eu	0.38	0.49	0.50	0.72	0.71	0.69	0.58	0.49
Gd	1.37	1.71	1.84	2.58	2.60	2.48	2.00	1.87
Tb	0.25	0.31	0.33	0.47	0.47	0.41	0.35	0.32
Dy	1.64	2.07	2.19	3.14	3.20	2.85	2.44	2.24
Ho	0.36	0.45	0.48	0.69	0.70	0.62	0.53	0.50
Er	1.00	1.27	1.39	1.95	1.98	1.77	1.53	1.43
Tm	0.16	0.21	0.21	0.31	0.31	0.28	0.24	0.23
Yb	1.01	1.24	1.30	1.96	1.90	1.73	1.48	1.40
Lu	0.15	0.19	0.20	0.29	0.29	0.26	0.23	0.21
Hf	0.71	0.99	1.13	1.61	1.54	1.40	2.11	1.94
Pb	100.00	16.00	1.80	3.50	0.60	1.60	8.00	0.52
Th	0.10	0.11	0.08	0.16	0.15	0.39	0.25	0.12
U	0.13	0.06	0.03	0.17	0.05	0.55	0.41	0.07

A 6 (continued) Trace element data (ppm) from ICP-MS analyses

Padloping Island								
sample	PI-33	PI-34	PI-35	PI-38	PI-36	PI-37	PI-39	PI-40
La	2.99	1.51	1.79	1.39	1.34	1.61	0.98	1.18
Ce	8.27	4.49	5.02	4.1	4.04	4.05	2.93	3.55
Pr	1.33	0.76	0.84	0.69	0.67	0.62	0.48	0.59
Nd	7.03	4.13	4.37	3.66	3.58	3.23	2.7	3.22
Sm	2.44	1.51	1.48	1.27	1.23	1.06	0.96	1.11
Eu	0.89	0.54	0.53	0.45	0.44	0.43	0.34	0.4
Gd	3.18	2.01	1.93	1.7	1.64	1.42	1.29	1.49
Tb	0.55	0.35	0.33	0.31	0.3	0.26	0.23	0.27
Dy	3.82	2.44	2.29	2.03	2	1.73	1.54	1.81
Ho	0.85	0.53	0.51	0.46	0.44	0.38	0.35	0.4
Er	2.41	1.55	1.43	1.29	1.27	1.07	1	1.17
Tm	0.37	0.24	0.22	0.21	0.2	0.17	0.16	0.18
Yb	2.26	1.49	1.36	1.28	1.23	1.07	0.96	1.13
Lu	0.35	0.23	0.21	0.2	0.19	0.16	0.15	0.18
Hf	1.68	2.16	1.12	2.54	2.84	0.83	35.27	2.97
Pb	4.3	1.4	2.3	0.8	1.7	5	1.7	2.45
Th	0.3	0.14	0.32	0.13	0.19	0.17	0.1	0.17
U	0.25	0.08	0.51	0.08	0.11	0.16	0.06	0.11

Padloping Island				
sample	PI-41	PI-42	PI-43	PI-44
La	1.12	1.16	1.34	1.44
Ce	3.56	3.61	4.11	4.64
Pr	0.62	0.63	0.7	0.76
Nd	3.42	3.43	3.93	4.24
Sm	1.18	1.18	1.38	1.55
Eu	0.44	0.47	0.5	0.55
Gd	1.62	1.61	1.9	2.03
Tb	0.29	0.29	0.34	0.37
Dy	1.91	1.91	2.24	2.46
Ho	0.42	0.42	0.49	0.54
Er	1.2	1.2	1.45	1.56
Tm	0.19	0.19	0.22	0.25
Yb	1.17	1.16	1.37	1.5
Lu	0.18	0.17	0.21	0.22
Hf	0.98	0.99	1.26	1.05
Pb	0.7	1	0.7	0.7
Th	0.07	0.07	0.96	0.09
U	0.02	0.03	0.38	0.03

Durban Island								
sample	DI-13	DI-14	DI-15	DI-16	DI-17	DI-18	DI-19	DI-20
La	3.73	2.01	1.49	1.52	1.45	1.56	1.70	3.36
Ce	9.88	5.72	4.46	4.03	4.41	4.51	4.79	8.52
Pr	1.53	0.97	0.75	0.72	0.76	0.76	0.80	1.30
Nd	7.98	5.32	4.14	3.88	4.15	4.15	4.31	6.75
Sm	2.62	1.78	1.39	1.33	1.40	1.38	1.41	2.25
Eu	0.96	0.64	0.49	0.46	0.50	0.51	0.50	0.83
Gd	3.33	2.36	1.84	1.77	1.90	1.85	1.84	3.00
Tb	0.59	0.42	0.33	0.31	0.34	0.33	0.33	0.54
Dy	3.82	2.76	2.15	2.07	2.27	2.22	2.18	3.61
Ho	0.83	0.61	0.46	0.46	0.49	0.48	0.48	0.77
Er	2.41	1.76	1.34	1.28	1.41	1.38	1.36	2.23
Tm	0.37	0.27	0.21	0.20	0.22	0.21	0.22	0.35
Yb	2.25	1.64	1.27	1.20	1.34	1.29	1.31	2.13
Lu	0.33	0.25	0.19	0.18	0.21	0.20	0.20	0.32
Hf	1.54	1.29	0.88	0.83	1.11	0.89	0.91	2.00
Pb	1.10	0.80	5.00	0.60	0.80	1.30	0.80	1.30
Th	0.28	0.12	0.11	0.11	0.08	0.10	0.13	0.38
U	0.10	0.04	0.08	0.11	0.03	0.06	0.14	0.10

Durban Island								
sample	DI-21	DI-22	DI-23	DI-24	DI-25	DI-26	DI-27	DI-28
La	5.86	4.75	3.48	1.60	1.84	2.19	1.46	1.64
Ce	11.80	10.10	8.16	3.99	5.34	6.15	4.34	4.77
Pr	1.74	1.47	1.11	0.71	0.93	0.98	0.74	0.84
Nd	8.25	7.07	5.36	3.91	5.17	5.16	4.24	4.68
Sm	2.35	2.05	1.55	1.31	1.82	1.72	1.57	1.63
Eu	0.82	0.73	0.58	0.50	0.67	0.64	0.57	0.60
Gd	2.99	2.63	2.00	1.86	2.45	2.30	2.13	2.21
Tb	0.52	0.47	0.35	0.33	0.45	0.42	0.40	0.40
Dy	3.39	3.02	2.25	2.26	3.09	2.87	2.64	2.61
Ho	0.72	0.65	0.50	0.49	0.67	0.62	0.59	0.58
Er	2.09	1.88	1.40	1.42	1.95	1.79	1.70	1.66
Tm	0.32	0.29	0.22	0.22	0.30	0.28	0.27	0.26
Yb	1.95	1.75	1.32	1.35	1.86	1.70	1.65	1.56
Lu	0.30	0.26	0.20	0.21	0.28	0.26	0.25	0.24
Hf	1.56	2.14	1.40	0.85	1.45	1.45	1.31	0.98
Pb	1.80	1.20	3.00	0.80	1.00	0.70	0.80	1.50
Th	0.66	0.57	0.45	0.09	0.14	0.19	0.11	0.11
U	0.30	0.10	0.15	0.07	0.04	0.06	0.04	0.10

Durban Island	
sample	DI-29
La	1.39
Ce	4.63
Pr	0.78
Nd	4.39
Sm	1.61
Eu	0.56
Gd	2.09
Tb	0.39
Dy	2.54
Ho	0.57
Er	1.59
Tm	0.25
Yb	1.53
Lu	0.23
Hf	1.11
Pb	0.80
Th	0.09
U	0.02

A 7.1 Sr- and Nd- isotope ratios from TIMS analyses

Cape Searle sample	$^{87}Sr/^{86}Sr$	2 *se*	$(^{87}Sr/^{86}Sr)_{60}$	εSr	$^{143}Nd/^{144}Nd$	2 *se*	$(^{143}Nd/^{144}Nd)_{60}$	εNd
CS-13	0.703757	15	0.703714	-12.97	0.513027	8	0.512926	7.13
CS-11	0.703749	14	0.703711	-13.01	0.513023	7	0.512922	7.05
CS-8	0.704870	14	0.704780	2.16	0.512847	9	0.512747	3.64
CS-7	0.704999	17	0.704912	4.03	0.512830	11	0.512730	3.31
CS-12	0.703765	18	0.703690	-13.32	0.513006	15	0.512907	6.75
CS-32	0.703090	17	0.703079	-21.99	0.513106	7	0.513022	8.99
CS-31	0.704975	21	0.704929	4.28	0.513110	6	0.513026	9.07
CS-30	0.703480	17	0.703459	-16.59	0.513112	6	0.513030	9.16
CS-29	0.703440	11	0.703404	-17.37	0.513107	11	0.513023	9.02
CS-27	0.703370	17	0.703343	-18.23	0.512977	6	0.512907	6.76
CS-26	0.703672	18	0.703658	-13.77				
CS-24	0.703503	23	0.703473	-16.38	0.513000	6	0.512927	7.14
CS-22	0.703475	17	0.703420	-17.14	0.512998	6	0.512923	7.06
CS-19	0.703459	17	0.703445	-16.78	0.512997	6	0.512924	7.08
CS-18	0.703417	12	0.703410	-17.29	0.512988	6	0.512913	6.87
CS-15	0.703764	14	0.703750	-12.46	0.513036	7	0.512962	7.83
CS-10	0.703744	21	0.703705	-13.10	0.512986	5	0.512912	6.86
CS-4	0.703959	23	0.703867	-10.80	0.512932	7	0.512854	5.73
CS-3	0.703719	18	0.703665	-13.66	0.512960	6	0.512885	6.32
CS-14	0.703448	17	0.703423	-17.10	0.512996	8	0.512919	6.99
CS-6	0.703474	20	0.703445	-16.79	0.513005	7	0.512929	7.19
CS-5	0.703328	20	0.703314	-18.65	0.512993	13	0.512921	7.03
CS-1	0.703265	17	0.703246	-19.61	0.513049	9	0.512973	8.04

A 7.1 (continued) Sr- and Nd- isotope ratios from TIMS analyses

sample	$^{87}Sr/^{86}Sr$	2 *se*	$(^{87}Sr/^{86}Sr)_{60}$	εSr	$^{143}Nd/^{144}Nd$	2 *se*	$(^{143}Nd/^{144}Nd)_{60}$	εNd
Padloping Island								
PI-16	0.705377	18	0.705323	9.86	0.512995	6	0.512896	6.5
PI-18	0.704060	15	0.704049	-8.21	0.512912	8	0.512837	5.4
PI-19	0.703986	23	0.703968	-9.36				
PI-20	0.704051	20	0.704023	-8.58	0.512883	11	0.512815	5.0
PI-21	0.704252	18	0.704236	-5.56	0.512875	11	0.512805	4.8
PI-22	0.703948	17	0.703921	-10.03	0.512916	6	0.512847	5.6
PI-25	0.703151	24	0.703142	-21.08	0.513110	6	0.513030	9.1
PI-26	0.703177	24	0.703181	-20.54	0.513097	6	0.513019	8.9
PI-27	0.703086	21	0.703076	-22.02	0.513107	8	0.513026	9.1
PI-28	0.703167	21	0.703162	-20.80	0.513099	6	0.513016	8.9
PI-31	0.703106	18	0.703099	-21.70	0.513107	7	0.513025	9.0
PI-34	0.703017	21	0.703013	-22.91	0.513134	20	0.513047	9.5
PI-35	0.703331	18	0.703321	-18.54	0.513069	6	0.512989	8.3
PI-37	0.703232	15	0.703225	-19.92	0.513108	10	0.513030	9.2
PI-40	0.703023	15	0.702992	-23.22	0.513103	20	0.513021	9.0
PI-41	0.703417	17	0.703407	-17.32	0.513105	13	0.513023	9.0
PI-44	0.703107	15	0.703096	-21.74	0.513100	6	0.513013	8.8
Durban Island								
DI-13	0.703317	13	0.70330059	-18.84	0.513065	7	0.51298712	8.32
DI-14	0.703339	15	0.703339	-18.29	0.513122	13	0.513042632	9.40
DI-16	0.703386	21	0.70336715	-17.89	0.513106	40	0.513024688	9.05
DI-19	0.703795	14	0.70377926	-12.04	0.51308	12	0.513002398	8.62
DI-20	0.703820	21	0.70381424	-11.55	0.512953	6	0.512873933	6.11
DI-21	0.704236	18	0.70423396	-5.59	0.512875	7	0.512807435	4.81
DI-22	0.704129	12	0.70412109	-7.19	0.51287	5	0.512801223	4.69
DI-23	0.703988	20	0.70396424	-9.42	0.512914	19	0.512845407	5.55
DI-24	0.703579	20	0.70357213	-14.98	0.513091	6	0.513011526	8.79
DI-26	0.703388	17	0.70337825	-17.73	0.513044	7	0.512964931	7.88
DI-27	0.703382	21	0.70337173	-17.83	0.513064	8	0.512976166	8.10
DI-29	0.703289	24	0.70328249	-19.09	0.513108	7	0.513021005	8.98

Table A7.2 Pb-isotope ratios from MC-ICP-MS analysis

sample	$^{206}Pb/^{204}Pb$	1 SE (%)	$^{207}Pb/^{204}Pb$	1 SE (%)	$^{208}Pb/^{204}Pb$	1 SE (%)
Cape Searle						
CS-8	16.99	0.01	15.06	0.01	37.29	0.01
CS-7	16.62	0.02	14.63	0.02	36.11	0.02
CS-12	17.33	0.03	15.13	0.03	37.23	0.03
CS-32	17.69	0.02	15.33	0.02	37.21	0.02
CS-29	17.60	0.01	15.31	0.01	37.18	0.01
CS-27	17.76	0.01	15.24	0.02	37.40	0.02
CS-22	17.61	0.02	15.14	0.02	37.01	0.02
CS-10	17.90	0.02	15.28	0.02	37.59	0.02
CS-14	17.99	0.01	15.30	0.01	37.60	0.01
CS-6	18.03	0.01	15.35	0.01	37.71	0.01
Padloping Island						
PI-16	16.94	0.01	15.50	0.01	36.80	0.01
PI-18	17.03	0.01	15.41	0.01	36.93	0.01
PI-19	17.61	0.01	15.44	0.01	37.54	0.01
PI-20	17.79	0.01	15.41	0.01	37.77	0.01
PI-21	17.47	0.01	15.44	0.01	37.41	0.01
PI-22	16.98	0.01	15.44	0.01	36.77	0.01
PI-23	16.88	0.01	15.50	0.01	36.67	0.01
PI-27	16.86	0.02	15.14	0.02	36.22	0.02
PI-40	16.95	0.01	15.36	0.01	36.58	0.01
PI-41	18.04	0.02	15.36	0.02	37.73	0.02
Durban Island						
DI-13	17.63	0.01	15.33	0.01	37.29	0.01
DI-19	17.42	0.03	15.13	0.03	36.85	0.03
DI-20	17.58	0.02	15.33	0.02	37.73	0.02
DI-21	17.83	0.02	15.27	0.02	37.71	0.02
DI-22	17.78	0.01	15.24	0.01	37.65	0.01
DI-24	17.51	0.02	15.22	0.02	36.98	0.03
DI-29	17.58	0.01	15.13	0.01	36.95	0.01

Table A7.3 Hf-isotope ratios from PIMMS analyses

sample	$^{176}Hf/^{177}Hf$	1 SE (%)	$(^{176}Hf/^{177}Hf)_{60}$	εHf	ΔεHf
Cape Searle					
CS-7	0.283090	0.0008	0.283051	11.22	3.63
CS-12	0.283223	0.0009	0.283171	15.46	3.29
CS-32	0.283268	0.0007	0.283234	17.69	2.54
CS-10	0.283193	0.0008	0.283164	15.23	2.92
CS-5	0.283190	0.0009	0.283159	15.06	2.52
Padloping Island					
PI-16	0.283215	0.0008	0.283162	15.15	3.26
PI-22	0.283107	0.0011	0.283085	12.44	1.83
PI-27	0.283258	0.0008	0.283229	17.52	2.25
PI-35	0.283262	0.0009	0.283231	17.60	3.31
PI-41	0.283267	0.0010	0.283237	17.79	2.60
Durban Island					
DI-13	0.283236	0.0012	0.283201	16.53	2.28
DI-16	0.283273	0.0011	0.283237	17.81	2.58
DI-22	0.283073	0.0007	0.283053	11.29	1.86
DI-24	0.283271	0.0007	0.283231	17.58	2.69
DI-29	0.283254	0.0006	0.283220	17.21	2.08

Table A7.4 He-isotope ratios

Sample	*in vacuo* crushing of olivines				olivine powders (produced by *in vacuo* crushing) melted			
	$^3He/^4He$ (R_a)	±	^4He ($10^{-9}cm^3STP\ g^{-1}$)	±	$^3He/^4He$ (R_a)	±	^4He ($10^{-9}cm^3STP\ g^{-1}$)	±
Cape Searle								
CS-7	43.9	0.6	130.6	0.6	7.4	0.5	33.6	0.2
CS-19	23.0	1.3	10.0	0.3				
CS-6	37.9	1.2	20.9	0.2	4.7	0.7	6.9	0.6
CS-5	26.3	2	4.4	0.2	0.2	0.0	169.6	0.9
Padloping Island								
PI-23	43.9	0.6	39.8	0.2	2.1	0.1	23.4	0.1
PI-25	49.5	1.6	11.0	0.1	0.1	0.0	164.7	0.8
PI-26	43.9	0.5	24.1	0.1	17.3	0.8	6.6	0.1
PI-27	43.1	0.5	45.6	0.2	9.9	1.2	11.8	0.1
Durban Island								
DI-23	14.5	0.5	22.4	0.3	2.1	0.1	64.3	0.3
DI-24	37.5	0.6	5.1	0.0	10.5	0.8	6.2	0.3
DI-27	38.6	1.5	17.4	0.4	6.9	0.8	7.0	0.1

A8 Calculated liquid compositions

	DI-15 (ol1 c2)			DI-17 (ol3 c1)		
	Rock[1]	Olivine	Calculated parental liquid composition	Rock[1]	Olivine	Calculated parental liquid composition
% add/sub			29.23(sub)			39.13(sub)
SiO_2	46.09	40.21	48.11	46.32	39.75	49.48
Al_2O_3	9.05	0.05	12.12	9.78	0.05	14.46
FeO	10.04	9.50	10.23	9.97	11.13	9.42
MgO	24.54	49.51	16.01	23.85	48.05	12.22
CaO	7.94	0.30	10.55	7.99	0.32	11.67
Na_2O	1.08		1.45	0.86	0.02	1.26
K_2O	0.03		0.04	0.02	0.00	0.04
TiO_2	0.65		0.87	0.69	0.02	1.01
MnO	0.18	0.16	0.19	0.18	0.16	0.19
NiO	0.14	0.44	0.04	0.14	0.26	0.08
CrO	0.26	0.12	0.31	0.20	0.04	0.27
Total	100.00	100.28	99.90	100.00	99.80	100.09

	DI-20 (ol2 c3)			DI-21 (ol4 c2)		
	Rock[1]	Olivine	Calculated parental liquid composition	Rock[1]	Olivine	Calculated parental liquid composition
% add/sub			1.26(sub)			11.9(sub)
SiO_2	49.47	39.09	49.60	47.50	39.59	48.51
Al_2O_3	16.26	0.08	16.46	14.12	0.06	15.91
FeO	9.29	14.57	9.22	9.73	12.00	9.44
MgO	9.03	45.09	8.57	15.27	47.36	11.20
CaO	12.91	0.33	13.07	10.58	0.31	11.88
Na_2O	1.68	0.02	1.70	1.41		1.58
K_2O	0.06	0.00	0.06	0.05		0.06
TiO_2	1.06	0.02	1.07	0.98		1.10
MnO	0.18	0.20	0.18	0.17	0.19	0.17
NiO	0.02	0.18	0.02	0.06	0.32	0.03
CrO	0.06	0.07	0.06	0.13	0.07	0.14
Total	100.00	99.66	100.00	100.00	99.90	100.01

[1]: Rock recalculated to 100% on a volatile-free basis

A8 (continued)

	DI-23 (ol1 c7)			DI-24 (ol7 c1)		
	Rock[1]	Olivine	Calculated parental liquid composition	Rock[1]	Olivine	Calculated parental liquid composition
% add/sub			45.85(sub)			32.27(sub)
SiO_2	45.93	39.51	49.68	45.92	39.90	48.22
Al_2O_3	9.74	0.06	15.41	9.80	0.08	13.52
FeO	10.12	11.98	9.03	9.80	9.52	9.90
MgO	24.28	47.42	10.74	24.59	48.88	15.28
CaO	7.51	0.32	11.72	7.80	0.29	10.68
Na_2O	1.05		1.66	0.86		1.18
K_2O	0.07		0.11	0.03		0.04
TiO_2	0.71		1.12	0.63		0.88
MnO	0.18	0.18	0.19	0.18	0.17	0.18
NiO	0.13	0.38	0.00	0.15	0.45	0.03
CrO	0.28	0.07	0.40	0.26	0.13	0.31
Total	100.00	99.92	100.05	100.00	99.42	100.22

	DI-25 (ol5 c3)			DI-27 (ol5 c4)		
	Rock[1]	Olivine	Calculated parental liquid composition	Rock[1]	Olivine	Calculated parental liquid composition
% add/sub			10.18(sub)			3.8(sub)
SiO_2	48.21	39.31	49.17	47.80	40.48	48.08
Al_2O_3	14.48	0.05	16.04	11.83	0.08	12.29
FeO	9.98	14.50	9.49	9.25	8.10	9.29
MgO	12.52	45.57	8.96	18.73	50.77	17.48
CaO	12.20	0.30	13.48	9.91	0.31	10.29
Na_2O	1.36		1.50	1.28		1.33
K_2O	0.02		0.02	0.04		0.04
TiO_2	0.93		1.03	0.71		0.74
MnO	0.18	0.23	0.18	0.17	0.12	0.17
NiO	0.03	0.27	0.01	0.09	0.46	0.08
CrO	0.08	0.05	0.09	0.19	0.10	0.19
Total	100.00	100.27	99.97	100.00	100.41	99.98

[1]: Rock recalculated to 100% on a volatile-free basis

A8 (continued)

	DI-29 (ol9 c5)			CS-7 (ol3 c1)		
	Rock[1]	Olivine	Calculated parental liquid composition	Rock[1]	Olivine	Calculated parental liquid composition
% add/sub			35.36(sub)			7.47(sub)
SiO_2	46.33	39.45	49.27	47.69	40.37	48.26
Al_2O_3	10.97	0.05	15.63	11.55	0.09	12.45
FeO	9.90	11.95	9.03	8.81	7.50	8.91
MgO	21.58	47.09	10.69	20.28	50.24	17.94
CaO	8.93	0.34	12.60	9.72	0.31	10.46
Na_2O	0.97		1.38	0.93		1.00
K_2O	0.02		0.03	0.05		0.05
TiO_2	0.78		1.11	0.47		0.51
MnO	0.18	0.17	0.18	0.17	0.12	0.17
NiO	0.12	0.34	0.02	0.11	0.42	0.08
CrO	0.22	0.07	0.28	0.23	0.17	0.23
Total	100.00	99.47	100.22	100.00	99.20	100.06

	CS-29 (ol3 c4)			CS-18 (ol4 c2)		
	Rock[1]	Olivine	Calculated parental liquid composition	Rock[1]	Olivine	Calculated parental liquid composition
% add/sub			35.75(sub)			15.75(sub)
SiO_2	46.15	40.02	48.81	47.76	39.54	49.17
Al_2O_3	9.95	0.07	14.22	14.24	0.06	16.67
FeO	9.88	10.28	9.71	9.49	13.16	8.86
MgO	24.12	48.24	13.69	14.71	46.10	9.33
CaO	7.59	0.31	10.73	11.11	0.34	12.95
Na_2O	0.98		1.40	1.41		1.65
K_2O	0.04		0.06	0.04		0.04
TiO_2	0.74		1.06	0.90		1.05
MnO	0.18	0.17	0.19	0.18	0.18	0.18
NiO	0.14	0.41	0.02	0.05	0.28	0.01
CrO	0.23	0.11	0.28	0.12	0.05	0.13
Total	100.00	99.59	100.18	100.00	99.72	100.05

[1]: Rock recalculated to 100% on a volatile-free basis

A8 (continued)

	PI-16 (ol1 c2)			PI-41 (ol2 c3)		
	Rock[1]	Olivine	Calculated parental liquid composition	Rock[1]	Olivine	Calculated parental liquid composition
% add/sub			18.89(add)			57.56(sub)
SiO_2	49.17	40.62	47.70	45.22	39.94	49.36
Al_2O_3	13.94	0.12	11.57	8.66	0.07	15.39
FeO	9.28	6.91	8.87	9.68	10.73	8.85
MgO	13.14	51.24	19.67	27.89	48.24	11.95
CaO	12.10	0.29	10.07	6.78	0.32	11.83
Na_2O	1.38		1.14	0.54		0.97
K_2O	0.05		0.04	0.07		0.12
TiO_2	0.63		0.52	0.57		1.02
MnO	0.17	0.12	0.16	0.17	0.17	0.17
NiO	0.05	0.48	0.12	0.17	0.39	0.00
CrO	0.10	0.18	0.12	0.25	0.09	0.38
Total	100.00	99.94	99.99	100.00	99.96	100.03

[1]: Rock recalculated to 100% on a volatile-free basis

11. Hänggi, P. & Bartussek, R. *Lecture Notes in Physics* Vol. 476 (eds Parisi, J., Müller, S. C. & Zimmermann, W.) 294–308 (Springer, Berlin, 1996).
12. Astumian, R. D. Thermodynamics and kinetics of a brownian motor. *Science* **276**, 917–922 (1997).
13. Astumian, R. D. & Hänggi, P. Brownian motors. *Phys. Today* **55**(11), 33–39 (2002).
14. Linke, H. (ed.) Ratchets and Brownian motors: basics, experiments and applications. *Appl. Phys. A* (Special Issue) **75**(2), (2002).
15. Cabodi, M., Chen, Y.-F., Turner, S. W. P., Craighead, H. G. & Austin, R. H. Continuous separation of biomolecules by the laterally asymmetric diffusion array with out-of-plane sample injection. *Electrophoresis* **23**, 3496–3503 (2002).
16. Müller, F. *et al.* Membranes for micropumps from macroporous silicon. *Phys. Stat. Sol. A* **182**, 585–590 (2000).
17. Kettner, C., Reimann, P., Hänggi, P. & Müller, F. Drift ratchet. *Phys. Rev. E* **61**, 312–323 (2000).
18. Kettner, C., Hänggi, P. & Müller, F. Verfahren und Vorrichtung zur größenabhängigen Sortierung mikroskopisch kleiner Teilchen auf der Basis von rauschinduziertem Transport. German patent pending (DE 199 07 564 A 1), submitted 22 Feb. 1999.
19. Lehmann, V. & Föll, H. Formation mechanism and properties of electrochemically etched trenches in n-type silicon. *J. Electrochem. Soc.* **137**, 653–659 (1990).
20. Lehmann, V. The physics of macropore formation in low doped n-type silicon. *J. Electrochem. Soc.* **140**, 2836–2843 (1993).
21. Schilling, J. *et al.* 3D photonic crystals made out of macroporous silicon by modulation of pore diameter. *Appl. Phys. Lett.* **78**, 1180–1182 (2001).
22. Lehmann, V. & Grüning, U. The limits of macropore array fabrication. *Thin Solid Films* **297**, 13–17 (1997).
23. Tong, Q. Y. & Gösele, U. *Semiconductor Wafer Bonding* 53–54 (Wiley and Sons, New York, 1999).

Supplementary Information accompanies the paper on **www.nature.com/nature**.

Acknowledgement We thank U. Gösele for backing the ratchet project over many years. We also gratefully acknowledge discussions on the theory of the ratchet-effect with P. Hänggi, Ch. Kettner, P. Reimann and R. Eichhorn as well as critical reading of the manuscript by K. Scheerschmidt and R. B. Wehrspohn.

Competing interests statement The authors declare that they have no competing financial interests.

Correspondence and requests for materials should be addressed to F.M. (Frank.Mueller@mpi-halle.de).

High $^3He/^4He$ ratios in picritic basalts from Baffin Island and the role of a mixed reservoir in mantle plumes

Finlay M. Stuart*, Solveigh Lass-Evans*†, J. Godfrey Fitton† & Robert M. Ellam*

** Isotope Geosciences Unit, Scottish Universities Environmental Research Centre, East Kilbride G75 0QF, UK*
† School of GeoSciences, University of Edinburgh, Edinburgh EH9 3JW, UK

The high $^3He/^4He$ ratio of volcanic rocks thought to be derived from mantle plumes is taken as evidence for the existence of a mantle reservoir that has remained largely undegassed since the Earth's accretion[1–3]. The helium isotope composition of this reservoir places constraints on the origin of volatiles within the Earth and on the evolution and structure of the Earth's mantle. Here we show that olivine phenocrysts in picritic basalts presumably derived from the proto-Iceland plume at Baffin Island, Canada, have the highest magmatic $^3He/^4He$ ratios yet recorded. A strong correlation between $^3He/^4He$ and $^{87}Sr/^{86}Sr$, $^{143}Nd/^{144}Nd$ and trace element ratios demonstrate that the ^3He-rich end-member is present in basalts that are derived from large-volume melts of depleted upper-mantle rocks. This reservoir is consistent with the recharging of depleted upper-mantle rocks by small volumes of primordial volatile-rich lower-mantle material at a thermal boundary layer between convectively isolated reservoirs. The highest $^3He/^4He$ basalts from Hawaii and Iceland plot on the observed mixing trend. This indicates that a ^3He-recharged depleted mantle (HRDM) reservoir may be the principal source of high $^3He/^4He$ in mantle plumes, and may explain why the helium concentration of the 'plume' component in ocean island basalts is lower than that predicted for a two-layer, steady-state model of mantle structure.

Ocean island basalts (OIB) derived from mantle plumes commonly have $^3He/^4He$ ratios that are higher than mid-ocean ridge basalts (MORB) that originate in the upper, asthenospheric mantle[1–3]. High $^3He/^4He$ and solar-like Ne isotope ratios[4] reflect a higher proportion of primordial volatiles in the source region and, in the current paradigm, indicate that plumes tap a deep mantle reservoir that is significantly less degassed than the asthenospheric mantle. Although a number of locations have been proposed for this reservoir[5], a lower mantle that has been convectively isolated below the 670-km seismic discontinuity for the lifetime of the Earth[6] is consistent with the mass balance of the depleted mantle and continental crust[7]. However, layered mantle models are seemingly at odds with seismic studies that demonstrate convective flow across the 670-km boundary[8] and require a 100- to 200-fold depletion of the He concentration in the upper, degassed mantle relative to the deep undegassed mantle reservoir[6]. Plume-derived OIB from, for example, Loihi seamount, Hawaii, have lower He concentrations than basalts from the degassed upper mantle[2] and have posed a persistent problem for a unified geochemical model of Earth structure[6]. The apparent paradox can be explained, at least in part, by more extensive degassing of ocean island basalts[9]. However, basalts from Iceland and the Hawaiian islands have linear, rather than strongly hyperbolic, He–Pb isotope mixing arrays that are consistent with relatively small He concentration contrasts between the degassed mantle and less degassed (high $^3He/^4He$) mantle reservoirs[9,10].

Picritic basalts erupted on Baffin Island, northeast Canada, 61 Myr ago correlate with the Anaanaa Member of the Vaigat Formation in West Greenland[11], and are among the earliest manifestations of the ancestral Iceland mantle plume[12]. Trace-element and Sr–Nd isotope ratios show that they were generated by mixing of two discrete sources; relatively depleted mantle with $(La/Sm)_n < 1$, $^{87}Sr/^{86}Sr \approx 0.7030$, $^{143}Nd/^{144}Nd \approx 0.5130$, and relatively enriched mantle with $(La/Sm)_n > 1$, $^{87}Sr/^{86}Sr \approx 0.7042$ and $^{143}Nd/^{144}Nd \approx 0.51282$ (ref. 13). The depleted basalts are similar to the most depleted Icelandic basalts and North Atlantic MORB[14]. The enriched basalts are similar to, though slightly more extreme (higher $^{87}Sr/^{86}Sr$ and lower $^{143}Nd/^{144}Nd$ ratios) than the most enriched basalts erupted by the Iceland plume and across the North Atlantic igneous province[15].

The isotopic composition of He released by *in vacuo* crushing olivine phenocrysts from picritic basalts from three stratigraphically distinct cliff sections in northeast Baffin Island (Table 1) ranges from $14.4R_a$ to $49.5R_a$ (where R_a is the atmospheric $^3He/^4He$ ratio; 1.39×10^{-6}). These ratios are far higher than MORB values and extend the range measured in contemporaneous picrites from West Greenland[16]. The high ratios cannot result from contamination by *in situ* cosmogenic ^3He because (1) *in vacuo* crushing does not release cosmogenic He from the olivine lattice[17], (2) cosmogenic ^3He production was negligible because the samples were collected from eroding, near-vertical sea cliff faces, and (3) the $^3He/^4He$ of powders produced by crushing are systematically lower than crush values (Table 1) indicating that radiogenic He dominates the olivine lattice. Nucleogenic ^3He production from ^6Li is negligible in Palaeocene basalts[16].

Crush release of radiogenic ^4He in the olivine lattice and melt inclusions by post-eruptive U and Th decay tends to lower $^3He/^4He$, so measured ratios may underestimate the source $^3He/^4He$. Any such effect would be most pronounced in samples with the lowest He content. $^3He/^4He$ are not correlated with He concentration (Table 1), implying that post-eruptive radiogenic He is insignificant to the crush-release He. Crustal contamination of the basalts by amphibolite- and granulites-facies basement rocks would also lower

Table 1 **He, Sr and Nd isotope ratios, and trace-element data for Baffin Island basalts**

Sample	$^4He^*$ (10^{-9} cm^3 STP g^{-1})	$^3He/^4He^*$ (R/R_a)	^4He† (10^{-9} cm^3 STP g^{-1})	$^3He/^4He$† (R/R_a)	$^{143}Nd/^{144}Nd$‡	$^{87}Sr/^{86}Sr$‡	$(La/Sm)_n$	ΔNb
Cape Searle								
CS/19	10.0 ± 0.3	23.0 ± 1.3			0.512924 ± 6	0.703420 ± 17	1.82	0.26
CS/7	130.6 ± 0.6	43.9 ± 0.6	33.6 ± 0.17	7.4 ± 0.5	0.512730 ± 11	0.704912 ± 17	0.92	−0.11
CS/6	20.9 ± 0.2	37.9 ± 1.2	6.9 ± 0.58	4.7 ± 0.7	0.512929 ± 7	0.703445 ± 20	1.78	0.20
CS/5	4.4 ± 0.2	26.3 ± 2.0	169.6 ± 0.86	0.16 ± 0.04	0.512921 ± 13	0.703314 ± 20	1.86	0.19
Padloping Island								
PI/23	39.8 ± 0.2	43.9 ± 0.6	23.4 ± 0.12	2.1 ± 0.1	0.513051 ± 8	0.703248 ± 20	1.00	−0.17
PI/25	11.0 ± 0.1	49.5 ± 1.6	164.7 ± 0.82	0.12 ± 0.02	0.513030 ± 6	0.703142 ± 24	1.04	−0.05
PI/26	24.1 ± 0.1	43.9 ± 0.5	6.6 ± 0.05	17.3 ± 0.8	0.513019 ± 6	0.703181 ± 24	1.15	−0.23
PI/27	45.6 ± 0.2	43.1 ± 0.5	11.8 ± 0.07	9.9 ± 1.2	0.513026 ± 8	0.703076 ± 21	1.00	−0.12
Durban Island								
DI/23	22.4 ± 0.3	14.5 ± 0.5	64.3 ± 0.33	2.1 ± 0.13	0.512845 ± 9	0.703964 ± 20	2.25	0.26
DI/24	5.1 ± 0.04	37.5 ± 0.6	6.2 ± 0.33	10.5 ± 0.8	0.513012 ± 6	0.703572 ± 20	1.22	−0.25
DI/27	17.4 ± 0.4	38.6 ± 1.5	7.0 ± 0.08	6.9 ± 0.8	0.512976 ± 8	0.703372 ± 21	0.93	−0.23

*Helium was extracted by *in vacuo* crushing 1–2 g of olivine and analysed at SUERC using procedures reported previously[19]. $^3He/^4He$ ratios (R) are normalized to the atmospheric ratio (1.39×10^{-6}; R_a) and corrected for blanks. ^4He blanks averaged 4×10^{-11} cm^3 STP and ^3He blanks (5×10^{-15} cm^3 STP) were always less than 5% of the measured ^3He. Correction for atmospheric He on the basis of Ne abundances is insignificant.

†Olivine powders (~100 mg) produced by *in vacuo* crushing were melted at 1,850 °C in a double-walled resistance furnace. Hot furnace ^4He blanks averaged 2×10^{-11} cm^3 STP g^{-1}. ^3He blanks were the same as crush extractions.

‡Whole-rock Sr and Nd isotopic ratios[28] have been corrected to 60 Myr ago on the basis of measured Rb/Sr and Sm/Nd. This reduces $^{87}Sr/^{86}Sr$ by less than 0.007% and $^{143}Nd/^{144}Nd$ by less than 0.002%. Uncertainties (2σ) are in the last decimal place. Rare-earth element concentrations were measured by ICP-MS[29]. $(La/Sm)_n$ is chondrite normalized, and has an uncertainty of ± 3% (2σ). Nb, Y and Zr concentrations were measured in triplicate by X-ray fluorescence and the averages used[24]. $\Delta Nb = 1.74 + \log(Nb/Y) - 1.92 \times \log(Zr/Y)$[30]. Uncertainty in ΔNb never exceeds ± 10%.

$^3He/^4He$. Pb isotopes are sensitive to crustal contamination in North Atlantic margin Palaeocene basalts, because the Precambrian basement has distinctively unradiogenic Pb (ref. 18). The Baffin Island picrites show no correlation between Pb isotope composition and other isotopic tracers (Sr, Nd, He). Thus, while the Pb isotopes may indicate some crustal interaction, its effect on other elements appears negligible. We have previously demonstrated that basalts whose whole-rock Pb isotope compositions are clearly affected by crustal contamination retain uncontaminated He (ref. 19), either because the olivine crystallized before crustal assimilation, or because the deep crust is He-poor. In this study, we observe a similar effect: dyke sample CS/7 has high $^3He/^4He$ ($43.3 \pm 0.6R_a$) but has high $^{87}Sr/^{86}Sr$ and low $^{143}Nd/^{144}Nd$ that are best attributed to crustal contamination. As crustal contamination is expected to lower $^3He/^4He$, we conclude that crush-release He is insensitive to any contamination. The inability of magmatic or post-magmatic processes to alter He isotope ratios, and the strong correlation with Sr and Nd isotopes and trace elements (see below), means that the sample (PI/25) with the highest helium isotope ratio provides the best estimate yet ($49.5 \pm 1.5R_a$) of the minimum He isotope composition of the less degassed mantle reservoir.

The olivine $^3He/^4He$ ratio correlates strongly with whole-rock $^{143}Nd/^{144}Nd$, $^{87}Sr/^{86}Sr$ and trace-element ratios such as La/Sm (see Fig. 1). The absence of co-variation of $^{87}Sr/^{86}Sr$ and $^{143}Nd/^{143}Nd$ with indices of contamination such as Ba/Nb and Pb isotope ratios suggests that crustal contamination has not significantly affected Sr and Nd isotopes (with the exception of the dyke sample CS/7). Furthermore, high-$^3He/^4He$ Palaeogene basalts from Iceland[3] that cannot have been contaminated by continental crust have He–Nd and He–Sr isotopic compositions that plot on the trend. Consequently, the He isotope correlations with La/Sm and the lithophile isotope ratios record binary mixing between large-volume melts of a ^3He-rich, relatively depleted mantle reservoir, and small-volume melts from a mantle reservoir with low $^3He/^4He$, rich in incompatible elements.

The depleted mantle end-member inferred from the most extreme Sr and Nd isotope compositions requires a mantle source region with $^{87}Sr/^{86}Sr \approx 0.70305$, $^{143}Nd/^{144}Nd \approx 0.51305$ and $^3He/^4He > 50R_a$. The Sr and Nd isotope ratios are indistinguishable from the most depleted basalts erupted on Iceland and only slightly less depleted than North Atlantic MORB erupted away from the Iceland plume ($^{87}Sr/^{86}Sr < 0.7030$, $^{143}Nd/^{144}Nd > 0.5131$). Icelandic and North Atlantic MORBS define parallel, non-overlapping arrays on a plot of log(Nb/Y) against log(Zr/Y). The excess or deficiency in Nb is defined by the ΔNb notation such that Icelandic basalts have $\Delta Nb > 0$ and MORB have $\Delta Nb < 0$ (ref. 24). The high $^3He/^4He$ Baffin Island basalts have strongly negative ΔNb (Table 1) indicating derivation from the North Atlantic MORB-source mantle rather than the depleted Iceland plume.

It is, first, important to note that this He-, Sr- and Nd-isotopic composition cannot represent MORB source mantle at 61 Myr ago as the $^3He/(U+Th)$ of the MORB reservoir is incapable of significantly changing $^3He/^4He$ in hundreds of millions of years. If He is less incompatible than U during melting, high-$^3He/^4He$ would correspond with the most depleted basalts[20]. Low-$^{87}Sr/^{86}Sr$, high-$^{143}Nd/^{144}Nd$ and high-$^3He/^4He$ basalts are indicative of a

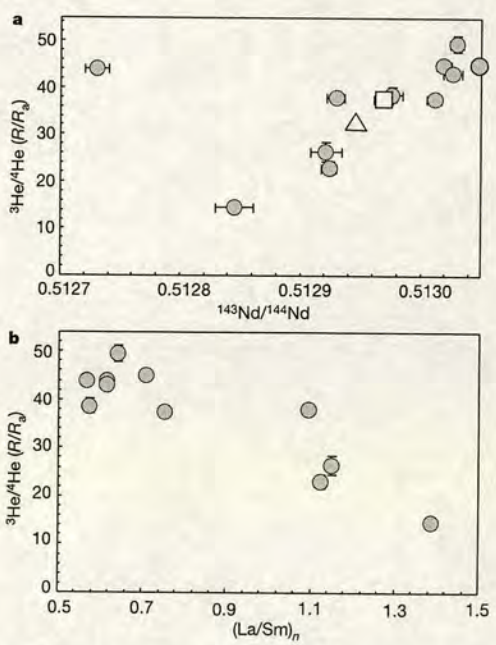

Figure 1 Plots of olivine $^3He/^4He$ versus $^{143}Nd/^{144}Nd$ and $(La/Sm)_n$ for early Palaeocene basalts from Baffin Island. **a**, Whole-rock Nd isotopic composition; also shown are the data for a Palaeogene ankaramite from NW Iceland (square) and basaltic glass from Loihi seamount (triangle). **b**, Whole-rock $(La/Sm)_n$.

depleted, 'regassed' component which would be generated in a reservoir with low U/He which grows ^{4}He less quickly than MORB source mantle. The mechanism proposed to generate the low-U/He source[20] requires (shallow) melt-gas separation to fractionate He from U and the other lithophile trace elements. It is difficult to reconcile the linear He–Sr and He–Nd isotope arrays (Fig. 1) with such a component since a high-He/Sr and -He/Nd ratio component mixed with 'normal' He/Sr and He/Nd mantle would result in strongly hyperbolic mixing arrays. Instead, we make the assumption that the dominant control on isotopic heterogeneity in the mantle is the same for all elements—that is, solid-melt distribution coefficients—and that He is highly incompatible during mantle melting[21]. Therefore any reservoir with low Rb/Sr and high Sm/Nd, because it is residual to partial melting, will have lost most of its He and would evolve low-^{3}He/^{4}He, low-^{87}Sr/^{86}Sr and high-^{143}Nd/^{144}Nd ratios. The subduction of interplanetary dust particles is incapable of delivering enough solar noble gases to the upper mantle to change its He and Ne isotopic composition significantly[22]. In the absence of alternatives we show below that the high-^{3}He/^{4}He component is most probably the product of mantle mixing.

If Earth accreted with ^{3}He/^{4}He = $120R_a$, bulk silicate Earth U (21 p.p.b.) and U/Th = 3.8, an undegassed mantle reservoir with ^{3}He/^{4}He = $50R_a$ has a ^{3}He concentration of 8×10^{10} atoms g^{-1}. If moderately incompatible lithophile element concentrations in the depleted mantle reservoir are less than a factor of two lower than undepleted mantle[23], mixing a small proportion of ^{3}He-rich mantle with depleted upper mantle ($1.2–4.6 \times 10^9$ ^{3}He atoms g^{-1}; ref. 6) severely changes ^{3}He/^{4}He without significantly altering trace element concentrations and Sr and Nd isotope ratios. Consequently the isotopic composition of the high ^{3}He/^{4}He end-member can be generated by mixing depleted mantle and primordial ^{3}He-rich mantle reservoir. The Baffin Island data define approximately linear mixing arrays in He–Sr and He–Nd isotope space, implying that the He/Nd and He/Sr ratios and, therefore, He concentrations, of both reservoirs are similar. The absence of strongly hyperbolic mixing trends supports the contention that the high ^{3}He/^{4}He end-member is not simply undegassed mantle.

The enriched mantle end-member, estimated by extrapolating the He–Nd and He–Sr isotope trends to the most extreme values measured in uncontaminated Baffin Island basalts (^{143}Nd/^{144}Nd = 0.51282; ^{87}Sr/^{86}Sr = 0.7042), has a ^{3}He/^{4}He similar to, or lower than, the MORB ratio ($8 \pm 1R_a$). The positive Nb value of this end-member, and the coincidence of the high ^{3}He/^{4}He ankaramite from northwest Iceland[3] with the mixing trend, supports an origin for this enrichment in the mantle asthenosphere. Although the ultimate origin is unclear, the low ^{3}He/^{4}He ratio requires that it has been isolated from the high-^{3}He/^{4}He reservoir prior to melting. It may represent fusible heterogeneities in the upper mantle or the plume that are large enough to prevent isotopic homogenization yet small enough to be preferentially sampled by melting.

The convergence of Sr–Nd–Pb isotope trends in ocean island basalt (OIB) and MORB have been used to identify a common deep mantle reservoir that is the carrier of the high-^{3}He/^{4}He plume component. The most primordial ^{3}He-rich basalts from Iceland and Hawaii lie on the He–Nd and He–Sr isotope mixing trends identified here suggesting that the extreme end of the Baffin Island picrite trend is the best estimate of a common, high-^{3}He/^{4}He mantle component. This is at the depleted end of the ranges proposed previously for a common mantle reservoir[24,25], but the negative ΔNb requires that it originates in the depleted upper mantle, rather than the lower mantle. The thermal boundary layer between upper- and lower-mantle regions is one potential reservoir for such material[26,27], although it cannot be ruled out that the mixing occurs as the plume head disperses in the upper mantle. The dominance of the ^{3}He-recharged, depleted component in mantle plumes is consistent with a low mass flux from the lower mantle and explains why basalts from Iceland and Hawaii appear to have lower He concentrations than predicted for undegassed mantle[9,10]. □

Received 12 December 2002; accepted 29 April 2003; doi:10.1038/nature01711.

1. Kurz, M. D., Jenkins, W. J. & Hart, S. R. Helium isotope systematics of ocean islands and mantle heterogeneity. *Nature* **297,** 43–46 (1982).
2. Honda, M., McDougall, I., Patterson, D. B., Doulgeris, A. & Clague, D. A. Noble gases in submarine pillow basalt glasses from Loihi and Kilauea, Hawaii—a solar component in the Earth. *Geochim. Cosmochim. Acta* **57,** 859–874 (1993).
3. Hilton, D. R., Gronvold, K., Macpherson, C. & Castillo, P. Extreme ^{3}He/^{4}He ratios in northwest Iceland: constraining the common component in mantle plumes. *Earth Planet. Sci. Lett.* **173,** 53–60 (1999).
4. Dixon, E. T., Honda, M., McDougall, I., Campbell, I. H. & Sigurdsson, I. Preservation of near-solar neon isotopic ratios in Icelandic basalts. *Earth Planet. Sci. Lett.* **180,** 309–324 (2000).
5. Porcelli, D. & Ballentine, C. J. Origin of noble gases in terrestrial planets. *Rev. Mineral. Geochem.* **47,** 411–480 (2002).
6. Porcelli, D. & Wasserburg, G. J. Mass transfer of helium, neon, argon, and xenon through a steady-state upper mantle. *Geochim. Cosmochim. Acta.* **59,** 4921–4937 (1995).
7. DePaolo, D. J. & Wasserburg, J. G. Inferences about magma sources and mantle structure from variations in ^{143}Nd/^{144}Nd. *Geophys. Res. Lett.* **3,** 743–746 (1976).
8. van der Hilst, R. D., Widiyantro, S. & Engdahl, E. R. Evidence for deep mantle circulation from global tomography. *Nature* **386,** 578–584 (1997).
9. Hilton, D. R., Thirlwall, M. F., Taylor, R. N., Murton, B. J. & Nichols, A. Controls on magmatic degassing along the Reykjanes Ridge with implications for the helium paradox. *Earth Planet. Sci. Lett.* **183,** 43–50 (2000).
10. Eiler, J. M., Farley, K. A. & Stolper, E. M. Correlated He and Pb isotope variations in Hawaiian lavas. *Geochim. Cosmochim. Acta* **63,** 1977–1998 (1998).
11. Pedersen, A. K., Larsen, L. M., Riisager, P. & Dueholm, K. S. in *The North Atlantic Igneous Province: Stratigraphy, Tectonic, Volcanic and Magmatic Processes* (eds Jolley, D. W. & Bell, B. R.) 157–181 (Geol. Soc. Lond. Spec. Publ. 197, 2002).
12. Francis, D. The Baffin Bay lavas and the value of picrites as analogues of primary magmas. *Contrib. Mineral. Petrol.* **89,** 144–154 (1985).
13. Robillard, I., Francis, D. & Ludden, J. N. The relationship between E- and N-type magmas in the Baffin Bay lavas. *Contrib. Mineral. Petrol.* **112,** 230–241 (1989).
14. Saunders, A. D., Fitton, J. G., Kerr, A. C., Norry, M. J. & Kent, R. W. in *Large Igneous Provinces* (eds Coffin, M. F. & Mahoney, J. J.) 45–94 (Am. Geophys. Union, Washington DC, 1997).
15. Prestvik, T., Goldberg, S., Karlsson, H. & Gronvold, K. Anomalous strontium and lead isotope signatures in the off-rift Oraefajokull central volcano in south-east Iceland: Evidence for enriched end-member(s) of the Iceland plume? *Earth Planet. Sci. Lett.* **190,** 211–220 (2001).
16. Graham, D. W. *et al.* Helium isotope composition of the early Iceland mantle plume inferred from the Tertiary picrites of West Greenland. *Earth Planet. Sci. Lett.* **160,** 241–255 (1998).
17. Kurz, M. D. Cosmogenic helium in a terrestrial igneous rock. *Nature* **320,** 435–439 (1986).
18. Whitehouse, M. J., Kalsbeek, F. & Nutman, A. P. Crustal growth and crustal recycling in the Nugssugtoquidian orogen of West Greenland: constraints from radiogenic isotope systematics and U-Pb zircon geochronology. *Precambrian Res.* **91,** 365–381 (1998).
19. Stuart, F. M., Ellam, R. M., Harrop, P. J., Fitton, J. G. & Bell, B. R. Constraints on mantle plumes from the helium isotopic composition of basalts from the British Tertiary Igneous Province. *Earth Planet. Sci. Lett.* **177,** 273–285 (2000).
20. Anderson, D. A model to explain the various paradoxes associated with mantle noble gas geochemistry. *Proc. Natl Acad. Sci. USA* **95,** 9087–9902 (1998).
21. Marty, B. & Lussiez, P. Constraints on rare gas partition coefficients from analysis of olivine-glass from a picritic mid-ocean ridge basalt. *Chem. Geol.* **106,** 1–7 (1993).
22. Stuart, F. M. Comment on "Speculations about the cosmic origin of He and Ne in the interior of the Earth". *Earth Planet. Sci. Lett.* **122,** 245–247 (1994).
23. McKenzie, D. M. & O'Nions, R. K. The source regions of ocean island basalts. *J. Petrol.* **36,** 133–159 (1995).
24. Hanan, B. B. & Graham, D. W. Lead and helium isotope evidence from oceanic basalts for a common deep source of mantle plumes. *Science* **272,** 991–995 (1996).
25. Hauri, E. H., Whitehead, J. A. & Hart, S. R. Fluid dynamic and geochemical aspects of entrainment in mantle plumes. *J. Geophys. Res.* **99,** 24275–24300 (1994).
26. Fitton, J. G., Saunders, A. D., Norry, M. J., Hardarson, B. S. & Taylor, R. N. Thermal and chemical structure of the Iceland plume. *Earth Planet. Sci. Lett.* **153,** 197–208 (1997).
27. Marty, B., Pik, R. & Gerzhagan, Y. Helium isotopic variation in Ethiopean plume lavas: nature of magma sources and limit on lower mantle contribution. *Earth Planet. Sci. Lett.* **144,** 223–237 (1996).
28. Hardarson, B. S., Fitton, J. G., Ellam, R. M. & Pringle, M. Rift relocation—a geochemical and geochronological investigation of a palaeo-rift in northwest Iceland. *Earth Planet. Sci. Lett.* **153,** 181–196 (1997).
29. Olive, V., Ellam, R. M. & Wilson, L. A protocol for the determination of the rare Earth elements at picomole level in rocks by ICP-MS: Results on geological reference materials USGSPCC-1 and DTS-1. *Geostand. Newsl. J. Geostand. Geoanal.* **25,** 219–228 (2001).
30. Fitton, J. G., Saunders, A. D., Larsen, L. M., Hardarson, B. S. & Norry, M. J. Volcanic rocks from the southeast Greenland margin at 63°N: composition, petrogenesis and mantle sources. *Proc. ODP Sci. Res.* **152,** 331–350 (1998).

Acknowledgements The samples used in this study were collected by I. Snape, C. Cole and S. Brown during an expedition partly funded by the Sheila Hall Trust. This work was supported by NERC scholarship to S.L.-E. and NERC funding to F.M.S. and R.M.E.

Competing interests statement The authors declare that they have no competing financial interests.

Correspondence and requests for materials should be addressed to F.M.S. (f.stuart@suerc.gla.ac.uk).